VARIATIONS ON SELF-ASSEMBLY OF SURFACTANT-BASED CONFINED SYSTEMS

Cognome / Surname   Mattiello   Nome / Name Sara

Matricola / Registration number   726873

Tutore / Tutor: Prof. Luca Beverina

Coordinatore / Coordinator: Prof. Marco Bernasconi

Contents

Chapter 1

Introduction - a personal perspective

"Begin at the beginning," the King said gravely, "and go on till you come to the end: then stop."

Lewis Carrol
ALICE IN WONDERLAND

At the beginning of this dissertation you would expect to find a very well defined picture of the nanotechnology field and market, because, if you want to be realistic, you need a very good reason to work on a particular idea, and there is no better reason than money. For example, nanotechnology research was funded globally for more than 10 billion USDs in 2015,[1] with 200000 papers published and a marked value of generated products evaluated for nearly 40 billion for year 2016.[2]

And after a wide overview of good reasons to step into nanotechnology research, looking at the title, you would expect I will explain you how important and wondrous is self-assembly to create and manipulate nanostructures, maybe starting from the story of the tobacco mosaic virus[3] and ending up with DNA origami.[4]

However, if I have to be true to you, at the beginning of this story there is nothing more special than soap, and this is exactly the point I am going to start from. The reason is that, at the very beginning of this dissertation, I would really like to highlight not the importance of money, market, or fundamental scientific theories, but how exciting should be for scientists to look at simple things and find wonder inside them. That is what you find out thinking how much of nanotechnology you can discover, well hidden, in something as simple as soap.

As the work presented in the following chapters may look a bit heterogeneous, this Introduction is needed to give a *ratio* of all the projects followed. I will start with a (short) overview of the class of materials studied, a constant of this thesis, their characteristics and applications, and I will then outline the big picture of this work, building confined systems through a simple self-assembly approach of small organic molecules.
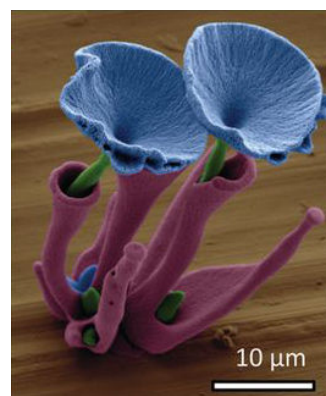
Marvelous self-assembly: false-colored SEM showing $SrCO_3$ – SiO_2 "corals". Reproduced with permission from [5]. Copyright © 2013 American Association for the Advancement of Science.

1.1 A short journey through surfactant world

1.1.1 A variety of surfactants

As I decided to begin from soap, I will start giving a first general definition of the substances soap is made of, namely surfactants. A surfactant -what a gross word- is "a substance which reduce the surface tension of a liquid in which it is dissolved".[6] Translating this property, we could picture surfactants as "mediators" for immiscible fluids, whose mutual antipathy decreases in their presence. The reason for this behaviour is the peculiar structure-property relationship that surfactants exhibit. Giving a second general definition, a surfactant is a molecule "composed of a polar head group that likes water and a nonpolar tail group that dislikes water [...] The head and tail groups of the surfactant cannot leave one another because they are covalently connected".[7] For this reason, a surfactant in a biphasic environment (both liquid-liquid or gas-liquid) will try to wet both the fluids, locating the head in the more polar phase and the tail in the less polar one, thus lowering the interfacial tension.

The particular nature of both the head and the tail spans a large variety of possibilities: cationic, anionic, zwitterionic, non-ionic for the head; hydrocarbon, fluorocarbon, siloxane based tail; tail length varying from small molecule to polymer, with linear or branched chains, or containing rings. Particular classes of surfactants possess two heads ("bola surfactants"), or both a double head and tail (they are called "gemini").[7, 8] Figure 1.1 summarizes possible chemical compositions and morphologies of common surfactants.
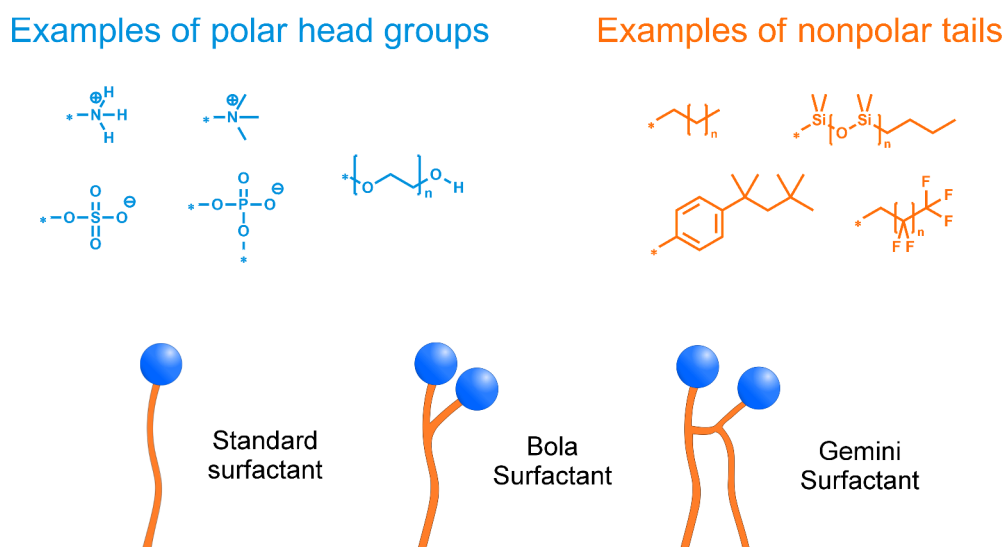
Figure 1.1 Examples of widespread chemical compositions for the head (blue) and tail (orange) of surfactants. On the bottom, a cartoon shows three possible morphologies for surfactant molecules. This color convention will be maintained within the whole dissertation.

Someone defined surfactants "schizophrenic" molecules:[9, 10] they can make surfaces wettable by a liquid or repellent, form or disrupt foams, increase or reduce the viscosity of a slurry, accelerate or retard the rate of organic reactions, suspend a solid in water or precipitate it, and, of course, solubilize hydrocarbons in water.

Surf*cat*tant

1.1.2 Basic surfactants behaviours

Micellization

Despite this large variety of natures and morphologies, looking through the eye of Dynamic Light Scattering, you will find out a systematic behaviour for all surfactants: if dissolved in water, above a particular concentration, they will spontaneously assemble into micelles. A micelle (literally, "tiny crumb") is the colloidal aggregate (few to few tens nanometers in size) that surfactants form when dispersed into a liquid unable to solubilize one of the two portions of the molecule (water is a classic). Figure 1.2 shows the cartoon of an ideal micelle: the apolar tails aggregate and interact through non-covalent interactions, while the heads form a "protective layer" which preserves the tails from seeing water.
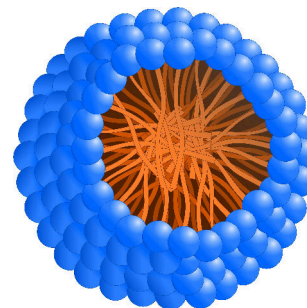
Figure 1.2 Cartoon of an ideal micelle.

From 1948, the year Debye gave his first theory on micellization,[11] several scientists proved themselves in describing this phenomenon, thus providing us a strong theoretical background which, today, allows us to compute micellar structures.[7] To make this long story short, micellization occurs when the energy required to keep the hydrophobic tails in a polar environment is bigger than the loss of entropy that follows the aggregation process. Depending on the considered parameters, models can be developed which are more or less refined. The first predictive theory on self-assembly, size and shape of micelles from structural considerations was developed by Israelachvili in 1976,[12] and it's still well considered, as it just requires three parameters (deducible from geometric considerations) and gives reliable results.

Critical micellar concentration
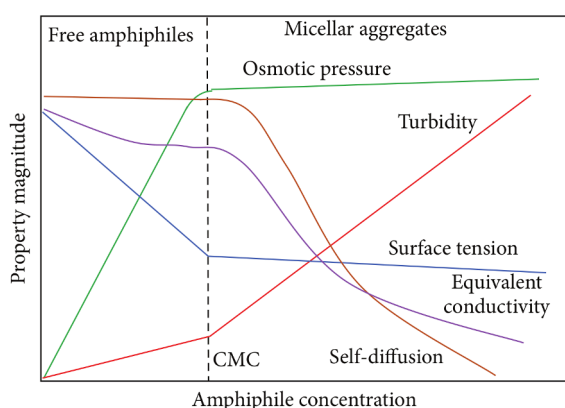
Figure 1.3 Behavior of some physical properties and their discontinuity associated with the formation of micelles at the critical micelle concentration. Reproduced with permission from [8].

The concentration of surfactant needed for micellization to occur is called critical micellar concentration (cmc), and it is specific of each surfactant. Its value can be determined experimentally through a number of different methods. In fact, when a surfactant is gradually added in water, it starts populating the air/water interface, packing into micelles only after interfacial saturation. As shown in figure 1.3, at the onset of cmc several physical properties of the surfactant solution change sharply.[8, 10] Measurements of interfacial tension, conductivity (for ionic species), osmotic pressure, self-diffusion, turbidity or chemical shift[13] can all be used for the purpose, and they allow measuring the cmc directly. Another common method is instead based on the use of a fluorescent probe, whose emission

spectrum changes depending on the neighboring environment. Pyrene is perhaps the most common probe used for this purpose,[14] as it has a structured emission spectrum, whose vibronic bands change intensity depending on the polarity of the environment. In pre-micellar stage, the pyrene accommodates in water, and beyond micellization, it partitions itself between water and hydrocarbon-like micellar core. As pyrene is strongly apolar, its partition coefficient is large, and the variation in the replica intensity is easily detectable. As we used this method for analytical purposes, I will come back to this point for a deeper insight in Chapter 4.

Strongly connected with cmc are the micellar aggregation number (the average number of molecules composing a micelle, a_M) and micellar weight (of course, the product of a_M and surfactant molecular weight).

Micelles stability and related issues

A micelle is not a stable entity. As it is formed by small molecules kept together by non-covalent interactions, it is a dynamic object, whose lifetime is limited (we are generally speaking of times in the milliseconds to seconds order of magnitude). This clearly means that a micelle is also far from being the ideal sphere depicted in figure 1.2, as surfactant molecules change continuously their arrangement. Thus a micelle might look more like that shown in figure 1.4. The presence of apolar chains at the surface of micelles creates a "percolation path" which allows loading of these structures with lipophilic species, which otherwise would not be able to pass the hydrophilic heads barrier.[15]
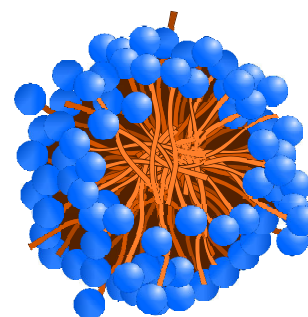
Figure 1.4 Cartoon of a more realistic micelle.

A lot has been debated about the degree of hydration of the micellar core;[16, 17] rivers of ink flew on the effect of surfactant morphology and tail length on the final properties (and stability) of the micelle;[7, 8, 12] but I promised to be short.

Because of the inherent dynamicity of surfactant molecules in a micellar dispersion, micelles cannot be considered as an entirely new phase with respect to the aqueous one. In fact, despite having properties which are way different from the outer aqueous environment, micelles continuously break and reform, unable to behave as stable entities. Thus, the related literature refer to them as a pseudophase. I'll discuss a little more on this in Chapter 3.

Stability of micellar pseudophase is also affected by temperature and the presence of additives. I will explore more this topic in Chapter 4, together with the HLB (Hydrophilic-Lipophilic Balance) theory.

1.1.3   One word on industrial applications

One word is more than enough, nearly everyone knows how ubiquitous surfactants are in everyday life. They are the active components in detergents and disinfectants, promote drugs assimilation, make possible the formulation of a variety of different substances, such as inks, cosmetics or pesticides, and are added to our food to improve its looking and taste.[15, 18]

1.2 The big picture

The only true voyage of discovery [...] would be not to visit strange lands, but to possess other eyes.

M. Proust
THE CAPTIVE

Speaking about academic research, surfactants are mainly used for their micellization property. Strictly speaking, this is not really different from the use industry makes of these molecules. The effect we look for is always the compatibilization of species which, otherwise, would not look at each other.

Nonetheless, this is not totally true. The way we look at the process is in fact completely different, and, coming back to what said at the beginning, this makes what we do different. For a long time, surfactant science moved on mainly thanks to industry contributions, looked more like "cooking" than science. If this is not true anymore, it is not due to the development of new materials or processes, but to new ways to look at them. So, what is a simple "ingredient" for a process engineer, might be a tool to operate for a scientist.

In our hands, surfactants are instruments to manipulate matter on the nanoscale. A micelle does not simply define a different (pseudo)phase in water, it becomes the box where we make processes happen. As the process depends only on the species loaded, it can be very general: we explored photophysics (Chapter 2) and reactivity of organic molecules (Chapter 3), but these are only two of many possible options.

In a few words, aim of this work was building confined nano-systems through the use of very common molecules -materials soap bubbles are made of-, and very simple processes -dissolution, precipitation, reprecipitation, colloidal chemistry tools. Self-assembly is our engine: simply tailoring interactions strength between players changes the outcome of our process. This is true for the localization of a molecule in a micelle (Chapter 4), as well as for the crystallization of a hybrid material which explores both ionic and non-covalent forces (Chapter 5).

For these reasons, this dissertation is divided in four chapters. In Chapter 2, photophysics in a micellar system is presented. In Chapter 3, the same micelles become nano-reactors. With Chapter 4, we deal with the problem of micellar stability to build a "polysoap". Finally, Chapter 5 tells a somewhat different story about surfactants, which, consistently with their "schizophrenic" nature, like actors wear new clothes -these of ligands- just to play the same role.

Bibliography
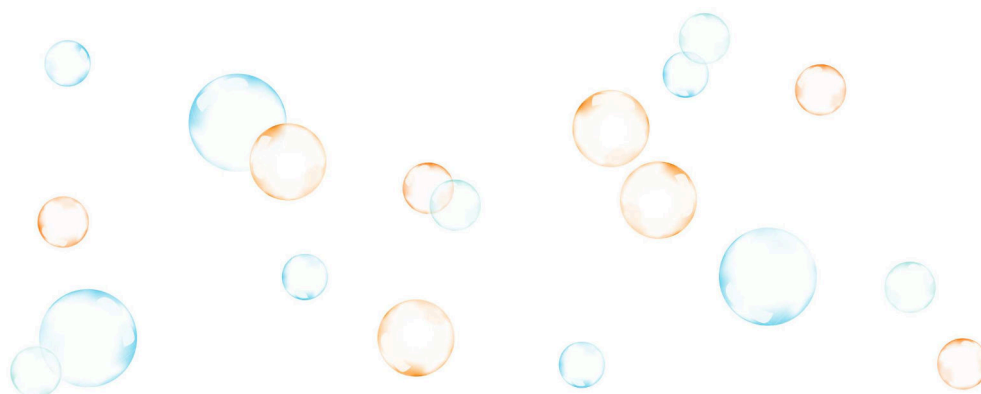
[1] http://nanotech.conferenceseries.com. Accessed 26-12-2017.

[2] McWilliams, A. *The Maturing Nanotechnology Market: Products and Applications.* Tech. rep., BCC Research, **2016**. Report ID: NAN031G.

[3] Klug, A. *Philos. Trans. Royal Soc. B* **1999**, *354*, 531–535. doi: 10.1098/rstb.1999.0404.

[4] Rothemund, P. W. K. *Nature* **2006**, *440*, 297–302. doi: doi:10.1038/nature04586.

[5] Noorduin, W. L., Grinthal, A., Mahadevan, L., and Aizenberg, J. *Science* **2013**, *340*, 832–837. doi: 10.1126/science.1234621.

[6] http://en.oxforddictionaries.com/definition/surfactant. Accessed 26-12-2017.

[7] Nagarajan, R. *One Hundred Years of Micelles*, in *Surfactant Science and Technology: Retrospects and Prospects.* Taylor & Francis, **2014**, pp. 3–52. ISBN 978-1-4398-8296-2.

[8] Lombardo, D., Kiselev, M., Magazù, S., and Calandra, P. *Adv. Cond. Matter Phys.* **2015**, *2015*, 1–22. doi: 10.1155/2015/151683.

[9] Mittal, K. L. (Editor). *Micellization, solubilization, and microemulsions*, vol. 1. Springer US, New York, **1977**. ISBN 978-1-4684-2348-8.

[10] Chakraborty, T., Chakraborty, I., and Ghosh, S. *Arab. J. Chem.* **2011**, *4*, 265–270. doi: 10.1016/j.arabjc.2010.06.045.

[11] Debye, P. *J. Colloid Sci.* **1948**, *3*, 407–409. doi: 10.1016/0095-8522(48)90025-7.

[12] Israelachvili, J. N., Mitchell, D. J., and Ninham, B. W. *J. Chem. Soc., Faraday Trans. 2* **1976**, *72*, 1525–1568. doi: 10.1039/f29767201525.

[13] Söderman, O., Stilbs, P., and Price, W. S. *Concepts Magn. Reson. A* **2004**, *23*, 121–135. doi: 10.1002/cmr.a.20022.

[14] Kalyanasundaram, J. K. and Thomas, K. *J. Am. Chem. Soc.* **1977**, *99*, 2039–2044. doi: 10.1021/ja00449a004.

[15] Mollet, H. and Grubenmann, A. *Formulation Technology: Emulsions, Suspensions, Solid Forms.* John Wiley & Sons, **2008**. ISBN 3-527-30201-8.

[16] Svens, B. and Rosenholm, B. *J. Colloid Interface Sci.* **1973**, *44*, 495–504. doi: 10.1016/0021-9797(73)90327-5.

[17] Stigter, D. *J. Phys. Chem.* **1974**, *78*, 2480–2485. doi: 10.1021/j100617a013.

[18] Hargreaves, A. E. *Chemical formulation: An overview of surfactant based chemical preparations used in everyday life.* Royal Society of Chemistry, Cambridge, UK, **2003**. ISBN 0-85404-635-6.

Chapter 2

Up-converting micelles

Light is therefore colour.

J. M. W. Turner

In this first case of study, the surfactant is used for his principal ability: creation of a loading system. Micelles are the vehicles we used to carry out up-conversion in water. We need them to define the space, in terms of polarity, where the chosen luminophores will interact. As the up-conversion photophysics requires proximity of the involved molecules, the micelle has also the function to keep them close enough to interact efficiently. We can think about these micelles as "photonic boxes".

This work was performed in collaboration with the Stem Cell Laboratory in the Department of Pathophysiology and Transplantation - University of Milano, and Istituto Italiano di Tecnologia (IIT).

2.1 Photon frequency conversion processes

Up-Conversion (UC) is the photophysical process through which the sequential absorption of two (or more) low-energy photons leads to the emission of a single high energy photon.[1, 2] This is not the only known process which allows the photon frequency conversion, since both second harmonic generation (SHG) and two-photon absorption (TPA), sketched in fig. 2.1, are well-established methods which allow to obtain this result. In these cases, however, high density photon flux and coherent

Figure 2.1 Simplified picture of the energy diagrams in photon frequencies conversion processes.

light are required, because virtual non-stationary states are involved in the photophysical process, and (nearly) simultaneous absorption of the photons is needed. On the other side, up-conversion processes are based on long-living excited states, thus enabling the transitions possibly without the need of high intensity and coherent light sources.[2]

In the literature, two categories of materials are reported to show up-conversion properties: lanthanide ions and organic molecules with suitable triplet states. In both cases, the up-conversion process requires the presence of a sensitizer and an emitter.

Lanthanide-based up-conversion nanoparticles (Ln-UCNPs) are generally composed of a sensitizer, emitter, and host lattice. The sensitizer is usually a NIR absorbing ion (like Nd^{3+} or Yb^{3+}), while several elements are used as emitters, like Er^{3+}, Tm^{3+}, Eu^{3+} or Sm^{3+}. The host lattice is usually made of an alkaline metal/optically inert rare earth fluoride, such as NaYF. The choice of host lattice is fundamental, since the crystal field dramatically changes the optical properties of the lanthanide ions, and the lattice vibrations could be advantageous or detrimental in achieving good UC luminescence efficiency. Several mechanisms are known to be involved in the UC process, such as excited-state absorption, energy transfer UC, photon avalanche, cooperative UC, and energy migration-mediated UC.[3–5] Besides the advantages of Ln-UCNPs, like the high stability, low toxicity and tunable (even multicolor) emission, their main drawback is their low UC luminescence efficiency, because of both the poor photon harvesting capabilities of lanthanide ions and the quenching of the sensitizer through deexcitation processes like thermal relaxation or energy transfer to surface defects or solvent.

2.2 A general overview of TTA-UC

UC processes in organic systems, on the other side, take advantage of sensitization of long-living triplet energy levels. Triplet-Triplet Annihilation (TTA), Thermally Activated Delayed Fluorescence (TADF), Inorganic Nanocrystals and direct Singlet-to-Triplet absorption are the known means which make possible this sensitization.[6] For this project, we concentrated on the TTA process, which has a solid track in the dedicated literature. The other cited methods are relatively new to the field of up-conversion, and reports on their application are very recent.[7–9]

2.2.1 Photophysics of TTA-UC: energy transfer mechanisms, power dependence and quantum yield

TTA-UC mechanism is based on the energy transfer from the sensitizer (S) to the emitter (E) through long-living triplet states: due to spin selection rules, in fact, phosphorescence from a triplet state is a "forbidden" transition, thus it gives time enough for energy transfer processes to occur. An appropriate pair of molecular species is needed to observe the phenomenon. Figure 2.2 shows a sketch of the process.[10, 11]
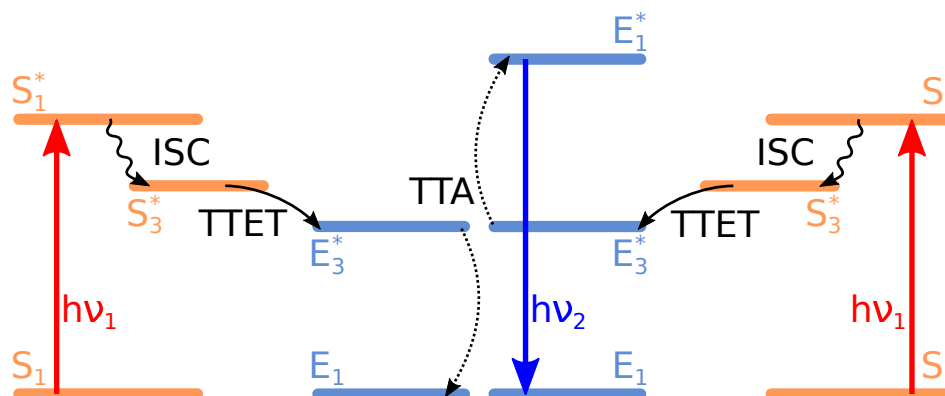

Figure 2.2 Sketch of the TTA-UC photophysical process. Energy levels of the sensitizer (S) are depicted in orange, while levels of the emitter (E) are in blue.

In the TTA process, the sensitizer molecule absorbs light of energy $h\nu_1$, being excited in the first singlet excited state S_1^*. It then decays rapidly into the first excited triplet state via Intersystem Crossing (ISC). If an emitter molecule is close enough to the sensitizer, Triplet-Triplet Energy Transfer (TTET) occurs, thus the sensitizer comes back to the ground state, while the emitter is excited to its first triplet excited state E_3^*. Finally, the collision of two excited triplets (TTA) leads to the promotion of one of them to the first singlet excited state of the emitter, which is fluorescent with emission energy $h\nu_2 > h\nu_1$.

The TTA-UC process is dependent on the concentration of triplet excited states, and therefore also on the power density of the incident light. Several groups have studied the power dependence to gain insights into the mechanistic aspects of the up-conversion process. Originally, a quadratic dependence of the upconverted light intensity to the incident power density was found,[12] and attributed to the bi-molecular nature of the annihilation step. However, Monguzzi first[13] and other groups later[14] demonstrated that the quadratic power dependence is the result of experimental conditions that prevent reaching a regime in which the concentration of triplets is sufficiently high for the annihilation route to be favored over alternative relaxation pathways (e.g. nonradiative triplets spontaneous decay). Thus, if the incident power density is increased beyond a certain threshold, the relationship between the upconverted intensity on the incident power density becomes linear, as visible in figure 2.3. This is possible when the annihilation process becomes faster than other relaxation channels, a condition achieved at a high population of triplets. Haefele[15] demonstrated that rigorously removing oxygen – a well-known triplet quencher – from the UC system allows to shift the transition from the quadratic regime to the linear regime with non-coherent light in solution towards much lower power densities.

The up-conversion quantum yield (QY_{UC}) of the overall UC process, which is the number of emitted photons per absorbed photons, can be written as[16]
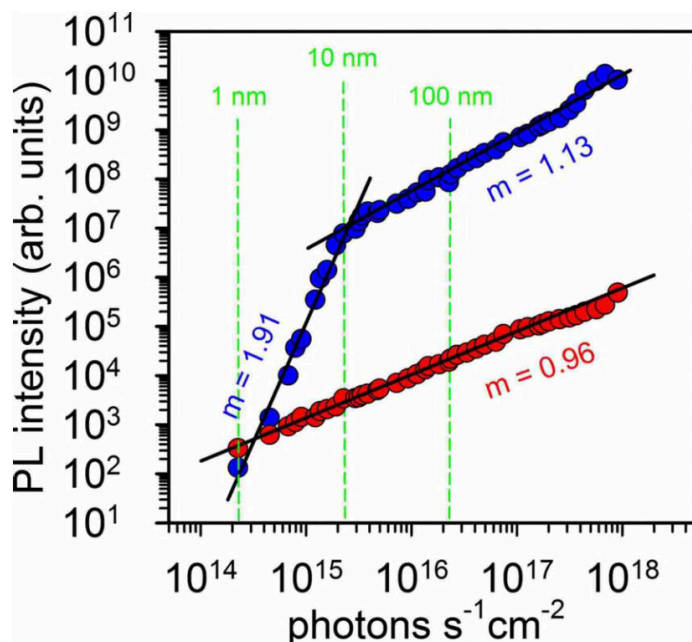
Figure 2.3 DPA fluorescence (blue circles) and PtOEP phosphorescence (red circles) intensity as function of the excitation power density for a PtOEP/DPA solution in 1,1,2-trichloroethane. The green vertical lines indicate the power density supplied by the sun at 532 nm under AM 1.5 condition integrated over 1, 10, and 100 nm, respectively. Reproduced with permission from ref. [13]. Copyright © 2008 American Chemical Society.

$$\text{QY}_{\text{UC}} = \frac{\#\,\text{emitted photons}}{\#\,\text{absorbed photons}} = \frac{1}{2} f \cdot \eta_{ISC} \cdot \eta_{TTET} \cdot \eta_{TTA} \cdot \eta_E = \frac{1}{2} f \cdot \phi_{ET} \qquad (2.1)$$

where η_{ISC}, η_{TTET}, η_{TTA} and η_E are the quantum yields of the ISC, TTET and TTA processes, and the fluorescence quantum yield of the emitter respectively (which can be summarized in the sensitizer-to-emitter energy transfer efficiency ϕ_{ET}), and f is the statistical probability of obtaining a singlet excited state after annihilation of two triplet states. On the basis of spin distribution statistics, the highest possible value for the latter has been debated for a long time;[14, 17–20] depending on the annihilator, values up to 85% have been demonstrated.[21, 22] The factor 1/2 is needed as two low-energy photons are required for the emission of one up-converted photon. This means that, under the best possible conditions, the highest theoretical yield of the process approaches 43%. At the present time, QY_{UC} as high as 34% has been demonstrated.[22]

2.2.2 Sensitizers and emitters requirements

In order for TTA-UC to occur, it is important that the sensitizer and the emitter molecule satisfy several requirements.

The sensitizer should have a large absorption cross-section, possibly in the low-energy portion of the spectrum, it should show efficient ISC and have a small energy gap between the singlet and the triplet state, and the triplet state lifetime should be as long as possible, in order for the TTET to occur efficiently.[23]

Since the most compelling requirement is the efficiency of ISC, the most popular luminophores are heavy metal atom containing coordination complexes. The reason is that the presence of an heavy atom promotes spin-orbit coupling, which is necessary to observe transitions between states with different spin multiplicity [24, p. 481-484]. Porphyrins, phthalocyanines and heavy metal complexes[23, 25–27] are thus the most popular sensitizers.

However, some fully organic systems are also know, which include heavy atom substituted fluorophores,[28, 29] C_{60}-chromphore hybrids[30, 31] and a few ketocoumarines[32] and boron-dipyrromethene (BODIPY)[33] dimers. Only recently, luminophores reported for thermally activated delayed fluorescence (such as 4CzTPN-Ph) are gaining attention also as sensitizers for TTA-UC.[8, 34, 35] Figure 2.4 shows some examples of sensitizers used in TTA-UC.
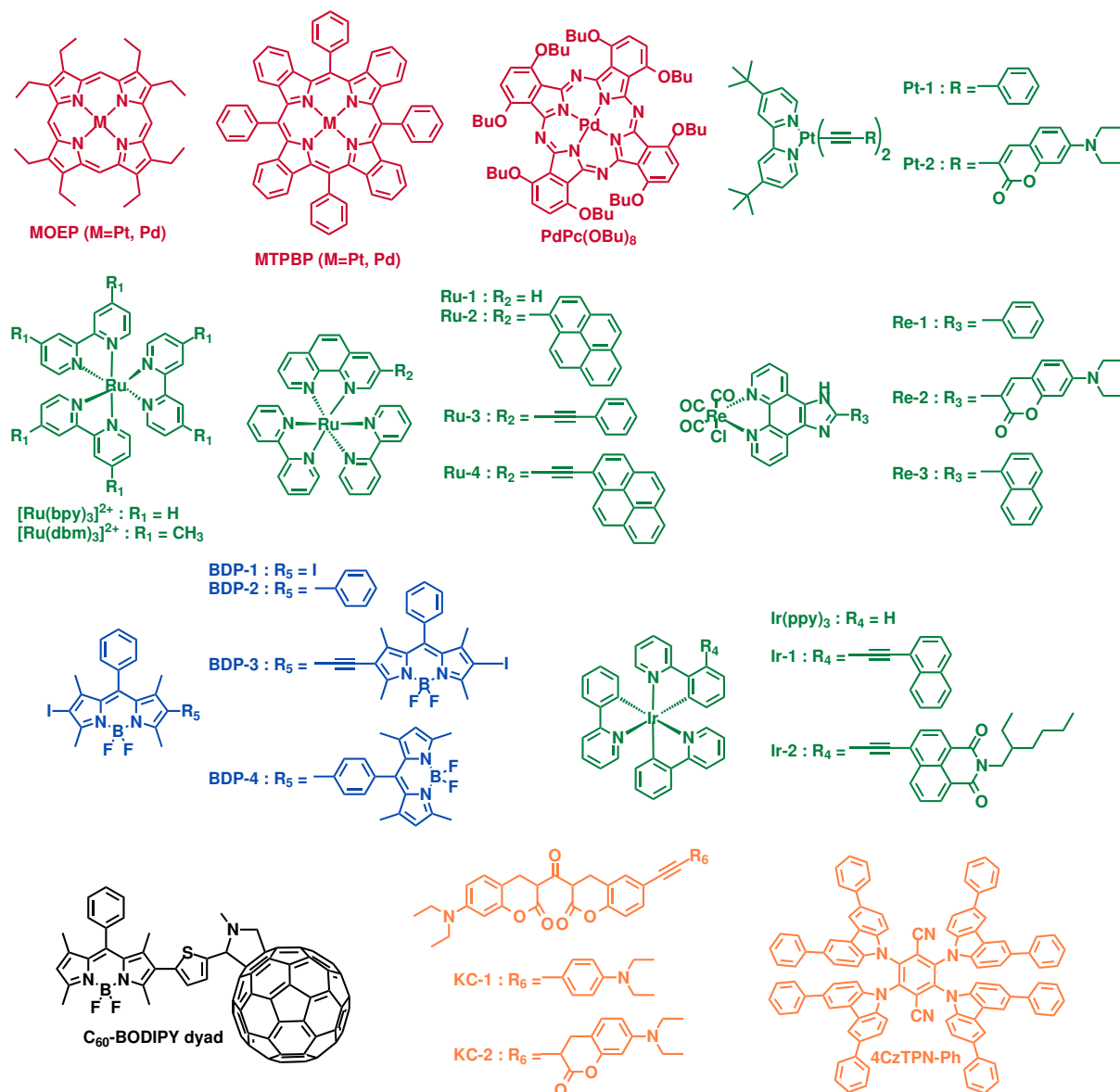
Figure 2.4 Examples of sensitizers used for TTA-UC. In red: porphyrins and phthalocyanines. In green: heavy metal complexes. In blue: heavy atom fluorophores. In black: $C_{60}-$BODIPY dyad. In orange: fully organic luminophores with good ISC efficiencies.

On the other side, the emitter should not absorb the excitation energy, should have a high fluorescence quantum yield and appropriate triplet energy state (lower than the triplet energy state of the sensitizer, but higher than half his singlet energy state) and long lifetime in order for TTA to occur.[23] The majority of annihilators pertains to the polycyclic aromatic hydrocarbons class (in particular, derivatives of anthracene, tethracene, perylene, pyrene and fluorene have been reported), but some heteroaromatic fluorophores are also

known, such as BODIPY[33] and perylene-3,4,9,10-tetracarboxylic diimide[36] derivatives. Figure 2.5 shows some examples of emitters used for TTA-UC, and photoluminescence (PL) spectra of some of these molecules, demonstrating it is possible to obtain upconverted emission in both UV and visible spectral regions.
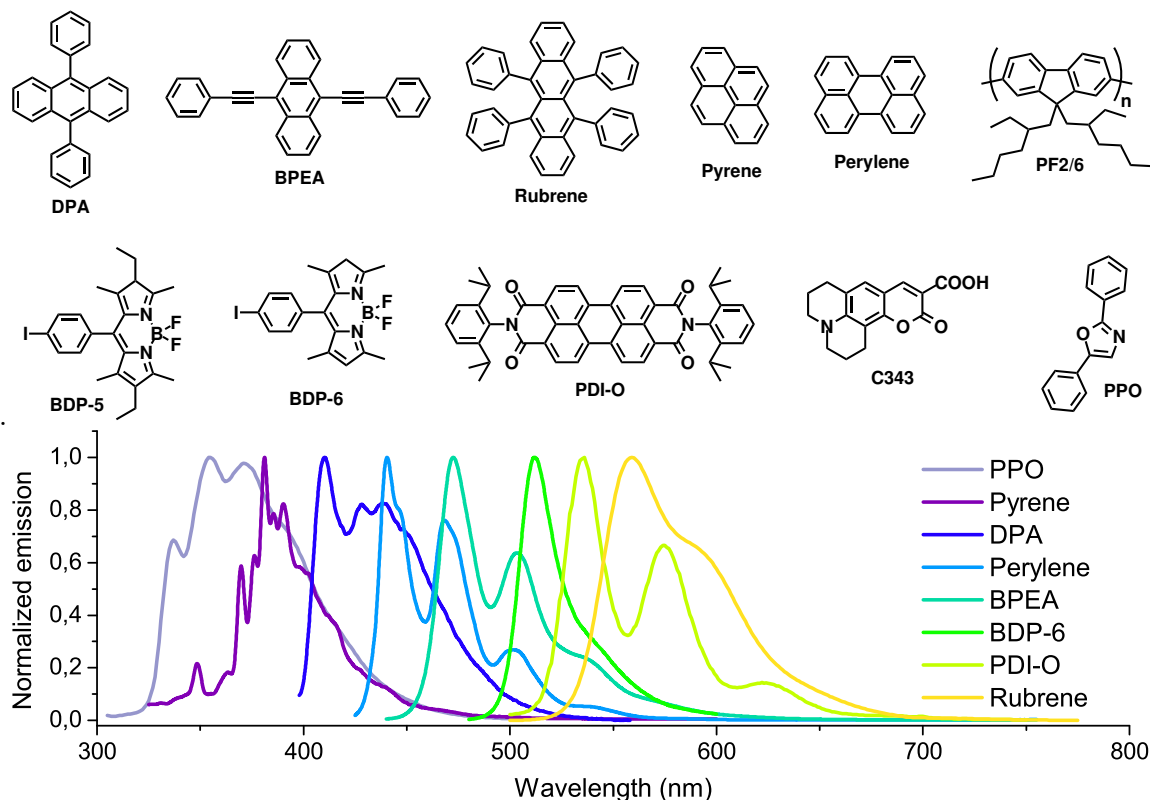
Figure 2.5 Examples of emitters used for TTA-UC and fluorescence spectra of selected ones.

A few works are reported, where a single molecule (or polymer) plays both the sensitizer and emitter role.[37–39] Such systems solve the problem of proximity between the two active components, but generally suffer of low UC efficiency because of occurring phenomena of back energy transfer.

2.2.3 Development of TTA-UC: advantages, drawbacks, applications and supramolecular approaches

In the overview of photon frequency conversion processes, TTA-UC offers several advantages: requires cheap, commercially available substances of low toxicity, low power sources to be observable (sunlight has already proven to be sufficient[40–42]), and can display high efficiencies under appropriate conditions. The main drawback of this process is that "appropriate conditions" means first of all an oxygen-free environment. In fact, the ground state of the oxygen molecule is a triplet, and can readily deexcite any present triplet excited state with formation of singlet oxygen. This process is at the base of photodynamic therapy,[43, 44] moreover recently TTA-UC has been demonstrated extremely effective for oxygen sensing in a broad range of concentrations.[45] As second drawback, the process requires close proximity of the sensitizer and emitters, as the energy is transferred between molecules mainly through a Dexter type mechanism in solution.[46] These two drawbacks

have limited the use of TTA-UC in devices since efficient methods of encapsulation for the dyes have been developed. This process may be not trivial, as aggregation induced quenching of fluorescence is common for these chromophores.[47]

In general, the up-conversion process has a variety of possible applications: all the processes that require the use of light might take advantage of it. Just to make a few examples, it has been theorized that sunlight collection in intermediate band solar cells would beneficiate from the introduction of an up-converter, with improvement of efficiencies up to 43,6%,[18, 48] and an improvement in photocurrent of 35% has been demonstrated for a DSSC coupled with a sub-bandgap up-converter.[49] As electrical excitation in OLEDs usually produces singlet and triplet excitons with a 25%:75% ratio owing to the laws of spin statistics, TTA-UC may improve the efficiencies of devices based on fluorescent materials.[50, 51] In the field of bio-imaging, the use of NIR to Vis up-conversion can solve both the problem of autofluorescence and radiation damage, as excitation irradiances less than $1 \, \mathrm{mW \, cm^{-2}}$ can be used, with energy suitable to match the transparency window of biological tissues.[1, 52, 53] Visible to UV up-conversion may allow to perform photoelectrochemistry and photocatalysis in sunlight,[54–56] without the need of expensive light sources. Niche applications have also been reported: Jiang[57] used the upconverted emission to trigger a photomechanical response in a soft actuator; Han[58] recently demonstrated that TTA in chiral emitters enhances circularly polarized luminescence.

To perform all of these processes, several methods have been developed, to enable both an efficient interaction between dyes, and the formation of a barrier against oxygen. Dispersion of the chromophores in a polymeric matrix with glass transition lower than room temperature allows casting films of up-converting rubbery materials.[11, 53] Use of glassy matrices is possible as well,[59] even if the impossibility for the dyes to diffuse and their aggregation are detrimental for the UC efficiency. Solution of the dyes have been encapsulated to form polymeric nanoparticles[60] or nanocapsules.[52, 54, 61] The dyes can be assembled in co-crystals[62] or metal-organic frameworks (MOFs).[63] Tailoring the structure of the chosen chromophores (e.g. attaching non-conjugated side chains) allows to take advantage of supramolecular approaches, such as the formation of self-assembled structures in water,[64, 65] or up-converting liquids.[66] The formation of an anoxic environment is usually achieved through the use of encapsulating materials with oxygen-barrier properties, such as poly(vinyl alcohol) (PVA),[67, 68] cellulose[69] or other similar natural derivatives.[61] Figure 2.6 shows a selection of the developed UC systems. All these approaches allow to obtain up-converting particles or structures with high efficiencies in aerated conditions, but require a complex multi-step synthetic procedure of the assembled system, or the chemical modification of the up-conversion couple.
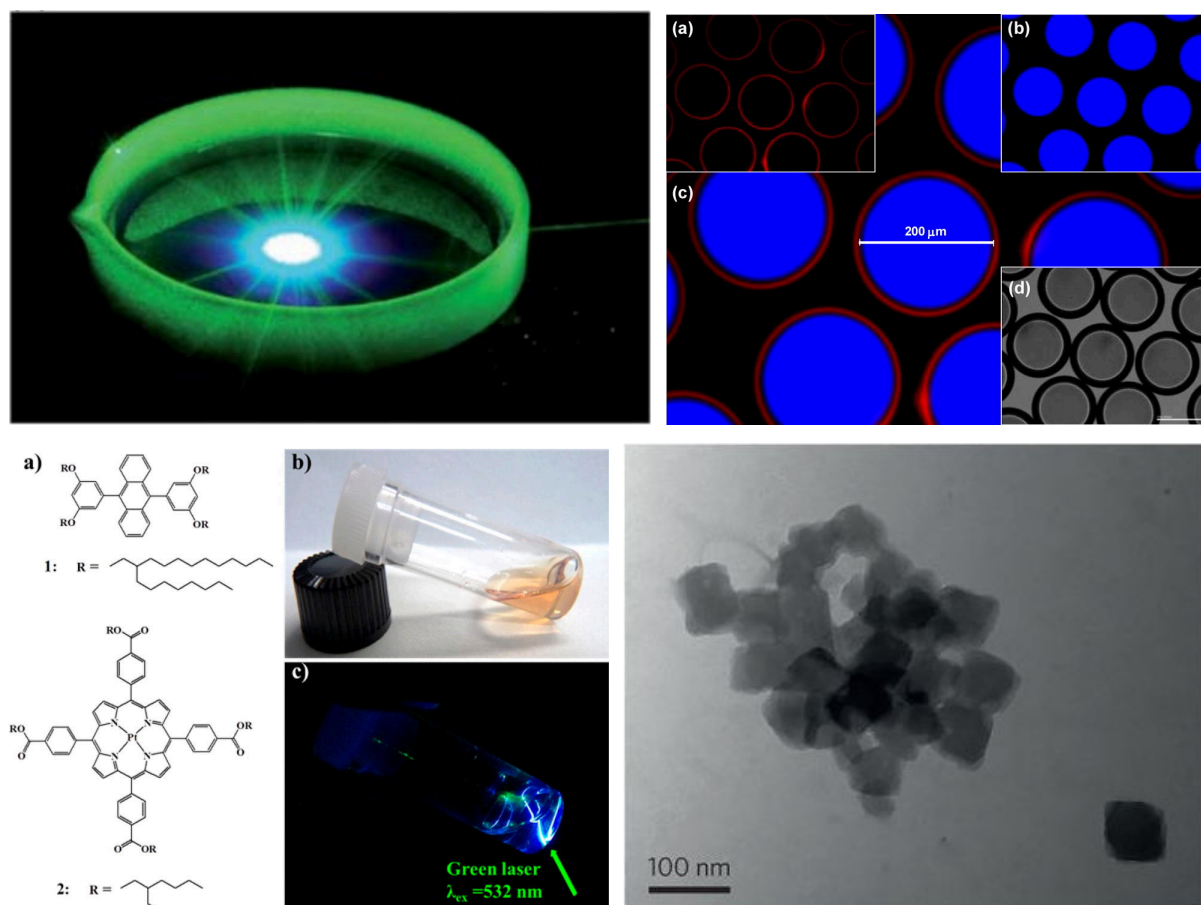
Figure 2.6 Top, left: Polymeric disk containing PdOEP/DPA UC couple. Reprinted with permission from ref. [53]. Copyright © 2012 The Royal Society of Chemistry. Top, right: confocal (a, b, c) and optical (d) microscopy pictures of polymeric capsules containing a solution of PtOEP/DPA UC couple. Reprinted with permission from ref. [54]. Copyright © 2012 American Chemical Society. Bottom, left: (a) chemical structure of liquid UC couple. Photographs of the mixed liquids exposed to (b) white light and (c) a green laser. Reprinted with permission from ref. [66]. Copyright © 2013 American Chemical Society. Bottom, right: TEM image of UC MOF nanocrystals. Reprinted with permission from ref. [63]. Copyright © 2015 Macmillan Publishers Limited, part of Springer Nature.

2.3   Aim of the work

We aimed, instead, at developing an easy procedure to prepare a surfactant-based UC system, specifically for bioimaging. This system, besides obviously asking to be a confined, oxygen proof box, needs to fulfill two more requirements: it has to be stable in water, and biocompatible. The former requirement is not as obvious as it looks like. A micelle is stable since the concentration of the surfactant is higher than the cmc: at lower concentrations, it will disaggregate into its components, delivering its load, in our case with loss of UC emission. As it's impossible to determine the concentration of surfactant in the cellular environment, a low cmc surfactant is the best guess. The latter requirement, on the other side, is particularly compelling, and we decided to deal with it using a surfactant approved by the Food and Drug Administration (FDA) for delivery purposes. The greatest advantage of a surfactant based system is that it provides an environment with a very high concentration of the dyes, which are insoluble in water, but it behaves as a viscous liquid, preventing aggregation induced quenching of the emission.

2.4 Up-converting Kolliphor Ⓡ micelles

We decided to use Kolliphor Ⓡ EL, a well-known, commercially available and cheap surfactant, which is approved by FDA as emulsifier for highly insoluble drugs (such as Paclitaxel and Miconazole).[70] This emulsifier is industrially synthesized by reaction of castor oil with ethylene oxide in a molar ratio of 1:35. Figure 2.7 shows the principal components of this mixture: triricinoleate esters of ethoxylated glycerol and polyethylene glycol ricinoleate. The double bond configuration is *cis*, as in the starting castor oil. Other present species are free fatty acids, and low molecular weight polyethylene glycol (PEG).[71, 72] Its reported critical micellar concentration is 0,02% in water, and we used it at a $\sim 1,3\%$ concentration in water, to have a margin in case of dilutions were needed before use in cellular environment. A measurement of Dynamic Light Scattering (DLS) allowed to estimate micelles hydrodynamic diameter as ~ 11 nm (v. *infra*, fig. 2.9). The

Figure 2.7 Principal components of Kolliphor Ⓡ EL: **(1)** triricinoleate esters of ethoxylated glycerol; **(2)** polyethylene glycol ricinoleates

HLB (Hydrophilic-Lipophilic Balance) value of this surfactant is quite high, lying between 12 and 14, owed to the high ethylene glycol content with respect to the castor oil (62 wt% of the total), thus Kolliphor is a very polar mixture.

We chose to use PtOEP (platinum(II) 2,3,7,8,12,13,17,18-octaethyl-21H,23H-porphyrin) and DPA (9,10-diphenylanthracene) as model sensitizer and emitter, because they are among the most studied and performing chromophores for TTA-UC, the porphyrin being the sensitizer and the DPA the emitter.

2.4.1 Synthesis of up-converting micelles (UCMs)

The synthesis of UC micelles is based on a typical formulation approach, thus is very simple. All the organic species (the surfactant mixture and the UC couple) are dissolved in an appropriate solvent, possibly miscible with water (such as THF), and sonicated for 30 minutes in order to homogenize the solution. If not otherwise stated, relative concentration of the sensitizer to the emitter is 1 mol%. The solvent is then removed by evaporation at reduced pressure, and deionized water or phosphate buffer saline (PBS) solution is added. The surfactant immediately assembles in micelles containing the UC couple, so a transparent solution is obtained, as visible in figure 2.8. Further details on the synthesis are given in the experimental section. Excitation of this solution with a commercial green pointer (λ_{ex}=532 nm) produces a blue emission in a few seconds, which is visible by the naked eye. It is important to underline that all the synthetic procedures are performed in air.
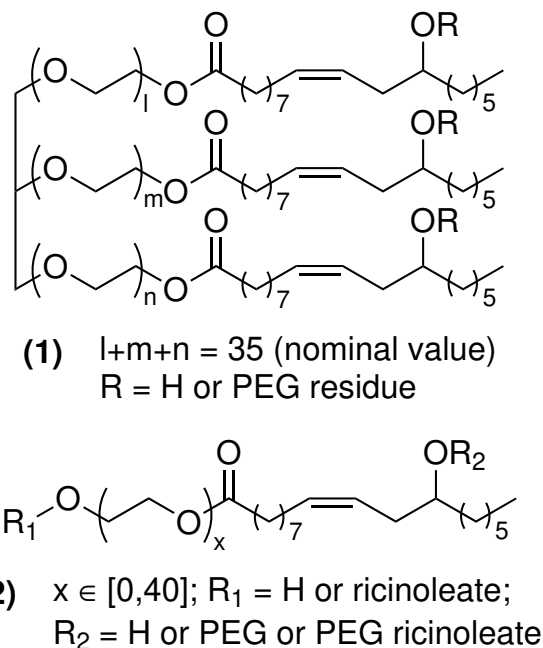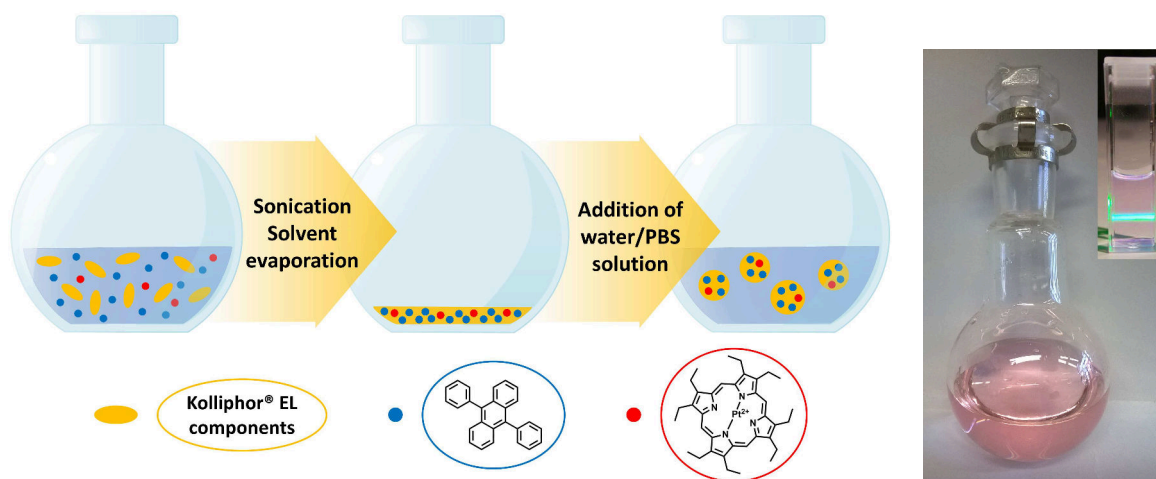
Figure 2.8 On the left, scheme of UCMs synthesis: Kolliphor is represented in yellow, PtOEP as red circles, and DPA as blue circles. On the right, a picture of the as-prepared UCMs solution. The inset shows a picture of the same UCMs dispersion under irradiation with a commercial green pointer (λ_{ex}=532 nm): the blue emission is visible by naked eye.

2.4.2 Morphology and optical properties of UCMs

We studied the morphology of the system through DLS and Cryo-EM measurements. As previously stated, the surfactant alone spontaneously form micelles in water with diameter of ~ 11 nm. As micelles are loaded with the UC couple, it is possible to see a small increase in their diameter to ~ 15 nm. Cryo-EM measurements, on the other side, shows nearly spherical particles (shape was determined through 3D tomography) with an average diameter of $\sim 6{,}2$ nm. This discrepancy is common when comparing DLS with an imaging technique. In fact, the diameter measured by DLS correspond to the dimension of the whole micelle swollen by water, while the Cryo-EM allows to see only the dense hydrophobic core of the micelles, as the hydrated PEG-ylated chains do not differ enough from the aqueous environment to be detectable. Figure 2.9 shows DLS measurements of Kolliphor and UCMs in water, a Cryo-EM picture of UCMs with their size distribution, and their 3D reconstruction.

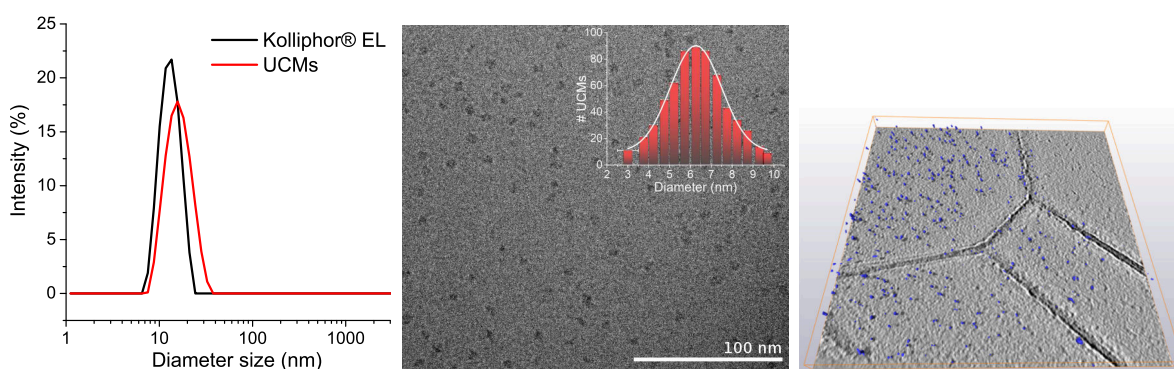**Figure 2.9** Left: DLS measurements of as prepared UCMs in water, and a dispersion of Kolliphor alone at the same concentration. Center: Cryo-EM picture of a UCMs solution in water; inset: size distribution of micellar diameters. Right: 3D model of the micelles obtained through reconstruction of a cryo-electron tomogram.

Both the overall dimensions and the diameter of inner core and of micelles are necessary

information: we used the former to estimate the number of micelles in solution, and the latter to ideally define the size of the "box" where PtOEP and DPA interact (v. *infra*).

Figure 2.10 shows the absorption spectrum of a ten times diluted dispersion of UCMs, and its deconvolution in the separated contributions of PtOEP and DPA. On the basis of the extinction coefficient of the two chromophores, we calculated a molar ratio of 1:96 of PtOEP to DPA, in line with the feeding ratio of 1:100. As no precipitate was observable after the formulation of the chromophores, we concluded that the large majority of the material was dispersed within the micelles, and the formulation approach was not selective toward one of the two components.
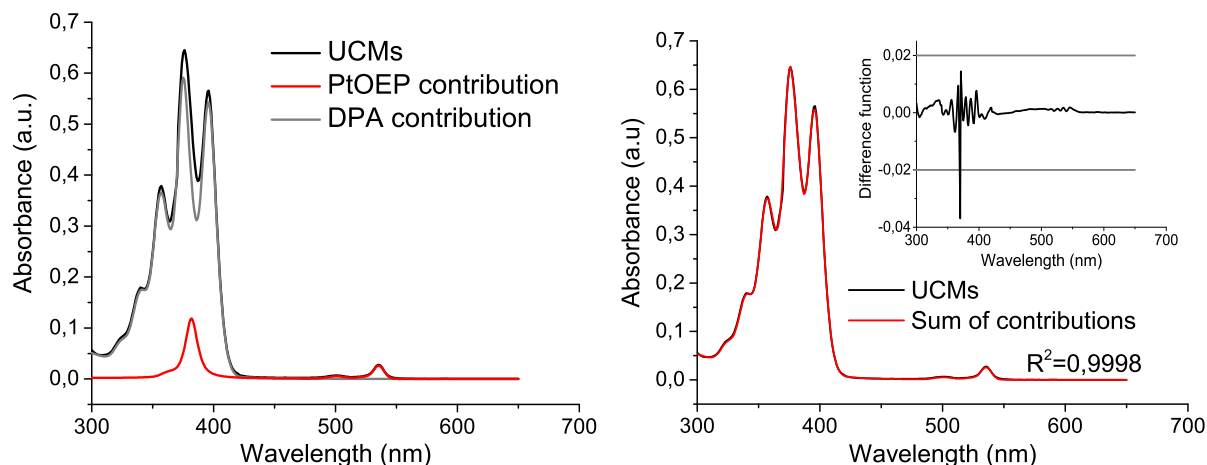

Figure 2.10 Left: UV-Vis absorption spectrum of a ten times diluted UCMs dispersion, and the separated contributions of PtOEP (red) and DPA (gray). Right: comparison between the collected UCMs spectrum and the linear combination of PtOEP and DPA contributions (1:96 molar ratio). The inset shows the difference function between experimental and calculated values; the gray horizontal lines represents the experimental error.

Fluorescence measurements (fig. 2.11) definitively demonstrate the successful loading of the UC couple: irradiation of the dispersion with a green laser (λ_{ex}=532 nm) matching the PtOEP absorption produces both the red phosphorescence of the sensitizer, and the blue UC emission of the DPA. This means that both the species are closely packed within the micelles core, where TTA occurs through diffusion of the excitons without any need of molecular motion. To support this theory, a simple Monte Carlo calculation was performed to simulate the distribution of DPA molecules within a sphere of 6,2 nm of diameter (the inner core of the micelle). Basing on the total amount of Kolliphor and DPA used,

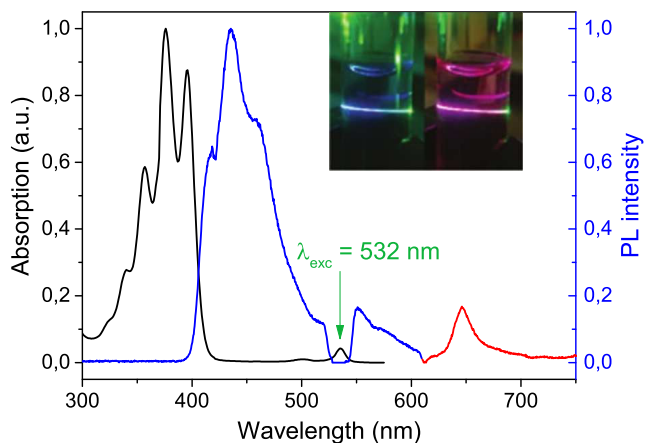**Figure 2.11** Absorption (black line) and up-converted emission (blue line) of UCMs dispersion under excitation with a green laser (λ_{ex}=532 nm). The red line represents the residual PtOEP phosphorescence. The inset shows the UCMs dispersion in PBS under laser excitation with (left) and without (right) a high-pass blue filter.

and the hydrodynamic diameter of the micelle, we estimated an average number of 56

DPA molecules per micelle, which were depicted as hard spheres of 1 nm of diameter (accordingly to the steric hindrance of DPA, whose molecular radius is 0,45 nm). The presence of PtOEP is not accounted in the calculation. Results of this simulation are visible in figure 2.12.
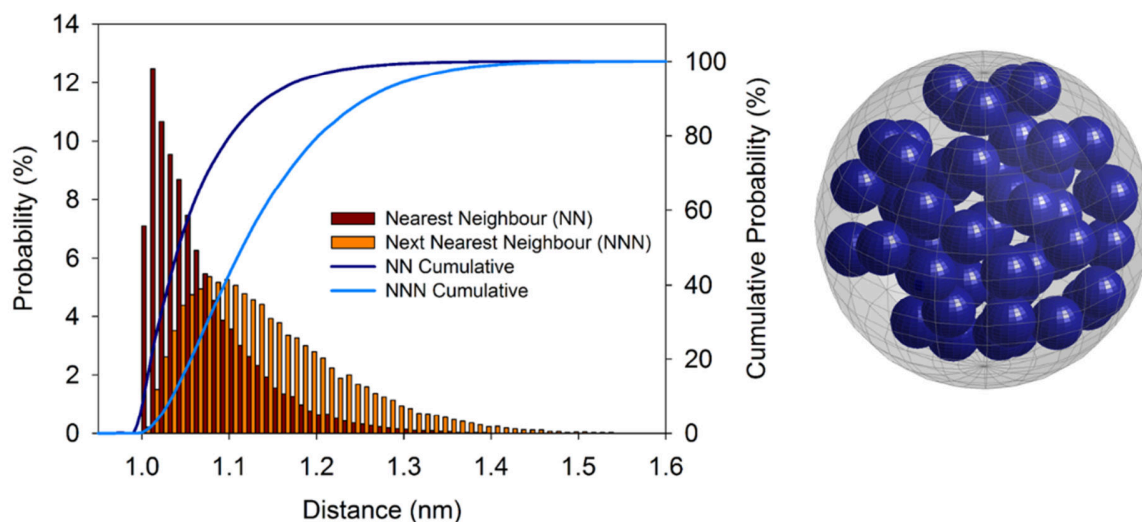

Figure 2.12 Left: histogram of the intermolecular stochastic nearest-neighbor (NN) and next nearest-neighbor (NNN) distance distribution of an ensemble of 56 DPA molecules embedded in a spherical UCM of radius 6,2 nm. The continuous line are the corresponding cumulative probabilities. Right: One example of the 10^5 randomly generated distributions.

All the dyes have a nearest-neighbour closer than 1,3 nm and a next nearest-neighbour closer than 1,5 nm. These values are comparable with the distances at which the exchange interactions are effective,[46] confirming that the excitation energy can migrate via exchange-mediated homomolecular hopping within the ensemble of emitters within the micellar volume to experience TTA.
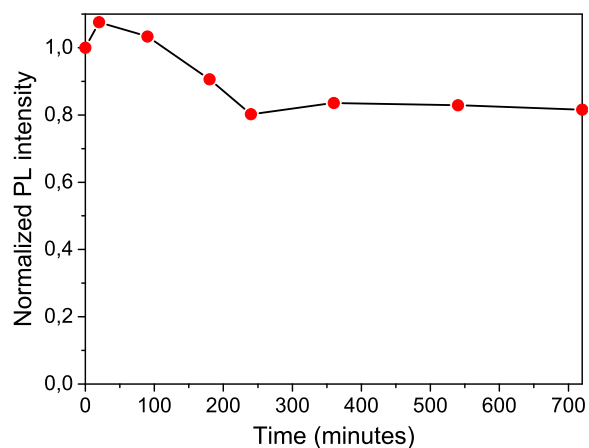
Figure 2.13 Variation of UCM photoluminescence intensity over time

Apart from an initial drop of ∼ 20%, the UC intensity remains constant for more than 12 hours after synthesis of UCMs (as visible in figure 2.13), demonstrating that this system is quite stable even in oxygenated environment. The initial drop is probably due to the consumption of oxygen present in the micellar environment by DPA molecules.

We don't have any obvious explanation for the ability of Kolliphor to protect the UC couple from quenching from oxygen, nonetheless we hypothesized that this unusual behaviour may be due to the high content of PEG (both in the principal components of Kolliphor and as free polymer). In fact, this polymer is known to behave as a protective barrier against oxygen.[73] The ricinoleate residues, with their double bonds, are natural antioxidants, and might play a role as well.

2.4.3   Photophysics of UCMs: performance analyses

As previously described, usually UC efficiency depends on the excitation power, raising with increasing excitation intensity (I_{exc}) up to a saturation value. In our case, instead, we observed a linear dependence of UC intensity for every irradiances above few tens of $mW\,cm^{-2}$, meaning that we are always in the saturation regime, corresponding to a constant QY_{UC}. Figure 2.14 shows the linear dependence of UC intensity from I_{exc} for two different concentrations of the sensitizer in the starting solution. For the highest concentration of PtOEP, we measured a noteworthy QY_{UC} of $\approx 6,5\%$. This value, even if notable for such a simple system in oxygenated environment, is way lower than the value which can be obtained for the same concentration of dyes in deoxygenated solution in an organic solvent, which is above 20%.[16] Moreover, the measured sensitizer-to-emitter energy transfer efficiency ϕ_{EM}

Figure 2.14 UC photoluminescence dependence from excitation intensity at 532 nm for two UCMs dispersion prepared with a starting sensitizer concentration of 40 µM and 400 µM. The straight lines represent the fitting of the data with a linear function with slope m. The inset shows the QY_{UC} measured at different excitation intensities.

is 55% in these conditions, so, using equation 2.1, and considering $f \approx 0,5$ for DPA, a $QY_{UC} \approx 13,5\%$ is expected for the system. To explain this discrepancy, the distribution of dyes within the micelles needed to be analyzed through deeper photophysical studies. We prepared two different series of UCMs, varying in both of them the sensitizer concentration c_{sens} in the range 20-400 µM in the starting solution. In the first series we introduced no DPA, while in the second one we introduced it at a fixed concentration of 4 mM. Figure 2.15 shows the results relative to the first series. All the samples of this series show the typical red emission of PtOEP, but the recorded lifetime is extremely different one from each other: in fact, at the lowest concentration (20 µM), the PL decay is way faster than the intrinsic radiative decay time of PtOEP (120 µs), and the lifetime lengthens by increasing c_{sens}. At the highest tested concentration, the lifetime cannot be described by a single exponential decay, and the long-time component is evaluated as $\tau_{long} = 82$ µs (represented by the green line). The short lifetime observed at low sensitizer concentrations is typically due to oxygen quenching: this suggest that the PtOEP localizes in a compartment of the micelle where oxygen is present. As the concentration of sensitizer increases, more PtOEP is pushed inside the micelle in order to accommodate all the molecules (see cartoon in fig. 2.15). The fact that more PtOEP concentrates in the micelles core, and is less affected by oxygen, matches our hypothesis that PEG constitutes the oxygen barrier layer of the micellar structure. We expect this behaviour for DPA as well, but we cannot detect it, as the oxygen sensitive triplet state of this molecule is completely dark (it does not phosphoresce), and no UC is detectable in presence of any quenching agent. This finding suggest that the efficiency of the system may be limited by the low number of "active" sensitizer.
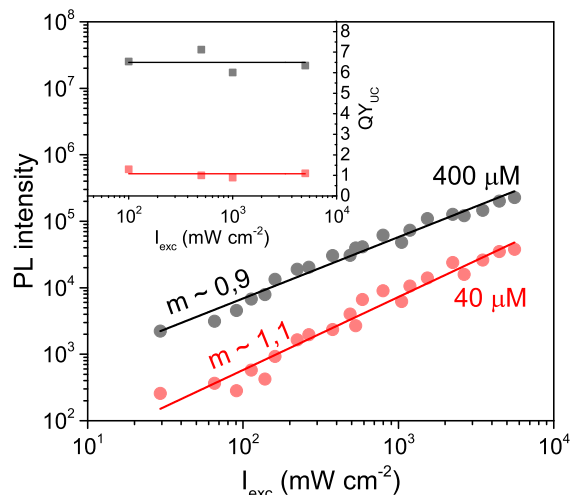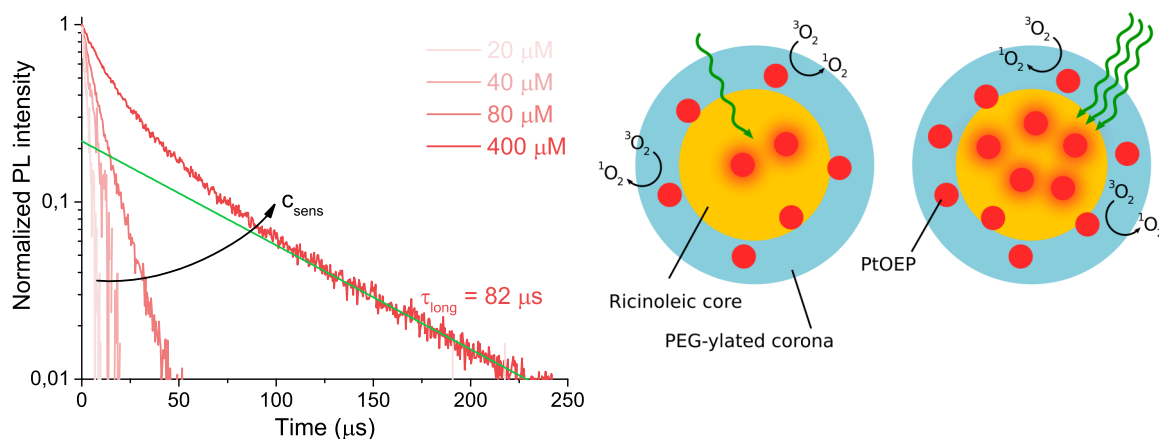
Figure 2.15 Left: time-resolved PL decay at 645 nm measured for a series of UCMs prepared with different PtOEP initial concentrations c_{sens}. The green line is the long-time component of the decay. Right: cartoon showing the proposed model to explain the variation of PtOEP lifetime with concentration within the micelles.

Following the picture outlined by the first series of UCMs, we expected to see an increase of the overall UC quantum yield with increasing sensitizer concentration for the second series of UCMs. The measurements supported this general view. Figure 2.16 shows the QY_{UC} values measured as function of PtOEP concentration, which increases from $\sim 0,4\%$ for $c_{sens} = 20\,\mu$M to 6,5% for $c_{sens} = 400\,\mu$M. The measured up-converted light decay, moreover, is the same for all the sample in the series, thus the TTA is perfectly efficient in all the conditions, and the QY_{UC} does not depend on it. This finding strongly support the conclusion that the limited efficiency of UC is not due to an inefficient TTA-UC process (which, in fact, is extremely performing unregarding the sensitizer concentrations and the power density), but rather to a not optimized distribution of the sensitizer within the micelles. In simple terms, the majority of the sensitizers are inactive, but those which are shielded from oxygen grant a perfect performance.
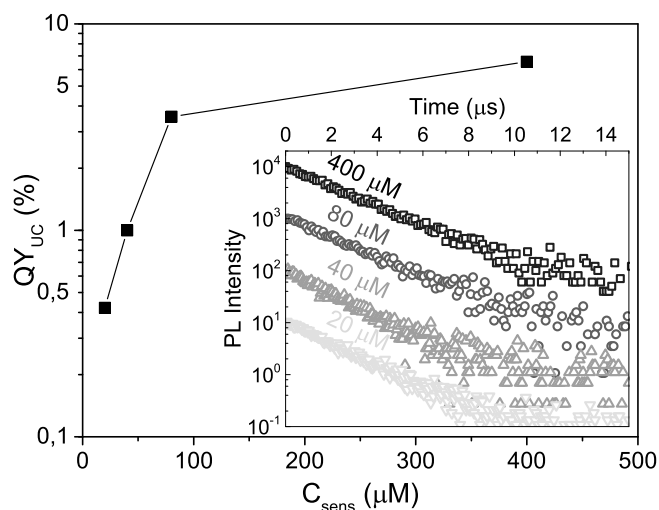
Figure 2.16 QY_{UC} measured for the second series of UCMs as function of c_{sens}. The inset shows the up-converted light decay at 435 nm for each sample of the series.

2.4.4 In-vitro fluorescence imaging

In order to demonstrate the applicative potential of our UCMs, and to verify their stability in biological media, we performed in vitro labeling of 3T3 murine fibroblast cells. First of all, we proved the absence of any cytotoxic effects induced by the UCMs by performing a

cell viability assessment by means of Live/Dead staining on cells labeled with increasing UCMs concentration. As visible in figure 2.17, the 1:50 dilution of the mother solution gave the best trade-off between good cell viability, without signs of stress and cell injuries, and UCMs concentration providing satisfactory fluorescence imaging. At this dilution, Kolliphor concentration in PBS is 0,026%, thus still above its cmc.
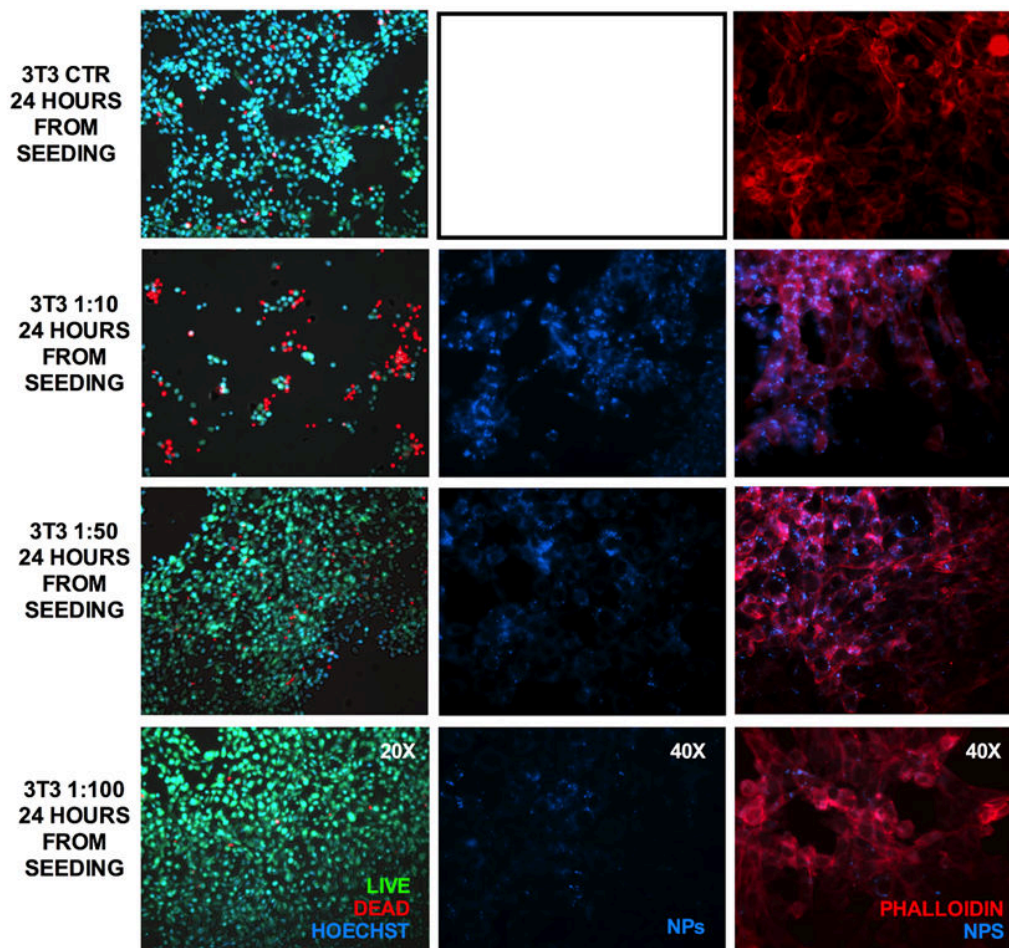
Figure 2.17 Cells viability assessment on 3T3 cells labeled with increasing UCMs concentration. The first row is the control, thus cells are not labeled. From 2 [nd] to 4 [th] row, the as prepared UCMs dispersion is used after 10 times dilution, 50 times dilution and 100 times dilution with PBS respectively. Left column: Live/Dead test results on 3T3 fibroblast stem cells stained with Hoechst. The green colour means the cells are alive, red means they are dead. Central column: fluorescence imaging of 3T3 cells stained with UCMs under UV excitation. Right column: fluorescence imaging of 3T3 cells stained with UCMs (blue) and phalloidin (red) under UV excitation.

Accordingly, we tested this concentration for further experiments aimed at evaluating the UCMs cytocompatibility throughout the time. One of the most frequently reported nanoparticle-associated toxicities is the generation of reactive oxygen species (ROS). ROS are chemically reactive compounds that are formed as a by-product of the cellular oxygen metabolism. However, environmental stress factors such as exposure to intense light or excessive heating, common consequences of a prolonged irradiation in diagnostic circumstances, can boost the intracellular ROS concentration to cytotoxic levels, causing damage to cell structures and possible cell death.[74] Moreover, oxidative stress induced by the staining with nano-objects can cause further pathophysiological effects including genotoxicity, inflammation, and fibrosis as demonstrated by activation of associated cell

signaling pathways.[75] Since oxidative stress is a key determinant of UCMs-induced injury, it is necessary to characterize the ROS response resulting from the labeling. Cell Titer-Glo viability and ROS evolution assessments have been performed on labeled 3T3 cells throughout 72 h. Figure 2.18 show the result of the viability and ROS tests, respectively. Although the CellTiter-Glo shows a slower proliferation rate for the UCMs labeled cells compared to the unlabeled control sample, the overall labeled cell viability has been maintained constant through the experiment course. At the same time, the amount of ROS released from labeled 3T3 cells has been kept on physiological levels, since the ROS production test did not display differences between control and stained samples, confirming the highly biocompatible composition of the UCMs.
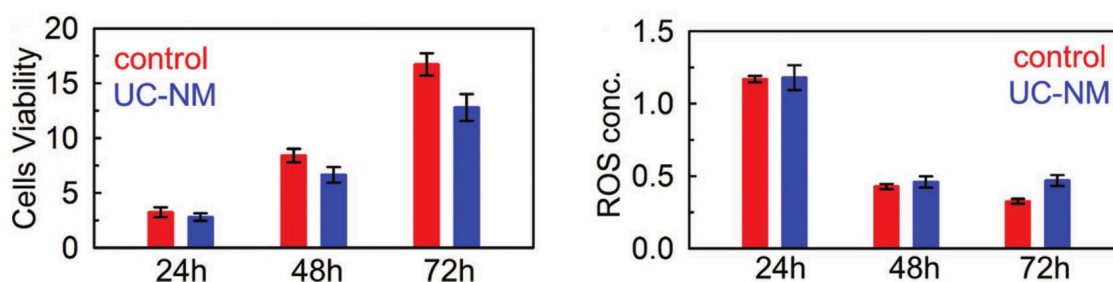
Figure 2.18 Cell Titer-Glo viability test (left) and ROS test (right) on 3T3 cells stained with UCMs at 1:50 dilution of the mother solution, monitored at three time points (24 h, 48 h, and 72 h)

Finally, we proceeded to acquire fluorescence confocal microscope images of paraformaldehyde fixed 3T3 cells stained with UCMs (blue) and phalloidin positive F actin (red) using a green laser excitation at 532 nm. As shown in figure 2.19, the blue UC light is generated in the cytoplasm region mostly around the cell nucleus, as expected for dyes not functionalized with target-specific ligands. In contrast, the phalloidin is a well-known standard dye employed for the specific staining of the cytoskeleton. Therefore, thanks to the overlay of the blue and red channels of the optical detector, we are able to record a nice, high-contrast, dual-channel image of the 3T3 cells by using the same excitation source. This colocalization staining clearly shows that the UCMs are effectively internalized by the 3T3 cells, leading to a perinuclear localization and confirming their good stability in the biological medium.

Figure 2.19 Confocal fluorescence image of 3T3 cell stained with UCMs (blue) and phalloidin positive F actin (red) under laser excitation at 532 nm.

2.5 Conclusions

We developed an exceedingly easy protocol to prepare up-converting micelles in water, which show efficient sensitized up-conversion emission at low excitation power. The procedure is general, and can ideall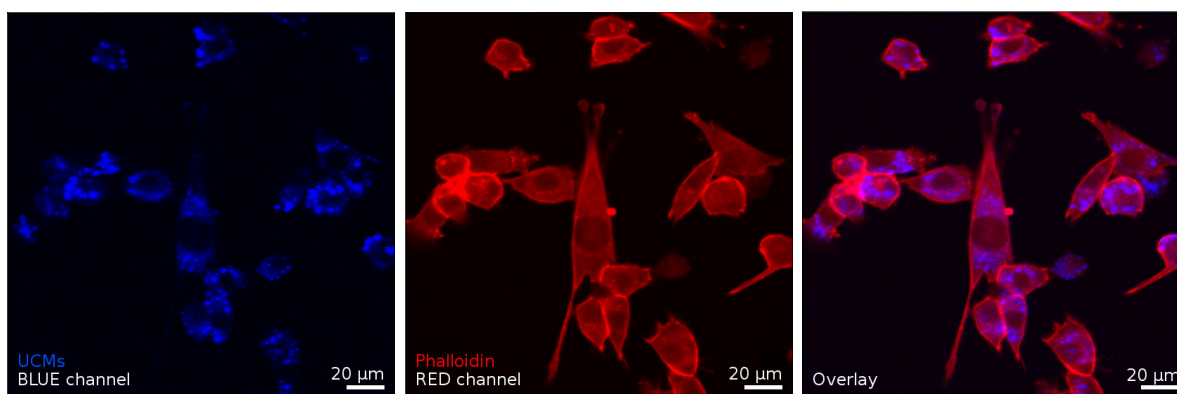y be extended to other organic species. Micelles demonstrated to be suitable systems to perform TTA-UC, as they provide a liquid-like environment which inhibits crystallization of the dyes, at the same time keeping them close enough to explore energy transfer processes. Thanks to a deep analysis of their optical properties, we have been able to optimize UCMs efficiency, which reaches 6,5% in water under oxygenated atmosphere. The stability of these anti-Stokes emitters in the biological medium, in conjunction with suitable biocompatibility, enabled us to obtain a multichannel, high-contrast optical imaging of 3T3 cells using a single excitation wavelength.

To our knowledge, this is the first example of efficient bi-component up-converters prepared through such a simple formulation approach employing biocompatible materials approved by the international authority. Importantly, these results are promising in the perspective of UCMs applicability as optically active systems for advanced theranostic applications. As TTA-UC and the corresponding signal would be lost in the case of UCMs collapsing, this optical feedback could be used to image the controlled release of water-insoluble additional payloads embedded within the micelles.

2.6 Experimental

1,2-propanediol and KH_2PO_4 were purchased from Merck. Na_2HPO_4 was purchased from Alfa Aesar. Deionized water was purchased from Carlo Erba. All the others starting materials were purchased from Sigma-Aldrich. All materials and solvents were used as received.

Synthesis of up-converting micelles (UCMs)

PtOEP (0,30 mg, 0,41 μmol) and DPA (13,50 mg, 40,9 μmol) are dissolved in 10 mL of THF (concentration of the sensitizer $\sim$ 40 μM). 2 mL of this solution are poured in a roundbottom flask, and 0,2 mL of a 1,2-propanediol/Kolliphor EL mixture (3:10 vol/vol, $\sim$ 220 mg) are added. The obtained solution was sonicated for 30 min in a SONICA 3200 EP ultrasonic cleaner, then THF was removed under reduced pressure and the oily residue was taken up either with 15 mL of deionized water or PBS solution.

To synthesize UCM dispersions with a different sensitizer concentration, the same protocol is followed, dissolving different amounts of PtOEP in the starting THF solution.

Concentration 20 μM PtOEP (0,30 mg, 0,41 μmol) and DPA (27,00 mg, 81,8 μmol) are dissolved in 20 mL of THF.

Concentration 80 μM PtOEP (0,60 mg, 0,82 μmol) and DPA (13,50 mg, 40,9 μmol) are dissolved in 10 mL of THF.

Concentration 400 μM PtOEP (3,00 mg, 4,12 μmol) and DPA (13,50 mg, 40,9 μmol) are dissolved in 10 mL of THF.

Preparation of PBS solution

PBS solution was prepared dissolving 80 g of NaCl, 14,4 g of Na_2HPO_4, 2,4 g of KH_2PO_4, and 2 g of KCl in 1 L of deionized water, and diluting 10 times before use.

DLS characterization

Dynamic Light Scattering experiments were performed on a 90Plus Particle Size Analyzer (Brookhaven Instruments Corporation) with scattering angles of 15° and 90°, equipped with a 35 mW solid state 632,8 nm laser and a Brookhaven's TuboCorr correlator with 510 channels. Measurements were run at 20 °C, allowing Zetasizer software to optimize both measurement position and attenuator, choosing water as dispersant. Three consecutive measurements have been run on each sample, and mediated to obtain the final intensity distribution. Measurements were run on 1 mL of freshly prepared UCMs dispersion in a disposable cuvette.

Cryo-EM structural analyses

Cryo-EM analyses were performed by R. Marotta at Istituto Italiano di Tecnologia in Genova.

UCMs, once applied in thin film on glow discharged holey TEM grids, were plunge frozen in liquid ethane cooled at liquid nitrogen temperature using a FEI Vitrobot Mark IV semi-automated cryoplunger. Cryo-EM projection images and single-axis tilt series were recorded in low dose using an FEI Tecnai G2 F20 Schottky field emission gun transmission electron microscope, equipped with automated cryobox, and a Gatan Ultrascan 2kx2k CCD (Charge-Coupled Device) detector. The tilt series were acquired from $\pm 60°$ with a tilt angle of $2°$ at a magnification of 29000 times (pixel size of 0,39 nm) with a total electron dose between 60 and 80 $e^- \text{\AA}^{-2}s^{-1}$. Cryoelectron tomograms were calculated and filtered using Imod 3.8.40 (Mastronarde 1997). The 3D model was obtained using Amira software (FEI Visualization Group).

Photophysical characterization

Absorption spectra were recorded with a Cary 50 spectrometer in the normal incidence condition using quartz Suprasil cuvettes.

All the other characterizations were performed by J. Pedrini and A. Monguzzi at Dipartimento di Scienza dei Materiali, Università degli Studi Milano-Bicocca (Milano).

Photoluminescence spectroscopy measurements

CW PL (Continuous Wave Photoluminescence) signals were recorded by a nitrogen cooled CCD coupled with a double monochromator Triax-190 (Horiba Jobin-Yvon), with a spectral resolution of 0,5 nm. The recorded spectra were corrected for the setup optical response. The excitation intensity threshold was measured by modulating the power of a CW 532 nm doubled Nd:YAG laser Coherent Verdi V10. The excitation laser beam is Gaussian shaped, and the spot diameter containing 90% of the intensity was 340 µm. Shape and spot size were measured by the knife-edge method.

ϕ_{ET} measurements

The sensitizer-to-emitter ET efficiency ϕ_{ET} has been calculated from the measurements of the sensitizer residual PL in presence (I) and in absence (I_0) of the emitter as[76]

$$\phi_{ET} = 1 - \frac{I}{I_0}$$

QY_{UC} measurements

The up-conversion luminescence quantum efficiency of UCMs was determined by comparison with a DPA-PtOEP UC pair in deaerated tetrahydrofuran ([DPA] = 10 mM, [PtOEP] = 100 µM) used as secondary standard, according to[16]

$$QY_{UC} = QY_{std}\frac{A_{std}}{A_{UC}}\frac{I_{UC}}{I_{std}}\frac{P_{std}}{P_{UC}}\left(\frac{\eta_{std}}{\eta_{UC}}\right)^2$$

where QY, A, I, P and η represent quantum yield, absorptance at excitation intensity, integrated photoluminescence spectral profile, excitation power density, and refractive index of the medium. The subscripts "*std*" and "*UC*" indicate the reference and the sample, respectively. The UC quantum yield of the secondary standard is 0,24 at its maximum. The recorded spectra have been corrected for the setup optical response. The refraction indexes at 293 K are 1,41 for tetrahydrofuran and 1,33 for water. The secondary standard solution is freshly prepared and characterized before each run of measurements. The samples have been measured in a 1 mm optical path cuvette. The used setup works in a collinear geometry, which is insensitive to the position in which the photoluminescence is generated, enabling to compare also samples with different absorbance without incurring in trivial errors.

Time resolved PL measurements

The 532 nm laser was modulated with a TTi TG5011 wavefunctions generator, with a time resolution better than 0,1 µs (5 ns pulse width). Time resolved PL spectra were detected in photon-counting mode using an ORTEC digital multichannel scaler, with a temporal resolution of 0,1 ns.

Cells-related characterization

All the following characterizations were performed by C. Villa and Y. Torrente at Dipartimento di Fisiopatologia Medico-Chirurgica e dei Trapianti, Università degli Studi di Milano, Fondazione IRCCS Ca' Granda Ospedale Maggiore Policlinico, Centro Dino Ferrari (Milano).

Cells culture and staining protocols

3T3 cells (ATCC CRL-1658) were thawed and plated on cell culture dish in DMEM high glucose (Gibco) supplemented with 10% FBS (Fetal Bovine Serum, Euroclone) for 48 h before use. For immunofluorescence experiments, 3T3 cells were detached with 0,25% Trypsin (Gibco), resuspended in complete medium and plated in 12-well plates at a density of 5×104 cells per well. After 24 h from seeding, UCMs were added to the cells at different concentrations of the mother solution (1:10, 1:50, and 1:100). 24 h after labeling, cell viability was assessed by performing live dead fluorescent assay (Thermo Fisher), in accordance with protocol by manufacturer. Briefly, Calcein-AM (green-Live) and ethidium homodimer-1 (red-Death) were diluted 1:1000 in complete medium and incubated for 30 min at 37 °C. Cells were then washed twice with PBS (1×, Gibco) and visualized with an

inverted fluorescent microscope (Leica). 1:2000 Hoechst counter staining was performed for nuclei visualization. In order to visualize UCMs uptake within cells, actin cytoskeleton was labeled with phalloidin tetramethylrhodamine B isothiocyanate (TRITC). 3T3 cells were washed with PBS, fixed with 4% formaldehyde solution for 4 min, washed twice, and permeabilized by 0,1% Triton X-100 in PBS. After washing in PBS, cells were incubated for 30 min with 50 $\mu g\,mL^{-1}$ fluorescent phalloidin conjugated solution; afterward they were extensively washed before visualization. Unlabeled cells were used as control. Since labeling with UCMs 1:50 dilution allowed to maintain both a good cell viability and a high number of detectable nanoparticles, further experiments considered 1:50 diluted UCMs labeled 3T3 cells throughout time (24, 48, 72 h after labeling).

Cells viability and ROS test

For proliferation experiments, cells were seeded in a 96 well plate at 3×10^3 cells per well density in triplicate (n = 3 wells for each time point). Evaluation of ROS production from cells was performed 24, 48, and 72 h after 1:50 UCMs labeling. ROS-Glo H2O2 Assay (Promega) was used, following the producer protocol. Cells treated with 50 μM menadione were considered as positive control, while growth medium were reported as negative control. The nonlytic protocol was applied for proceeding with additional evaluations on the same cells assessed for ROS production. Specifically, the Cell Titer-Glo viability assay (Promega) was performed following the datasheet instruction. The CellTiter-Glo 3D Cell viability assay is a homogeneous method to determine the number of viable cells based on quantitation of the ATP (Adenosine Triphosphate) present, which is a marker for the presence of metabolically active cells. For both ROS and cell titer glow assays, relative luminescence units were measured by a plate reader (GloMax Discover, Promega).

Confocal fluorescence imaging

Images of UCMs/phalloidin stained 3T3 cells were acquired with a Nikon C1 confocal microscope coupled with the 532 nm laser focused on the sample with a 60× (1,4 NA) immersion oil objective. The spot size in this configuration is 460 nm. The fluorescence intensity was filtered with blue- and red-pass dichroic mirrors and detected with two photomultiplier tubes with independent gain, in order to record the UCMs up-converted blue luminescence and the phalloidin red fluorescence, respectively.

Bibliography

[1] Zhu, X., Su, Q., Feng, W., and Li, F. *Chem. Soc. Rev.* **2017**, *46*, 1025–1039. doi: 10.1039/C6CS00415F.

[2] Chen, X., Peng, D., Ju, Q., and Wang, F. *Chem. Soc. Rev.* **2014**, *44*, 1318–1330. doi: 10.1039/c4cs00151f.

[3] Auzel, F. *Chem. Rev.* **2004**, *104*, 139–174. doi: 10.1021/cr020357g.

[4] Chen, X., Liu, Y., and Tu, D. *Lanthanide-Doped Luminescent Nanomaterials.* Springer-Verlag Press, Berlin, **2014**. ISBN 978-3-642-40363-7.

[5] Zheng, W., Huang, P., Tu, D., Ma, E., Zhu, H., and Chen, X. *Chem. Soc. Rev.* **2015**, *44*, 1379–1415. doi: 10.1039/C4CS00178H.

[6] Yanai, N. and Kimizuka, N. *Acc. Chem. Res.* **2017**, *50*, 2487–2495. doi: 10.1021/acs.accounts.7b00235.

[7] Amemori, S., Sasaki, Y., Yanai, N., and Kimizuka, N. *J. Am. Chem. Soc.* **2016**, *138*, 8702–8705. doi: 10.1021/jacs.6b04692.

[8] Yang, Z., Mao, Z., Xie, Z., Zhang, Y., Liu, S., Zhao, J., Xu, J., Chi, Z., and Aldred, M. P. *Chem. Soc. Rev.* **2017**, *46*, 915–1016. doi: 10.1039/C6CS00368K.

[9] Mase, K., Okumura, K., Yanai, N., and Kimizuka, N. *Chem. Commun.* **2017**, *53*, 8261–8264. doi: 10.1039/C7CC03087H.

[10] Sternlicht, H., Nieman, G. C., and Robinson, G. W. *J. Chem. Phys.* **1963**, *38*, 1326–1335. doi: 10.1063/1.1733853.

[11] Singh-Rachford, T. N. and Castellano, F. N. *Coord. Chem. Rev.* **2010**, *254*, 2560–2573. doi: 10.1016/j.ccr.2010.01.003.

[12] Parker, C. A. and Hatchard, C. G. *Proc. Chem. Soc.* **1962**, *0*, 133–147. doi: 10.1039/PS9620000133.

[13] Monguzzi, A., Mézyk, J., Scotognella, F., Tubino, R., and Meinardi, F. *Phys. Rev. B* **2008**, *78*, 195112. doi: 10.1103/PhysRevB.78.195112.

[14] Auckett, J. E., Chen, Y. Y., Khoury, T., Clady, R. G. C. R., Ekins-Daukes, N. J., Crossley, M. J., and Schmidt, T. W. *J. Phys. Conf. Ser.* **2009**, *185*, 012002. doi: 10.1088/1742-6596/185/1/012002.

[15] Haefele, A., Blumhoff, J., Khnayzer, R. S., and Castellano, F. N. *J. Phys. Chem. Lett.* **2012**, *3*, 299–303. doi: 10.1021/jz300012u.

[16] Monguzzi, A., Tubino, R., Hoseinkhani, S., Campione, M., and Meinardi, F. *Phys. Chem. Chem. Phys.* **2012**, *14*, 4322–4332. doi: 10.1039/C2CP23900K.

[17] McLean, A. J. and Truscott, T. G. *J. Chem. Soc., Faraday Trans.* **1990**, *86*, 2671–2672. doi: 10.1039/FT9908602671.

[18] Ekins-Daukes, N. J. and Schmidt, T. W. *Appl. Phys. Lett.* **2008**, *93*, 063507. doi: 10.1063/1.2970157.

[19] Cheng, Y. Y., Khoury, T., Clady, R. G. C. R., Tayebjee, M. J. Y., Ekins-Daukes, N. J., Crossley, M. J., and Schmidt, T. W. *Phys. Chem. Chem. Phys.* **2010**, *12*, 66–71. doi: 10.1039/B913243K.

[20] Gray, V., Dzebo, D., Abrahamsson, M., Albinsson, B., and Moth-Poulsen, K. *Phys. Chem. Chem. Phys.* **2014**, *16*, 10345–10352. doi: 10.1039/C4CP00744A.

[21] Cheng, Y. Y., Fückel, B., Khoury, T., Clady, R. G. C. R., Tayebjee, M. J. Y., Ekins-Daukes, N. J., Crossley, M. J., and Schmidt, T. W. *J. Phys. Chem. Lett.* **2010**, *1*, 1795–1799. doi: 10.1021/jz100566u.

[22] Zhong, F. and Zhao, J. *Eur. J. Inorg. Chem.* **2017**, *2017*, 5196–5204. doi: 10.1002/ejic.201700656.

[23] Zhou, J., Liu, Q., Feng, W., Sun, Y., and Li, F. *Chem. Rev.* **2015**, *115*, 395–465. doi: 10.1021/cr400478f.

[24] Brehm, J. and Mullin, W. *Introduction to the structure of matter: a course in modern physics.* Wiley, New York, **1989**. ISBN 978-0-471-60531-7.

[25] Chi, Y. and Chou, P.-T. *Chem. Soc. Rev.* **2010**, *39*, 638–655. doi: 10.1039/B916237B.

[26] Zhao, J., Wu, W., Sun, J., and Guo, S. *Chem. Soc. Rev.* **2013**, *42*, 5323–5351. doi: 10.1039/C3CS35531D.

[27] McCusker, C. E. and Castellano, F. N. *Inorg. Chem.* **2015**, *54*, 6035–6042. doi: 10.1021/acs.inorgchem.5b00907.

[28] Gorman, A., Killoran, J., O'Shea, C., Kenna, T., Gallagher, W. M., and O'Shea, D. F. *J. Am. Chem. Soc.* **2004**, *126*, 10619–10631. doi: 10.1021/ja047649e.

[29] Kamkaew, A., Lim, S. H., Lee, H. B., Kiew, L. V., Chung, L. Y., and Burgess, K. *Chem. Soc. Rev.* **2013**, *42*, 77–88. doi: 10.1039/C2CS35216H.

[30] Huang, L., Yu, X., Wu, W., and Zhao, J. *Org. Lett.* **2012**, *14*, 2594–2597. doi: 10.1021/ol3008843.

[31] Liu, Y. and Zhao, J. *Chem. Commun.* **2012**, *48*, 3751–3753. doi: 10.1039/C2CC30345K.

[32] Specht, D. P., Martic, P. A., and Farid, S. *Tetrahedron* **1982**, *38*, 1203–1211. doi: 10.1016/0040-4020(82)85104-1.

[33] Singh-Rachford, T. N., Haefele, A., Ziessel, R., and Castellano, F. N. *J. Am. Chem. Soc.* **2008**, *130*, 16164–16165. doi: 10.1021/ja807056a.

[34] Wu, T. C., Congreve, D. N., and Baldo, M. A. *Appl. Phys. Lett.* **2015**, *107*, 031103. doi: 10.1063/1.4926914.

[35] Peng, J., Guo, X., Jiang, X., Zhao, D., and Ma, Y. *Chem. Sci.* **2016**, *7*, 1233–1237. doi: 10.1039/C5SC03245H.

[36] Singh-Rachford, T. N., Nayak, A., Muro-Small, M. L., Goeb, S., Therien, M. J., and Castellano, F. N. *J. Am. Chem. Soc.* **2010**, *132*, 14203–14211. doi: 10.1021/ja105510k.

[37] Kozlov, D. V. and Castellano, F. N. *Chem. Commun.* **2004**, *24*, 2860–2861. doi: 10.1039/B412681E.

[38] Baluschev, S., Keivanidis, P. E., Wegner, G., Jacob, J., Grimsdale, A. C., Müllen, K., Miteva, T., Yasuda, A., and Nelles, G. *Appl. Phys. Lett.* **2005**, *86*, 061904. doi: 10.1063/1.1857073.

[39] Boutin, P. C., Ghiggino, K. P., Kelly, T. L., and Steer, R. P. *J. Phys. Chem. Lett.* **2013**, *4*, 4113–4118. doi: 10.1021/jz402311j.

[40] Baluschev, S., Miteva, T., Yakutkin, V., Nelles, G., Yasuda, A., and Wegner, G. *Phys. Rev. Lett.* **2006**, *97*, 7–9. doi: 10.1103/PhysRevLett.97.143903.

[41] Baluschev, S., Yakutkin, V., Miteva, T., Avlasevich, Y., Chernov, S., Aleshchenkov, S., Nelles, G., Cheprakov, A., Yasuda, A., Müllen, K., and Wegner, G. *Angew. Chem., Int. Ed.* **2007**, *46*, 7693–7696. doi: 10.1002/anie.200700414.

[42] Monguzzi, A., Borisov, S. M., Pedrini, J., Klimant, I., Salvalaggio, M., Biagini, P., Melchiorre, F., Lelii, C., and Meinardi, F. *Adv. Funct. Mater.* **2015**, *25*, 5617–5624. doi: 10.1002/adfm.201502507.

[43] Wilson, B. C. *Can. J. Gastroenterol.* **2002**, *16*, 393–396. doi: 10.1155/2002/743109.

[44] Dolmans, D. E., Fukumura, D., and Jain, R. K. *Nat. Rev. Cancer* **2003**, *3*, 380–387. doi: 10.1038/nrc1071.

[45] Borisov, S. M., Larndorfer, C., and Klimant, I. *Adv. Funct. Mater.* **2012**, *22*, 4360–4368. doi: 10.1002/adfm.201200794.

[46] Monguzzi, A., Tubino, R., and Meinardi, F. *Phys. Rev. B* **2008**, *77*, 155122. doi: 10.1103/PhysRevB.77.155122.

[47] Varghese, S. and Das, S. *J. Phys. Chem. Lett.* **2011**, *2*, 863–873. doi: 10.1021/jz200099p.

[48] Briggs, J. A., Atre, A. C., and Dionne, J. A. *J. Appl. Phys.* **2013**, *113*, 124509. doi: 10.1063/1.4796092.

[49] Li, C., Koenigsmann, C., Deng, F., Hagstrom, A., Schmuttenmaer, C. A., and Kim, J.-H. *ACS Photonics* **2016**, *3*, 784–790. doi: 10.1021/acsphotonics.5b00694.

[50] Zhang, Y. and Forrest, S. R. *Phys. Rev. Lett.* **2012**, *108*, 267404. doi: 10.1103/PhysRevLett.108.267404.

[51] Wallikewitz, B. H., Kabra, D., Gélinas, S., and Friend, R. H. *Phys. Rev. B* **2012**, *85*, 045209. doi: 10.1103/PhysRevB.85.045209.

[52] Wohnhaas, C., Turshatov, A., Mailänder, V., Lorenz, S., Baluschev, S., Miteva, T., and Landfester, K. *Macromol. Biosci.* **2011**, *11*, 772–778. doi: 10.1002/mabi.201000451.

[53] Simon, Y. C. and Weder, C. *J. Mater. Chem.* **2012**, *22*, 20817–20830. doi: 10.1039/c2jm33654e.

[54] Kim, J.-H. and Kim, J.-H. *J. Am. Chem. Soc.* **2012**, *134*, 17478–17481. doi: 10.1021/ja308789u.

[55] Khnayzer, R. S., Blumhoff, J., Harrington, J. A., Haefele, A., Deng, F., and Castellano, F. N. *Chem. Commun.* **2012**, *48*, 209–211. doi: 10.1039/C1CC16015J.

[56] Ye, C., Wang, J., Wang, X., Ding, P., Liang, Z., and Tao, X. *Phys. Chem. Chem. Phys.* **2016**, *18*, 3430–3437. doi: 10.1039/C5CP05288B.

[57] Jiang, Z., Xu, M., Li, F., and Yu, Y. *J. Am. Chem. Soc.* **2013**, *135*, 16446–16453. doi: 10.1021/ja406020r.

[58] Han, J., Duan, P., Li, X., and Liu, M. *J. Am. Chem. Soc.* **2017**, *139*, 9783–9786. doi: 10.1021/jacs.7b04611.

[59] Jankus, V., Snedden, E. W., Bright, D. W., Whittle, V. L., Williams, J. A. G., and Monkman, A. *Adv. Funct. Mater.* **2013**, *23*, 384–393. doi: 10.1002/adfm.201201284.

[60] Monguzzi, A., Frigoli, M., Larpent, C., Tubino, R., and Meinardi, F. *Adv. Funct. Mater.* **2012**, *22*, 139–143. doi: 10.1002/adfm.201101709.

[61] Liu, Q., Yin, B., Yang, T., Yang, Y., Shen, Z., Yao, P., and Li, F. *J. Am. Chem. Soc.* **2013**, *135*, 5029–5037.

[62] Gatti, T., Brambilla, L., Tommasini, M., Villafiorita-Monteleone, F., Botta, C., Sarritzu, V., Mura, A., Bongiovanni, G., and Del Zoppo, M. *J. Phys. Chem. C* **2015**, *119*, 17495–17501. doi: 10.1021/acs.jpcc.5b01909.

[63] Mahato, P., Monguzzi, A., Yanai, N., Yamada, T., and Kimizuka, N. *Nat. Mater.* **2015**, *14*, 924–930. doi: 10.1038/nmat4366.

[64] Ogawa, T., Yanai, N., Monguzzi, A., and Kimizuka, N. *Sci. Rep.* **2015**, *5*, 10882. doi: 10.1038/srep10882.

[65] Kouno, H., Ogawa, T., Amemori, S., Mahato, P., Yanai, N., and Kimizuka, N. *Chem. Sci.* **2016**, *7*, 5224–5229. doi: 10.1039/C6SC01047D.

[66] Duan, P., Yanai, N., and Kimizuka, N. *J. Am. Chem. Soc.* **2013**, *135*, 19056–19059. doi: 10.1021/ja411316s.

[67] Wohnhaas, C., Friedemann, K., Busko, D., Landfester, K., Baluschev, S., Crespy, D., and Turshatov, A. *ACS Macro Letters* **2013**, *2*, 446–450. doi: 10.1021/mz400100j.

[68] Sasaki, Y., Amemori, S., Kouno, H., Yanai, N., and Kimizuka, N. *J. Mater. Chem. C* **2017**, *5*, 5063–5067. doi: 10.1039/C7TC00827A.

[69] Svagan, A. J., Busko, D., Avlasevich, Y., Glasser, G., Baluschev, S., and Landfester, K. *ACS Nano* **2014**, *8*, 8198–8207. doi: 10.1021/nn502496a.

[70] Petros, R. A. and De Simone, J. M. *Nat. Rev. Drug Discov.* **2010**, *9*, 615–627. doi: 10.1038/nrd2591.

[71] Reintjes, T. (Editor). *Solubility Enhancement with BASF Pharma Polymers. Solubilizer Compendium.* BASF SE Pharma Ingredients & Services, 68623 Lampertheim, Germany, **2011**.

[72] http://products.basf.com/documents/pim;view/en/8805244447189.Kolliphor%C2% AE%20EL%20-%20Technical%20Information.pdf. Accessed 26-12-2017.

[73] Mongin, C., Golden, J. H., and Castellano, F. N. *ACS Appl. Mater. Interfaces* **2016**, *8*, 24038–24048. doi: 10.1021/acsami.6b05697.

[74] Tay, C. Y., Yu, Y., Setyawati, M. I., Xie, J., and Leong, D. T. *Nano Res.* **2014**, *7*, 805–815. doi: 10.1007/s12274-014-0441-z.

[75] Amruta, M., Liying, W., and Rojanasakul, Y. *Biomed. Res. Int.* **2013**, *2013*, 942916. doi: 10.1155/2013/942916.

[76] Inokuti, M. and Hirayama, F. *J. Chem. Phys.* **1965**, *43*, 1978–1989. doi: 10.1063/1.1697063.

Chapter 3

Micelles as nanoreactors

> *Once you're over the hill, you begin to pick up speed.*
>
> Charles M. Schulz

The work here described followed directly from the results obtained within the frame of up-converting micelles project described in Chapter 2 - in fact the surfactant we used is the same, Kolliphor® EL. In this case, we decided to take advantage of the newly discovered oxygen barrier property of Kolliphor to perform oxygen-sensitive Suzuki-Miyaura reactions in water. Micelles transform from photonic boxes into nanoreactors. As the test proved successful, we challenged Kolliphor in the synthesis of more complex structures, such as organic semiconductors, whose production is generally poorly sustainable.

The chapter begins with a brief introduction to Green Chemistry and micellar reactions as a green methodology to perform organic synthesis. Results on the use of Kolliphor® EL as surfactant in Suzuki-Miyaura micellar coupling will be subsequently reported.

3.1 Micellar reactions as Green Chemistry tools

3.1.1 A brief overview of Green Chemistry principles

The concept of Green Chemistry was born in 1991 with the launch of the Green Chemistry Program by the United States Environmental Protection Agency (EPA). Aim of the program was "to promote the research, development, and implementation of innovative chemical technologies that accomplish pollution prevention in both a scientifically sound and cost-effective manner".[1] Since then, Green Chemistry has become a powerful idea, which now appears in thousands of papers, and it is subject of teaching in universities, due to its ability to link environmental and economic goals simultaneously. One of the most important aspects of the program was the development of metrics, in order to change the idea that synthetic yield is the only parameter that describe the efficiency of a chemical process. In 1998, Anastas and Warner formulated twelve principles,[2] which purpose is "the design of chemical products and processes that reduce or eliminate the use or generation of hazardous substances".[1] As reporting their whole statements will end up in a (really not green) waste of paper, I will just cite their summarized acronym, PRODUCTIVELY:[3]

P -	Prevent wastes
R -	Renewable materials
O -	Omit derivatization steps
D -	Degradable chemical products
U -	Use safe synthetic methods
C -	Catalytic reagents
T -	Temperature, pressure ambient
I -	In-process monitoring
V -	Very few auxiliary substances
E -	E-factor, maximize feed in product
L -	Low toxicity of chemical product
Y -	Yes, it is safe

The point is very clear: the aim of Green Chemistry is to develop safe, non-polluting strategies to synthesize possibly non-toxic, degradable products with the minimum amount of waste necessary. Industrially speaking, application of these principles helps in reducing costs of production on various fronts: less waste, energy consuming processes, and hazards across all the life-cycle stages.[4]

Some explanation is maybe required about point E. The E(nvironmental)-factor is the metric defined as the ratio between the mass of waste produced for mass unit of product[5]

$$E = \frac{\text{Mass of waste (kg)}}{\text{Mass of product (kg)}}$$

It is worth to underline that any used recyclable material (solvents, catalysts, reused reactants) is not considered waste, so it does not contribute to the E-factor, while auxiliary materials, including those used in work-up or purification steps, are taken into account.[6] Other metrics are Atom Economy, Reaction Mass Efficiency and Process Mass Intensity,[5] but their description is out of the scope of this work, and they will not be discussed further.
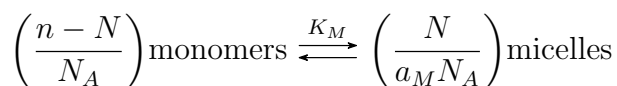
3.1.2 Principles of micellar reactions

From the point of view of the methods, micellar reactions are considered quite a green methodology:[7, 8] the use of water (and soap) in place of an organic solvent to conduct a reaction hits points P, R, U, T, V and E of the PRODUCTIVELY principles. In fact, solvents often account for the vast majority of mass wasted in syntheses and processes, while water is a safe, renewable, and recyclable material.[4]

However, micellar catalysis was known well before the birth of Green Chemistry: the first systematic studies on the effects of micelles on the rate and equilibrium constants of chemical reactions appeared during the 1960s,[9–12] and the field attracted more and more interest during subsequent years (see, for example, [13]). A consistent model able to explain the variety of effects observable in a chemical reaction in presence of a micellar environment does not exist, as it would fall into a molecular description not only of the reaction mechanism (which is already a complicated matter), but also of the surfactant structure, and the surfactant-reactant(s) complex formation and binding. Nonetheless, some simplified models have been developed to quantify the effect of micelles in enhancing or inhibiting organic reactions, the most popular relying on the pseudophase model.[13–16]

As mentioned in the Introduction, micelles cannot be described as an entirely new phase with respect to the aqueous environment, thus they usually refer to them as a *pseudophase*. The main characteristics of this pseudophase can be summarized as
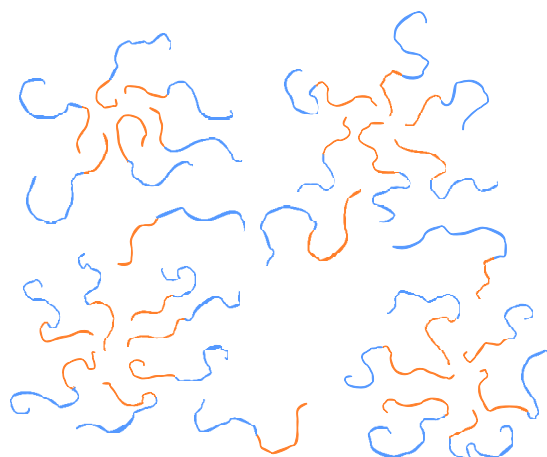

Cartoon of a micellar pseudophase.

1. micelles and bulk aqueous solvents are regarded as distinct regions;

2. an equilibrium between the free monomeric surfactant and the associative colloid exists, described by

$$\left(\frac{n-N}{N_A}\right) \text{monomers} \xrightleftharpoons{K_M} \left(\frac{N}{a_M N_A}\right) \text{micelles}$$

where n represents the total number of surfactant molecules, N is the total number of surfactant molecules used up in the formation of micelles, a_M is the mean aggregation number of a micelle, N_A is Avogadro's number and K_M is the equilibrium constant for the formation of the micelle.

Moving from the description of an associative colloid to that of a nanoreactor means that reactants must be taken into account in the description of the system. This could look like quite a complicated step, but for simple unimolecular or bimolecular reactions it can be done easily under a series of assumptions:

1. substrate does not perturb micellization;

2. the rates of formation and disintegration of micelle are independent of the corresponding rates of micellar intake and exit of a solubilizate;

3. solubilization of the substrate in micelle is way faster than its reaction rate in water;

4. equilibrium constants for micellar incorporation of different solubilizates are independent one from each other;

5. for a bimolecular reaction, the reaction between a reactant in the micellar pseudophase and the other reactant in the aqueous pseudophase does not occur;

6. micellar effects on reaction rates are insensitive to changes in shape and size of micelle

On these bases, simple models for the calculations of reaction rates have been built, such as Berezin's model,[17] which demonstrated to be predictive. Even if we are not interested in kinetic aspects of the synthesis, it is worth to underline particularly the importance of statement 5. Experimental observations suggest that micellar pseudophase is not homogeneous in terms of micropolarity, water concentration, dielectric constant, and ionic strength (for ionic surfactants). To overcome this problem, Davies[18] suggested that the micellar pseudophase should be divided up into an arbitrary number of pseudophases. This might be especially true for nonionic surfactants, whose PEG-ylated chains are likely to behave very differently from both surrounding water and the apolar compartment. Statement 5, in this case, might be generalized to "reaction between reactants solubilized in different micellar pseudophases does not occur".
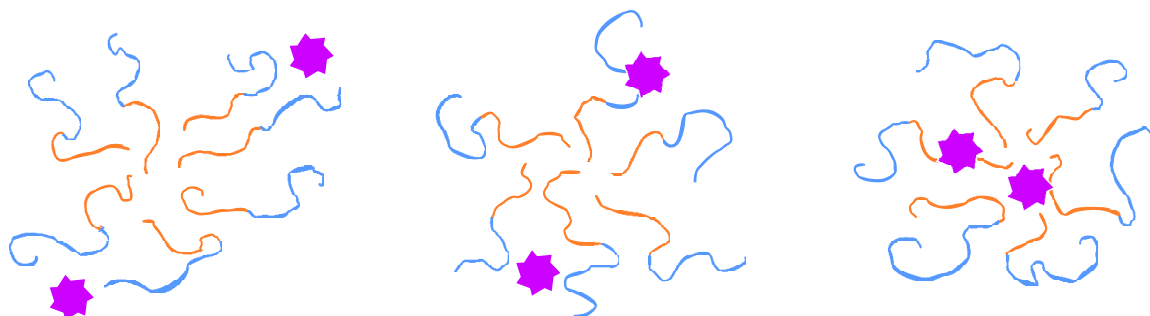
Cartoon showing possible localization sites for a solubilizate (depicted as a violet star) in a micelle: at surface (left), in the palisade layer (center), in the apolar core (right).

3.1.3   A variety of micellar reactions

Early reports on the study of micellar dispersions as media in organic synthesis mainly focused on hydrolyses and nucleophilic substitution reactions.[11–13, 19] Aim of the new-born research field was to understand mechanisms of micellar enhancement or inhibition of the reactions, not the synthesis of new molecules, and these kind of simple reactions were perfect for the purpose. The desire to apply the method on an industrial level followed soon, and reports on hydroformilation reactions in micellar environment started appearing during 1980s.[20] Today, the pool of synthetic routes working in micellar conditions is quite impressive. Developed C−C coupling reactions include Michael additions,[21] aldol[22, 23] and Diels-Alder[24] reactions, Fujiwara–Moritani, Heck, Suzuki-Miyaura, Stille and Sonogashira couplings.[25–28] Negishi[29] coupling has proven possible too, despite the incompatibility of organozinc reactants with water. C−heteroatom couplings are also

possible, such as Buchwald-Hartwig amination or Miyaura borylation.[26, 27] Many differ-
ent cyclization reactions have been performed in micellar environment, also giving het-
erocycles or spyro-unit containing products.[27, 28, 30, 31] Oxidation[32–35] and reduction[36–38]
reactions have been studied as well. Halogenation of electron-rich substrates has been
demonstrated.[31, 39] Examples of photochemical reactions in micelles are also known.[15, 40]
Examples of the cited reactions are given in figure 3.1.
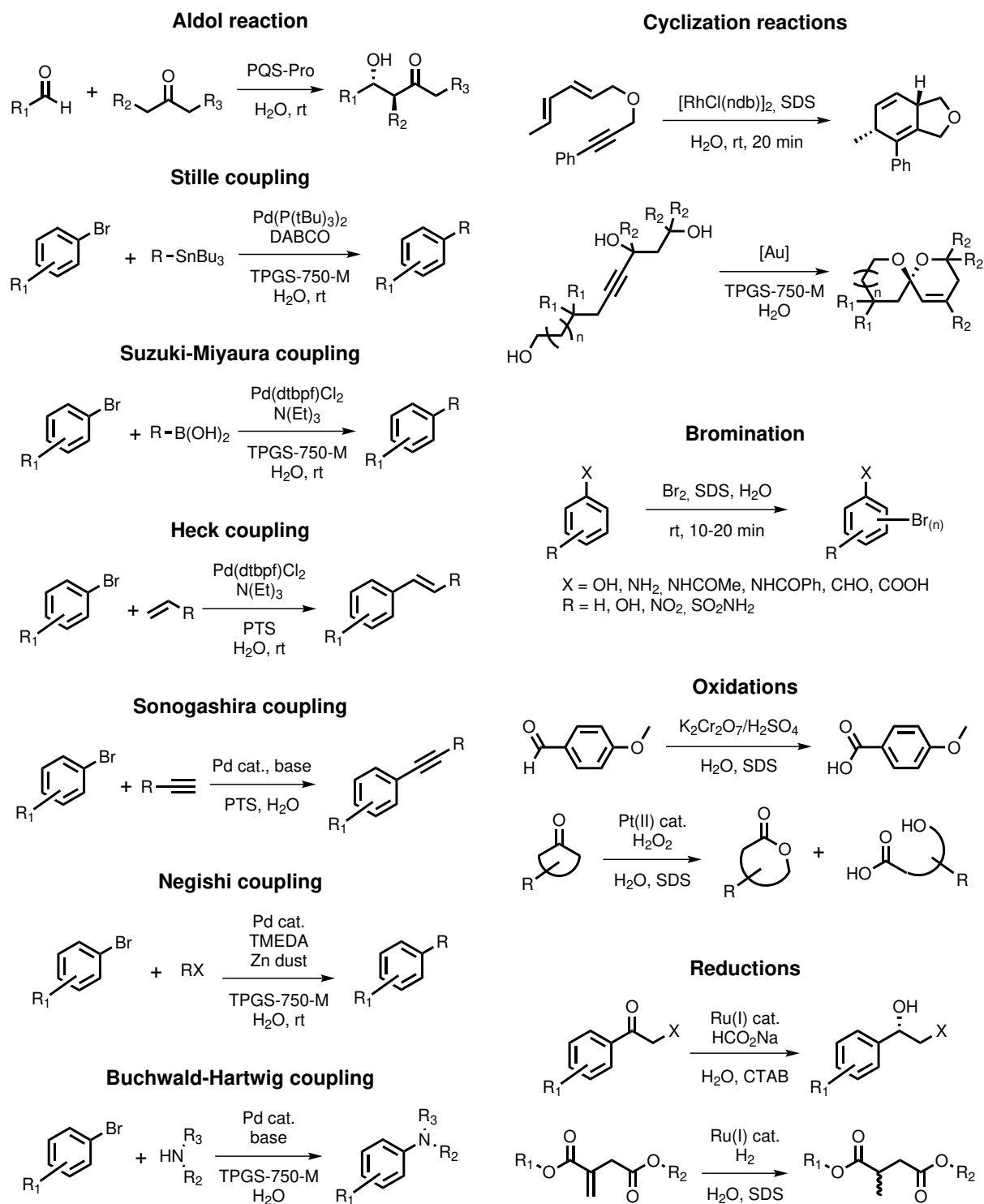
Figure 3.1 Examples of reactions carried out in micellar conditions.

3.2   Aim of the work

From the discovery of organic semiconductors, the big promise of Organic Electronic has been the possibility to create thin, flexible, printable, cheap devices.[41] OLED finally come to the market, but this is still not true for organic transistors or solar cells. There are several reasons for this, mainly not related to materials efficiencies. An important one, is that synthetic methodologies commonly applied in a chemistry laboratory are not sustainable on an industrial scale.[42–44]

Among the most used reactions to synthesize organic semiconductors there are coupling reactions, such as Stille or Suzuki-Miyaura. Although these couplings have been reported in micellar conditions, they have never been attempted specifically for the synthesis of organic semiconductors. The passage is not trivial, as organic semiconductors are usually heavily functionalized molecules, which structure can interfere with surfactant micellization. Aim of this project was therefore the synthesis of small molecule semiconductors using Suzuki-Miyaura coupling via micellar protocol.

As the catalyst in Suzuki coupling is an air-sensitive palladium complex, we decided to take advantage of the newly discovered oxygen-barrier property of Kolliphor® EL to develop Suzuki coupling in standard aerated atmosphere. We therefore started proving this point on simple substrates, and followed applying the protocol to the synthesis of small molecule semiconductors.

3.3   State of the art for the Suzuki-Miyaura coupling

Suzuki-Miyaura coupling was firstly reported in 1979 by Akira Suzuki and Norio Miyaura,[46] his inventor being awarded by the 2010 Nobel Prize in Chemistry for the discovery. It is a coupling reaction, the coupling partners being a boronic acid/ester and an organohalide, catalyzed by a palladium(0) complex. Figure 3.2 shows mechanism of the reaction. The first step is the oxidative addition of the catalyst to the halide to give a organopalladium species. Reaction of this intermediate with a base gives the species which reacts through transmetalation with the boronate, giving a new organopalladium species. Finally, reductive elimination of the desired product restores the catalyst.

Figure 3.2 Reaction mechanism of Suzuki-Miyaura coupling[45]

Suzuki-Miyaura coupling is a kind of reaction that strongly beneficiates from application of Green Chemistry principles: for example, development of protocols allowing elimination of organic solvents may decrease the E-factor of a reaction by an order of magnitude.[7, 27] From its discovery, a lot has been done to increase the reaction scope and sustainability. Nickel,[47] copper,[48] iron[49, 50] and ruthenium[51] have been demonstrated to be suitable as metal catalysts. Amides have
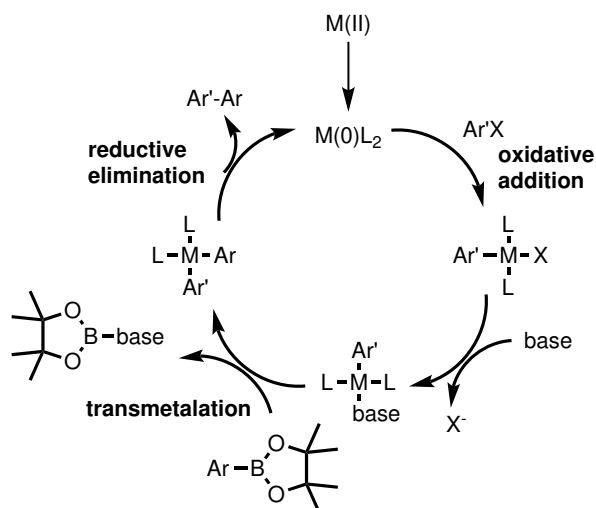
been reported as suitable coupling substrates instead of halides, despite their greater inertness.[52] Green solvents, such as PEG,[53] glycerol,[54] supercritical CO_2[55] and water,[56] can be used to carry out the reaction.

Although several groups reported Suzuki coupling in micellar conditions,[57–59] the most intense research in the field has been performed by Lipshutz and co-workers. Beyond research on catalyst optimization,[50, 60] they gained much credit from the development of designer surfactants specifically for coupling reactions,[26, 61, 62] which are now available on the market and provide green environments not only for Suzuki-Miyaura, but also for Stille, Buchwald−Hartwig, Heck, and Sonogashira couplings, and cross- and ring-closing-metathesis reactions. These surfactants are benign by construction, as they are obtained coupling a natural lipophilic compound (vitamin-E or β-sitosterol) with a PEG-ylated long chain (in appropriate doses, PEG is not considered harmful for human health, and it is approved as food additive[63]).

3.4 Kolliphor® EL in Suzuki-Miyaura micellar reactions

3.4.1 Suzuki-Miyaura coupling reaction in air

We here show that Kolliphor® EL micelles provide a suitable medium for the Suzuki-Miyaura cross coupling in water at room temperature under an oxygenated environment.

In order to comparatively test Kolliphor® EL with established coupling promoting surfactants, we tested the method under a set of experimental conditions generally accepted as appropriate in the dedicated literature:[62] room temperature, a 2 wt% solution of the surfactant in distilled water, 0,5 M concentration of the halide (bromide in all our reactions), [1,1'-bis(di-tert-butylphosphino)ferrocene]dichloropalladium(II) (Pd(dtbpf)Cl$_2$) 2 mol% with respect to the bromide as the catalyst, and triethylamine (N(Et)$_3$) as the base. Reaction scope is shown with examples of cross-coupling reactions in scheme 3.1.

Derivatives **2−5** have isolated yields comparable with literature data obtained with two popular and efficient designer surfactants, Nok and TPGS-750-M.[61, 62] Results are generally comparable, with the relevant difference of Kolliphor reactions being carried out under standard oxygenated environment. Table 3.2 reports all tested reaction conditions, including reactions carried out with less reactive catalysts like [1,1'-bis(diphenylphosphino)ferrocene]dichloropalladium(II) (Pd(dppf)Cl$_2$), palladium(II) acetate (Pd(OAc)$_2$) and bis(triphenylphosphine)palladium(II) dichloride (Pd(PPh$_3$)$_2$Cl$_2$). Whenever a thiophene residue was present, the use of Pd(dtbpf)Cl$_2$ gave the best results.

We carried out a comparative study on the coupling of 3-thienylboronic acid and 3-bromoquinoline by using two popular micelle-forming surfactants: Triton X-100 and the designer surfactant TPGS-750-M. Table 3.1 shows that under otherwise identical conditions the reaction with Kolliphor leads to 90% yield while the reactions with Triton X-100 and TPGS-750-M afford the product in a more modest 68% and 69% yield, respectively. As an extra benefit, in the case of Kolliphor, the coupling product can be readily isolated by filtration. This prompted us to recycle the aqueous phase for a second consecutive reaction without adding a fresh catalyst. The reaction behaved satisfactorily, leading to an isolated yield of 70% after 2 h. The role of oxygen in explaining the different behavior
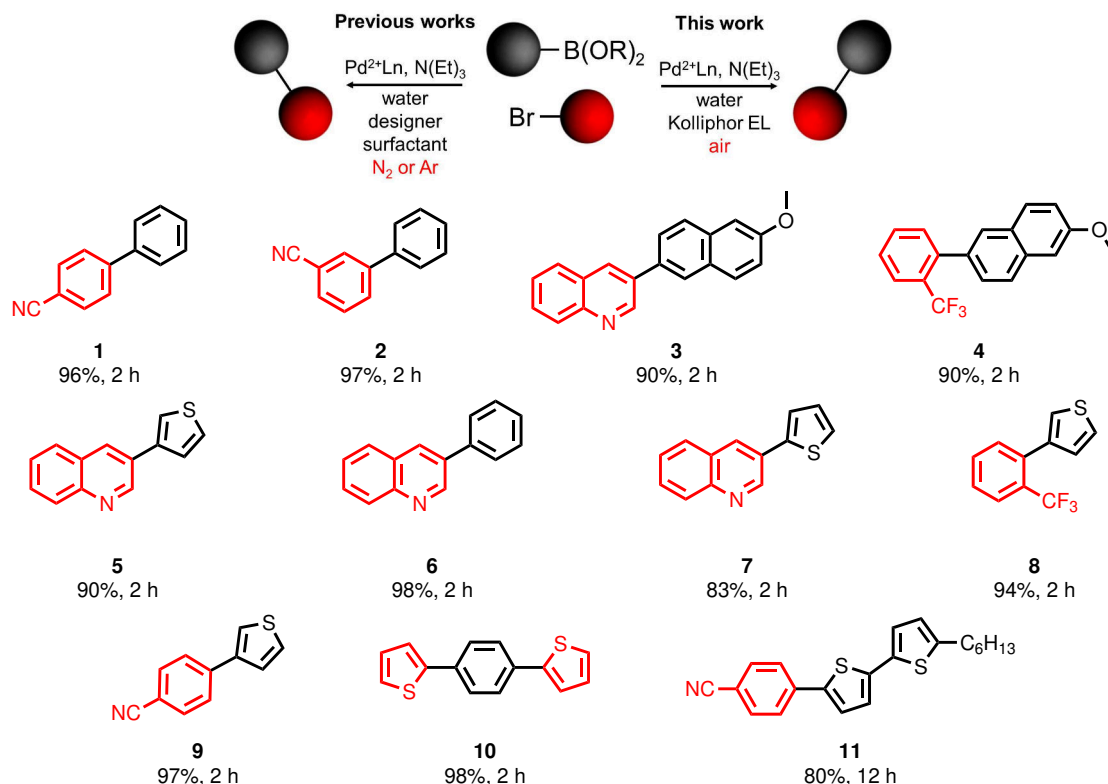
Scheme 3.1 Micellar couplings in water under oxygenated environment. Aryl bromides (in red) and arylboronic acids (in black) were coupled in 2 wt% Kolliphor EL solution in deionized water. Isolated yields and reaction times are given.

of Kolliphor-, Triton-, and TPGS-750-M-enhanced reactions was further confirmed by repeating the reactions with Triton X-100 and TPGS-750-M under nitrogen atmosphere and with nitrogen-saturated water. Indeed, we were able to increase the yield from 68 to 80% in the case of Triton X-100 and from 69 to 95% in the case of TPGS-750-M. The absolute higher yield obtained with the latter is not surprising; TPGS-750-M is a designer surfactant, specifically engineered to perform cross-coupling reactions. Conversely, Kolliphor EL is just an emulsifier, unoptimized for micellar couplings. The real gain when using Kolliphor is the oxygen insensitivity rather than the absolute performance (remarkable in any case).

Entry	Surfactant	Run	Atmosphere	Time (h)	Yield (%)
1	Kolliphor EL	I	air	1	90
2	Kolliphor EL	II	air	2	70
3	Triton X-100	I	air	2	68
4	Triton X-100	I	N_2	2	80
5	TPGS-750-M	I	air	2	69
6	TPGS-750-M	I	N_2	2	95

Table 3.1 Reaction of 3-bromoisoquinoline with 3-thienylboronic acid in different surfactant dispersions.
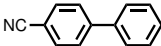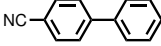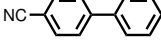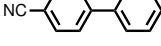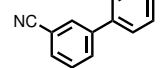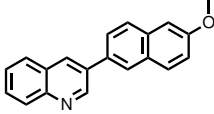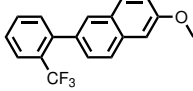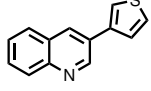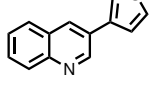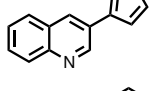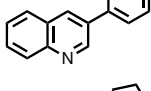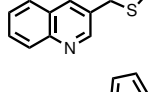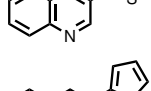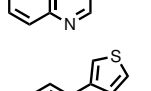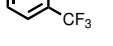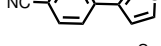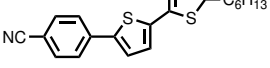
Entry	Product	Catalyst	Time (h)	Yield (%)
1		Pd(dtbpf)Cl$_2$	2	96
2		Pd(dppf)Cl$_2$	2	96
3		Pd(OAc)$_2$	2	95
4		Pd(PPh$_3$)$_2$Cl$_2$	2	97
5		Pd(dtbpf)Cl$_2$	2	97
6		Pd(dtbpf)Cl$_2$	2	90
7		Pd(dtbpf)Cl$_2$	2	90
8		Pd(dtbpf)Cl$_2$	2	90
9		Pd(dppf)Cl$_2$	24	<10
10		Pd(OAc)$_2$	24	No reaction
11		Pd(dtbpf)Cl$_2$	2	98
12		Pd(dtbpf)Cl$_2$	2	83
13		Pd(dppf)Cl$_2$	24	<10
14		Pd(OAc)$_2$	24	No reaction
15		Pd(dtbpf)Cl$_2$	2	94
16		Pd(dtbpf)Cl$_2$	2	97
17		Pd(dtbpf)Cl$_2$	2	88
18		Pd(dtbpf)Cl$_2$	12	80

Table 3.2 Complete datasets for coupling reactions described in scheme 3.1.

To further substantiate this point, we carried out an additional experiment using the oxygen-sensitive catalyst tetrakis(triphenylphosphine)palladium(0) (Pd(PPh$_3$)$_4$). We prepared two identical dispersions, one with Kolliphor EL and one with TPGS-750-M, of 10 mg of Pd(PPh$_3$)$_4$ in 2 mL of 2% by weight surfactant solution in water. Such dispersions, both featuring the characteristic yellow coloration of fresh Pd(PPh$_3$)$_4$, were allowed to stir at room temperature for 24 h in a standard laboratory environment. After aging, the TPGS-750-M dispersion darkened significantly (figure 3.3a-b). Both dispersions were thus charged with 6-methoxynaphthalene-2-boronic acid, 9-bromoanthracene, and N(Et)$_3$ (figure 3.3c reports the reaction scheme). Figure 3.3d shows the GC-MS trace of both reactions after 3 h of stirring. The Kolliphor EL dispersion gives the expected product; conversely, the TPGS-750-M reaction leads to negligible conversion, coherent with extensive catalyst degradation.

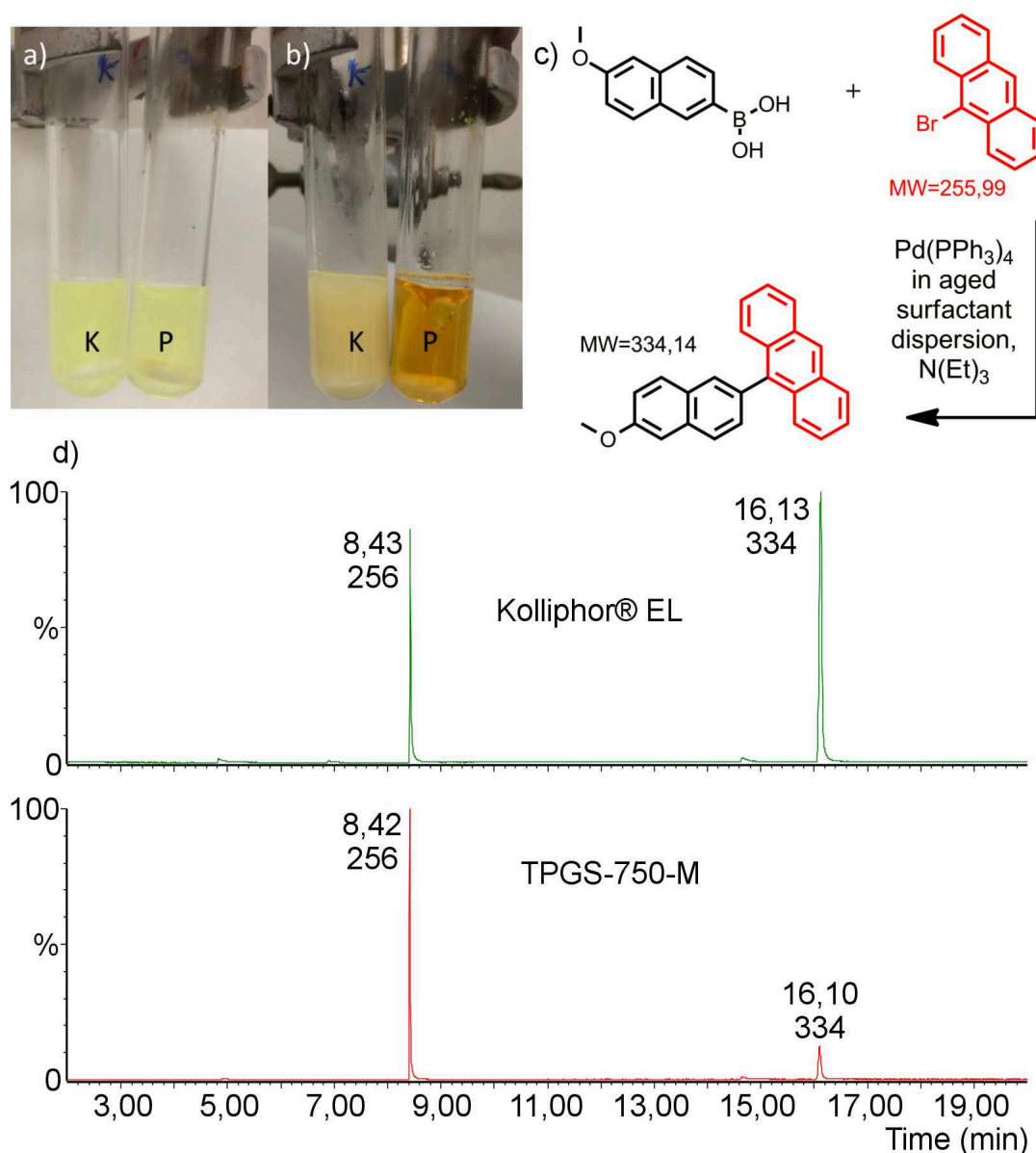**Figure 3.3** a) As-prepared dispersions of 10 mg of Pd(PPh$_3$)$_4$ in Kolliphor EL (denoted with K) and TPGS-750-M (denoted with P). b) Dispersions after 24 h aging at room temperature and under oxygenated environment. c) Scheme of the reaction carried in aged Pd(PPh$_3$)$_4$ dispersions. d) GC-MS traces of reaction in aged Kolliphor® EL (green) and TPGS-750-M (red)

3.4.2   Synthesis of organic semiconductors

Kolliphor EL is mostly known for being an excellent dispersant of relatively insoluble drugs such as Taxol and its derivatives.[64] We decided to challenge its dispersion capabilities in a series of cross-coupling reactions involving organic semiconductors pertaining to the classes of 9,10-diarylanthracenes, diketopyrrolopyrroles, diarylbenzothiadiazoles, perylenediimides, and isoindigos. Such compounds possess solid track records in a variety of organic devices.[65, 66] Working with such starting compounds required further optimization of the reaction conditions. Scheme 3.2 shows a series of reactions involving 9,10-dibromoanthracene (DBA) and four arylboronic acids bearing different functional groups. The reaction with phenylboronic acid was tested to optimize reaction conditions. We consistently obtained the highest yield by increasing reaction mixture concentrations. In particular, dilution of the reaction mixture favored formation of the homocoupling biphenyl side product. This process is commonly connected with oxygen being present in the reaction mixture.[67] Conversely, when working at 1 M bromide concentration, we obtained a 95% yield after crystallization and no isolated biphenyl.

12

0.50 M	25%, 24 h
0.25 M	10%, 24 h
1.00 M	95%, 12 h

13
69%, 12 h

14
95%, 12 h

15
90%, 12 h
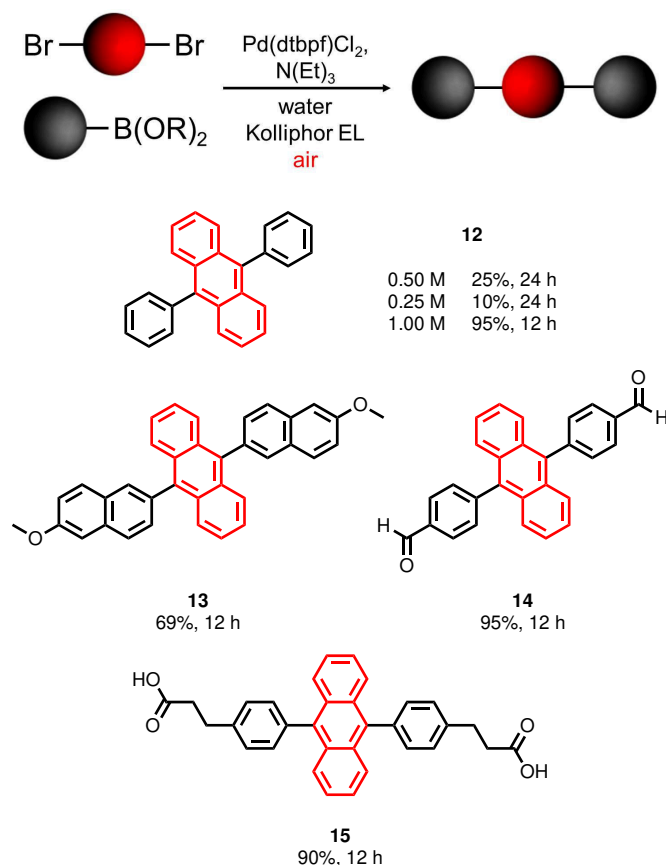
Scheme 3.2 Couplings of 9,10-dibromoanthracene (in red) and different arylboronic acids (in black) performed in a 2 wt% Kolliphor EL solution in deionized water. Isolated yields, after crystallization, are given.

Working under the same conditions, we isolated all other cross-coupling products with yields between 69 and 95%. Table 3.3 shows details for every reaction, including the structure and yield of the homocoupling products (where present). As a tentative rationalization of such behavior, we postulate that the obtainment of the homo- versus cross-coupling products depends upon the localization of the reactive species within the micelle. Results obtained with up-converting micelles described in Chapter 2 provided us evidences that Kolliphor micelles are constituted by two compartments, only one of which - the low polarity one - is oxygen free. Two of the three components of the model reaction, DBA and the catalyst, have a very low polarity and are thus likely to localize in the nonpolar, oxygen free compartment of the micelle. The boronic acid is more likely to localize in the polar outer pseudophase of the micelle, diffusing into the core due to concentration gradient. Thus, if the reaction mixture is very diluted, the boronic acid is unlikely to diffuse towards the core. Reaction in the oxygenated palisade layer explains the formation of the homocoupling product, as well as progressive deactivation of the catalyst. Conversely at very high concentration, the boronic acid is pushed towards the core, thereby reacting
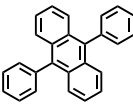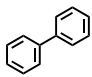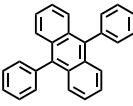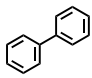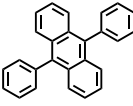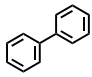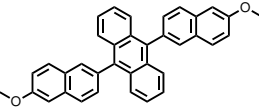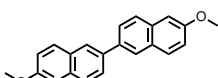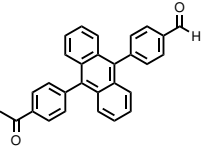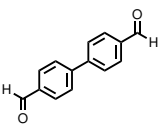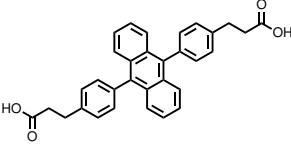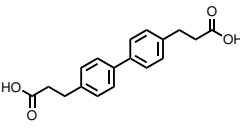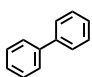
Entry	Concentration of DBA (M)	Product	Time (h)	Isolated yield (%)
1	0,5		24	25
				5
2	0,25		24	10
				10
3	1		12	95
				traces
4	1		12	69
				traces
5	1		12	95
				traces
6	1		12	90
				traces
7	1[a]		12	20

Table 3.3 Micellar couplings of 9,10-dibromoanthracene and different arylboronic acids performed in a 2% by weight Kolliphor EL solution in deionized water. [a]Concentration of the boronic acid.

with the bromide in the absence of oxygen and leading to the cross-coupling product.

To substantiate this tentative mechanism, we made a countercheck reaction: entry 7 in table 3.3 describes a reaction performed under standard condition but without introducing the halide. Indeed, we observed gradual formation of the homocoupling product, with an isolated yield of 20%. The reaction mixture readily turned very dark and the mixture could not be used a second time, a further indication that the reaction takes place in a pseudophase where the catalyst can be gradually converted to inactive palladium black. Incidentally, such a model would also agree with the observation of preferential double reaction in the case of bifunctional bromides. In fact, the mono cross-coupling between DBA and one equivalent of boronic acid leads to a low polarity compound, still preferentially localized within the low polarity, oxygen free compartment of the micelle, where a second coupling readily gives DPA.

Reaction conditions leading to diarylanthracenes were also successfully employed for the synthesis of the organic semiconductors shown in Scheme 3.3.
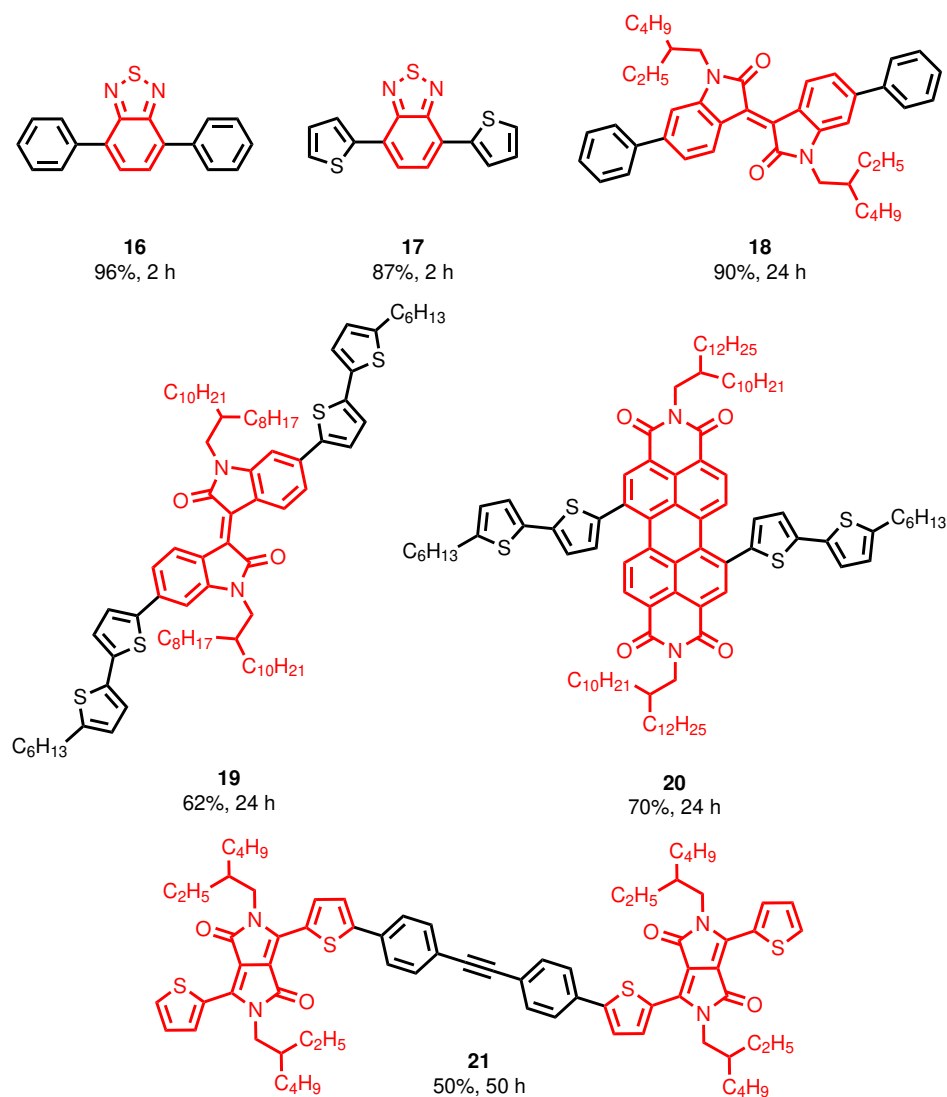
Scheme 3.3 Couplings of brominated precursors (in red) and arylboronic acids or esters (in black) performed in a 2 wt% Kolliphor EL solution in deionized water. Isolated yields and reaction times are given.

Derivatives **16** and **17** are known fluorescent molecules and behave in a way similar to that of diarylanthracene compounds. These are poorly soluble crystalline derivatives; they can be directly filtered from the reaction medium and purified by crystallization. Derivatives **18** and **19** are examples of heavily functionalized compounds that could interfere with the micellar structure of Kolliphor EL in solution. Characteristics of such isoindigo derivatives made the reaction mixture difficult to efficiently stir, as most of the material formed an oily and sticky residue on the walls of the reaction flask. To deal with the problem, we mechanically shook the reaction mixture and increased the reaction time to 24 h. Derivatives **20** and **21** are examples of a coupling reaction involving a boronic ester instead of an acid. The reactions proved to be significantly slower, again mostly due to the high viscosity of the reaction mixture. All products could, in any case, be isolated after chromatographic purification in moderate to good yields. Further optimization of our method will likely require the devising of improved mixing procedures. The use of cosolvents might also be helpful.[68]

3.5 Conclusions

We have demonstrated that Kolliphor EL, a cheap, readily available, and well-established drug emulsifier and surfactant, can be used with a simple room-temperature method to access a wide variety of Suzuki—Miyaura coupling products affording high yield in air. The scope of the reaction is demonstrated with the coupling of a wide variety of aryl and heteroaryl bromides with various boronic acids and esters, including examples of well-established organic molecular semiconductor cores. All reactions can be carried out directly in a standard oxygenated environment in deionized water. In the case of crystalline compounds, the reaction medium can be recycled, and the coupling products can be isolated directly by filtration. By comparing Kolliphor EL to other designer surfactants, we have demonstrated that Kolliphor EL alone provides an environment suitable for efficient oxygen-insensitive reactions. In short, we demonstrated an exceedingly simple, economically convenient, and sustainable benchtop protocol for efficient Suzuki—Miyaura coupling.

Still, we can improve a lot in the synthesis of organic semiconductors: this method, in fact, demonstrated its limitations when heavily functionalized substrates where present, as the reaction could not be stirred appropriately. This problem is particularly obvious in presence of substrates having long alkyl chains, which behave as sticky waxes. We are now testing improved stirring methods, including the use of a peristaltic pump, to deal with the problem. The use of a cosolvent also demonstrated to greatly enhance the final yields, with no loss of oxygen barrier activity.[69]

Within such premises, we are currently exploring polymerization reactions of semiconductor polymers with very encouraging results.

3.6 Experimental

Catalysts were purchased from Alfa Aesar. Deionized water was purchased from Carlo Erba. Boronic acids and esters were purchased from TCI. All the others starting materials were purchased from Sigma-Aldrich. All materials and solvents were used as received.

NMR spectra were acquired on a Bruker NMR 500 Avance.

General procedure for micellar coupling

Reactions leading to products **1-11** were performed in a microwave vessel (10 mL vessel, available from CEM Corporation) with magnetic stirring and under standard laboratory atmosphere. In a typical procedure, bromide (0,5 mmol) and boronic acid (0,75 mmol) were weighted in the vessel and 1 mL of the 2% by weight surfactant solution (either Kolliphor EL, Triton X-100, TPGS-750-M) was added under stirring. To the suspension, $Pd(dtbpf)Cl_2$ (0,01 mmol) and $N(Et)_3$ (1,5 mmol) were added. The viscous reaction mixture was vigorously stirred for the appropriate time (see table 3.2, table 3.3 and scheme 3.3) and worked up according to one of the two following procedures.

Route A The reaction mixture was suction filtered through a frit funnel. The solid precipitate was washed thoroughly with water directly on the filter. The solid residue was thus dried to constant weight and crystallized in the appropriate solvent (see below).

Route B The mixture was diluted with 10 mL of CH_2Cl_2 and filtered through a pad of silica. The filtrated was evaporated under reduced pressure and purified by chromatography (see details below).

Reactions leading to products **12-17** were performed analogously, but doubling the concentration of reagents in the micellar dispersion.

Reactions leading to products **18-21** were performed analogously, but concentration needed to be adjusted, case by case, to the highest one allowing to stir the reaction.

For new compounds, elemental analysis as well as ^{1}H and ^{13}C NMR spectra are reported.

Details on single specific reactions

Synthesis of 4-cyanobiphenyl (*1*)
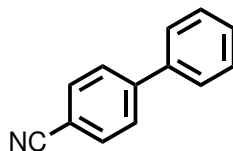
From phenylboronic acid (91 mg), 4-bromobenzonitrile (91 mg), $N(Et)_3$ (151 mg) and $Pd(dtbpf)Cl_2$ (7,0 mg). Route B, purified on SiO_2 column with CH_2Cl_2:n-heptane 1:3. Off white solid, 86 mg, yield 96%.

^{1}H NMR (CDCl3, 500 MHz): δ 7.42-7.45 (m, 1H), 7.49 (t, J = 7.5 Hz, 2H), 7.59-7.60 (m, 2H), 7.68- 7.70 (m, 2H), 7.73-7.74 (m, 2H).

^{13}C NMR (CDCl3, 125.7 MHz): δ 111.8, 119.8, 128.1, 128.6, 129.5, 130.0, 133.5, 140.1, 146.6. See [70] for comparison.

Synthesis of 3-cyanobiphenyl (*2*)
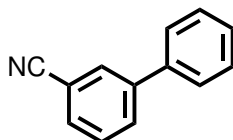
From phenylboronic acid (91 mg), 3-bromobenzonitrile (91 mg), N(Et)$_3$ (151 mg) and Pd(dtbpf)Cl$_2$ (7,0 mg). Route B, purified on SiO$_2$ column with CH$_2$Cl$_2$:n-heptane 1:3. Waxy solid, 87 mg, yield 97%.

^{1}HNMR (CDCl$_3$, 500 MHz): δ 7.41-7.44 (m, 1H), 7.47-7.50 (m, 2H), 7.53-7.57 (m, 3H), 7.62-7.64 (m, 1H), 7.80-7.82 (m, 1H), 7.85 (m, 1H).

^{13}C NMR (CDCl$_3$, 125.7 MHz): δ 113.8, 119.8, 128.0, 129.3, 130.0, 130.5, 131.63, 131.64, 132.4, 139.7, 143.3. See [70] for comparison.

Synthesis of 3-(2-methoxynaphthalen-6-yl)quinolone (*3*)
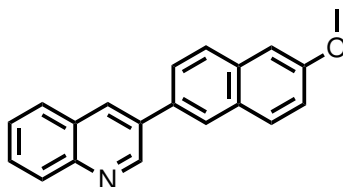
From 2-methoxynaphthalene-6-boronic acid (150 mg), 3-bromoquinoline (104 mg), N(Et)$_3$ (151 mg) and Pd(dtbpf)Cl$_2$ (7,0 mg). Route B, purified on SiO$_2$ column with CH$_2$Cl$_2$:AcOEt 3:1. Off white solid, 128 mg, 90% yield.

^{1}H NMR (CDCl$_3$, 500 MHz): δ 3.97 (s, 3H), 7.20 (d, J = 2.6 Hz, 1H), 7.22 (m, 1H), 7.60 (m, 1H), 7.73 (m, 1H), 7.82 (m, 1H), 7.86 (d, J = 8.8 Hz, 1H), 7.91 (m, 2H), 8.11 (d, J = 1.3 Hz, 1H), 8.16 (d, J = 8.3 Hz, 1H), 8.40 (d, J = 2.2 Hz, 1H), 9.31 (d, J = 2.2 Hz, 1H).
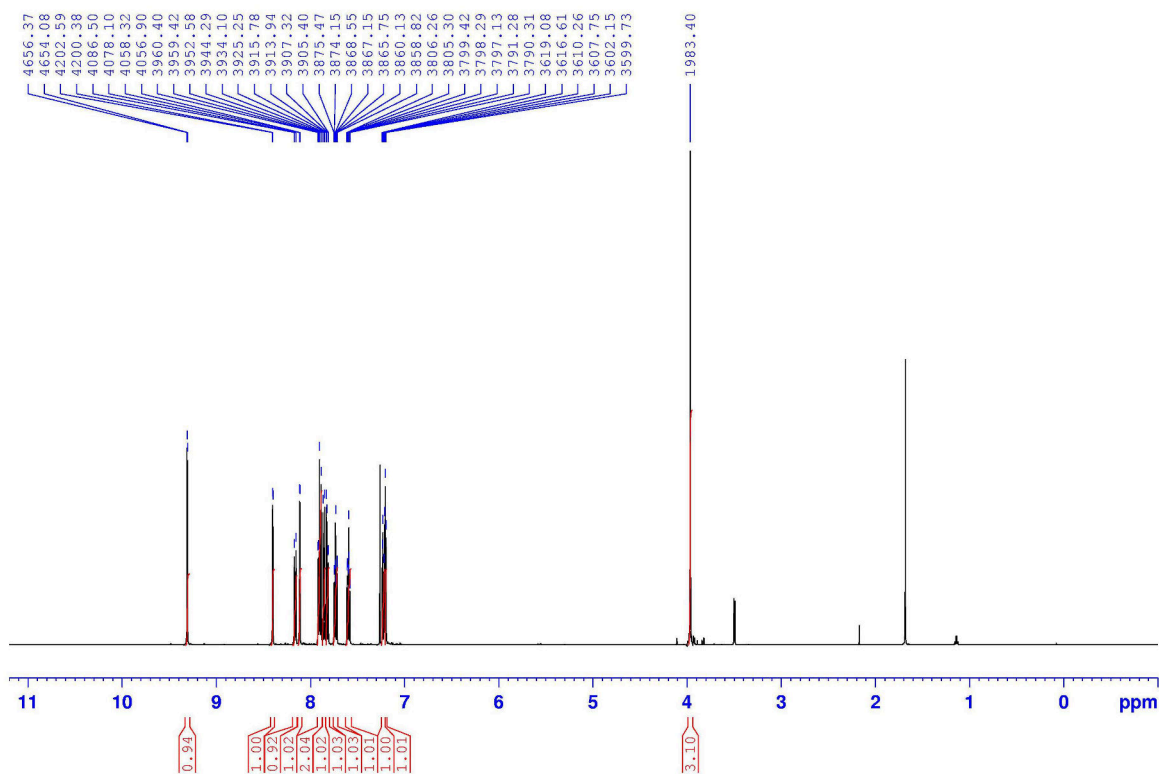
^{13}C NMR (CDCl$_3$, 125.7 MHz): δ 56.3, 106.5, 120.5, 126.6, 127.1, 127.9, 128.7, 128.9, 129.0, 130.1, 130.2, 130.7, 133.8, 134.0, 134.7, 135.0, 148.1, 151.0, 159.1.
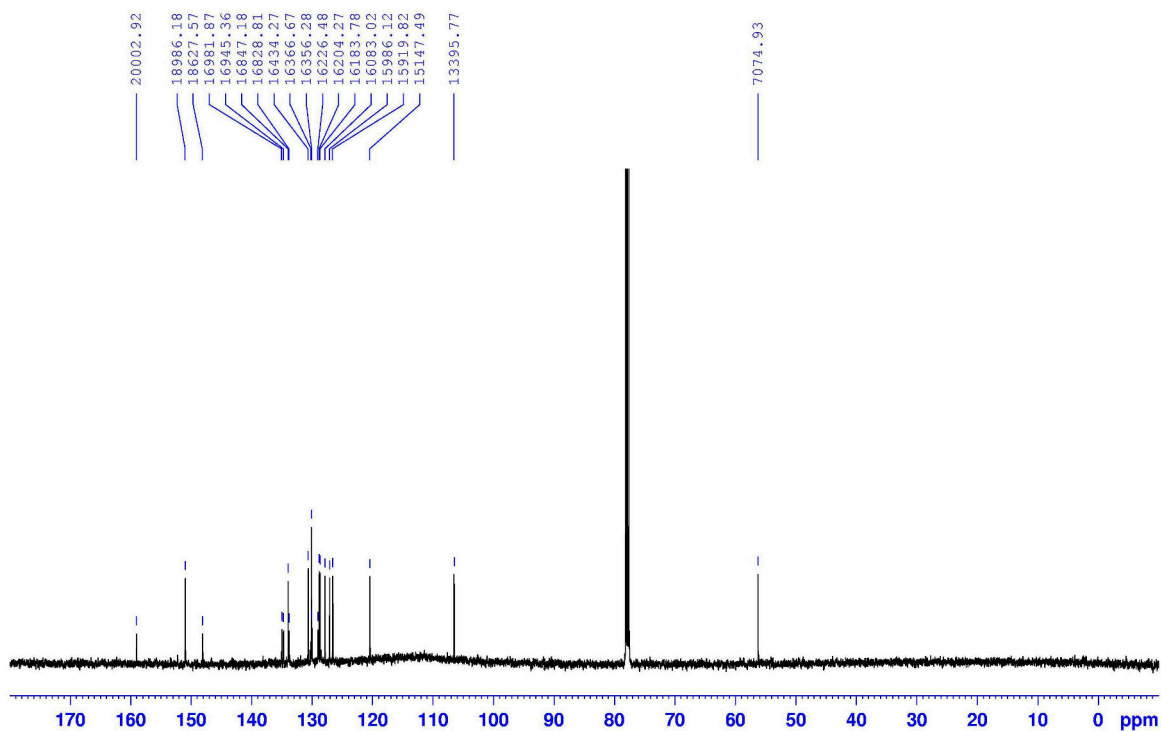
Anal. calcd. for C$_{20}$H$_{15}$NO: C, 84.19; H, 5.30; N, 4.91. Found: C, 84.01; H, 5.40; N, 4.62.

Synthesis of 2-(2-(trifluoromethyl)phenyl)-6-methoxynaphthalene (*4*)
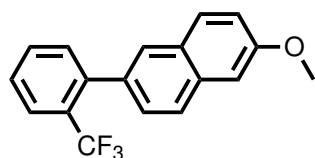
From 2-methoxynaphthalene-6-boronic acid (150 mg), 2-bromotrifluoromethylbenzene (113 mg), N(Et)$_3$ (151 mg) and Pd(dtbpf)Cl$_2$ (7,0 mg). Route B, purified on SiO$_2$ column with CH$_2$Cl$_2$:n-heptane 1:2. Off white solid, 136 mg, yield 90%.

^{1}H NMR (CDCl$_3$, 500 MHz): δ 3.95 (s, 3H), 7.19-7.20 (m, 2H), 7.42 (t, J = 7.6 Hz, 2H), 7.49 (t, J = 7.6 Hz, 1H), 7.59 (t, J = 7.6 Hz, 1H), 7.72 (m, 1H), 7.75-7.79 (m, 3H).

^{13}C NMR (CDCl$_3$, 125.7 MHz): δ 56.3, 106.5, 120.1, 125.1 (q, J = 275.2 Hz), 126.9-127.1 (m), 128.1, 128.6, 129.2, 129.5 (q, J = 30.3 Hz), 130.5, 132.2, 133.3, 134.7, 136.0, 142.4 (q, J = 2.1 Hz), 158.8. See [62] for comparison.

Synthesis of 3-(thiophen-3-yl)quinoline (*5*)
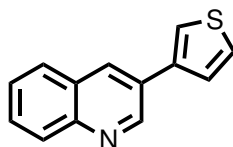
From thienyl-3-boronic acid (96 mg), 3-bromoquinoline (104 mg), N(Et)$_3$ (151 mg) and Pd(dtbpf)Cl$_2$ (7,0 mg). Route A, followed by chromatographic purification on silica gel column with gradient eluent from CH$_2$Cl$_2$ to CH$_2$Cl$_2$:AcOEt 5:1. White solid, 95 mg, yield 90%.

^{1}H NMR (CDCl$_3$, 500 MHz): δ 7.47-7.48 (m, 1H), 7.50-7.52 (m, 1H), 7.55 (m, 1H), 7.64 (dd, J1 = 3.1 Hz, J2 = 1.3 Hz, 1H), 7.67-7.70 (m, 1H), 7.83 (d, J = 7.8 Hz, 1H), 8.11 (d, J = 8.3 Hz, 1H), 8.25 (d, J = 2.2 Hz, 1H), 9.20 (d, J = 2.2 Hz, 1H).

^{13}C NMR (CDCl$_3$, 125.7 MHz): δ 122.5, 127.0, 128.00, 128.02, 128.8, 129.0, 129.6, 130.1, 130.2, 132.9, 139.8, 148.1, 150.4. See [71, 72] for comparison.

Synthesis of 3-phenylquinoline (*6*)
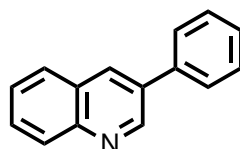
From phenylboronic acid (91 mg), 3-bromoquinoline (104 mg), N(Et)$_3$ (151 mg) and Pd(dtbpf)Cl$_2$ (7,0 mg). Route A, followed by chromatographic purification on silica gel column with gradient eluent from CH$_2$Cl$_2$ to CH$_2$Cl$_2$:AcOEt 9:1. Waxy solid, 101 mg, yield 98%.

^{1}H NMR (CDCl$_3$, 500 MHz): δ 7.43-7.46 (m, 1H), 7.52-7.55 (m, 2H), 7.57-7.60 (m, 1H), 7.73 (d, J1 = 7.9 Hz, 3H), 7.89 (d, J = 8.3 Hz, 1H), 8.15 (d, J = 8.3 Hz, 1H), 8.31 (d, J = 2.2 Hz, 1H), 9.20 (d, J = 2.6 Hz, 1H).

^{13}C NMR (CDCl$_3$, 125.7 MHz): δ 127.9, 128.3, 128.9, 129.0, 130.1, 130.2, 130.3, 134.1, 134.8, 138.8, 148.2, 150.9. See [73] for comparison.

Synthesis of 3-(thiophen-2-yl)quinoline (*7*)
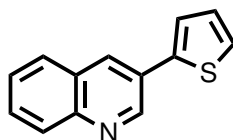
From thienyl-2-boronic acid (96 mg), 3-bromoquinoline (104 mg), N(Et)$_3$ (151 mg) and Pd(dtbpf)Cl$_2$ (7,0 mg). Route A, followed by chromatographic purification on silica gel column with gradient eluent from CH$_2$Cl$_2$ to CH$_2$Cl$_2$:AcOEt 5:1. Yellow solid, 88 mg, yield 83%.

^{1}H NMR (CDCl$_3$, 500 MHz): δ 7.17-7.19 (m, 1H), 7.40-7.42 (m, 1H), 7.51-7.52 (m, 1H), 7.56- 7.59 (m, 1H), 7.70-7.72 (m, 1H), 7.85 (d, J = 7.9 Hz, 1H), 8.10 (d, J = 8.3 Hz, 1H), 8.29 (d, J = 2.2 Hz, 1H), 9.22 (d, J = 2.2 Hz, 1H).

^{13}C NMR (CDCl$_3$, 125.7 MHz): δ 125.3, 127.0, 128.1, 128.5, 128.7, 128.8, 129.3, 130.2, 132.3, 141.7, 148.3, 149.6. See [72, 74] for comparison.

Synthesis of 3-(2-(trifluoromethyl)phenyl)thiophene (*8*)
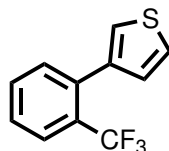
From 2-bromotrifluoromethylbenzene (113 mg), thienyl-3-boronic acid (96 mg), N(Et)$_3$ (151 mg) and Pd(dtbpf)Cl$_2$ (7,0 mg). Route B, purified on SiO$_2$ column with CH$_2$Cl$_2$:n-heptane 1:1. Oil, 108 mg, yield 94%.

^{1}H NMR (CDCl$_3$, 500 MHz): δ 7.17 (d, J = 5.3 Hz, 1H), 7.31 (m, 1H), 7.37 (m, 1H), 7.42 (d, J = 7.9 Hz, 1H), 7.46 (t, J = 7.5 Hz, 1H), 7.56 (t, J = 7.5 Hz, 1H), 7.76 (d, J = 7.5 Hz, 1H).

^{13}C NMR (CDCl$_3$, 125.7 MHz): δ 125.0 (q, J = 273.7 Hz), 124.61 (d, 2.5 Hz), 125.7, 127.0 (q, J = 5.6 Hz), 128.3, 129.45 (q, J = 29.6 Hz), 129.9, 132.3, 133.0, 137.1 (d, J = 2.5 Hz), 140.4. See [62] for comparison.

Synthesis of 4-(thiophen-3-yl)benzonitrile (*9*)
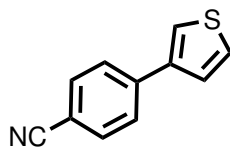
From thienyl-3-boronic acid (96 mg), and 4-bromobenzonitrile (91 mg), N(Et)$_3$ (151 mg) and Pd(dtbpf)Cl$_2$ (7,0 mg). Route B, purified on SiO$_2$ column with CH$_2$Cl$_2$:n-heptane 1:1. White solid, 180 mg, yield 97%.

^{1}H NMR (CDCl$_3$, 500 MHz): δ 7.40 (dd, J$_1$ = 5.3 Hz, J$_2$ = 1.3 Hz, 1S), 7.44-7.45 (m, 1H), 7.58 (dd, J$_1$ = 3.1 Hz, J$_2$ = 1.3 Hz, 1H), 7.69 (s, 4H).

^{13}C NMR (CDCl$_3$, 125.7 MHz): δ 111.4, 119.8, 123.5, 126.8, 127.7, 128.1, 133.6, 141.0, 141.3. See [75] for comparison.

Synthesis of 2-(4-(thiophen-2-yl)phenyl)thiophene (*10*)
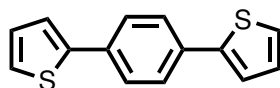
From benzene-1,4-diboronic acid (497 mg, 3 mmol), 2-bromothiophene (978 mg, 6 mmol), N(Et)$_3$ (151 mg) and Pd(dtbpf)Cl$_2$ (7,0 mg). Route B, purified on SiO$_2$ column with CH$_2$Cl$_2$:n-heptane 1:1. Crystallized from isopropanol. Light yellow solid, 639 mg, yield 88%.

^{1}H NMR (CDCl$_3$, 500 MHz): δ 7.10 (t, J = 4.2 Hz, 2H), 7.30 (d, J = 4.8 Hz, 2H), 7.35 (d, J = 3.1 Hz, 2H), 7.63 (s, 4H).

^{13}C NMR (CDCl$_3$, 125.7 MHz): δ 124.0, 125.8, 127.2, 129.0, 134.4, 144.8. See [76] for comparison.

Synthesis of 4-(5-(5-hexylthiophen-2-yl)thiophen-2-yl)benzonitrile (*11*)
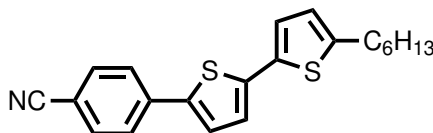
From 5-Hexyl-2,2-bithiophene-5-boronic acid (221 mg), 4-bromobenzonitrile (91 mg), N(Et)$_3$ (151 mg) and Pd(dtbpf)Cl$_2$ (7,0 mg). Route B, purified on SiO$_2$ column with gradient eluent from CH$_2$Cl$_2$:n-Heptane 1:2 to CH$_2$Cl$_2$. Crystallized from methanol. Light yellow solid, 140 mg, yield 80%.

^{1}H NMR (CDCl$_3$, 500 MHz): δ 0.90 (t, J = 7.0 Hz, 3H), 1.32-1.34 (m, 4H), 1.36-1.42 (m, 2H), 1.69 (qui, J = 7.5 Hz, 2H), 2.81 (t, J = 7.5 Hz, 2H), 6.72 (d, J = 3.1 Hz, 1H), 7.05 (d, J = 4.0 Hz, 1H), 7.10 (d, J = 3.5 Hz, 1H), 7.32 (d, J = 4.0 Hz, 1H), 7.65 (m, 4H).

^{13}C NMR (CDCl$_3$, 125.7 MHz): δ 15.0, 23.5, 29.6, 31.1, 32.4, 111.1, 119.8, 124.9, 125.9, 126.4, 126.7, 133.6, 134.9, 139.3, 140.5, 140.7, 147.4. See [77] for comparison.

Synthesis of 9,10-diphenylanthracene (*12*)
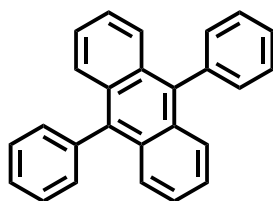
From 9,10-dibromoanthracene (168 mg), phenylboronic acid (183 mg), $N(Et)_3$ (303 mg) and $Pd(dtbpf)Cl_2$ (15 mg) in 0,5 mL of Kolliphor EL 2% solution. Route A. Crystallized from acetic acid. White crystal, 157 mg, yield 95%.

^{1}H NMR (CDCl$_3$, 500 MHz): δ 7.32-7.34 (m, 4H), 7.48-7.50 (m, 4H), 7.54-7.57 (m, 2H), 7.60-7.62 (m, 4H), 7.69-7.71 (m, 4H).

^{13}C NMR (CDCl$_3$, 125.7 MHz): δ 125.9, 127.8, 128.3, 129.3, 130.7, 132.2, 138.0, 140.0. See [78] for comparison.

Synthesis of 9,10-di(2-methoxynaphthalen-6-yl) anthracene (*13*)
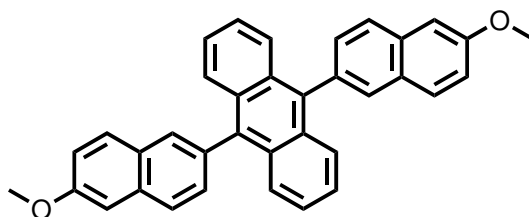
From 9,10-dibromoanthracene (168 mg), 2-methoxynaphthalene-6-boronic acid (303 mg), $N(Et)_3$ (303 mg) and $Pd(dtbpf)Cl_2$ (15 mg) in 0,5 mL of Kolliphor EL 2% solution. Route A. Crystallized from dimethyl sulfoxide. White crystal, 169 mg, yield 69%.

^{1}H NMR (CDCl$_3$, 500 MHz): δ 4.03 (s, 6H), 7.28 (d, J = 2.6 Hz, 1H), 7.30-7.32 (m, 4H), 7.33 (d, J = 2.6 Hz, 2H), 7.59 (dt, J_1 = 8.3 Hz, J_2 = 1.8 Hz, 2H), 7.75 (m, 4H), 7.82-7.84 (m, 3H), 7.92 (br, 2H), 7.98 (d, J = 8.3, 2H).

^{13}C NMR (CDCl$_3$, 125.7 MHz): δ 56.4, 106.7, 120.2, 125.9, 127.7, 128.0, 129.8, 130.5, 130.9, 131.0, 131.1, 134.8, 135.1, 138.0, 158.9. See [79] for comparison.

Synthesis of 9,10-di(4-formylphenyl) anthracene (*14*)
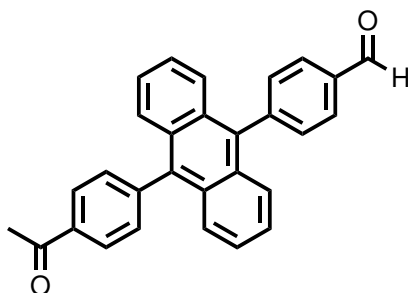
From 9,10-dibromoanthracene (168 mg), 4-formylphenylboronic acid (225 mg), $N(Et)_3$ (303 mg) and $Pd(dtbpf)Cl_2$ (15 mg) in 0,5 mL of Kolliphor EL 2% solution. Route A. Crystallized from acetic acid. White crystal, 183 mg, yield 95%.

^{1}H NMR (CDCl$_3$, 500 MHz): δ 7.37-7.39 (m, 4H), 7.61-7.63 (m, 4H), 7.69 (d, J = 7.9 Hz, 4H), 8.16 (d, J = 7.9 Hz, 4H), 10,22 (s, 2H).

^{13}C NMR (CDCl$_3$, 125.7 MHz): δ 126.6, 127.4, 130.3, 130.8, 133.0, 136.7, 137.1, 146.6, 192.9. See [80] for comparison.

Synthesis of 9,10-di(phenyl-4-propanoic acid) anthracene (*15*)
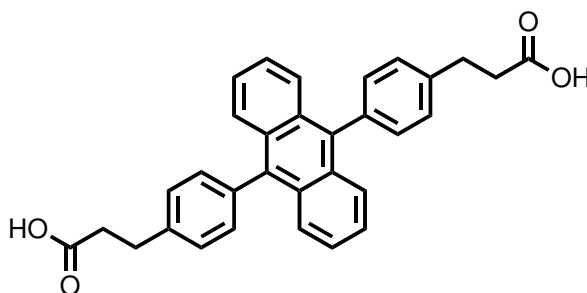
From 9,10-dibromoanthracene (168 mg), 3-(4-bromophenyl)propanoic acid (291 mg), $N(Et)_3$ (303 mg) and $Pd(dtbpf)Cl_2$ (15 mg) in 0,5 mL of Kolliphor EL 2% solution. Prior to filtration, mixture was diluted with 10 mL of 1% HCl. Route A. Crystallized from acetic acid. White crystal, 214 mg, yield 90%.

[1]H (DMSO-d6, 500 MHz): δ 2.73 (t, J = 7.5 Hz, 4H), 3.06 (t, J = 7.5 Hz, 4H), 7.38 (d, J = 7.9 Hz 8H), 7.4-7.42 (m, 4H), 7.53 (d, J = 7.9 Hz, 4H), 7.61-7.63 (m, 4H), 12.00 (br, 2H).
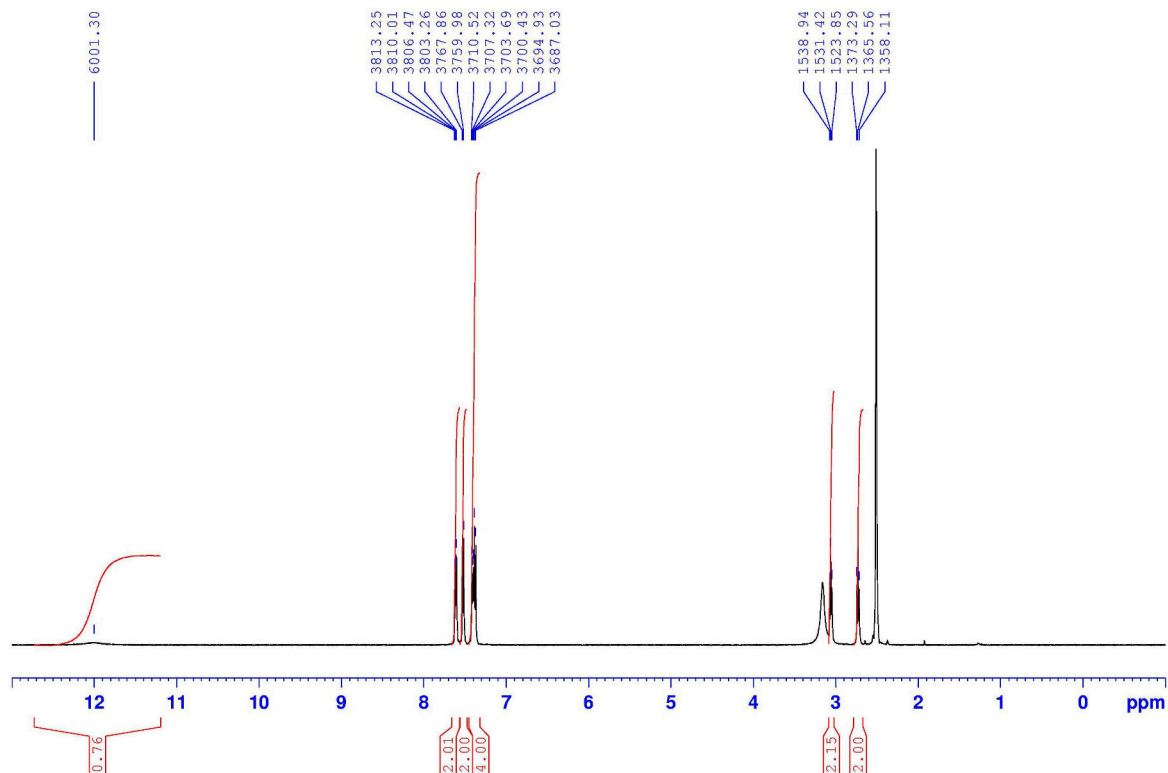
^{13}C (DMSO-d6, 125.7 MHz): δ 31.7, 36.5, 126.7, 127.9, 129.9, 130.8, 132.3, 137.3, 137.9, 141.8, 175.1.
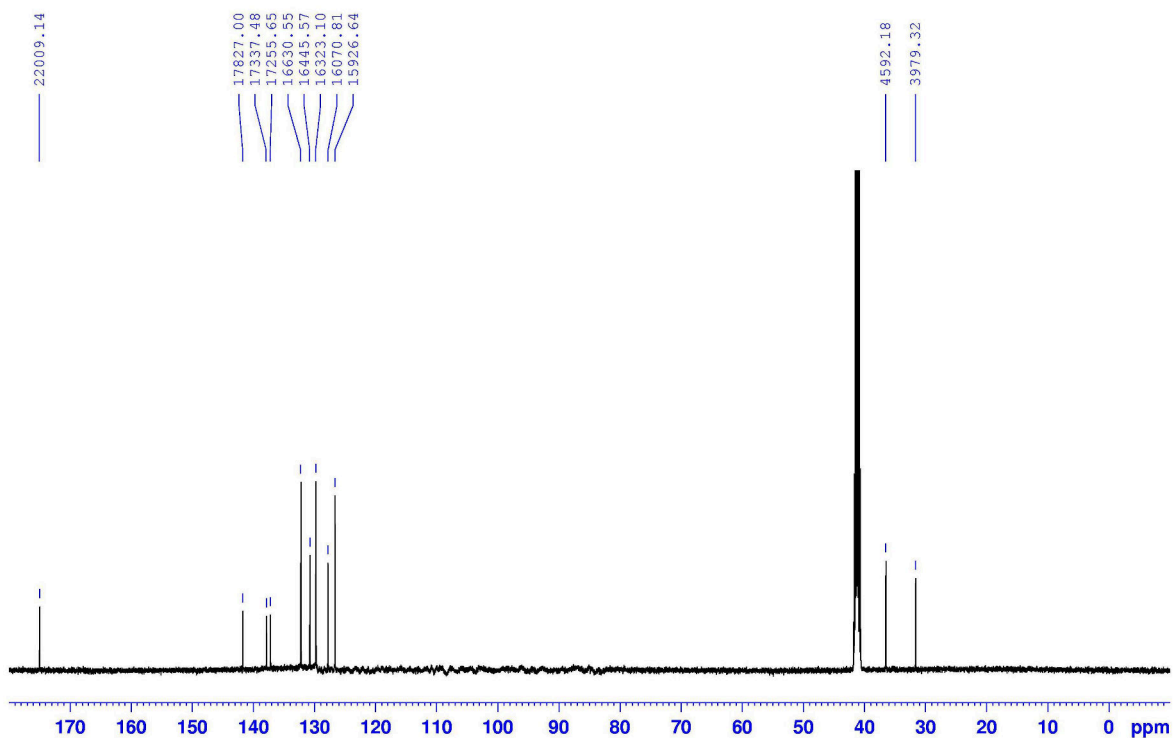
Anal. calcd. for $C_{32}H_{26}O_4$: C, 80.99; H, 5.52. Found: C, 81.16; H, 5.48.

Synthesis of 4,7-diphenylbenzo[c][1,2,5]thiadiazole (*16*)
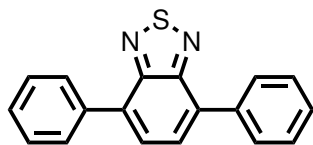
From phenylboronic acid (183 mg), 4,7-dibromobenzo[c][1,2,5]thiadiazole (147 mg), $N(Et)_3$ (303 mg) and $Pd(dtbpf)Cl_2$ (15 mg) in 0,5 mL of Kolliphor EL 2% solution. Route B, purified on SiO_2 column with CH_2Cl_2. Bright yellow solid, 139 mg, yield 96%.

^{1}H NMR ($CDCl_3$, 500 MHz): δ 7.47 (m, 2H), 7.56 (t, J = 8.0 Hz, 4H), 7.80 (s, 2H), 7.97 (d, J = 8.0 Hz, 4H).

^{13}C ($CDCl_3$, 125.7 MHz): δ 129.0, 129.3, 129.5, 130.1, 134.3, 138.3, 155.0. See [81] for comparison.

Synthesis of 4,7-di(thiophen-2-yl)benzo[c][1,2,5]thiadiazole (*17*)
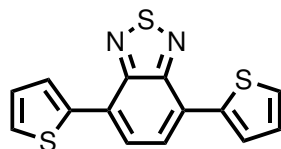
From thienyl-2-boronic acid (192 mg), 4,7-dibromobenzo[c][1,2,5]thiadiazole (147 mg), $N(Et)_3$ (303 mg) and $Pd(dtbpf)Cl_2$ (15 mg) in 0,5 mL of Kolliphor EL 2% solution. Route B, purified on SiO_2 column with CH_2Cl_2. Bright red solid, 130 mg, yield 87%.

^{1}H NMR ($CDCl_3$, 500 MHz): δ 7.20-7.22 (m, 2H), 7.45-7.47 (m, 2H), 7.86 (s, 2H), 8.11-8.12 (m, 2H).

^{13}C NMR ($CDCl_3$, 125.7 MHz): δ 126.7, 126.9, 127.7, 128.4, 128.9, 140.2, 153.5. See [82] for comparison.

Synthesis of 6,6'-diphenyl-N,N'-(2-ethylhexyl)-isoindigo (*18*)
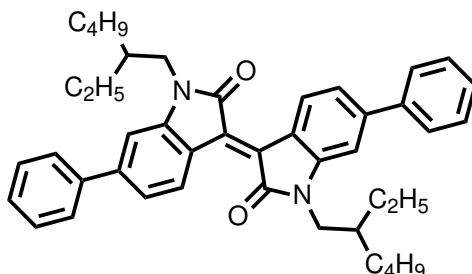
From 6,6'-dibromo-N,N'-(2-ethylhexyl)-isoindigo (322 mg, 0,5 mmol), phenylboronic acid (183 mg, 1,5 mmol), $N(Et)_3$ (303 mg, 3,0 mmol) and $Pd(dtbpf)Cl_2$ (15 mg, 0,02 mmol) in 1,5 mL of Kolliphor EL 2% solution. Route A. Crystallized from isopropanol. Dark red solid, 287 mg, 90%.

^{1}H (CDCl$_3$, 500 MHz): δ 0.90 (m, 6H), 0.96 (m, 6H), 1.32-1.43 (m, 16H), 1.92 (m, 2H), 3.68-3.79 (m, 4H), 6.99 (s, 2H), 7.29 (d, J = 7.9 Hz, 2H), 7.41 (m, 2H), 7.49 (m, 4H), 7.65 (d, J = 7.0 Hz, 4H), 9.24 (d, J = 8.3 Hz, 2H).
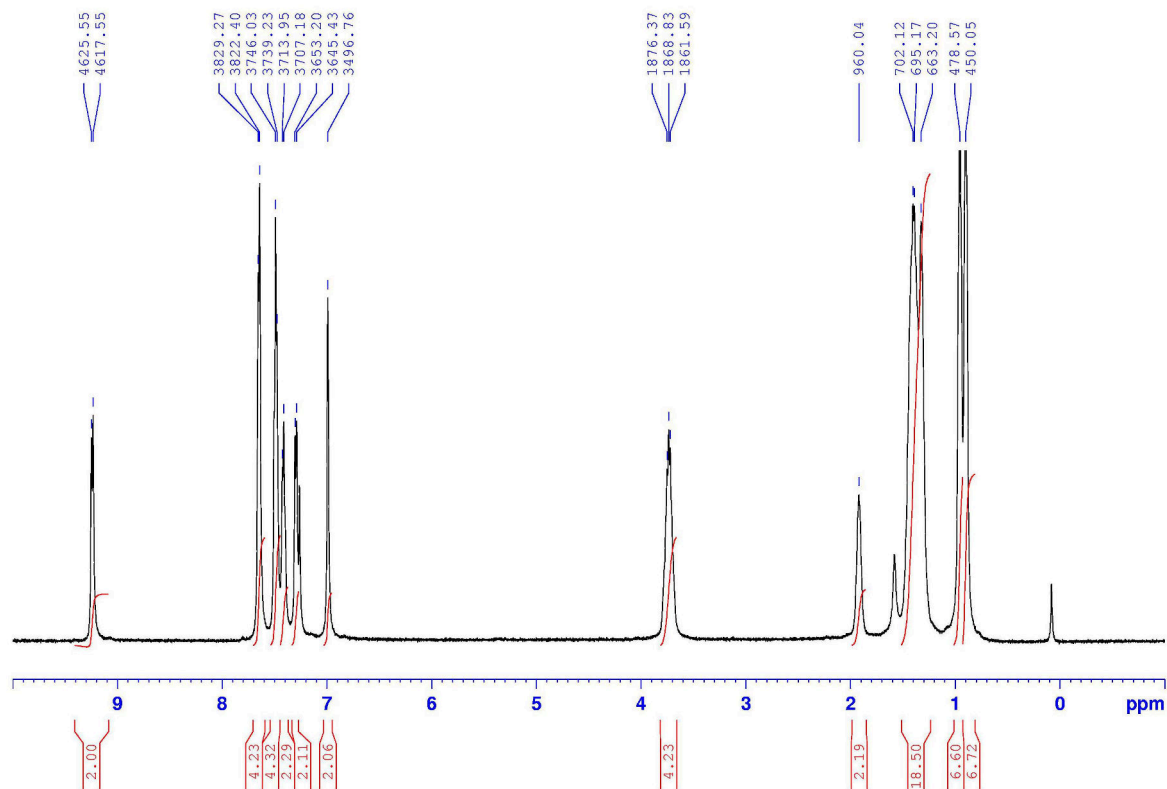
^{13}C (CDCl$_3$, 125.7 MHz): δ 11.6, 15.0, 24.0, 25.0, 29.7, 31.6, 38.6, 45.1, 107.5, 121.7, 121.8, 127.9, 129.1, 129.8, 131.0, 133.5, 141.5, 145.9, 146.6, 169.6.
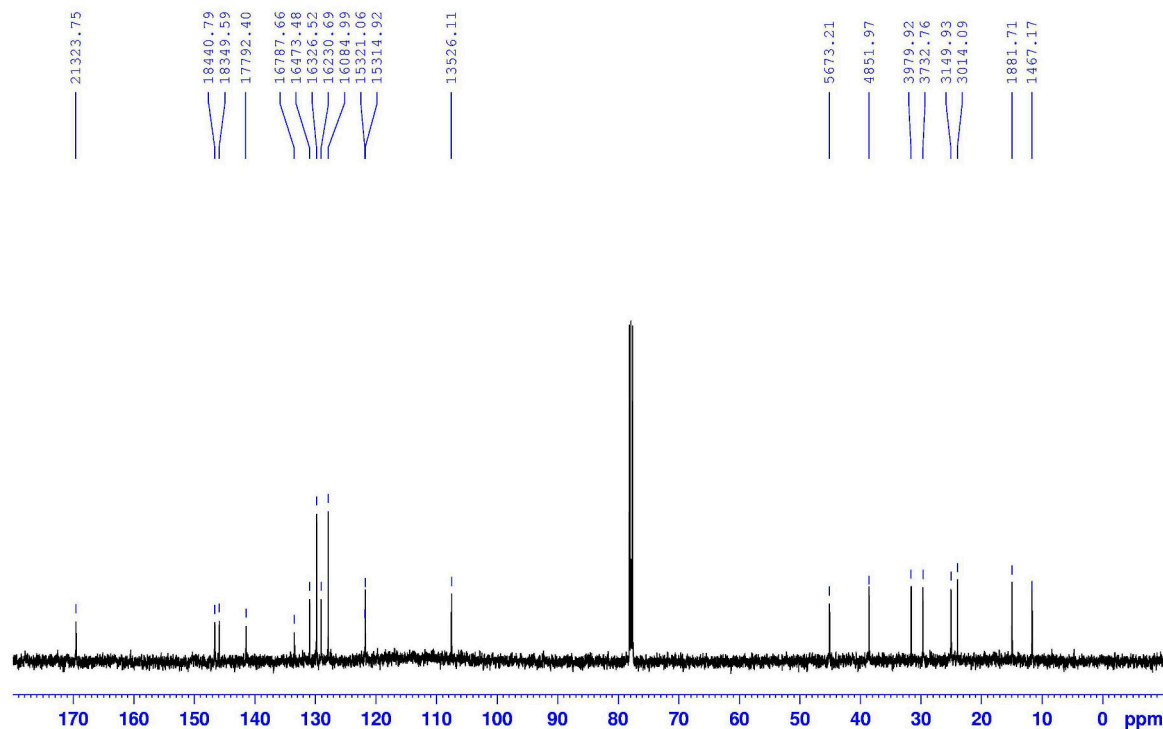
Anal. calcd. for $C_{44}H_{50}N_2O_2$: C, 82.72; H, 7.89; N, 4.38. Found: C, 83.01; H, 8.16; N, 4.16.

Synthesis of 6,6'-di(5'-hexyl-2,2-bithiophene-5-yl)-N,N'-(2-ethylhexyl)-isoindigo (*19*)
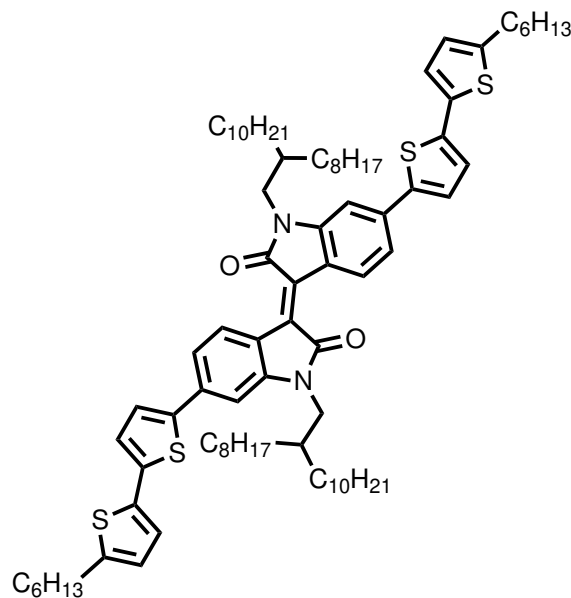
From 6,6'-dibromo-N,N'-(2-ethylhexyl)-isoindigo (322 mg, 0,5 mmol), 5-hexyl-2,2-bithiophene-5 boronic acid pinacol ester (565 mg, 1,5 mmol), $N(Et)_3$ (303 mg, 3,0 mmol) and $Pd(dtbpf)Cl_2$ (15 mg, 0,02 mmol) in 1,5 mL of Kolliphor EL 2% solution. Route B, purified on SiO_2 column with CH_2Cl_2:n-heptane 1:1. Dark solid, 409 mg, 62%.

^{1}H NMR (CDCl$_3$, 500 MHz): δ 0.84-0.91 (m, 18H), 1.23- 1.40 (m, 76H), 1.70 (m, 4H), 1.89 (m, 2H), 2.81 (t, J = 7.5 Hz, 4H), 3.66 (d, J = 6.91 Hz, 4H), 6.70 (d, J = 3.0 Hz, 2H), 6.89 (s, 2H), 7.04 (d, J = 3.2 Hz, 2H), 7.08 (d, J = 3.6 Hz, 2H), 7.26 (m, 2H), 7.29 (d, J = 3.6 Hz, 2H), 9.14 (d, J = 8.4 Hz, 2H).
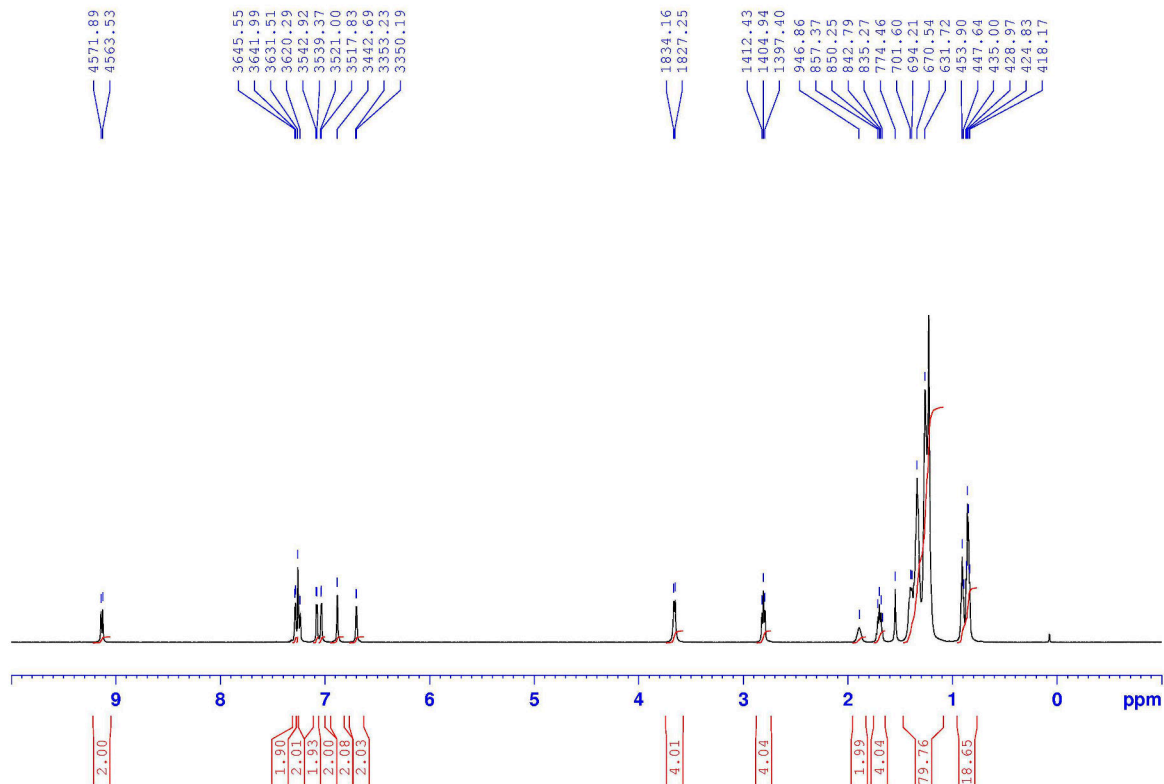
^{13}C NMR (CDCl$_3$, 125.7 MHz): δ 14.96, 14.99, 23.46, 23.56, 23.58, 27.6, 29.7, 30.2, 30.3, 30.56, 30.60, 30.9, 31.1, 32.44, 32.46, 32.68, 32.79, 32.82, 37.3, 45.3, 105.4, 119.6, 121.9, 124.7, 124.9, 125.8, 131.08, 132.56, 135.4, 138.3, 139.7, 142.9, 146.6, 147.0, 169.6.
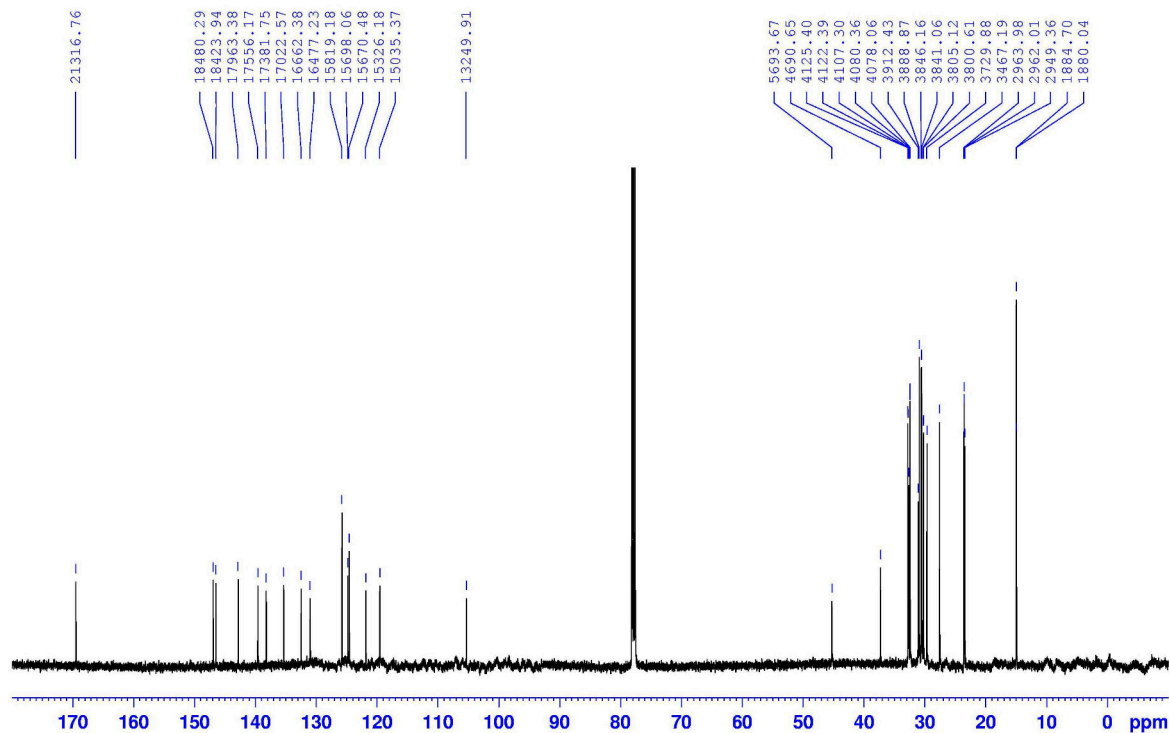
Anal. calcd. for $C_{84}H_{122}N_2O_2S_4$: C, 76.42; H, 9.32; N, 2.12. Found: C, 76.38; H, 9.48; N, 1.96.

Synthesis of N,N'-Bis(2-decyl-tetradecyl)-1,7-di(5'-hexyl-2,2-bithiophene-5-yl)-3,4,9,10-perylene diimide (*20*)
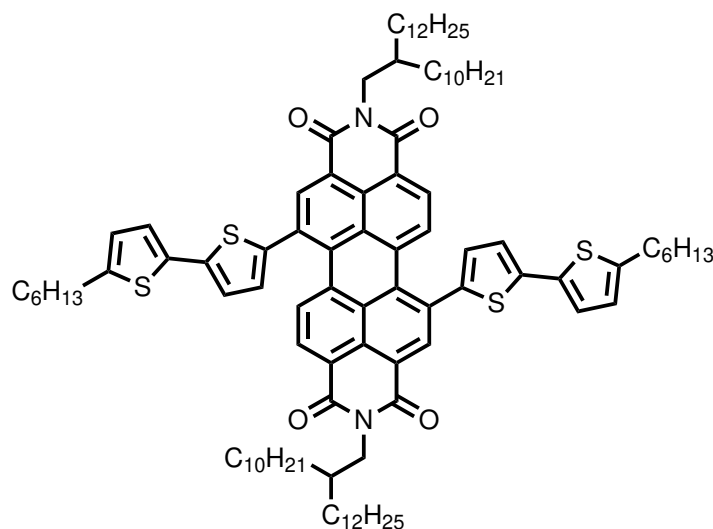
From N,N'-Bis(2-decyl-tetradecyl)-1,7-dibromo-3,4,9,10-perylene diimide (612 mg, 0,5 mmol), 5-hexyl-2,2-bithiophene-5 boronic acid pinacol ester (565 mg, 1,5 mmol), N(Et)$_3$ (303 mg, 3,0 mmol) and Pd(dtbpf)Cl$_2$ (15 mg, 0,02 mmol) in 1,5 mL of Kolliphor EL 2% solution. Route B, purified on SiO$_2$ column with AcOEt:n-heptane 1:30. Dark green solid, 546 mg, 70%.

^{1}H (CDCl$_3$, 500 MHz): δ 0.85-0.91 (m, 18H), 1.24-1.36 (m, 92H), 1.70 (m, 4H), 1.99 (m, 2H), 2.82 (t, J = 7.5 Hz, 4H), 4.12 (d, J = 7.1 Hz, 4H), 6.70 (d, J = 3.3 Hz, 2H), 7.00 (d, J = 3.4 Hz, 2H), 7.15 (d, J = 3.6 Hz, 2H), 7.23 (d, J = 3.6 Hz, 2H), 8.30 (m, 4H), 8.66 (s, 2H).
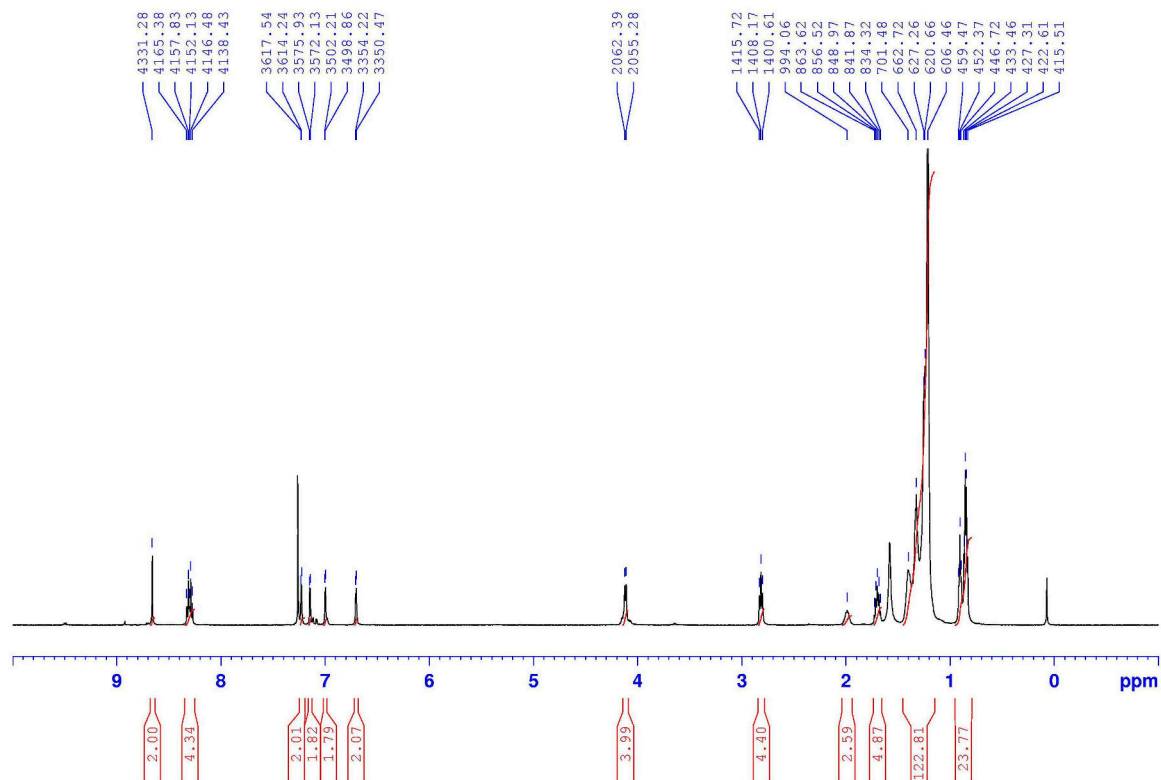
^{13}C (CDCl$_3$, 125.7 MHz): δ 15.0, 23.46, 23.56, 27.4, 29.6, 30.2, 30.53, 30.57, 30.9, 31.1, 32.45, 32.46, 32.6, 32.8, 37.5, 45.6, 123.1, 123.2, 125.1, 126.0, 128.8, 129.3, 130.2, 130.5, 130.7, 133.8, 133.9, 134.8, 135.5, 136.5, 142.0, 142.3, 147.5, 164.5.
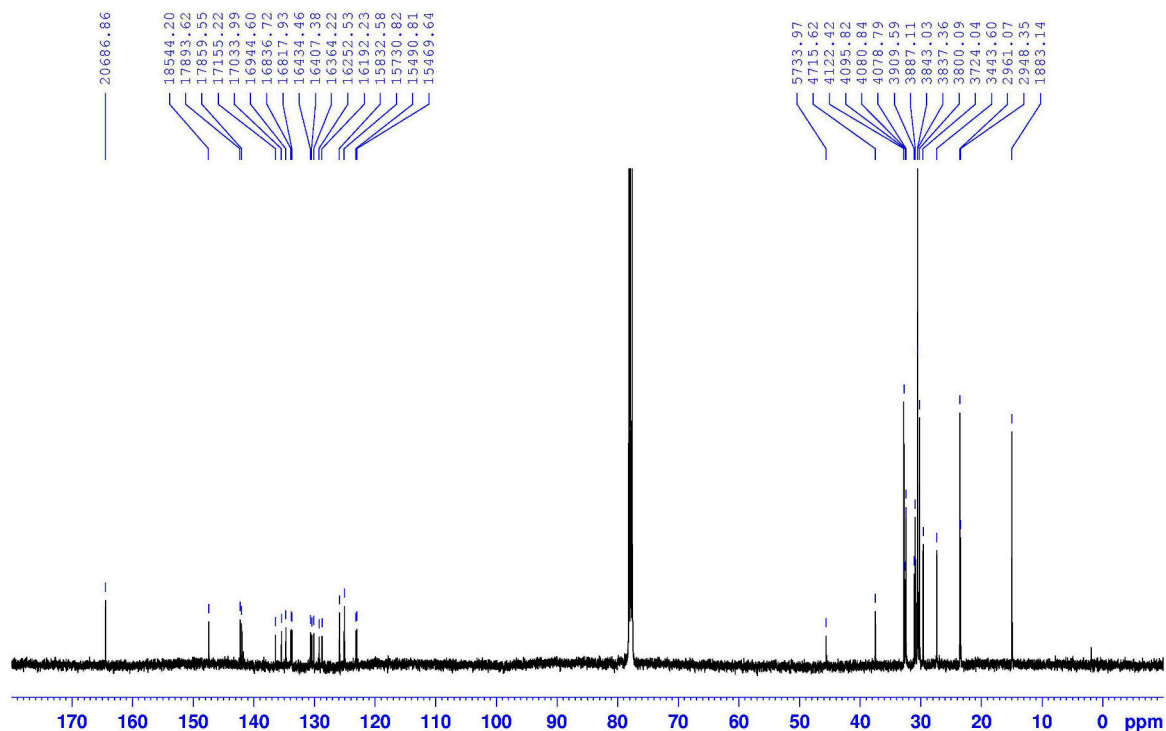
Anal. calcd. for $C_{100}H_{138}N_2O_4S_4$: C, 76.97; H, 8.91; N, 1.80. Found: C, 76.56; H, 8.95; N, 1.68.

Synthesis of Bis-DPP (*21*)
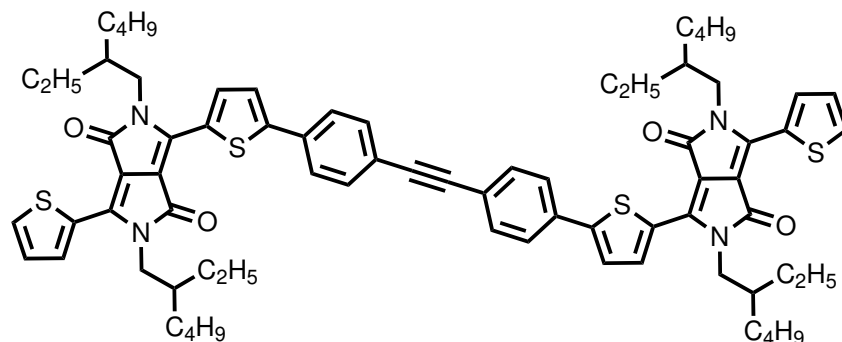
From 3-(5-bromothiophen-2-yl)-2,5-bis(2-ethylhexyl)-6-(thiophen-2-yl)pyrrolo[3,4-c]pyrrole-1,4(2H,5H)-dione (300 mg, 0,5 mmol), 4,4'-(acetylene-1,2-diyl)bis(phenylboronic acid pinacol ester) (86 mg, 0,2 mmol), N(Et)$_3$ (152 mg, 1,5 mmol) and Pd(dtbpf)Cl$_2$ (13 mg, 0,02 mmol) in 1,0 mL of Kolliphor EL 2% solution. Route B, purified on SiO$_2$ column with CH$_2$Cl$_2$:n-heptane 1:1. Dark red solid, 122 mg, 50%.

^{1}H (CDCl$_3$, 500 MHz): δ 0.85-0.94 (m, 24H), 1.25-1.43 (m, 32H), 1.87-1.93 (m, 4H), 4.00-4.12 (m, 8H), 7.28 (t, J = 7.3 Hz, 2H), 7.51 (d, J = 4.2 Hz, 2H), 7.59 (d, J = 8.4 Hz, 4H), 7.64 (s, 2H), 7.68 (d, J = 8.4 Hz, 4H), 8.90 (s, 2H), 8.95 (d, J = 4.2 Hz, 2H).
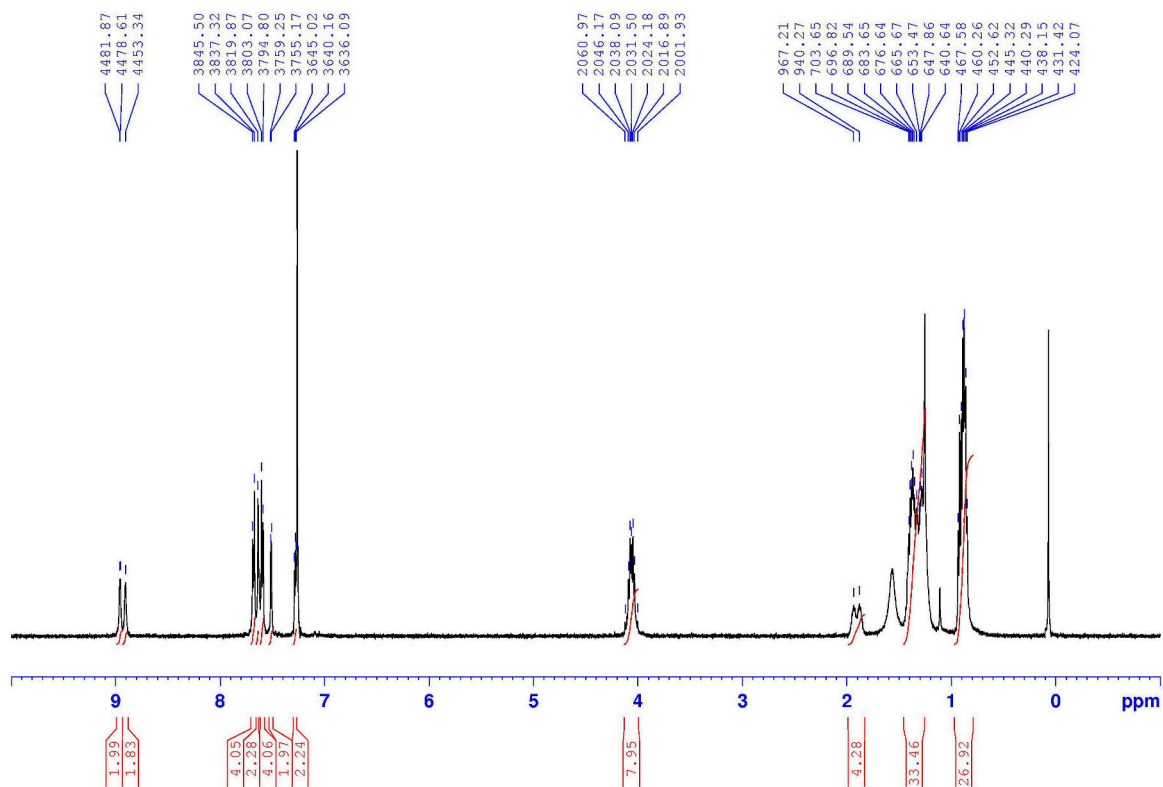
^{13}C (CDCl$_3$, 125.7 MHz): δ 1.9, 11.3, 11.4, 14.91, 14.97, 23.96, 23.99, 24.4, 24.6, 29.2, 29.5, 30.6, 31.1, 31.2, 40.0, 40.1, 46.8, 91.9, 109.0, 109.2, 124.2, 125.8, 126.8, 127.8, 129.3, 130.2, 130.7, 131.4, 133.0, 133.2, 134.0, 136.2, 137.6, 140.8, 141.1, 149.5, 162.5, 162.6.
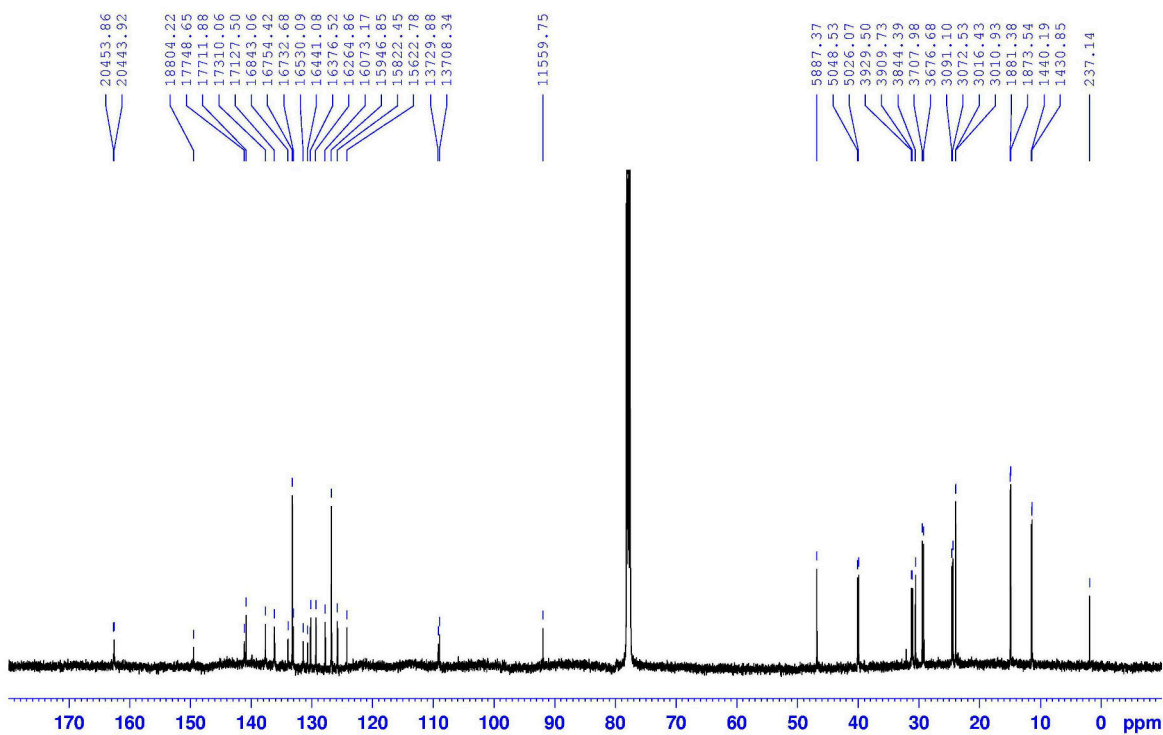
Anal. calcd. for $C_{74}H_{86}N_4O_4S_4$: C, 72.63; H, 7.08; N, 4.58. Found: C, 72.56; H, 7.15; N, 4.50.

Characterization of 9-(2-methoxynaphthalen-6-yl) anthracene
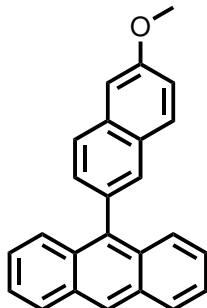
^{1}H (CDCl$_3$, 500 MHz): δ 4.02 (s, 3H), 7.26 (dd, J1 = 8.8 Hz, J2 = 2.6 Hz, 1H), 7.31-7.35 (m, 3H), 7.45-7.49 (m, 2H), 7.53 (dd, J_1 = 8.4 Hz, J_2 = 1.8 Hz,, 1H), 7.71-7.72 (m, 2H), 7.80 (d, J = 8.8 Hz, 1H), 7.86 (m, 1H), 7.95 (d, J = 8.3 Hz, 1H), 8.08 (d, J = 8.8 Hz, 2H), 8.53 (s, 1H).
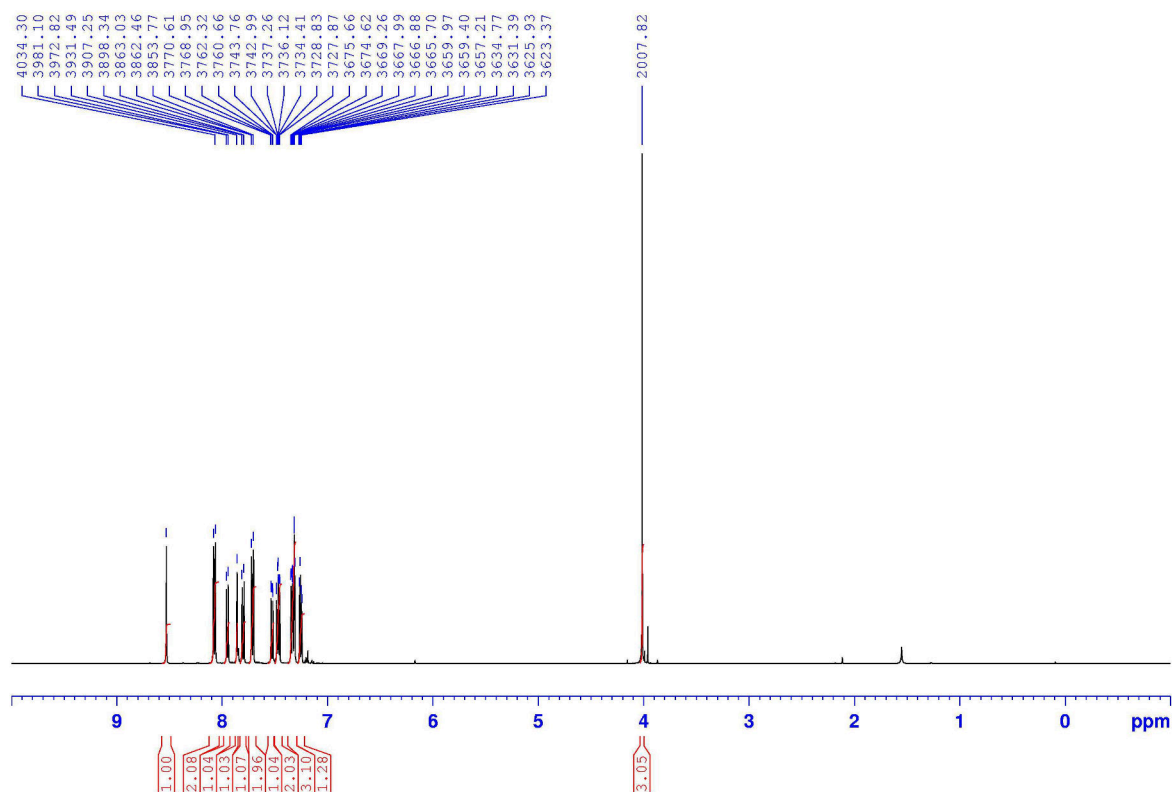
^{13}C (CDCl$_3$, 125.7 MHz): δ 56.3, 106.7, 120.1, 126.0, 126.2, 127.4, 127.6, 127.8, 129.3, 129.8, 130.5, 130.87, 130.94, 131.4, 132.3, 134.8, 134.9, 137.9, 158.9.
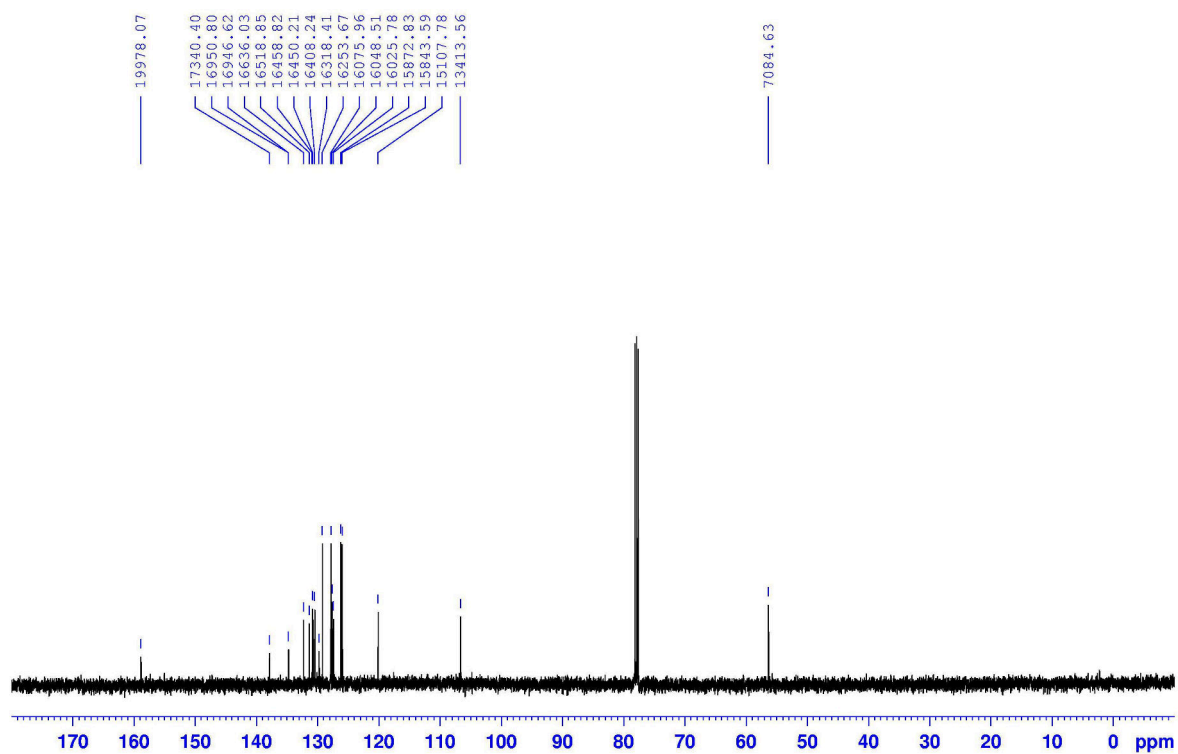
Anal. calcd. for $C_{25}H_{18}O$: C, 89.79; H, 5.43. Found: C, 89.92; H, 5.39.

Bibliography

[1] http://nepis.epa.gov/Exe/ZyPDF.cgi/P1004H5E.PDF?Dockey=P1004H5E.PDF. Accessed 26-12-2017.

[2] Anastas, P. and Warner, J. *Green Chemistry: Theory and Practice.* Oxford University Press, **1998**. ISBN 978-0-19-850234-0.

[3] Tang, S. L. Y., Smith, R. L., and Poliakoff, M. *Green Chem.* **2005**, *7*, 761–762. doi: 10.1039/B513020B.

[4] Anastas, P. and Eghbali, N. *Chem. Soc. Rev.* **2010**, *39*, 301–312. doi: 10.1039/B918763B.

[5] Henderson, R. K., Constable, D. J. C., and Jiménez-González, C. *Green Chemistry Metrics*, in *Green Chemistry in the Pharmaceutical Industry.* Wiley-VCH Verlag GmbH & Co. KGaA, **2010**, pp. 21–48. ISBN 978-3-527-62968-8.

[6] Albini, A. and Protti, S. *Paradigms in Green Chemistry and Technology.* Springer International Publishing, **2016**. ISBN 978-3-319-25895-9.

[7] Lipshutz, B. H., Isley, N. A., Fennewald, J. C., and Slack, E. D. *Angew. Chem., Int. Ed.* **2013**, *52*, 10952–10958. doi: 10.1002/anie.201302020.

[8] Shaughnessy, K. H. *Greener Approaches to Cross-Coupling*, chap. 14, in *New Trends in Cross-Coupling: Theory and Applications.* The Royal Society of Chemistry, **2015**, pp. 645–696. ISBN 978-1-84973-896-5.

[9] Duynstee, E. F. J. and Grunwald, E. *J. Am. Chem. Soc.* **1959**, *81*, 4540–4542. doi: 10.1021/ja01526a025.

[10] Duynstee, E. F. J. and Grunwald, E. *J. Am. Chem. Soc.* **1959**, *81*, 4542–4548. doi: 10.1021/ja01526a026.

[11] Bunton, C. A., Fendler, E. J., Sepulveda, G. L., and Yang, K.-U. *J. Am. Chem. Soc.* **1968**, *90*, 5512–5518. doi: 10.1021/ja01022a033.

[12] Bunton, C. A. and Robinson, L. *J. Am. Chem. Soc.* **1968**, *90*, 5972–5979. doi: 10.1021/ja01024a005.

[13] Fendler, J. H. and Fendler, E. J. *Catalysis in Micellar and Macromolecular Systems.* Academic Press, **1975**. ISBN 978-0-12-252850-7.

[14] Bunton, C. A. and Savelli, G. *Organic Reactivity in Aqueous Micelles and Similar Assemblies*, vol. 22 of *Advances in Physical Organic Chemistry* (edited by V. Gold and D. Bethell). Academic Press, **1986**, pp. 213–309. doi: 10.1016/S0065-3160(08)60169-0.

[15] Taşcioğlu, S. *Tetrahedron* **1996**, *52*, 11113–11152. doi: 10.1016/0040-4020(96)00669-2.

[16] Niyaz, M. *Micellar Catalysis*, vol. 133 of *Surfactant Science.* CRC Press, **2006**, ISBN 978-1-57444-490-2.

[17] Berezin, I. V., Martinek, K., and Yatsimirskii, A. K. *Russ. Chem. Rev.* **1973**, *42*, 787. doi: 10.1070/RC1973v042n10ABEH002744.

[18] Davies, D. M., Gillitt, N. D., and Paradis, P. M. *J. Chem. Soc., Perkin Trans. 2* **1996**, *0*, 659–666. doi: 10.1039/P29960000659.

[19] Behme, M. T. A. and Cordes, E. H. *J. Am. Chem. Soc.* **1965**, *87*, 260–265. doi: 10.1021/ja01080a022.

[20] Matsui, Y. and Orchin, M. *J. Organomet. Chem.* **1983**, *244*, 369–373. doi: 10.1016/0022-328X(83)80045-X.

[21] Bassetti, M., Cerichelli, G., and Floris, B. *Gazz. Chim. Ital.* **1991**, *121*, 527–532.

[22] Peng, Y.-Y., Ding, Q.-P., Li, Z., Wang, P. G., and Cheng, J.-P. *Tetrahedron Lett.* **2003**, *44*, 3871–3875. doi: 10.1016/S0040-4039(03)00692-0.

[23] Lipshutz, B. H. and Ghorai, S. *Org. Lett.* **2012**, *14*, 422–425. doi: 10.1021/ol203242r.

[24] Otto, S., Engberts, J. B., and Kwak, J. C. *J. Am. Chem. Soc.* **1998**, *120*, 9517–9525. doi: 10.1021/ja9816537.

[25] Dwars, T., Paetzold, E., and Oehme, G. *Angew. Chem., Int. Ed.* **2005**, *44*, 7174–7199. doi: 10.1002/anie.200501365.

[26] Lipshutz, B. H. and Ghorai, S. *Aldrichimica Acta* **2012**, *45*, 3–16.

[27] Lipshutz, B. H. and Ghorai, S. *Green Chem.* **2014**, *16*, 3660–3679. doi: 10.1039/C4GC00503A.

[28] La Sorella, G., Strukul, G., and Scarso, A. *Green Chem.* **2015**, *17*, 644–683. doi: 10.1039/C4GC01368A.

[29] Duplais, C., Krasovskiy, A., and Lipshutz, B. H. *Organomet.* **2011**, *30*, 6090–6097. doi: 10.1021/om200846h.

[30] Motoda, D., Kinoshita, H., Shinokubo, H., and Oshima, K. *Angew. Chem., Int. Ed.* **2004**, *43*, 1860–1862. doi: 10.1002/anie.200353123.

[31] Minkler, S. R. K., Isley, N. A., Lippincott, D. J., Krause, N., and Lipshutz, B. H. *Org. Lett.* **2014**, *16*, 724–726. doi: 10.1021/ol403402h.

[32] Ganguly, N. C. and Barik, S. K. *Synthesis* **2009**, *2009*, 1393–1399. doi: 10.1055/s-0028-1088023.

[33] Cavarzan, A., Scarso, A., Sgarbossa, P., Michelin, R. A., and Strukul, G. *ChemCatChem* **2010**, *2*, 1296–1302. doi: 10.1002/cctc.201000088.

[34] Bahrami, K., Khodaei, M. M., and Abbasi, J. *Synthesis* **2012**, *44*, 316–322. doi: 10.1055/s-0031-1289628.

[35] Saha, R., Ghosh, A., and Saha, B. *Chem. Eng. Sci.* **2013**, *99*, 23–27. doi: 10.1016/j.ces.2013.05.043.

[36] Denis, C., Laignel, B., Plusquellec, D., Le Marouille, J.-Y., and Botrel, A. *Tetrahedron Lett.* **1996**, *37*, 53–56. doi: 10.1016/0040-4039(95)02094-2.

[37] Das, D., Roy, S., and Das, P. K. *Org. Lett.* **2004**, *6*, 4133–4136. doi: 10.1021/ol0481176.

[38] Huang, S., Voigtritter, K. R., Unger, J. B., and Lipshutz, B. H. *Synlett* **2010**, *2010*, 2041–2044. doi: 10.1055/s-0030-1258540.

[39] Kumar, L., Mahajan, T., and Agarwal, D. D. *Ind. Eng. Chem. Res.* **2012**, *51*, 2227–2234. doi: 10.1021/ie2022916.

[40] Turro, N. J., Cox, G. S., and Paczkowski, M. A. *Photochemistry in Micelles*, in *Photochemistry and Organic Synthesis*. Springer-Verlag Berlin Heidelberg, **1985**, pp. 57–97. ISBN 978-3-540-15141-8.

[41] Forrest, S. R. *Nature* **2004**, *428*, 911–918. doi: 10.1038/nature02498.

[42] Po, R., Bernardi, A., Calabrese, A., Carbonera, C., Corso, G., and Pellegrino, A. *Energy Environ. Sci.* **2014**, *7*, 925. doi: 10.1039/c3ee43460e.

[43] Marrocchi, A., Facchetti, A., Lanari, D., Petrucci, C., and Vaccaro, L. *Energy Environ. Sci.* **2016**, *9*, 763–786. doi: 10.1039/C5EE03727A.

[44] Cho, J., Yu, S. H., and Chung, D. S. *J. Mater. Chem. C* **2017**, *5*, 2745–2757. doi: 10.1039/c6tc05535d.

[45] Miyaura, N. and Suzuki, A. *Chem. Rev.* **1995**, *95*, 2457–2483. doi: 10.1021/cr00039a007.

[46] Miyaura, N., Yamada, K., and Suzuki, A. *Tetrahedron Lett.* **1979**, *20*, 3437–3440. doi: 10.1016/S0040-4039(01)95429-2.

[47] Han, F.-S. *Chem. Soc. Rev.* **2013**, *42*, 5270–5298. doi: 10.1039/C3CS35521G.

[48] Yang, C.-T., Zhang, Z.-Q., Liu, Y.-C., and Liu, L. *Angew. Chem., Int. Ed.* **2011**, *50*, 3904–3907. doi: 10.1002/anie.201008007.

[49] Hatakeyama, T., Hashimoto, T., Kathriarachchi, K. K. A. D. S., Zenmyo, T., Seike, H., and Nakamura, M. *Angew. Chem., Int. Ed.* **2012**, *51*, 8834–8837. doi: 10.1002/anie.201202797.

[50] Handa, S., Wang, Y., Gallou, F., and Lipshutz, B. H. *Science* **2015**, *349*, 1087–1091. doi: 10.1126/science.aac6936.

[51] Na, Y., Park, S., Han, S. B., Han, H., Ko, S., and Chang, S. *J. Am. Chem. Soc.* **2004**, *126*, 250–258. doi: 10.1021/ja038742q.

[52] Weires, N. A., Baker, E. L., and Garg, N. K. *Nat. Chem.* **2016**, *8*, 75–79. doi: 10.1038/nchem.2388.

[53] de Souza, A. L. F., Silva, A. d. C., and Antunes, O. A. C. *Appl. Organomet. Chem.* **2009**, *23*, 5–8. doi: 10.1002/aoc.1455.

[54] Banik, B., Tairai, A., Shahnaz, N., and Das, P. *Tetrahedron Lett.* **2012**, *53*, 5627–5630. doi: 10.1016/j.tetlet.2012.08.026.

[55] Feng, X., Yan, M., Zhang, T., Liu, Y., and Bao, M. *Green Chem.* **2010**, *12*, 1758–1766. doi: 10.1039/C004250A.

[56] Jiang, N. and Ragauskas, A. *Tetrahedron Lett.* **2006**, *47*, 197–200. doi: 10.1016/j.tetlet.2005.10.158.

[57] Arcadi, A., Cerichelli, G., Chiarini, M., Correa, M., and Zorzan, D. *Eur. J. Org. Chem.* **2003**, *2003*, 4080–4086. doi: 10.1002/ejoc.200300356.

[58] Bhattacharya, S., Srivastava, A., and Sengupta, S. *Tetrahedron Lett.* **2005**, *46*, 3557–3560. doi: 10.1016/j.tetlet.2005.03.118.

[59] Saha, D., Chattopadhyay, K., and Ranu, B. C. *Tetrahedron Lett.* **2009**, *50*, 1003–1006. doi: 10.1016/j.tetlet.2008.12.063.

[60] Handa, S., Andersson, M. P., Gallou, F., Reilly, J., and Lipshutz, B. H. *Angew. Chem., Int. Ed.* **2016**, *55*, 4914–4918. doi: 10.1002/anie.201510570.

[61] Lipshutz, B. H., Ghorai, S., Abela, A. R., Moser, R., Nishikata, T., Duplais, C., Krasovskiy, A., Gaston, R. D., and Gadwood, R. C. *J. Org. Chem.* **2011**, *76*, 4379–4391. doi: 10.1021/jo101974u.

[62] Klumphu, P. and Lipshutz, B. H. *J. Org. Chem.* **2014**, *79*, 888–900. doi: 10.1021/jo401744b.

[63] http://www.fda.gov/food/ingredientspackaginglabeling/foodadditivesingredients/ucm091048.htm. Accessed 26-12-2017.

[64] Petros, R. A. and De Simone, J. M. *Nat. Rev. Drug Discov.* **2010**, *9*, 615–627. doi: 10.1038/nrd2591.

[65] Lin, Y., Li, Y., and Zhan, X. *Chem. Soc. Rev.* **2012**, *41*, 4245–4272. doi: 10.1039/C2CS15313K.

[66] Mishra, A. and Bäuerle, P. *Angew. Chem., Int. Ed.* **2012**, *51*, 2020–2067. doi: 10.1002/anie.201102326.

[67] Adamo, C., Amatore, C., Ciofini, I., Jutand, A., and Lakmini, H. *J. Am. Chem. Soc.* **2006**, *128*, 6829–6836. doi: 10.1021/ja0569959.

[68] Lipshutz, B. H., Gallou, F., and Handa, S. *ACS Sustainable Chem. Eng.* **2016**, *4*, 5838–5849. doi: 10.1021/acssuschemeng.6b01810.

[69] Rooney, M., Mattiello, S., Stara, R., Sanzone, A., Brazzo, P., Sassi, M., and Beverina, L. *Dyes and Pigments* **2018**, *149*, 893–901. doi: 10.1016/j.dyepig.2017.11.044.

[70] Hassan, J., Hathroubi, C., Gozzi, C., and Lemaire, M. *Tetrahedron* **2001**, *57*, 7845–7855. doi: 10.1016/S0040-4020(01)00752-9.

[71] Ishikura, M., Oda, I., and Terashima, M. *Heterocycles* **1985**, *23*, 2375–2386. doi: 10.3987/R-1985-09-2375.

[72] Dumouchel, S., Mongin, F., Trécourt, F., and Quéguiner, G. *Tetrahedron* **2003**, *59*, 8629–8640. doi: 10.1016/j.tet.2003.06.001.

[73] Hogan, A.-M. L. and O'Shea, D. F. *Org. Lett.* **2006**, *8*, 3769–3772. doi: 10.1021/ol061348n.

[74] Tamao, K., Kodama, S., Nakajima, I., Kumada, M., Minato, A., and Suzuki, K. *Tetrahedron* **1982**, *38*, 3347–3354. doi: 10.1016/0040-4020(82)80117-8.

[75] Molander, G. A. and Biolatto, B. *Org. Lett.* **2002**, *4*, 1867–1870. doi: 10.1021/ol025845p.

[76] Lois, S., Florès, J.-C., Lère-Porte, J.-P., Serein-Spirau, F., Moreau, J. J. E., Miqueu, K., Sotiropoulos, J.-M., Baylère, P., Tillard, M., and Belin, C. *Eur. J. Org. Chem.* **2007**, *2007*, 4019–4031. doi: 10.1002/ejoc.200601114.

[77] Mizuho, K., Jun-ichi, M., Kentaro, O., Hiroshi, S., and Nobuhiro, K. *Chem. Lett.* **2013**, *42*, 891–893. doi: 10.1246/cl.130365.

[78] Yagodkin, E. and Douglas, C. J. *Tetrahedron Lett.* **2010**, *51*, 3037–3040. doi: 10.1016/j.tetlet.2010.03.121.

[79] Zheng, S. and Shi, J. *Chem. Mater.* **2001**, *13*, 4405–4407. doi: 10.1021/cm0103702.

[80] Kwit, M., Skowronek, P., Kołbon, H., and Gawroński, J. *Chirality* **2005**, *17*, S93–S100. doi: 10.1002/chir.20119.

[81] Aldakov, D., Palacios, M. A., and Anzenbacher, P. *Chem. Mater.* **2005**, *17*, 5238–5241. doi: 10.1021/cm050985p.

[82] Kitamura, C., Tanaka, S., and Yamashita, Y. *Chem. Mater.* **1996**, *8*, 570–578. doi: 10.1021/cm950467m.

Chapter 4

Stabilization of micellar structures

The whole is more than the sum of the parts.

Aristotele
Metaphysica

A stellar dodecahedron is placed in the center and is enclosed in a translucent sphere like a soap bubble. This symbol of order and beauty reflects the chaos...

M. C. Escher on "Order and Chaos"
The Graphic Work Of M. C. Escher

The work presented in this chapter is wide, and might look like a bit cluttered and somewhat pioneering. It is. These are the results I am most proud of, even if they are definitely not the most scientifically relevant obtained. The work presented here was realized with the precious help of two enthusiastic master students, and what they taught me are the most important lessons I learnt within the whole PhD -resilience, teamwork, the art of finding makeshift solutions. And the importance of serendipity as well.

As already stated, a micelle is an associative colloid with a defined lifetime: each surfactant molecule continuously aggregates and disaggregates with other molecules, leading to formation and disruption of micelles within the dispersion. Even if, in many cases, this is not a relevant matter, there are applications for which one would need stable objects, or the possibility to take advantage of micelles properties out of the solution.

In this chapter, a method to stabilize micellar of non-ionic surfactant aggregates is discussed. The obtained micellar aggregates show improved stability to both dilution and temperature, indicative of a successful stabilization, and preliminary tests suggest they are suitable to build organic nanocrystals.

4.1 Micellar dynamics

As described in the previous chapters, in aqueous solutions surfactants self-associate into micelles at a concentration above the critical micellar concentration (cmc). The formation of micelles is therefore a cooperative process that can be described by the mass action law. Micelles can be considered as chemical species in equilibrium with free (non-micellized) surfactant; when a micellar dispersion is diluted below the cmc, the micelles disappeared within seconds. This is a description of the average equilibrium state of the system, but it says nothing about the dynamics of surfactant molecules within the dispersion.

The first investigation of dynamic properties in a micellar dispersion was performed in 1966 by means of the temperature-jump (T-jump) technique, which allowed to observe a relaxation process associated with micellar equilibria.[1] This process was assigned to the reversible exit (or dissociation) of one surfactant molecule from the micelle (also considered as the process of exchange of one surfactant molecule between two micelles). It is often referred to as surfactant exchange. Only twelve years later, in 1974, a pressure-jump and shock-tube study showed unambiguously that micellar solutions are characterized by two well separated relaxation processes, with way different relaxation times.[2] Several authors independently assigned the fast process to surfactant exchange, and the slow process to the micelle formation/breakdown. In the following months, Aniansson and Wall derived the first analytical expressions of the relaxation times characterizing the two processes based on this assignment,[3, 4] a treatment that was later refined and extended to ionic surfactant micelles and mixed micelles systems.[5–7] More recent studies of micellar dynamics concern aqueous solutions of gemini surfactants and amphiphilic block copolymers, as the behavior these species deviate from that reported for conventional surfactants.[8, 9]

Other processes may occur in micellar dispersions: internal motion of the surfactant alkyl chains within the micelles; exchange of counterions between free and micelle-bound states; and fast changes of micelle shape. In the case of solubilized systems (micellar solutions that have solubilized compounds that are sparingly soluble in water), the solubilizate may exchange between micelles and the aqueous pseudophase.[10]

We are not going to report the mathematical description of micellar dynamics, which is a difficult subject and fall out the scope of the work, especially because we had no means to characterize the relaxation times of the examined systems, which is typically done by stop-flow, T/p-jump, or ultrasonic absorption techniques.[10, 11] We will just report that typical relaxation times for surfactant exchange between micelles (τ_1) fall in the microseconds order of magnitude, while micellar formation/breakdown relaxation time (τ_2) might span from milliseconds to minutes depending on the surfactant nature (it is longer for non-ionic surfactants than for ionic).[12] For concentrations much higher than the cmc, micellar lifetime T_M can be calculated from the measured relaxation time τ_2 and aggregation number (a_M) as[13]

$$T_M \approx a_M \cdot \tau_2 \tag{4.1}$$

4.2   Surfmers, polysoaps and stabilization of micellar structures

In many cases, the existence of micellar dynamics is something one can forget about, as the properties of interest of the system arise from average conditions (such as for UC micelles in Chapter 2 and nanoreactors in Chapter 3). However, this is not always the case. As at the forefront of nanotechnology is the request to develop easily accessible reaction and templating media, offering compositional and/or architectural control on a nanometer scale, conventional self-assembled surfactants, due to their dynamic nature, are of limited use. Polymerizable surfactants ('surfmers'), on the other hand, offer potential for developing hybrid nanosized reaction and templating media with constrained geometries.

Early studies on surfmers and polymerized micelles can be tracked back to 1979, when γ-irradiation was used to polymerize micelles of sodium undecenoate,[14] and the interest for the obtained structures remained high for the following years. Many studies proved the benefits obtained from the use of polymerized micelles with respect to their unpolymerized counterparts. For example, Boutevin proved that hydrolysis of p-nitrophenyl hexanoate in surfmers based micelles depended on the polymerization degree, being more efficient in polymerized micelles due to a better solubilization of the substrate and a higher catalytic activity.[15] Stäler developed multicomponent polymeric micelles, formed by well-segregated hydrophobic hydro- and fluorocarbon domains along a hydrophilic polyacrylamide backbone, capable of specific solubilization of mutually incompatible hydrophobic compounds.[16, 17] Today, studies focus on the use of surfmers for the stabilization of emulsions,[18–20] synthesis and stabilization of polymeric nanoparticles,[21, 22] preparation of hydrogels,[23, 24] and some papers are appearing on the preparation of somewhat more exotic materials, such as hybrid or fluorescent particles.[25, 26]

Morphology of the obtained material after the polymerization is extremely dependent on the components employed during synthesis. In the case of polymerization of surfmer micelles, however, it is nearly never the case that intramicellar (topological) polymerization can be obtained. In fact, monomer exchange between micelles (characteristic times of $10^{-5} - 10^{-9}$ s) is usually way faster than the rate of chain propagation (characteristic times of $10^{-2} - 10^{-6}$ s), implying that monomer exchange occurs during polymerization.[27]
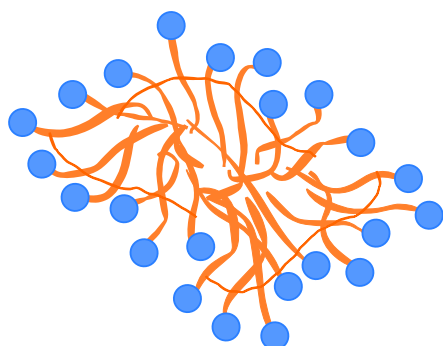
Figure 4.1 Cartoon of a polysoap as described in [27]

A more realistic representation might be the formation of a "polysoap", a self-assembled structure formed by oligomeric species that exhibits micellar-like physical properties, a cartoon of which is shown in figure 4.1. Evidences of this behaviour have been reported, for example, by Kline,[28] which, following the evolution of the system microstructure through small-angle neutron scattering, demonstrated that cetyltrimethylammonium 4-vinylbenzoate rod-like micelles preserved only partially their shape after polymerization, resulting in interpolymerized cylinders. These polymerized aggregates were reported to be insensitive to temperature changes and dilution, whereas their parent rod-like structures rearrange to spherical micelles at elevated temperatures. In many cases, polysoaps are also polyelec-

trolytes, as the starting surfmers are ionic species.[29] In more recent times, polysoaps gained attention as "compartmentalized" micellar systems,[30, 31] which have been used as compatibilizers[32, 33] and, recently, proved to be a suitable dispersant medium for donor-acceptor couples to build multilayer photoactive nanostructures.[34] These last finding primarily moved our interest.

As final consideration, we did not linger on polymerized/crosslinked micelles based on di- or tri-block copolymers. We want to underline that these are way different type of structures, with a different dynamic behaviour with respect to small-molecule based micelles, developed to obtain intrapolymerized, "monodisperse" objects. They are nano-objects by themselves, mainly developed as smart nano-carriers, not a platform to operate at the nanoscale.

4.3 Loading and localization of small molecules in micellar systems

Whatever the application for the stabilized system, one might probably want it to interact with other (organic) species. The basic interaction rule is, obviously, *like prefers like*.[35] Thus, the fist parameter to consider is the partition coefficient of the considered molecule between water and the micelle. For example, ionic species will likely partition in water if the chosen surfactant has their same charge or is nonionic, but will interact with micelles if they have an opposite charge. Decreasing the polarity, the species are more likely to localize within the micelles. Although the water-micelle partition coefficient is not usually immediately accessible, it shows a linear correlation with the water-octanol partition coefficient,[36, 37] which can also be used, to some extent, to predict the localization of the solute within the micelle.[38]

4.3.1 The HLB value of surfactants

In case of high amount of liquids (2-10 vol%, depending on the liquid) are added to the dispersion, swelling of micelles occur. Depending on the liquid nature, the swollen part might be the core (in the case of apolar oils) or the palisade layer (for polar liquids). The different localization also affects the type of obtained system when more and more load is added. Addition of very high amounts (>10 vol%) of polar, hydrophilic species usually ends up in a dehydration of the surfactant corona, which causes either the surfactant demixing (due to lowering of the cmc) or its complete dissolution in the mixed solvents environment.[39, 40] Addition of apolar liquids immiscible with water, on the other side, ends up in the formation of emulsions or mini-emulsions* (provided that the system is kept under appropriate conditions, otherwise phase separation is the only result). This eventuality is extremely interesting, as it provides a perfect box for a variety of applications, from synthesis, to encapsulation, to cosmetics, to theranostics.

Individuation of proper conditions to obtain a stable emulsion instead of phase separation is not an obvious task, as it requires a careful optimization of the amount and type of surfactant with respect to both the water and oil phase, the salinity of water phase, the

---

*A mini-emulsion is a bicontinuous path formed by channels of water and oil separated by surfactant walls.[10]

eventual presence of an alcohol and, obviously, the temperature. Nonetheless, evaluation of the right operative conditions is today accessible through the use of Hydrophilic-Lipophilic Deviation (HLD) approach.[41, 42] Although more accurate, this method has not yet replaced the HLB (Hydrophilic-Lipophilic Balance) system, which is in use since its formulation by Griffin,[43] especially on an industrial level, and way simpler. This method relies on the calculation of an HLB value for surfactants, which is an indicator to chose the right one to form the emulsion. For simple nonionic surfactants, the HLB value is defined as

$$\text{HLB} = \frac{\text{molar mass of the hydrophilic part}}{\text{molar mass of the emulsifier}} \cdot 20 \qquad (4.2)$$

thus it is an indicator of the polarity of the species, and can be calculated through a simple incremental method which assigns a value to each group of the surfactant. For more complex (or ionic) surfactants, other methods have been developed to calculate the HLB value, one of the most used being the PIT (Phase Inversion Temperature) method.[42, 44]

4.3.2 Building of nanocrystals

In the opposite case, when a high amount of solid material is introduced in the dispersion, crystallization might occur, possibly within the micelles. In this case, an organic nanoparticle/nanocrystal can be obtained.

During last 20 years, we saw a boom in studies related to nanometric structures, such as inorganic crystals and quantum dots (now we are witnessing the era of perovskites, but this is a story for the next chapter). We did not see the same enthusiasm for organic nanostructures (not considering graphene, of course), mainly because the physical properties of organic molecules do not change as an effect of quantization. Nonetheless, we might take advantage from the development of organic nanocrystals in many research fields, such as medicine, sensing, catalysis and electronics.[45–51] Effects like aggregation induced fluorescence of two-photon excited fluorescence might add value to these materials, particularly for imaging applications.[52, 53]

Organic nanocrystals might show a number of interesting properties which make them suitable materials for the aforementioned applications: high sensitivity to external stimuli, ability to reversibly change morphology, size and shape tunability, facile and cost-effective synthesis. Among the preparation methods, one of the most popular is a solvent-exchange process, specifically the reprecipitation method that has been extensively developed by Nakanishi's group.[54] It consists in dissolving the chosen species in an organic solvent miscible with water (such as THF or acetone) and swiftly inject the solution in the micellar dispersion under vigorous stirring. As the organic solvent is quickly displaced by water (the antisolvent) in the nearby of organic molecules, they will migrate into the micelles to minimize interactions with the aqueous environment. A surfactant (or other amphiphile) is usually needed to prevent the aggregation of obtained nanocrystals. This method is extremely easy and versatile, as it allows to play with several parameters (temperature, concentrations, amount of solvent/antisolvent, aging time, additives) to vary the particles size and morphology. Its main drawback is that heterogeneous by size particles are usually obtained, as the growth obeys thermodynamic and kinetic processes (diffusion, Ostwald ripening).

Before the beginning of this work, we tried to prepare organic nanocrystals of a π-conjugated dye (N,N'-dioctyl quinacridone, v. *infra* figure 4.35) using simple surfactants. This molecule is particularly suitable for the task, as it has an extended, flat core able to give strong π-π interactions, and lipophilic chains to solubilize within the micelles. Figure 4.2 shows the DLS measurements of the colloidal dispersions prepared reprecipitating the dye in a micellar solution of Triton X-100 or Tween 80, collected up to a week after the synthesis. The measurements clearly show that the size distribution of the obtained objects continuously change, not allowing to obtain crystals of defined size. In the case of Triton X-100, dye precipitation was observed (both by DLS and by eye) the day after the synthesis, before efficient crystallization within the micelles could take place.
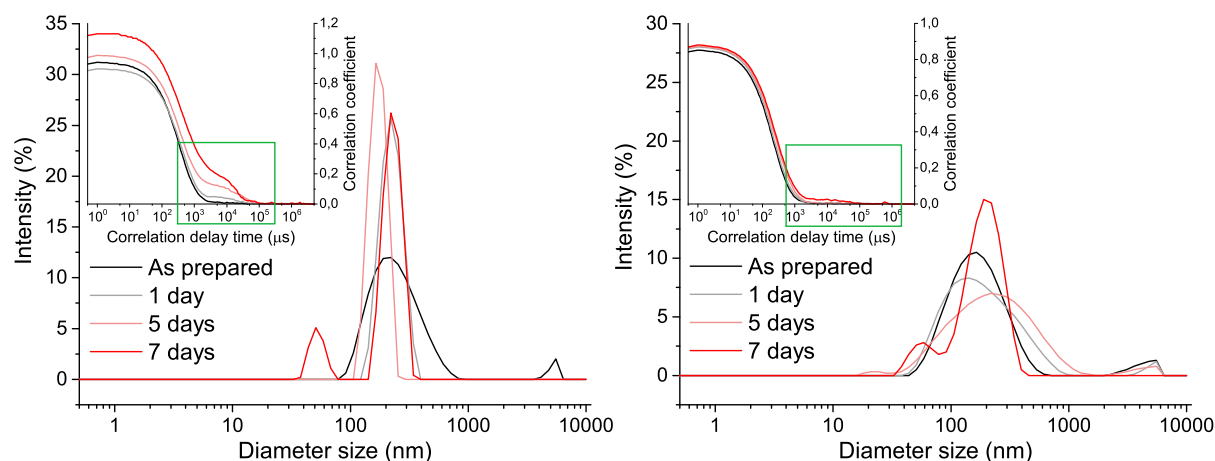
Figure 4.2 DLS measurements of a micellar dispersion of Triton X-100 (left) or Tween 80 (right) loaded with N,N'-dioctyl quinacridone. Insets show the correlograms of the measurements. In both cases, the size of the obtained particles changes over time, as micelles continuously form and disrupt, making impossible for the dyes to crystallize undisturbed. After one day (for Triton X-100) or a week (for Tween 80), precipitation of the material is detected by the measurement due to the increase in the baseline of the correlation coefficient for long correlation times, highlighted in green. A short Appendix on interpretation of DLS measurements is present at the end of the chapter.

4.4 Aim of the work

Aim of the work presented in this chapter was the development of a method to stabilize micelles, that means to create a "kinetically frozen" state for the micellar dispersion. At the same time, we wanted it to remain a "soft" and adaptable system, still able to load organic species, in order to obtain a material both removable from the dispersion and capable to give specific interactions.

Polymerization is quite a universal approach, for organic chemists, to improve the stabilization and rigidity of a system. As described previously, polymerized micellar structures are mainly based on surfmers, which dictates the ability of the final material to interact with other species. This introduces some rigidity into the system, as surfmers ability to polymerize is tied to their structure, reason why the majority of them are ionic salts.[27, 29] In order to gain more freedom on the specific interaction we wanted to insert, we decided to completely change approach to deal with the problem, in particular to decouple the surfactant from the polymerogenic unit. This is clearly an hazardous attempt, as, without chemical bonds between surfactants, nothing prevents the micelles to behave dynamically exactly as they were not polymerized. To reach the goal and also maintain the improved stability feature, we got inspired by the idea of Interpenetrated Polymer Networks (IPNs), "alloys" of cross-linked polymers, with no covalent bonds between them, which cannot be separated unless chemical bonds are broken.[55] The idea was to take advantage of the morphological characteristics of these systems, instead of direct bond formation, to form stabilized "soft" structures.

We decided to build a semi-IPN-like structure, using a classic surfactant based micelle as the "platform" around which growing a polymeric chain. To build the polymeric part of the semi-IPN, we decided to introduce a polymerizable co-surfactant within the micelles, and perform the polymerization after the dispersion. In this way, stabilization is reached as the effect of an increased difficulty for the system to disentangle.

As the outlined approach is original, the presented work is very preliminar, focused on the development of the method more than on testing applications. We will therefore show only a very small example for an application, the synthesis of organic nanoparticles, as it was convenient for a deeper characterization of the system.

4.5 Interpenetrating polymer networks

Topological studies on entangled structures form a vast field in the coordination network chemistry. Polycatenation, polythreading and polyknotting cover many of the reported strategies developed to produce "non-disentanglable" or self-penetrating motifs, three examples of which are shown in figure 4.3.

Although IPNs are not likewise visually intriguing, as they lack such a regular structure, still they do the job: creating a network which cannot be separated unless chemical bonds are broken. The combination of the polymers effectively produce an advanced multicomponent polymeric system with improved mechanical properties, and suppressed flow of the material.[57, 58] Figure 4.4 shows the structure of a classic IPN, formed by the entanglement of two crosslinked polymeric networks. However, this is not the only example of this kind of structure. Less entangled structures have also been studied, such
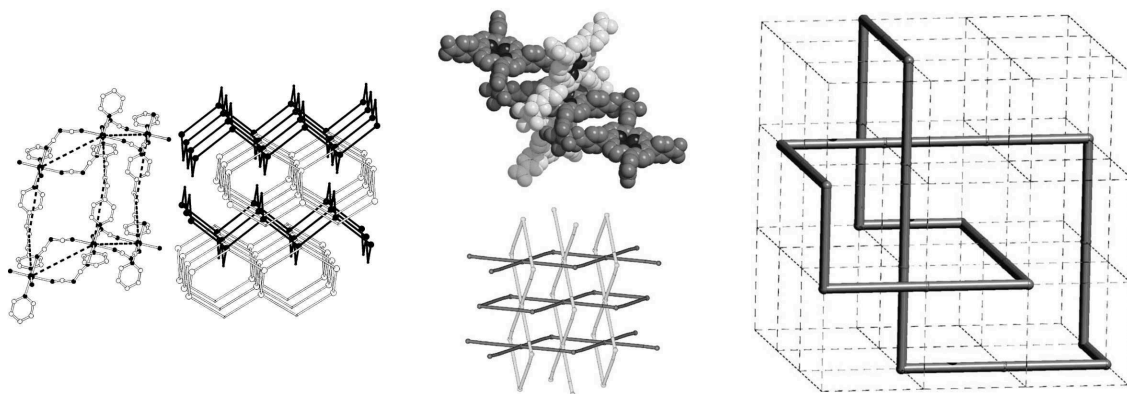
Figure 4.3 Examples of polycatenated (left), polythreaded (center), and polyknotted (right) structures. Figures are reproduced with permission from [56]. Copyright © 2003 Elsevier B.V.

as semi-IPNs, which are composed by a single crosslinked polymer, while the second one is linear or branched.

Inspired by these architectures, we thought about a "mechanically hindered" system, composed by a branched surfactant and a polymeric (linear or branched) chain. The properties we wanted to borrow from these systems are the much higher stiffness and toughness of mechanical properties with respect to the single components. The choice of a branched surfactant is quite fundamental: as we work with only one polymeric component, a linear surfactant would easily slip out from the polymerized chains. The polymer is obtained in-situ through the polymerization of a co-surfactant dispersed within the micelles.
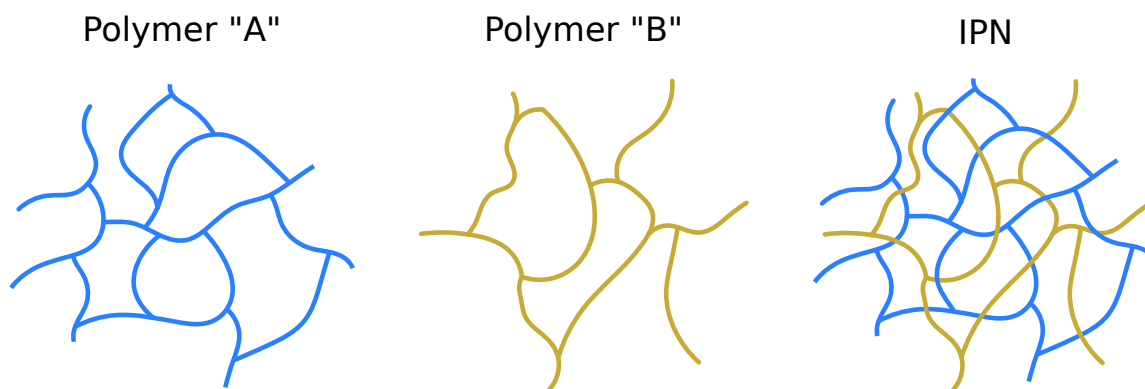
Figure 4.4 Structure of an IPN, as formed by two different crosslinked polymers. As in borromean rings, the loops cannot be disentangled without breaking the chains.

4.6   Stabilization through co-surfactant polymerization
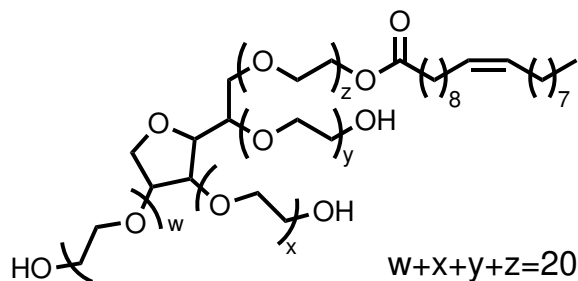
Figure 4.5 Structure of the main component of Tween 80 surfactant

average MW	~1310
composition	Oleic acid $\geq 58.0\%$ (balance primarily linoleic, palmitic, and stearic acids)
cmc	0,012 mM (0,0016%)
density	1.06 g/mL at 25 °C
clouding point	65 °C
aggregation number	60 (micellar weight ~79000 g/mol)
HLB value	15
τ_2	8-10 s

Table 4.1 Properties of Tween 80[11, 59]

Tween 80 (T80) is the surfactant we chose to realize stabilized micelles. Figure 4.5 represents the structure of its main component, table 4.1 summarizes its properties.

Tween is the name of a family of surfactants obtained from esterification of sorbitan with a fatty acid (the number following the name Tween identifies the acid), and subsequent etoxylation. Tween 80 is a mixture, whose main component presents the oleic chain, others being mainly linoleic/palmitic/stearic residues. The double bond configuration is *cis*, as in the starting oleic acid. A recent study based on quantitative ^{13}C NMR revealed that isosorbide PEGs/PEG esters and free PEGs/PEG esters are present as well.[60]

We chose this surfactant because we wanted a cheap, industrial, non-ionic product. As previously stated, the morphology of this molecule was also an important factor: the apolar portion represents only 25% of the total weight of the surfactant, arranged in a single chain, while the polar compartment is branched, thus probably more suitable to create an interpenetrated-like network.

As the 20 PEG units are distributed in four "arms", these are 5 PEG units long each on average. We used this information to design the polymerizable co-surfactant.

Using equation 4.1, micellar lifetime for T80 can be evaluated as $T_{\text{T80}} = 8 - 10$ minutes. This is quite a long time for an in-situ polymerization of a small amount (50-100) of co-surfactant molecules, giving us good chances to "freeze" the system in something that might look like a polysoap, although the loading of the co-surfactant will have an influence on the micellar lifetime.

4.6.1   Design of the co-surfactant

Figure 4.6 shows the derivative AP-E4 we designed as polymerizable co-surfactant. The polymerizable unit is a methacrylic group, very well-known and popular for the purpose.

We chose a four unit ethylene glycol (TEG) as hydrophilic chain, in order to have a molecule which could entirely localize within the palisade layer of T80. Finally, we needed and "anchor unit", lipophilic enough to keep the co-surfactant within the micelle instead of in solution. We chose to use the 2-tetrahydropyranyl prostetic group, whose addition reaction is easy from the synthetic point
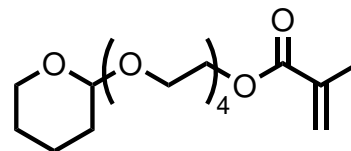
Figure 4.6 AP-E4 co-surfactant

of view, and it is more stable than linear prostetic groups. The methacrylic unit is not apolar enough to fulfill the "anchor" task: the HLB value of the unprotected molecule calculated using equation 4.2, in fact, is nearly 17, higher than that of T80, meaning that the molecule might not localize within the micelle. On the other side, HLB value of AP-E4 is around 14, lower than that of T80, thus this molecule should localize preferentially within T80 chains rather than water. Details on the synthesis are given in the Experimental section.

This derivative is quite reactive: if left at room temperature with no polymerization inhibitors for one night, it forms a colorless, jelly solid, which is the polymerization product. A scheme of the polymerization reaction is shown in figure 4.7.
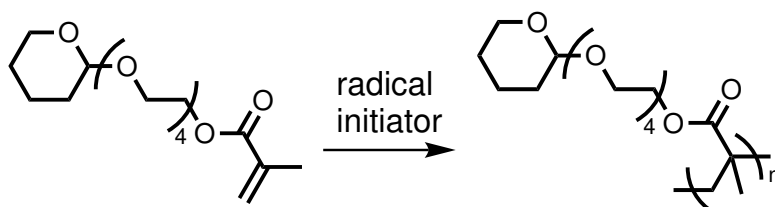
Figure 4.7 Generic radical polymerization reaction of AP-E4.

We collected IR spectra of both the AP-E4 monomer and polymer, which are shown in figure 4.8. The spectrum of the supposed polymer clearly show the disappearance of the signal relative to the methacrylic double bond, and the shift of the carbonyl peak at higher energies, consistent with a stiffening of the C=O bond, which is not conjugated anymore. We used this second feature to follow the micellar polymerization reaction (v. *infra*).

4.6.2 Characterization of AP-E4/T80 micellar dispersion

The idea of polymerizing a co-surfactant implicates the polymerizable unit will be diluted within the micelle. A trade-off is therefore needed between two opposite necessities: a high amount of co-surfactant is desirable as polymerization is more likely to occur, but if it is too high micelles will not to form, as the co-surfactant is not able to micellize by itself. We decided to use a 3:2 mixture of AP-E4 and T80, which we never changed along the work. We calculated the appropriate amount of AP-E4 on the basis of data reported in table 4.1.

To prepare the AP-E4/T80 micellar dispersion, we added the AP-E4 in a THF solution to a 0,22% dispersion of T80 in water. Further details on preparation are given in the Experimental section. Immediately after the addition of AP-E4, the transparent T80 dispersion turns milky.
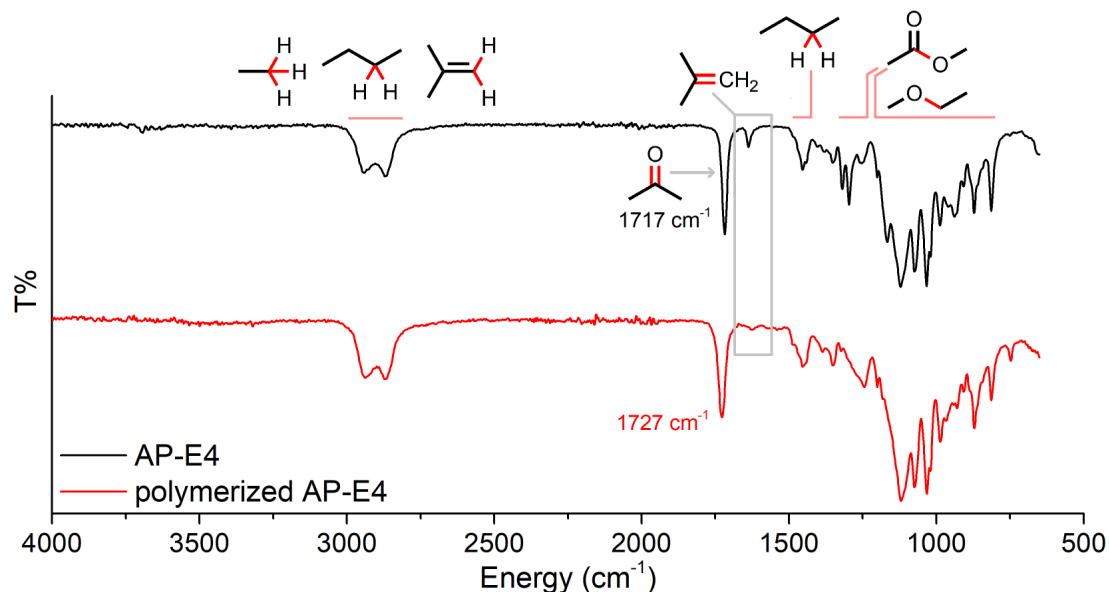
Figure 4.8 FT-IR spectra of as synthesized AP-E4 and polymerized AP-E4. The disappearance of C=C bond is highlighted in the gray rectangle, while the energy of C=O bond shifts from 1717 cm^{-1} to 1727 cm^{-1}. Other bands are assigned to corresponding bonds (for the sake of clarity, considered bonds are in red).

A DLS measurement, reported in figure 4.9, shows that the average dimensions of dispersed aggregates increase considerably, from ∼10 nm of the T80 dispersion to ∼160 nm. We hypothesized that this behaviour is due to a pre-clouding phenomenon*:[40, 61] the inclusion of polar species within the palisade layer of the micelles causes a loss of hydration, and subsequently their aggregation. Such dimensions are in fact due to formation of some sort of secondary aggregates, and obviously not to an increase in size of the single micelle.
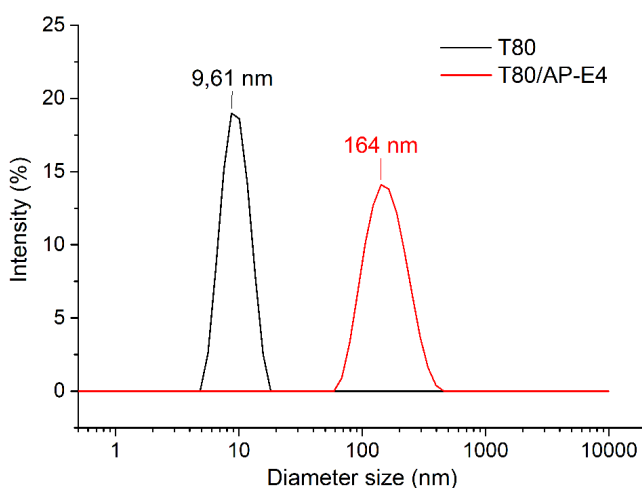
Figure 4.9 DLS measurements showing size distribution of T80 only and T80/AP-E4 dispersions

To gain information on the localization of AP-E4 within the micelles, we collected the NMR spectra of the AP-E4/T80 micellar dispersion in DMSO−d$_6$ and D$_2$O, shown in figure 4.10. As both T80 and AP-E4 are soluble in DMSO, we expected to see a well resolved spectrum in this solvent. On the other side, the system is subject to micellization and aggregation in D$_2$O, thus we expected to see broader peaks for the aggregated portions of the molecules (those present in the micellar core). Comparing the two spectra, it is clear that T80 micellized in water, as all the peaks relative to the alkylic chain are broader and less resolved. In the case of AP-E4, instead, the only peaks which change are related to the protons on the pyran ring. In particular, the peculiar splitting pattern

---

*Formation of a colloidal phase displaying a strong Tyndall effect before the effective clouding (phase separation) of the dispersion

observable in deuterated DMSO is lost in deuterated water. This change is significative: the two peaks in the range 1,6-1,8 ppm in DMSO$-$d$_6$ originate from the axial/equatorial configuration of protons labeled as 7 on the ring with respect to the PEG-ylated chain.[62] As they blend in a single peak and lose resolution of the splitting pattern in D$_2$O, the two conformations are not distinguishable, meaning that the ring is not in the isotropic environment of aqueous pseudophase. Signals of protons on the double bond, methyl group and ester (labeled as 1, 2, 3 and 4) instead, do not broad. We thus speculate that AP-E4 is dispersed within the palisade layer of T80, the pyran ring "anchorating" it to the micelle, the TEG chain and polymerizable end-group being solvated by water and T80 ethylene glycol chains.

4.6.3 Photopolymerizations, and role of compartmentalization

We firstly attempted to polymerize AP-E4 through a photopolymerization reaction. This kind of polymerization, in fact, is more suitable to micellar conditions than thermopolymerization, as higher temperatures might change the micellar organization or provoke clouding of the dispersion.

As we speculate that the cosurfactant localize within the palisade layer of the micelles, we needed to find a photoinitiator of suitable polarity to make the reaction happen. We attempted the polymerization with a number of photoinitiators and two different light sources, a mercury lamp (λ_{max}=256 nm) and a fluorescence UV-A lamp (λ_{max}=365 nm).

4.6.3.1 Light source: mercury lamp
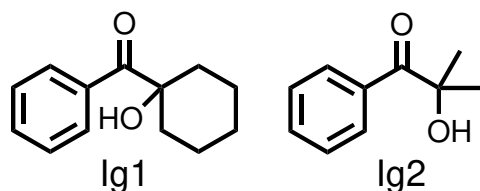
Figure 4.11 Photoinitiators paired with mercury lamp.

Two different photoinitiators were used, 1-hydroxycyclohexyl phenyl ketone and 2-hydroxy-2-methylpropiophenone (figure 4.11, Ig1 and Ig2 from now on), both featuring an absorption spectrum with maximum at $\sim$245 nm.[63] These two photoinitiators are quite popular, and their use has been reported for methylmethacrylate based monomers.[64] We preferred these over other initiators for the presence of an $-$OH group, which we thought might prove helpful to localize the molecules within the palisade layer of the micelles.

Photopolymerization setup is shown in figure 4.12. The lamp (a low pressure, 125 W mercury lamp) and the quartz reactor containing the micellar reaction are located in a wooden box with black internal walls. The reactor is located $\sim$15 cm far from the lamp. A stream of compress air, not shown in the picture, is used to avoid a raise of temperature within the chamber. Initiator is introduced as a THF solution in the micellar dispersion in a 4 mol% amount with respect to the co-surfactant. Reasons for choosing such a high concentration of initiator are discussed in the Experimental section.

The polymerization progress is checked after 3, 5 and 7 h through IR analysis. As previously stated, a shift in the carbonyl peak energy is visible when the double bond of the methyl methacrylate group reacts. In the Experimental section, IR spectra of AP-E4, T80 and their starting micellar dispersion are shown, and peaks assignment is discussed.
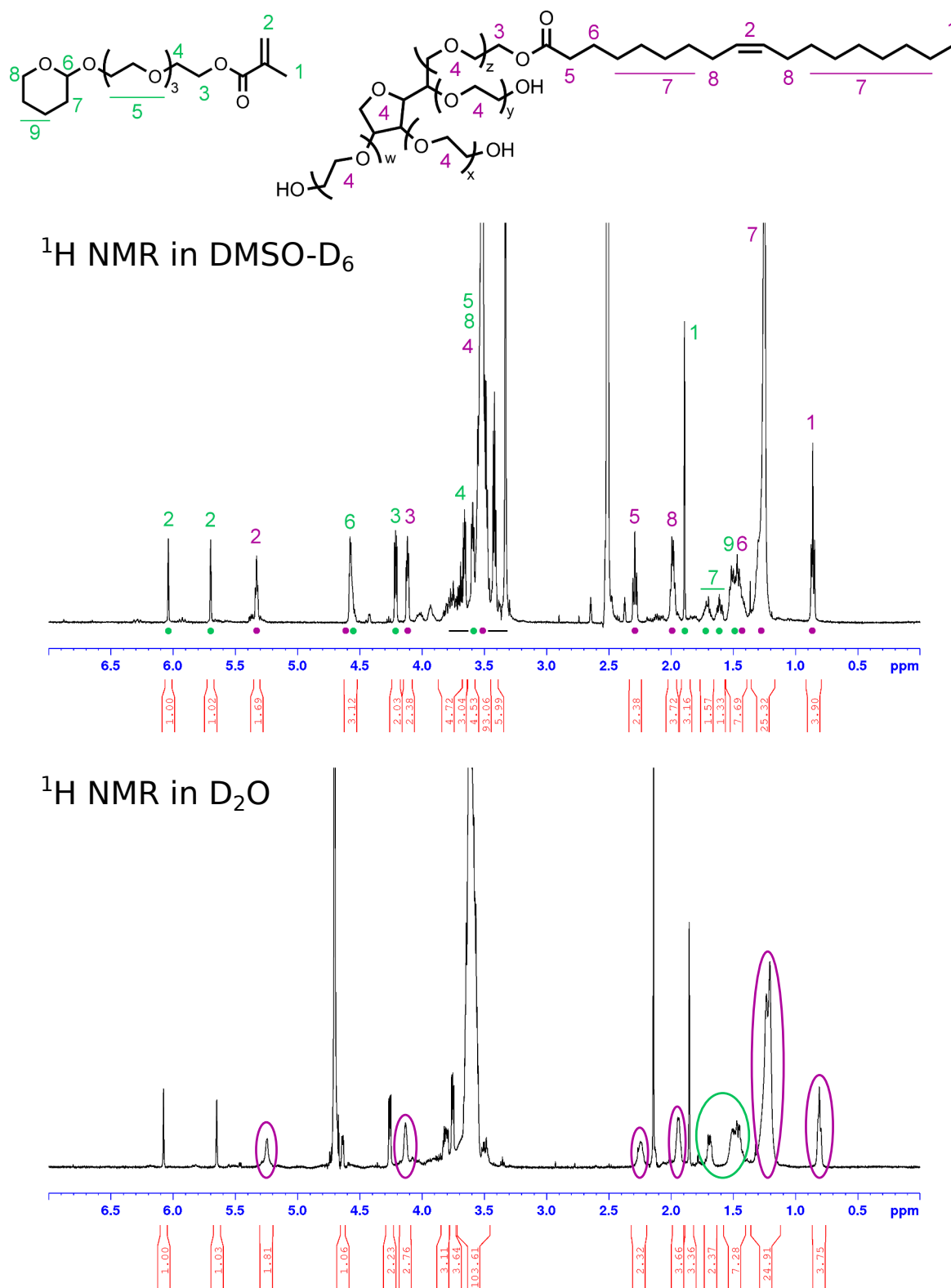
Figure 4.10 Top: ^{1}H NMR in DMSO$-$d$_6$ of a T80/AP-E4 mixture. Peaks of the AP-E4 are labeled in green, peaks of T80 in purple. Principal peaks are assigned: peaks of T80 are assigned as reported in [60], while assignment of AP-E4 peaks is discussed in the Experimental section. Bottom: ^{1}H NMR in D$_2$O of T80/AP-E4 mixture. Peaks which show a broadening and/or a less resolved splitting pattern are circled (green for AP-E4, purple for T80).
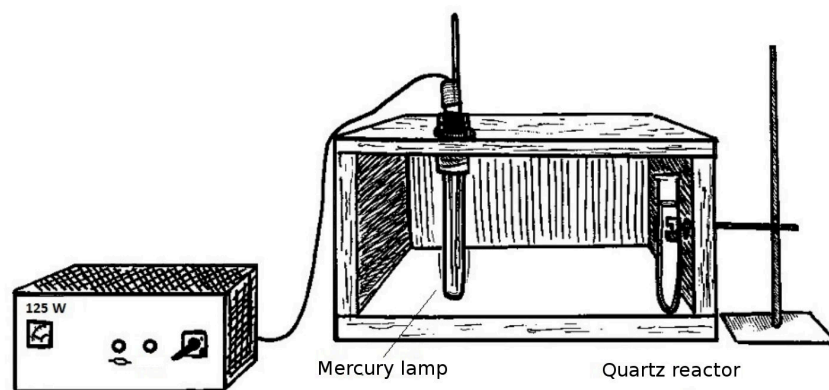
Figure 4.12 Illustration of the photoreactor setup used for micellar polymerization with mercury lamp. Credits: Anna Ramunni

As the carbonyl peak of AP-E4 is initially conjugated to a double bond, its vibrational mode is less energetic than that of T80, and the two peaks do not totally overlap. When the double bond reacts, these peaks merge, thus the aforementioned shift is observable despite the presence of T80 carbonyl peak. This is confirmed by IR collected during polymerization progress. Figure 4.13 show the peak of the carbonyls at every check of the polymerization. The peak maximum initially has an energy of 1720 cm^{-1}; as the polymerization moves forward, the position of the maximum changes, and after 7 h its energy is 1730 cm^{-1}.
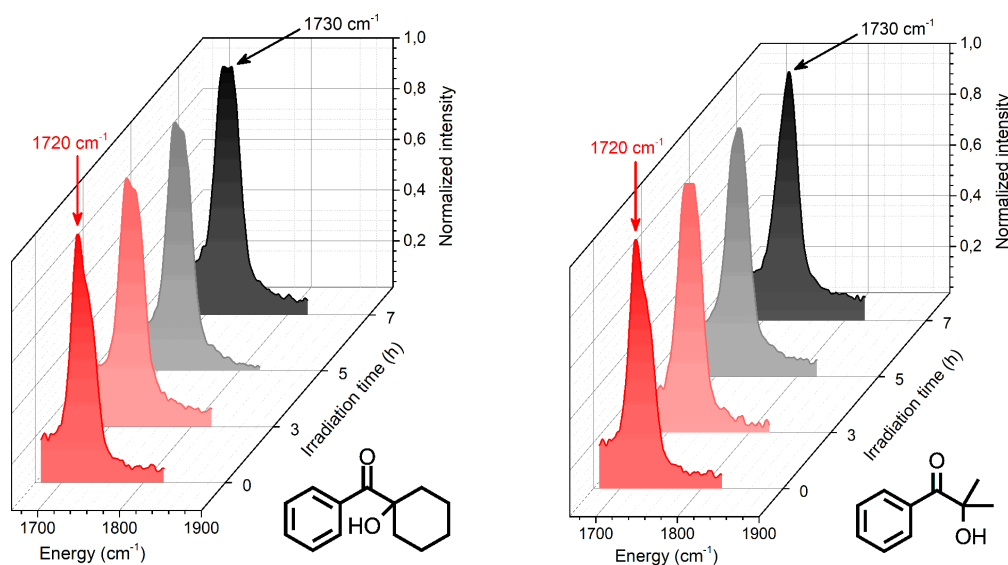
Figure 4.13 IR signal of carbonyl peak of AP-E4/T80 micellar dispersions containing Ig1 (left) or Ig2 (right) photoinitiator after 3, 5 and 7 h of irradiation.

Comparing the shift of the carbonyl peak in the two polymerizations, it is quite obvious that polymerization efficiency is not the same for the two initiators. In particular, the shift is way more accentuated for Ig2 initiator. This evidence is further confirmed by NMR spectra, reported in figure 4.14, which show that, after 7 h of continuative irradiation, no double bond signal for AP-E4 can be detected when Ig2 is used, while conversion is 49% in the case of Ig1. As Ig1 is less polar than Ig2, this difference in efficiency can be ascribed to a different localization of the initiator within the micelle. If Ig1 partitions more in the micellar core than in the palisade layer, it cannot be really effective as radical initiator,
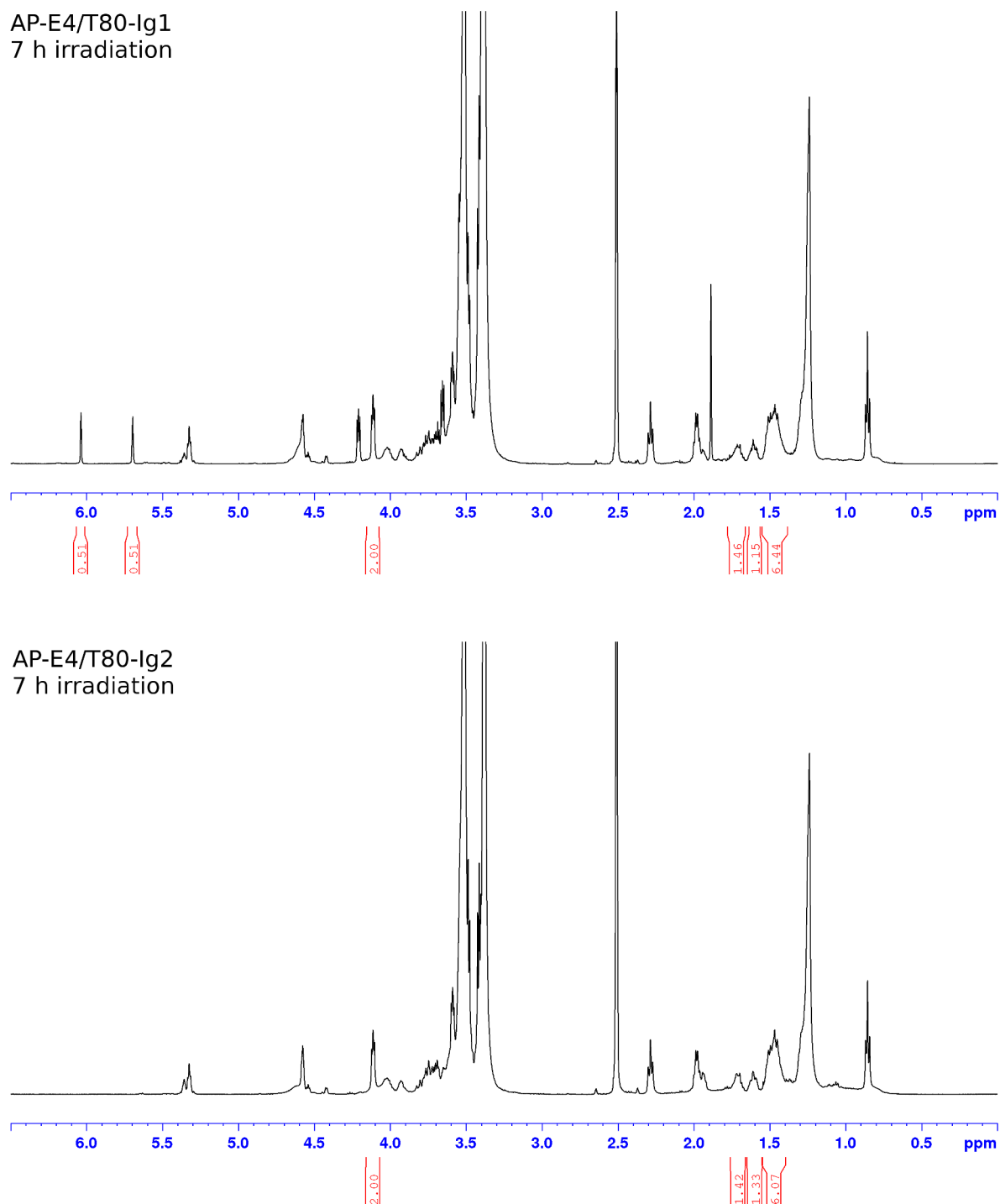
Figure 4.14 Top: ^{1}H NMR in DMSO$-$d$_6$ of a T80/AP-E4 mixture after polymerization with Ig1. Bottom: ^{1}H NMR in DMSO$-$d$_6$ of a T80/AP-E4 mixture after polymerization Ig2. Ester peak of T80 is used as reference. Integrals are reported to allow a comparison between relative amounts.

as the polymerogenic unit is not close enough to react with it.

During polymerization, DLS measurements were collected to check for any variation in the size distribution of micellar aggregates. Figure 4.15 shows the measurements: nearly no variation in size was observed in case of Ig1, while an increase was visible in case of Ig2. We speculate that a certain degree of interpolymerization within aggregates causes this behaviour, which is way less accentuated for Ig1 due to less extent of polymerization.
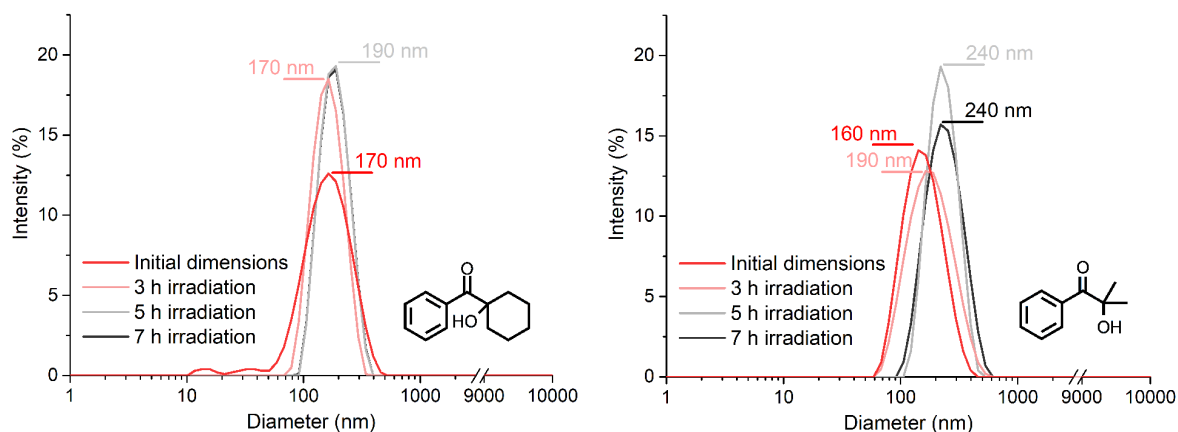
Figure 4.15 DLS measurements of AP-E4/T80 micellar dispersions containing Ig1 (left) or Ig2 (right) photoinitiator after 3, 5 and 7 h of irradiation.

As the system using Ig2 photoinitiator proved suitable to obtain a complete polymerization of the co-surfactant, we also developed the crosslinked version, adding a 5 mol% of crosslinker 4EDMA (tetraethylene glycol dimethacrylate, shown in figure 4.16) with respect to AP-E4 before polymerization. No issues were found with the polymerization upon addition of this species to the starting dispersion, and complete conversion of the monomers was always obtained.
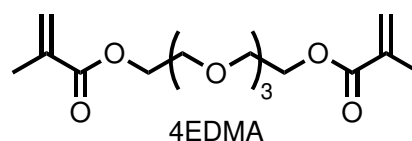
Figure 4.16 Crosslinker used in micellar polymerization

4.6.3.2   Light source: fluorescence UV-A lamp

Figure 4.17 "Nail-lamp" (UV-A) setup used for micellar polymerizations.

As we found able to perform the photopolymerization, we tried to replicate the same result using a less expensive, and less energy demanding fluoresence lamp. In particular, a picture of the light source used is shown in figure 4.17: it is a manicure setup, used by estheticians to polymerize semi-permanent nail polish. It can be bought for 10 € on the Internet.[65]

Photoinitiators working in the UV-A region are less common than these active in the deep UV. The majority of efficient radical photointiators for polymerization of vinyl groups are aromatic ketone compounds.[66] The mechanisms of radical

formation involves the triplet state of the molecule, which is sensitized by the carbonyl group.[67] Like aromatic ketones, α-diketones can be used as radical photoinitiator.[63]

We tested three different molecules as photoinitiators paired with the UV-A lamp: 4,4'-bis(dimethylamino)benzophenone (DABP), 2,3-dioxo-2,3-dihydroindole (better known as isatin, IS) and 2-di(3-thienyl)-1,2-ethanedione (DTE), shown in figure 4.18. Whilst DABP is a well-known photoinitiator, the other two species are just efficient triplet sensitizers; isatin has been sparingly used as photoinitiator,[68] while DTE has never been used specifically for the purpose of radical generation. The choice of these two latter molecules is quite unusual, and it comes from two considerations. The first one, is that there is a lack of polar photoinitiators working in the UV-A region: as aromatic species are reported to have a certain tendency to localize within the PEG-ylated shell of micelles instead of the core [10, 36, p. 130], and α-diketones usually have absorption shifted through the visible region,[69] we switched from molecules containing polar groups to these aromatic diketones. The second reason is that we already had these species in our reagents inventory.
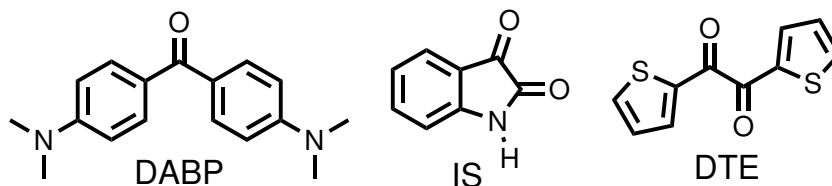
Figure 4.18 Photoinitiators paired with UV-A lamp.

Polymerization setup is quite different from that reported above: the chamber is mirrored, and way smaller than previous one, thus we could not cool down the system with compress air. This last difference is important: in all the cases, the polymerization occurred at a temperature of 40-45 °C due to heating by radiant energy.

Initiator	Medium	Conversion
DABP	water	50%
IS	water	33%
DTE	water	71%
DTE	PBS	92%

Table 4.2 Polymerization yields of AP-E4/T80 dispersions for every photoinitiator as calculated from NMR

As previously done, we injected the chosen initiator in the micellar dispersion, and followed the polymerization through IR and NMR. We observed occurrence of the polymerization for all three initiators, with strikingly different efficiencies. IR spectra after 7 h of irradiation are shown in figure 4.19, while table 4.2 reports polymerization conversions as calculated through NMR. In no case polymerization comes to completeness, however DTE proves to be the most efficient of the three species. Figures 4.20,4.21 and 4.22 show the collected NMR spectra.

Figure 4.23 shows the absorption spectra of the three initiators, and the luminescence spectrum of the lamp. It is quite obvious that, on the basis of the absorption only, DTE should be the less efficient of the three molecules. Nonetheless, it is the one which allows to obtain the highest conversion. We noticed, however, that after irradiation, the micellar dispersion containing DTE develops a greenish photoluminescence, which clearly cannot be ascribed to any of the starting molecules, but it is thought to be due to the formation of the radical anion of DTE.[70] In this case, besides compartmentalization, radical stability might play a role in the efficiency of the polymerization.
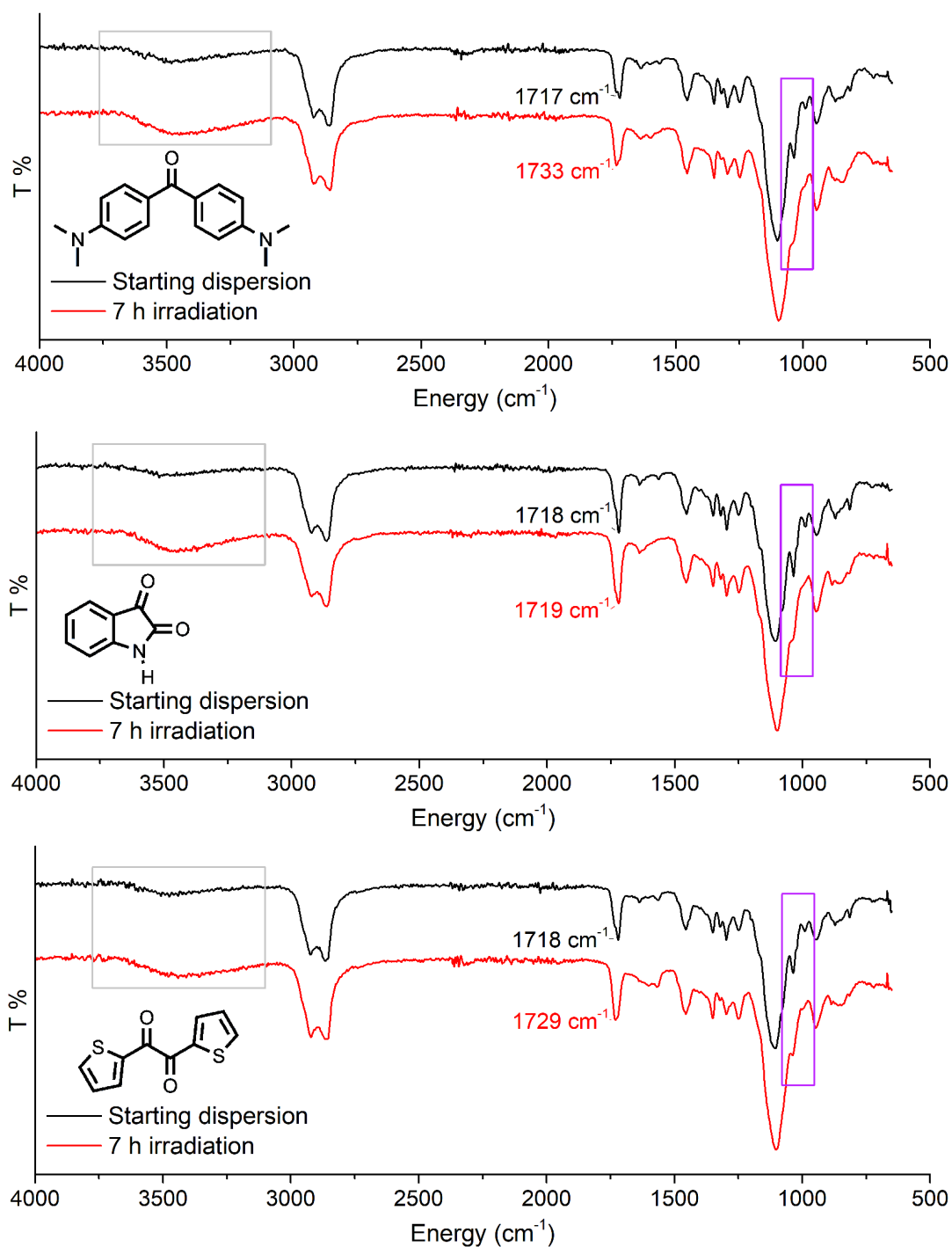
Figure 4.19 IR spectra of micellar dispersion before and after polymerization with different initiators: top, DABP; center, IS; bottom, DTE. The gray box highlight an increment in the −OH band, while the purple box highlight the disappearance of two bands of AP-E4 related to pyran ring.

Figure 4.20 Top: ^{1}H NMR in DMSO−d$_6$ of a T80/AP-E4 mixture before polymerization with DABP. Double bond peaks of AP-E4 are highlighted in red, pyran ring peaks are in purple, and ester peak of T80, used as reference, is in green. Bottom: ^{1}H NMR in DMSO−d$_6$ of a T80/AP-E4 mixture after polymerization. Integrals are reported to allow a comparison of relative amounts.
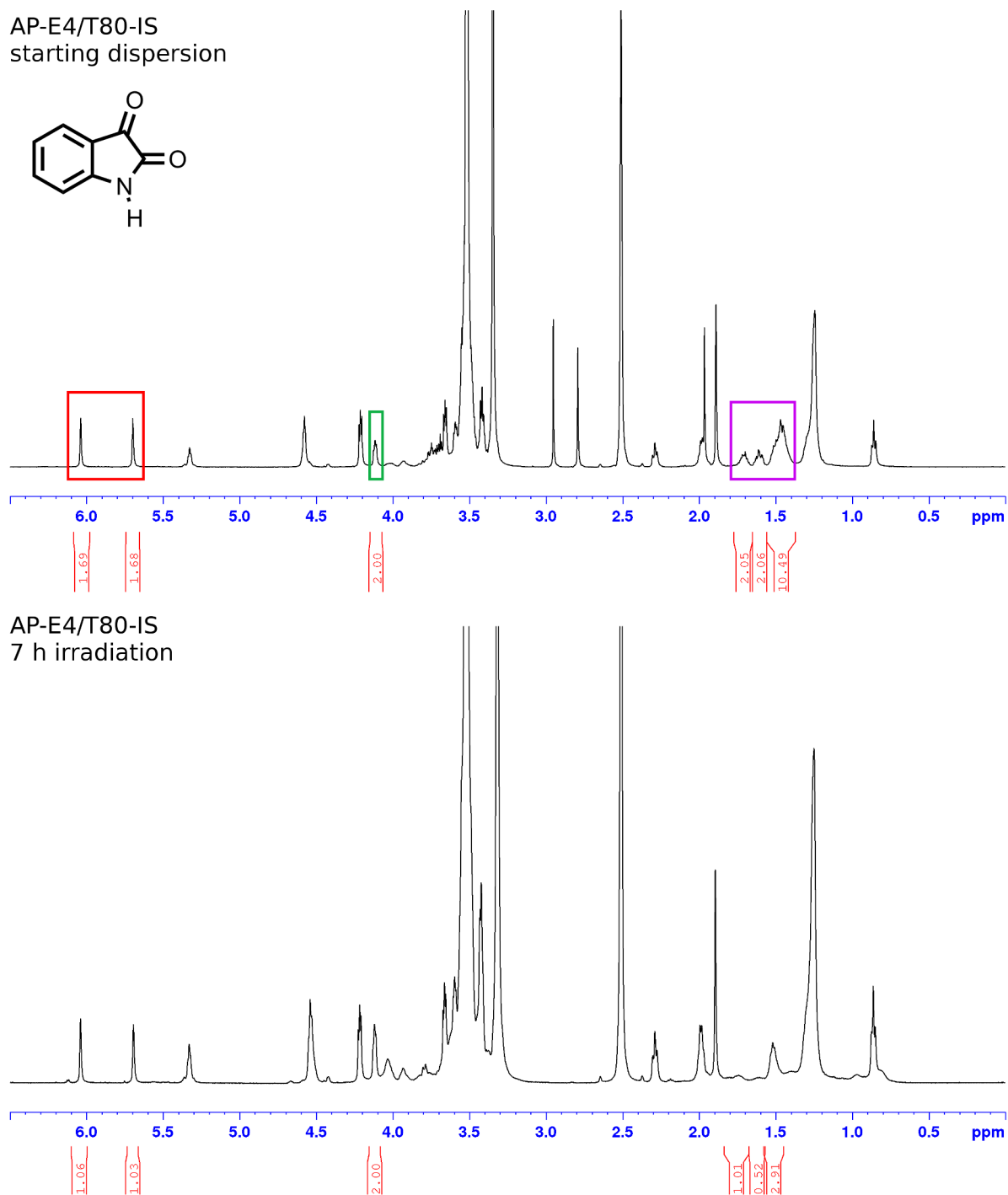
Figure 4.21 Top: ^{1}H NMR in DMSO$-$d$_6$ of a T80/AP-E4 mixture before polymerization with IS. Double bond peaks of AP-E4 are highlighted in red, pyran ring peaks are in purple, and ester peak of T80, used as reference, is in green. Bottom: ^{1}H NMR in DMSO$-$d$_6$ of a T80/AP-E4 mixture after polymerization. Integrals are reported to allow a comparison of relative amounts.
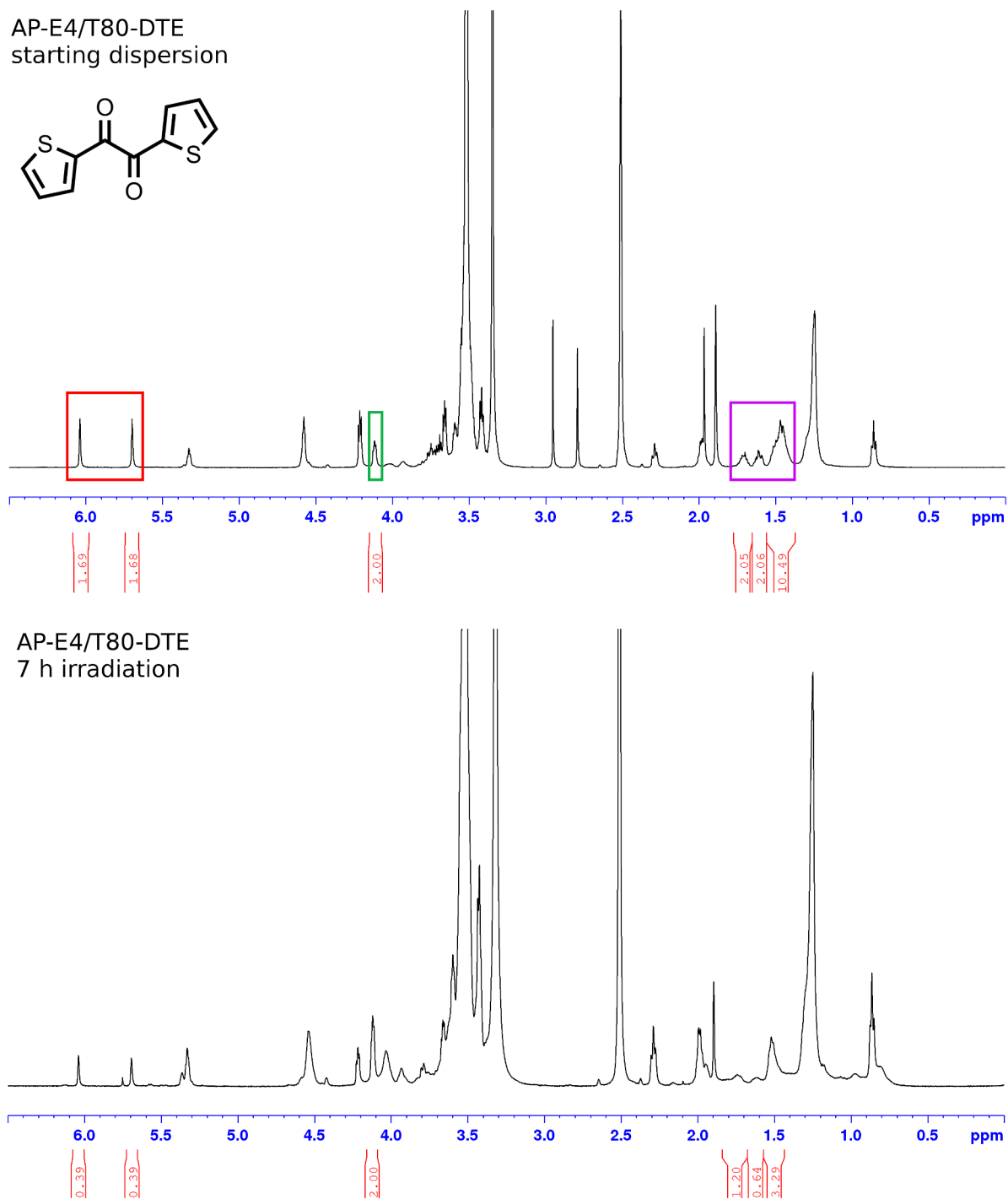
Figure 4.22 Top: ^{1}H NMR in DMSO$-$d$_6$ of a T80/AP-E4 mixture before polymerization with DTE. Double bond peaks of AP-E4 are highlighted in red, pyran ring peaks are in purple, and ester peak of T80, used as reference, is in green. Bottom: ^{1}H NMR in DMSO$-$d$_6$ of a T80/AP-E4 mixture after polymerization. Integrals are reported to allow a comparison of relative amounts.
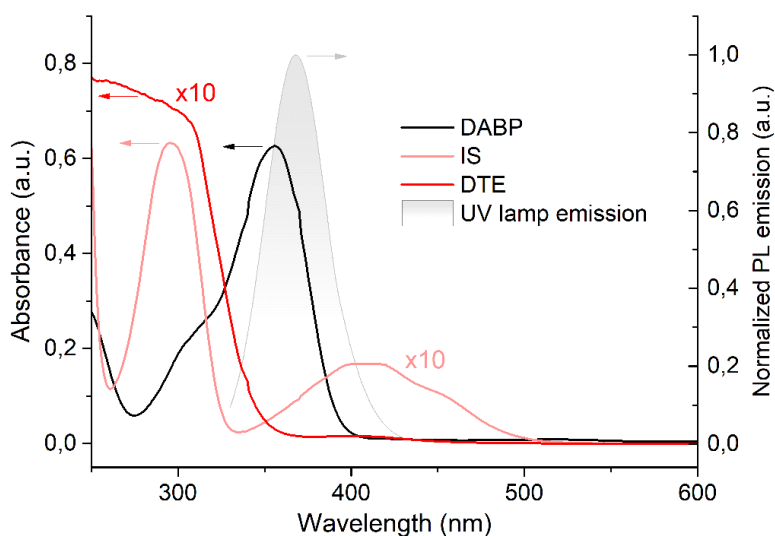
Figure 4.23 Absorption spectra of DABP, IS and DTE in CHCl$_3$ solution (10^{-4} M, 10^{-3} M and 10^{-3} M respectively), and emission spectrum of the used UV-A lamp.

IR spectra in figure 4.19 show not only the occurred polymerization, but also a change in the lower energy portion of the spectrum in correspondence to pyran peaks, which become way less intense (attribution of these peaks to the pyran ring is discussed in the Experimental section). NMR spectra show the same occurrence: signal relative to pyran ring are way less intense after irradiation. This behaviour was not observed in the case of irradiation with the mercury lamp. As we changed both the setup geometry and the initiators, we hypothesized two possible explanations:

- the higher temperature reached during polymerization is detrimental for the co-surfactant, which degrades

- the chosen initiators, which produce radicals through a proton extraction mechanism (while both Ig1 and Ig2 undergo a unimolecular bond cleavage[63]), develop some acidity as consequence of irradiation, which provokes the pyran ring opening

Deprotection of AP-E4 should end up in the formation of pentanal; however, in aqueous environment this species is subject to keto–enol tautomerism, and forms 1-penten-1-ol, which is hardly detectable in both IR and NMR spectra, as its peaks probably overlap to these of T80. The only easily detectable change is the increased intensity of a broad band at ~ 3400 cm^{-1}, typical of O$-$H stretching, which supports the hypothesis of occurred deprotection.

We had no ways to cool down the polymerization, as the chamber was too small to integrate the compress air flow. Therefore, we only tested if there was any development of acidity in the case of DTE initiator. To test this possibility, we performed a new polymerization in the same conditions, but using PBS solution instead of distilled water as medium. As PBS solution is a buffer, developed acidity should be inhibited, and the pyran ring should degrade less. Figure 4.24 shows the NMR of the performed polymerization in PBS. Comparing this to the results obtained in water (figure 4.22), we can see both an improved polymerization conversion (only 8% of the initial double bonds are still visible) and a less pronounced pyran degradation (78% of the starting value instead of 35%).
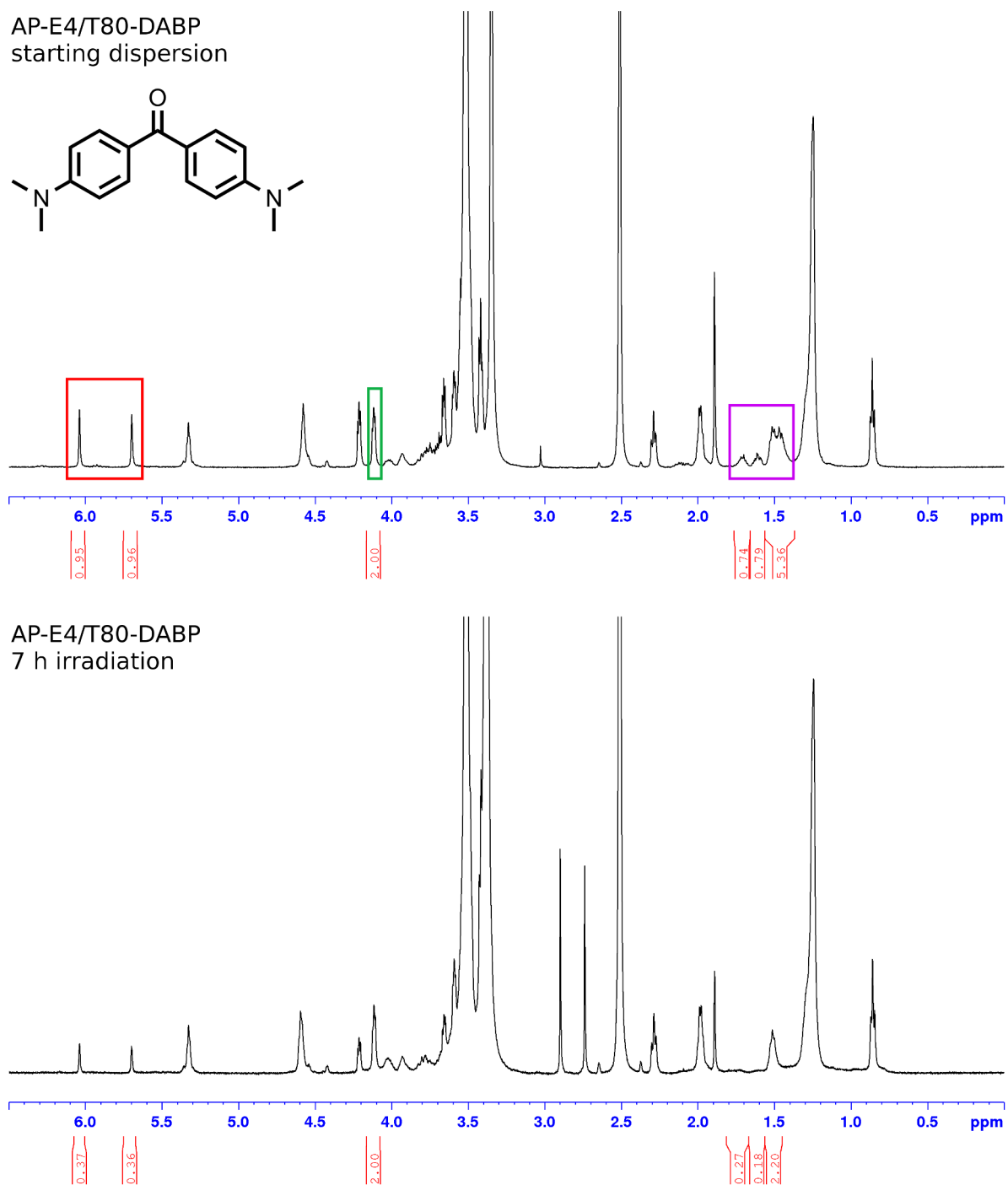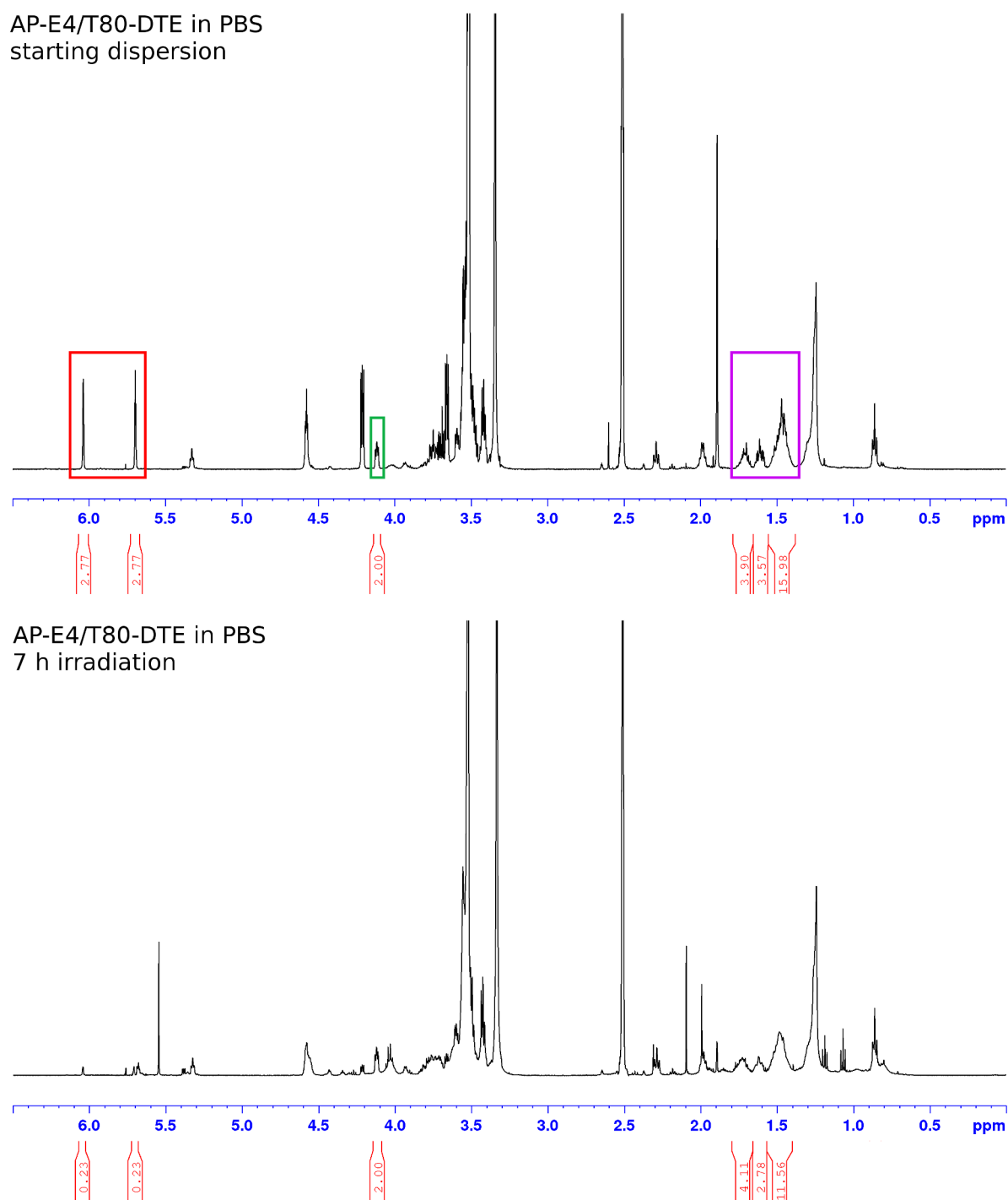
Figure 4.24 Top: ^{1}H NMR in DMSO−d$_6$ of a T80/AP-E4 mixture before polymerization with DTE in PBS. Double bond peaks of AP-E4 are highlighted in red, pyran ring peaks are in purple, and ester peak of T80, used as reference, is in green. Bottom: ^{1}H NMR in DMSO−d$_6$ of a T80/AP-E4 mixture after polymerization in PBS. Integrals are reported to allow a comparison of relative amounts.

4.6.4 Thermopolymerization attempts

Contemporarily to photopolymerization, we also tested radical thermal polymerization. We selected several radical initiators, shown in figure 4.25, with very different polarities, always with the aim to understand the importance of polarity on compartmentalization. Lauroyl peroxide (LPO) is a very apolar species, azobisisobutyronitrile (AIBN) has an intermediate polarity, and 2,2'-azobis(2-amidinopropane) dihydrochloride (AAPH) is soluble in water (but its partition coefficient in micelle is $\sim 91\%$[71]). All these three initiators have a low 10 h half life temperature (65 °C in toluene for LPO and AIBN,[72] 56 °C in water for AAPH[73]). We added the chosen initiator to the AP-E4/T80 dispersion, and heated it to 52 °C, checking the reaction after 1 h and 12 h. Details of procedures are reported in the Experimental section. The temperature was chosen after a preliminary check of the stability of the starting dispersion with raising temperature. DLS measurements at various temperatures showed no variations of aggregates size until 55 °C, and at 60 °C the measurement was not reliable anymore (see

Figure 4.25 Thermoinitiators used to attempt polymerization of AP-E4/T80 micellar dispersion.

figure 4.26). We therefore supposed no further aggregation (symptomatic of clouding) was happening until 55°C, and decided to perform the polymerization at 52 °C.
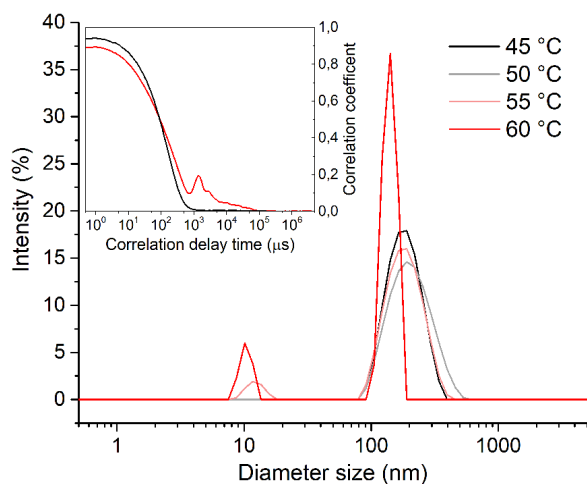
Figure 4.26 DLS measurements of micellar dispersions of AP-E4/T80 at various temperatures. The inset shows the correlograms of measurements performed at 45 °C and 60 °C. The shape of the function is a perfect sigmoid at 45 °C, which is lost at 60 °C. This is symptomatic of occurring aggregation, which heavily disturbs the measurement. For this reason, the sharp peaks visible at 60°C are not a reliable picture of the size dispersion of the system.

In all the cases, no polymerization reaction was observed. Both LPO and AAPH react in the chosen conditions: in the case of LPO, we were able to follow the disappearance of the carbonyl signal over time, confirming the formation of radicals was occurring, while AAPH has been used as radical initiator in micelles for the study of antioxidant properties of natural compounds.[71] As AIBN has the same 10 h half-life temperature of LPO, which is poorly dependent on the solvent,[73] we supposed it reacted as well. Figure 4.27 shows the IR spectra of the dispersion components before addition of the initiator and after 12 hour of reaction.

In all the cases, it is clearly possible to see that the carbonyl peak of AP-E4 remained unchanged, but signals relative to the pyran ring are less intense. As in the case of photopolymerization with UV-A lamp, the monomer is unstable at the chosen temperature. In this case, however, we had the additional problem that the kinetic of radical formation is too slow at 52 °C:
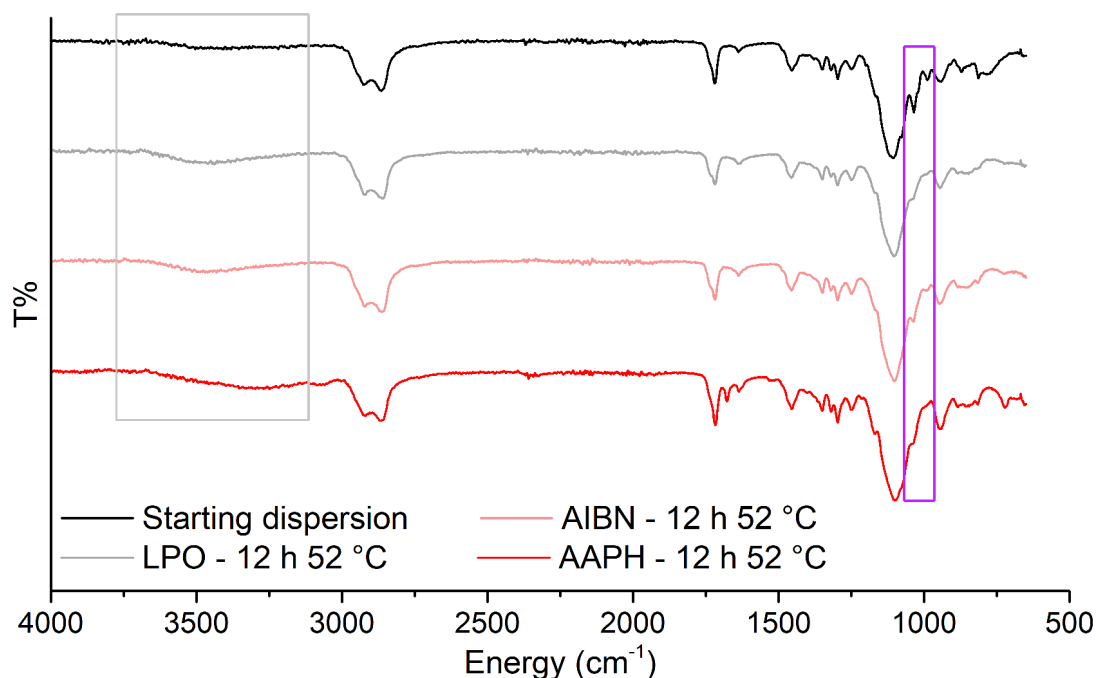
Figure 4.27 IR spectra of micellar dispersion before and after thermopolymerization with different initiators (LPO, AIBN, AAPH). The gray box highlight an increment in the −OH band, while the purple box highlight the disappearance of two bands of AP-E4 related to pyran ring.

the pyran ring got lost before polymerization could occur, probably with dispersion of the monomer in water and a complete inhibition of polymerization.

The photopolymerization and thermopolymerization attempts depicted quite clearly that the designed system can be effectively polymerized under tailored conditions. If the temperature is raised and the radical formation rate is not fast enough, the system degrades, and cannot be polymerized any longer. As we found one set only of conditions to obtain a complete polymerization without degradation of the co-surfactant, we kept using that method. All the following characterizations will be therefore made on the dispersion photopolymerized using Ig2 photoinitiator.

4.6.5   Morphology of polymerized micelles

As the AP-E4 cosurfactant immediately formed secondary aggregates when dispersed within T80, we tried to isolate the polymerized material to see if these aggregates were the only objects present in dispersion, or polysoap micelles were present too. In fact, DLS confirmed the presence of a single family of aggregates having dimensions of ∼250 nm, but this does not mean smaller particles were not present. As the scattering intensity is a function of particles dimensions, which goes as the 6th power of the size for particles smaller than the laser wavelength,[74] DLS is able to "sense" the presence of several families of different particles size only if smaller objects are sizably more than the bigger ones (80% or more of the total[75]).

We centrifuged the polymerized dispersion at 14000 rpm for 90 minutes, and compared DLS and IR measurements before and after centrifugation. Figure 4.28 shows the results.

After centrifugation, the DLS measurement of the supernatant clearly shows the peak of a family of small particles which was previously invisible. The conversion in hydrodynamic
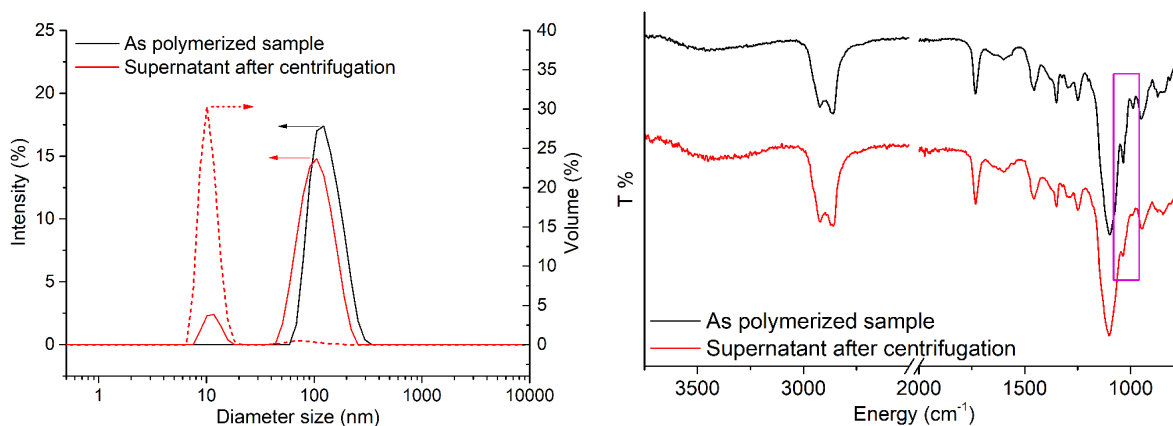
Figure 4.28 Characterization of an as-polymerized surfactant dispersion before and after ultracentrifugation. Left: DLS intensity (full lines) and volume (dashed line) distribution of particles dimensions . Right: IR spectra. The pyran peaks are highlighted in a purple rectangle.

volume suggests that only 2% of the supernatant is composed of big aggregates. The size is 11,5 nm, slightly bigger than that of T80 only micelles. IR spectra suggest that the composition of the supernatant is not as rich in AP-E4 as the precipitate. We speculate that AP-E4 preferentially polymerizes giving the semi-IPN-like structure, and partly forms micellar aggregates with T80. The small family of particles would be thus formed by partly polymerized T80/AP-E4 micelles. The morphology of the system as composed of small particles and micellar aggregates is also confirmed by SEM (v. *infra* figure 4.37). Figure 4.29 shows a cartoon of the expected morphology of the system.
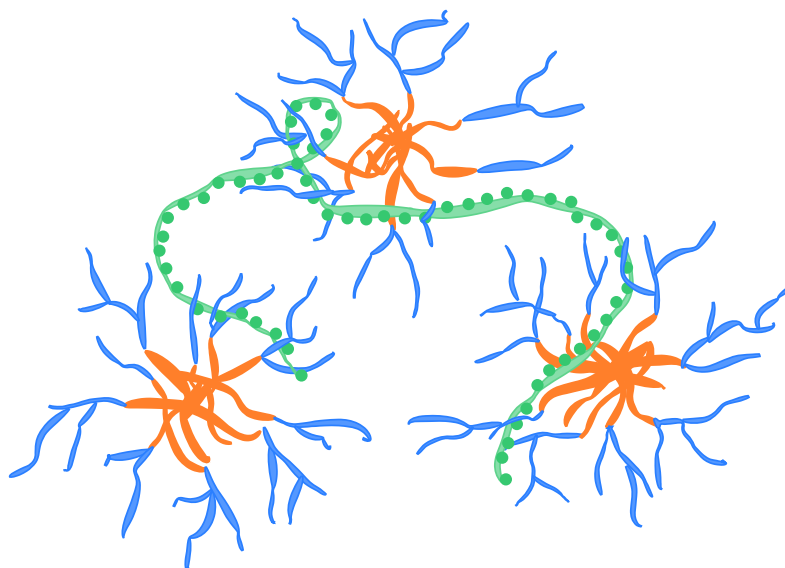
Figure 4.29 Cartoon showing the hypothesized morphology of the aggregated micellar dispersion. The green strand represents the polymerized co-surfactant.

4.6.6 Stability of micellar aggregates

4.6.6.1 Stability to dilution

To test if the polymerization was effective to stabilize the system, we proceeded to dilute it to a concentration lower than the cmc of T80.

Figure 4.30 show the DLS size distributions and correlograms of an as prepared micellar AP-E4/T80 dispersion diluted 3 times (concentration of 1 mg/mL), an as polymerized micellar AP-E4/T80 dispersion (concentration of 3 mg/mL), and the same dispersion diluted 400 times (concentration of $7,5 \cdot 10^{-3}$ mg/mL). The system diluted before polymerization is totally unstable, and unable to form a good dispersion. Dilution after polymerization, instead, show the presence of the same family of aggregated particles, which do not dissolve. This measurement is clearly an index of the impossibility, for the polymerized aggregates, to easily separate one from the others. We kept the 400-fold diluted dispersion, and performed a new measurement one month after the first one, which was reliable and showed no changes in the size distribution of the dispersion.
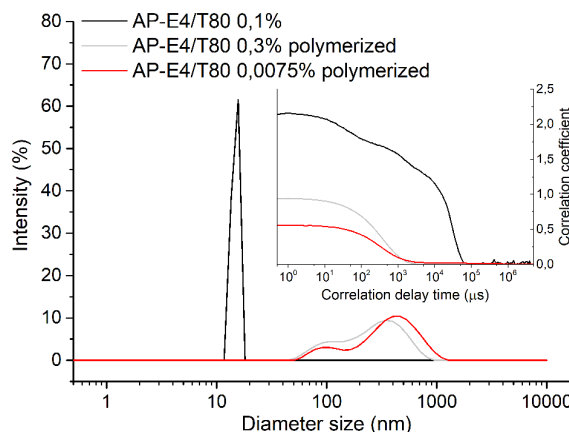
Figure 4.30 DLS measurements of AP-E4/T80 system upon dilution; the inset shows corresponding correlograms. Before polymerization, a three-fold dilution ends up in a terribly unreliable measurement, due to a strong aggregation which do not allow to recognize any feature of the dispersion (black line). After polymerization, the dispersion can be diluted 400 times, with no loss in the reliability of the measurement (red line). The DLS of the as polymerized dispersion is shown for comparison.

4.6.6.2 Stability to temperature
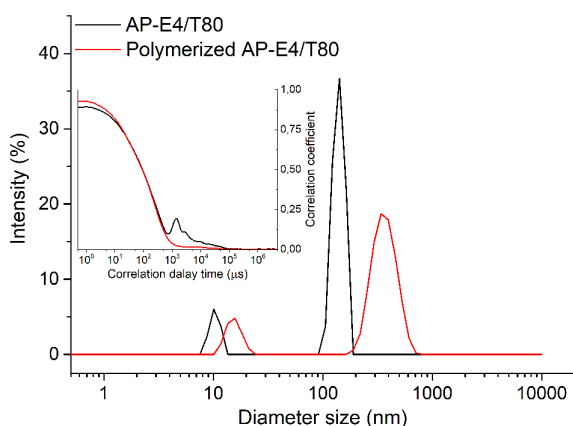
Figure 4.31 DLS measurements of micellar dispersions of AP-E4/T80 at 60 °C before and after polymerization; the inset shows the corresponding correlograms.

We also tested if polymerization allowed to stabilize the system at higher temperature. We performed a DLS measurement at 60 °C, which previously proved not reliable for the system before polymerization. The polymerized system, on the other side, showed no stress due to further aggregation/clouding phenomena. The appearing family of small particles, on the other side, might be due to "slipping" of small AP80 chains/T80 molecules out of the semi-IPN structure as effect of the increased thermal motion. Unfortunately, it was not advisable to perform the measurement at higher temperatures to study the phenomenon, as solvent evaporation and development of bubbles influence the result.

4.7 Loading of organic species

4.7.1 Pyrene: an old probe in micelle-related studies
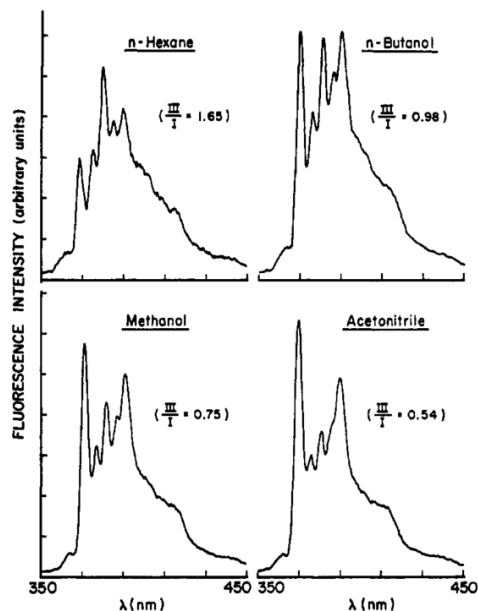
Figure 4.32 Solvent dependence of vibronic band intensities in pyrene monomer fluorescence: [pyrene] = 2 pM; λ_{exc} = 310 nm. Reproduced with permission from [76]. Copyright © 1977 American Chemical Society.

As first load for our micellar system, we used pyrene, a very popular probe for colloidal dispersions, whose structure is depicted in figure 4.33. This molecule has several photophysical interesting properties, in primis the structure of its photoluminescence spectrum strongly depends from the polarity of the surrounding environment. The spectrum, in fact, shows five replicas, which relative intensities change depending on the solvent, as visible in figure 4.32. The vibronic 0-0 band, in particular, shows an increased intensity with increasing solvent polarity, and the ratio of III/I replicas intensity is the most variable. This peculiar behaviour has been widely used to identify the cmc of surfactants, while its PL lifetime can be used to obtain the aggregation number of micellar systems. Moreover, pyrene shows excimer emission upon aggregation, which can be easily detected as it presents itself as a broad band centered at ∼480 nm.

Figure 4.33 shows the photoluminescence spectrum of a 4EDMA/AP-E4/T80 crosslinked dispersion after loading with pyrene. The III/I ratio is 0,96, a typical value for micellar dispersions, which is indicative of localization at the core-corona interface, where water should not be present. A strong excimer band is visible as well. This PL spectrum clearly proved the occurred micellization of pyrene. This test is only apparently trivial: as the system is designed to keep a load inside after its insertion, this also mean it might be able to prevent the loading from the beginning. This is especially true, as the typical micellar percolative path to the lipophilic core is at least partly clogged by the co-surfactant.

We used this probe to test the retaining of the load of our system after solvent evaporation. Figure 4.34 shows the normalized absorption spectra of pyrene in three micellar dispersions with different "network densities" after redispersion in water: T80 only (simple micelles), AP-E4/T80 (polymerized micelles), 4EDMA/AP-E4/T80 (crosslinked micelles).

Absorption spectra show that, after solvent evaporation and redispersion, the degree of retention increases with increasing network density. We speculate that, after solvent evaporation, when water is newly added, the previously loaded pyrene is more apt to crystallize than to promptly redisperse within the micelles, as the micelles formation is not instantaneous. In the case of T80 only micelles, therefore, only 48% of the initial pyrene amount is preserved. This value increases to 60% when the system is polymerized, and to 88% when it is crosslinked. We ascribe the improved retemption to the presence of the polymeric network: for polymerized micelles, re-organizing in new structures after solvent evaporation and addition of new solvent is a difficult process, while it is what
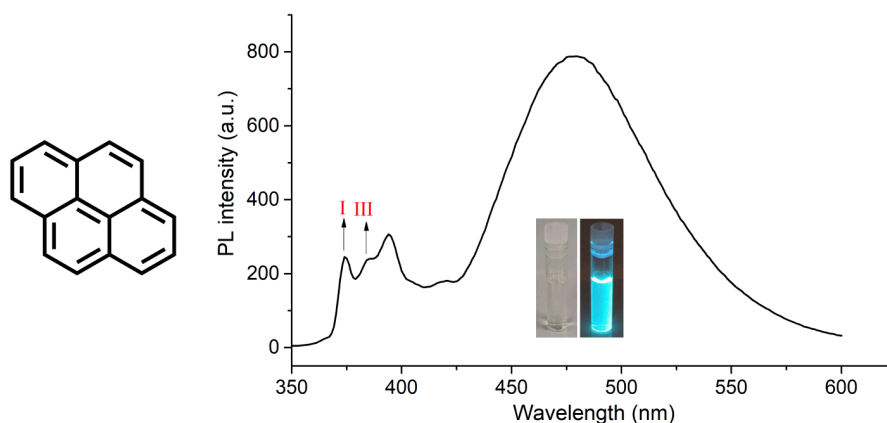
Figure 4.33 Left: structure of pyrene. Right: pyrene PL spectrum in a crosslinked micellar dispersion of 4EDMA/AP-E4/T80. The photographs show the same dispersion in white (left) and UV (right) light.
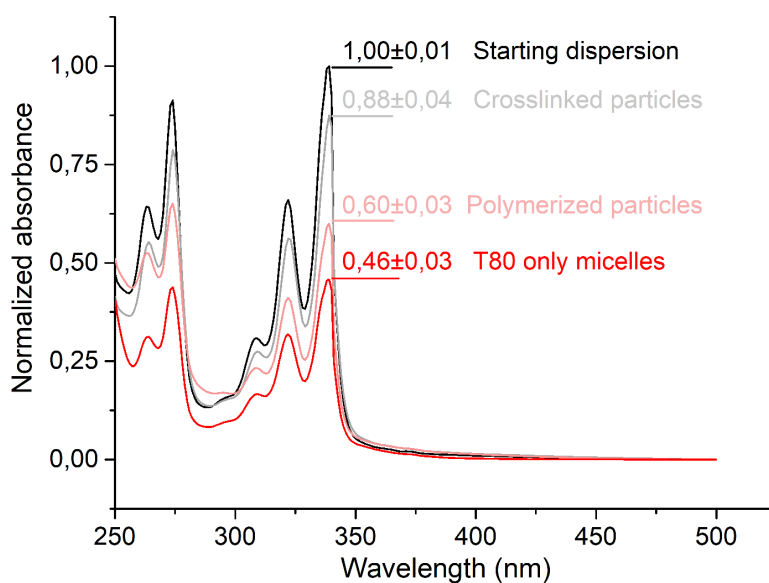
Figure 4.34 Absorbance spectra of micellar dispersion with different network densities loaded with pyrene after solvent evaporation and newly addition of water, normalized with respect to the starting absorbance.

happens for the T80 micelles. During this re-organization process, the loaded pyrene is likely to come out from a simple micellar structure, a more difficult process for a polymerized system, as the diffusion out from the micelles is hindered.

4.7.2 Quinacridone nanocrystals

As we finally proved the system was suitable to load and retain organic species, we tested it with a dye, Qn-Oct (N,N'-dioctyl substituted quinacridone, shown in figure 4.35). We chose this molecule because it has an extended, planar core, able to give strong π-interactions, and two alkyl chains which might help in the solubilization process within micellar cores of the AP-E4/T80 aggregates. Moreover, as many dyes, its absorption spectrum changes upon aggregation, in particular
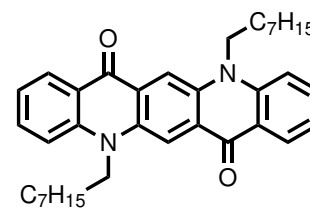
Figure 4.35 Qn-Oct structure

with the development of a red-shifted band, typical for J aggregates.[77]
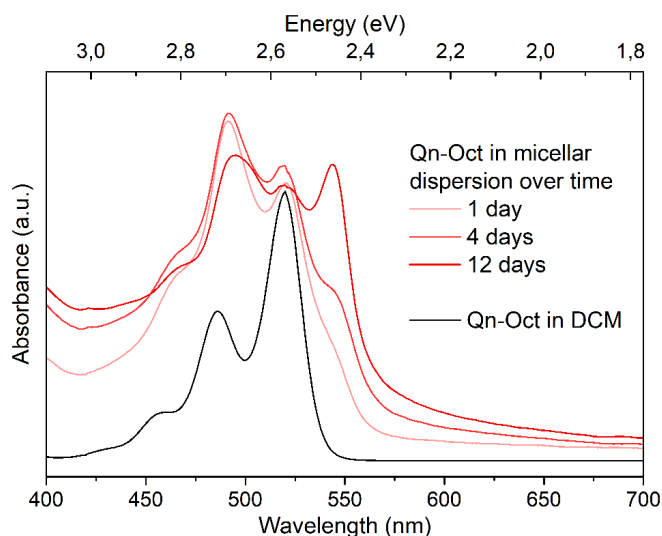
Figure 4.36 Absorption spectra of a crosslinked micellar dispersion loaded with Qn-Oct. Qn-Oct spectrum in CH_2Cl_2 solution is shown for comparison.

Figure 4.36 shows the evolution of the absorption spectrum of a Qn-Oct loaded 4EDMA/AP-E4/T80 crosslinked dispersion (the spectrum of Qn-Oct is shown for comparison). It is clearly visible a new, red-shifted band in the spectrum, which is not present for the molecule in solution, and rises over time. We speculate that the Qn-Oct molecules crystallize within the micelles, which can be thought as "molds" for the growth of these nanocrystals. The process takes time, as the micellar core behave like a viscous solvent, and π-stacking interactions are efficient only when molecules are close. After twelve days, we looked the dispersion under a SEM. Collected images are shown in figure 4.37.

The SEMs show aggregates with dimensions of $\sim$150-250 nm, formed by smaller objects of $\sim$15-20 nm. These are the same dimensions observed through DLS measurements (see above, figure 4.28). It is noteworthy that micellar aggregates, which usually do not survive out of solution, can be observed even after gold sputtering on the sample. We ascribe this improved resistance to the crystallization of Qn-Oct within the micelles.
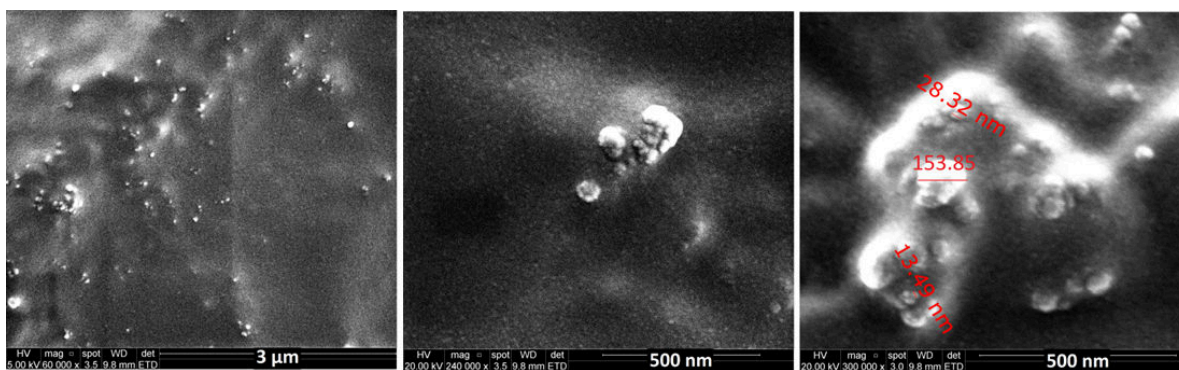
Figure 4.37 SEM pictures showing micellar aggregates of AP-E4/T80 loaded with Qn-Oct. As the dispersion was drop casted directly on the substrate, water caused its bloating.

4.8 Conclusions

We designed the specific, polymerogenic co-surfactant AP-E4 to be coupled with a branched surfactant (T80) to form, after polymerization, a semi-IPN-like structure with improved resistance. We attempted both the photo- and the thermo-polymerization of the system: results indicate that localization of the radical initiator as well as the rate of radical formation are important parameters. Moreover, the co-surfactant is not compatible with either high temperature and proton extractor radicals. Nonetheless, AP-E4 can be efficiently photopolymerized under tailored conditions, obtaining a full conversion into oligomeric/polymeric species.

The obtained final material is formed by aggregates of small nanoparticles, which show improved stability to both dilution and temperature, and can be loaded with organic species. A dye was crystallized in the form of nanoparticles inside the aggregates, which could be observed under SEM. We therefore conclude that the method is successful for the synthesis of a semi-IPN-like polysoap structure.

Future work will inspect the properties of the system as dispersant medium and as reactor for organic synthesis. As the system is designed to grant flexibility of the introduced building blocks, we also plan to synthesize a new co-surfactant containing extended aromatic groups to introduce domains specifically for π-interactions.

4.9 Experimental

Heptane and distilled water were purchased from Carlo Erba; p-toluensulfonic acid mono-hydrate and 3,4-dihydropyran were purchased from Alfa Aesar; DCM was purchased from VWR, and eventually anhydrificated over $CaCl_2$. All other reagents and solvents were purchased from Sigma-Aldrich and used as received.

$CDCl_3$ was purchased from Sigma-Aldrich; $DMSO-d_6$ was purchased from Euriso-top; D_2O was purchased from Merck. NMR spectra were acquired with a Bruker NMR 500 Avance.

Synthesis and characterization of AP-E4 derivative
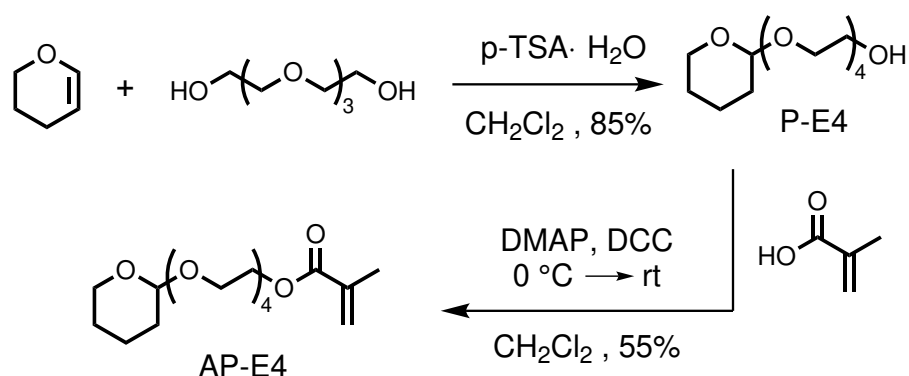
Step 1 - synthesis of P-E4 derivative

In a 1 L roundbottom flask, 250 g of tetraethylene glycol (TEG, 1,29 mol) are dissolved in 500 mL of CH_2Cl_2. p-Toulenesulfonic acid (p-TSA, 5,15 mmol, 0,98 g) is added. 3,4-dihydropyran (0,30 mol, 24,90 g) is added dropwise over 45 minutes. The reaction is stirred for a weekend. After evaporation of half of the solvent, the crude solution is extracted with 100 mL of $NaHCO_3$ aqueous solution, and subsequently 7×100 mL of brine. The solution is dried over anhydrous Na_2SO_4, and the solvent is finally evaporated, yielding the desired product (68,13 g, yield 81,6%) as a mixture of mono-protected and di-protected TEG (96%-4% respectively on the basis of NMR).

^{1}H NMR ($CDCl_3$, 500 MHz): δ 4.58 (q, J=5.13 Hz, 2H), 3.81 (m, J=13.03 Hz, 4H), 3.61 (m, J=32.96 Hz, 29H), 3.07 (s, 1H), 1.77 (m, J=15.10 Hz, 2H), 1.66 (m, J=14.51 Hz, 2H), 1.51 (m, J=33.26 Hz, 8H). See [78] for a comparison.

Step 2 - synthesis of AP-E4

In a 250 mL roundbottom flask cooled with a water/ice bath, all the reagents (P-E4: 10,44 g, 37,6 mmol; methacrylic acid: 3,33 g, 38,7 mmol; dimethylaminopyridine, DMAP: 0,58 g, 5,17 mmol; N,N'-dicyclohexylcarbodiimide, DCC: 8,06 g, 38,1 mmol) are weighted. 130 mL of anhydrous CH_2Cl_2 are then added, and the flask content is protected from moisture using a drying tube filled with $CaCl_2$. The reaction is stirred at room temperature for 24 h; during this time, a precipitate forms within the flask. The precipitate is filtered off, and the solution is washed with NH_4Cl aqueous solution (50 mL, two times), then $NaHCO_3$ aqueous solution (50 mL, two times), and finally brine (50 mL, two times). The solution is dried over anhydrous Na_2SO_4, and the solvent is finally evaporated, yielding an oily crude which is purified through flash column chromatography (eluent AcOEt:heptane 1:1). 7,10 g of desired product are obtained (yield 55%).

^{1}H NMR (CDCl$_3$, 500 MHz): δ 6.10 (s, 1H), 5,55 (t, J = 1.6 Hz, 1H), 4.60 (t, J = 3.6 Hz, 1H), 4.27 (t, J = 4.9 Hz, 2H), 3.86-3.82 (m, 2H), 3.72 (t, J = 4.9 Hz, 2H), 3.66-3.63 (m, 10H), 3.60-3.56 (m, 1H), 3.49-3.45 (m, 1H), 1.92 (s, 3H), 1.82-1.77 (m, 1H), 1.72-1.66 (m, 1H), 1.60-1.47 (m, 4H).
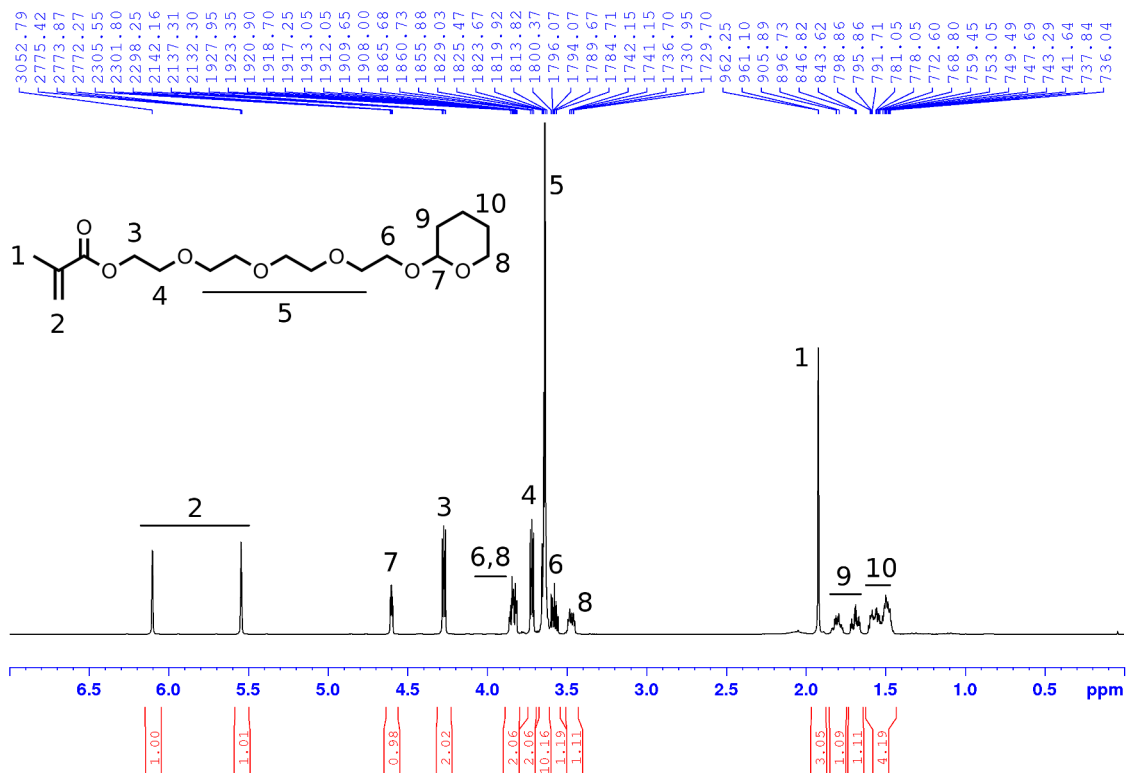
^{13}C NMR (CDCl$_3$, 125.7 MHz): δ 168.20, 137.01, 126.56, 99.79, 71.52, 71.47, 71.39, 70.00, 67.50, 64.74, 63.06, 31.41, 26.28, 20.33, 19.16.
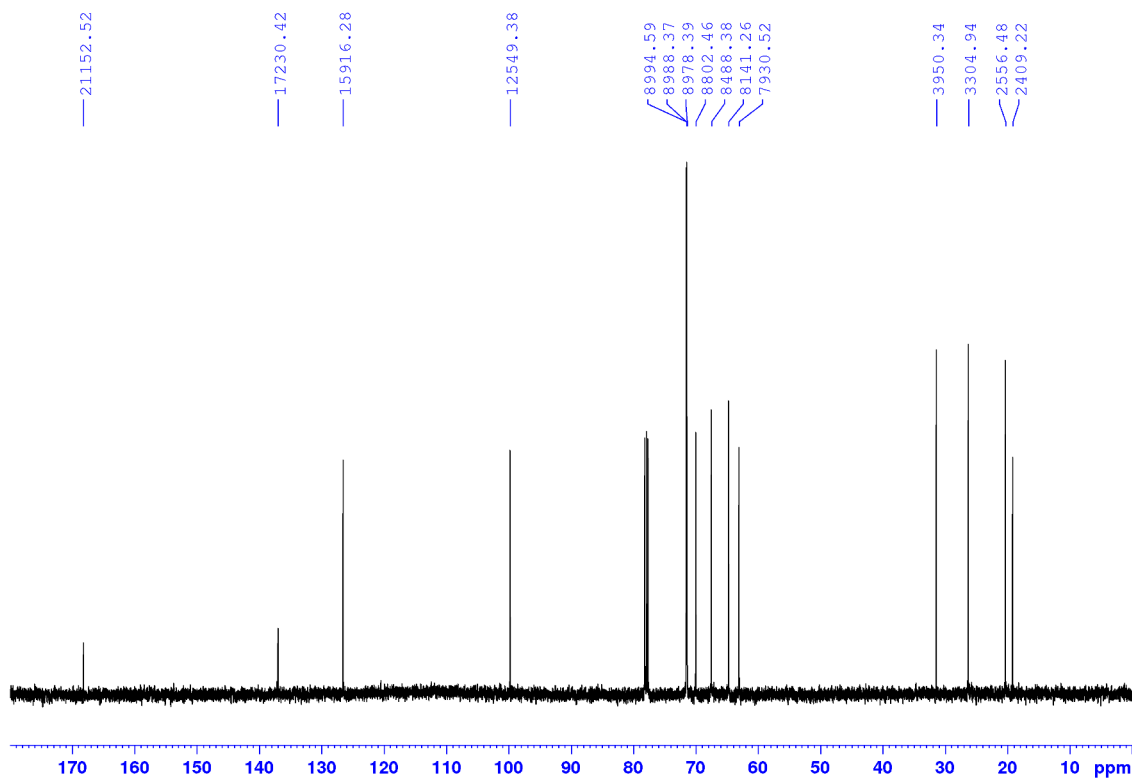
Discussion on assignment of ^{1}H NMR peaks for derivative AP-E4

Assignment of peaks labeled as 1, 2, 3, 5 and 7 is trivial, and is based on peaks integration and multiplicity. Proton labeled as 7 can be easily distinguished by these labeled as 2 comparing the spectrum with that of the derivative P-E4. Assignment of protons labeled as 8, 9 and 10 is tentative, and it is based on the splitting pattern observed in the spectrum of 2-(2-bromoethoxy-1,1,2,2-d$_4$)tetrahydro-2H-pyran (below). Protons labeled as 6 are assigned by process of elimination.
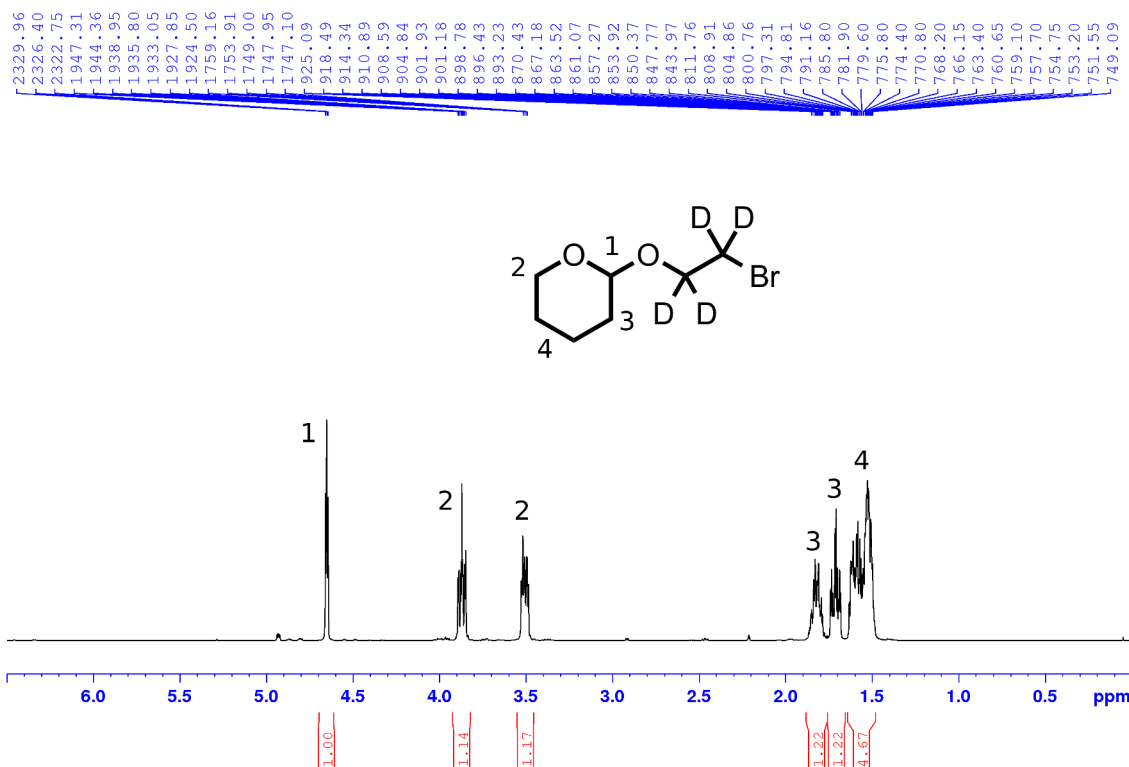
Discussion on assignment of IR peaks for derivative AP-E4
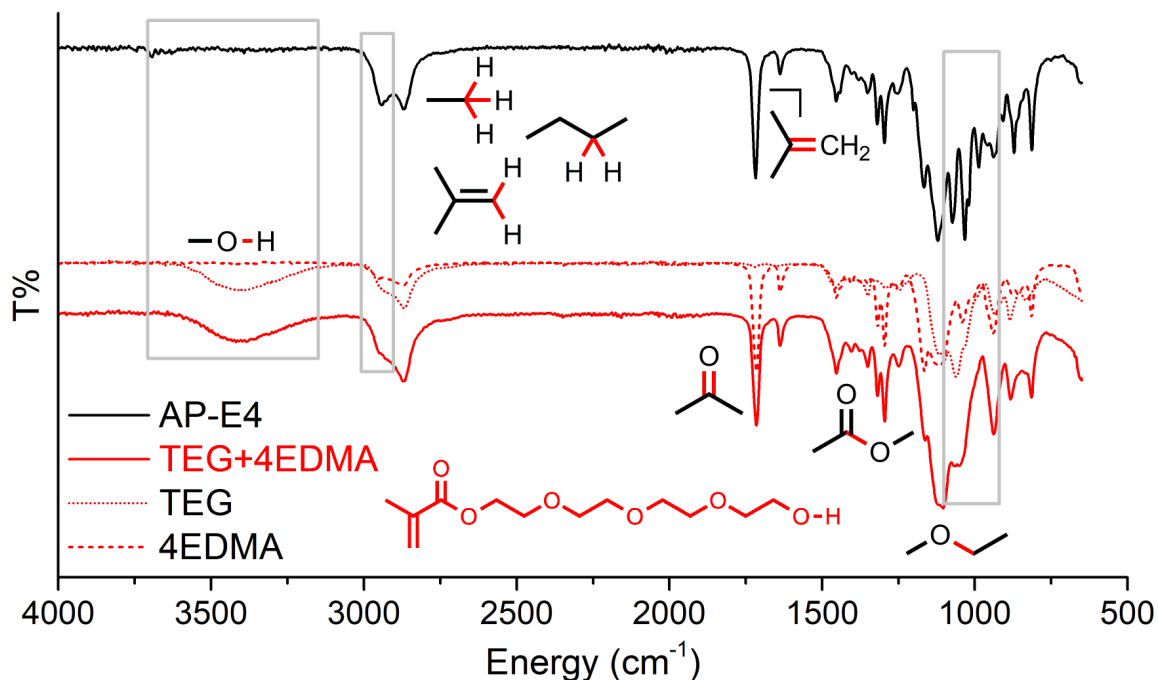
In both the spectra of AP-E4 and TEG+4EDMA, peaks relative to the double bond (~ 1640 cm^{-1}), the carbonyl (~ 1720 cm^{-1}) and the ester bond (1300-1320 cm^{-1}) are easily identifiable. Peaks relative to C$-$H bonds (2870-2950 cm^{-1}) are obvious as well, being more intense for AP-E4 for the presence of the pyran ring. The broad band around ~ 3400 cm^{-1} is due to the O$-$H, in fact is present in the TEG spectrum only. The

large band from 980 to 1200 cm^{-1} is related to signals of C$-$O ether bonds. The residual peaks in the spectrum of AP-E4 which do not have any counterpart in the TEG+4EDMA spectrum (985/1020/1033 cm^{-1}), should be related therefore to the pyran ring.

The figure shows the IR spectrum of AP-E4 derivative (black), TEG (red, dotted line), 4EDMA (red, dashed line) and their linear combination TEG+4EDMA (red, full line), which would ideally represent the derivative tetraethylene glycol methacrylate depicted in red. This derivative differs from AP-E4 for the absence of the pyran ring, differences being highlighted within gray rectangles.

IR peaks of AP-E4/T80 mixture
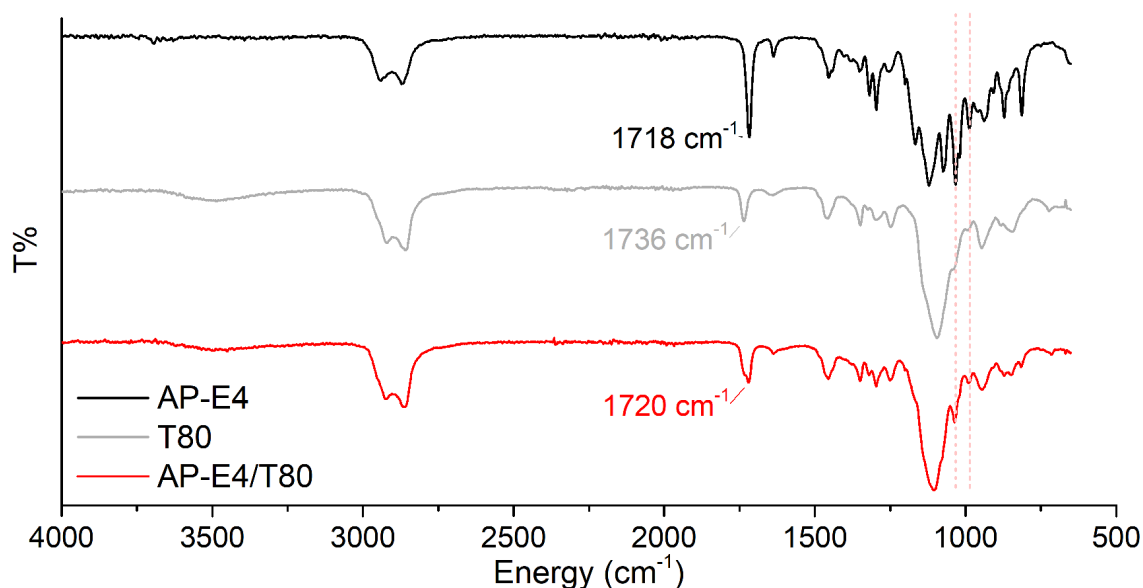
The figure shows IR spectra of AP-E4 (black), T80 (gray) and a mixture of both as prepared before a polymerization (red). Spectra of AP-E4 and T80 are qualitatively similar, as they are formed by similar components. However, the peak relative to the carbonyl group has a different energy for the two derivatives, the one of AP-E4 being conjugated to a double bond, and therefore less stiff (and consequently energetic). The peak of the double bond, on the other side, is not visible enough to be used as a reliable signal; moreover it has the same energy of one of the peaks of water, which would prevent the signals identification if the sample is not perfectly dry.

Although not extremely intense, two signals of the pyran ring of AP-E4 (pinpointed by the pink, dashed lines) remain visible in the spectrum of the mixture.

Synthesis of Qn-Oct
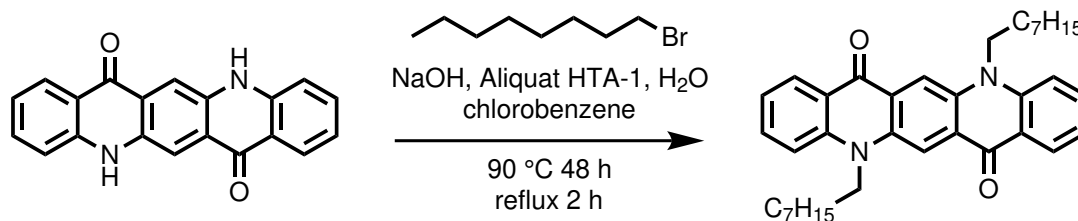
In a two-necked, 250 mL roundbottom flask NaOH (160 mmol, 6,40 g) and quinacridone (16 mmol, 5,00 g) are put under N_2 atmosphere, then Aliquat® HTA-1 (0,5 mL), water (5,9 mL) and chlorobenzene (50 mL) are added, and the mixture is stirred for 30 minutes. Octyl bromide (96 mmol, 18,54 g) is finally added, and the temperature is raised to 90 °C. After 48 hours, the mixture is refluxed for two hours before cooling at room temperature. The solvent is evaporated, and the solid residue is taken up with water. Toluene is added to the resulting suspension, and the mixture is filtered through a fritted funnel. The solid is collected, while the organic phase is washed with water and dried over anhydrous Na_2SO_4. After filtration, the solvent is removed under reduced pressure, and the solid collected with the previous one. This final crude is purified by flash chromatography using solvent gradient elution (CH_2Cl_2 to CH_2Cl_2/AcOEt 9:1). Final yield: 4,81 g, 56%

^{1}H NMR (CDCl$_3$, 500 MHz): δ 8.78 (s, 2H), 8.58 (dd, J_1=3.9 Hz, J_2=1.7 Hz), 7.76 (m, 2H), 7.52 (d, J=8.8 Hz, 2H), 7.28 (t, J=7.2 Hz, 2H), 4.52 (t, J=8.1 Hz, 4H), 2.02 (quin, J=7.9 Hz, 4H), 1.63 (quin, J=7.7 Hz, 4H), 1.47 (quin, J=7.5 Hz, 4H), 1.30-1.40 (m, 12H), 0.90 (t, J=7.0 Hz, 6H).
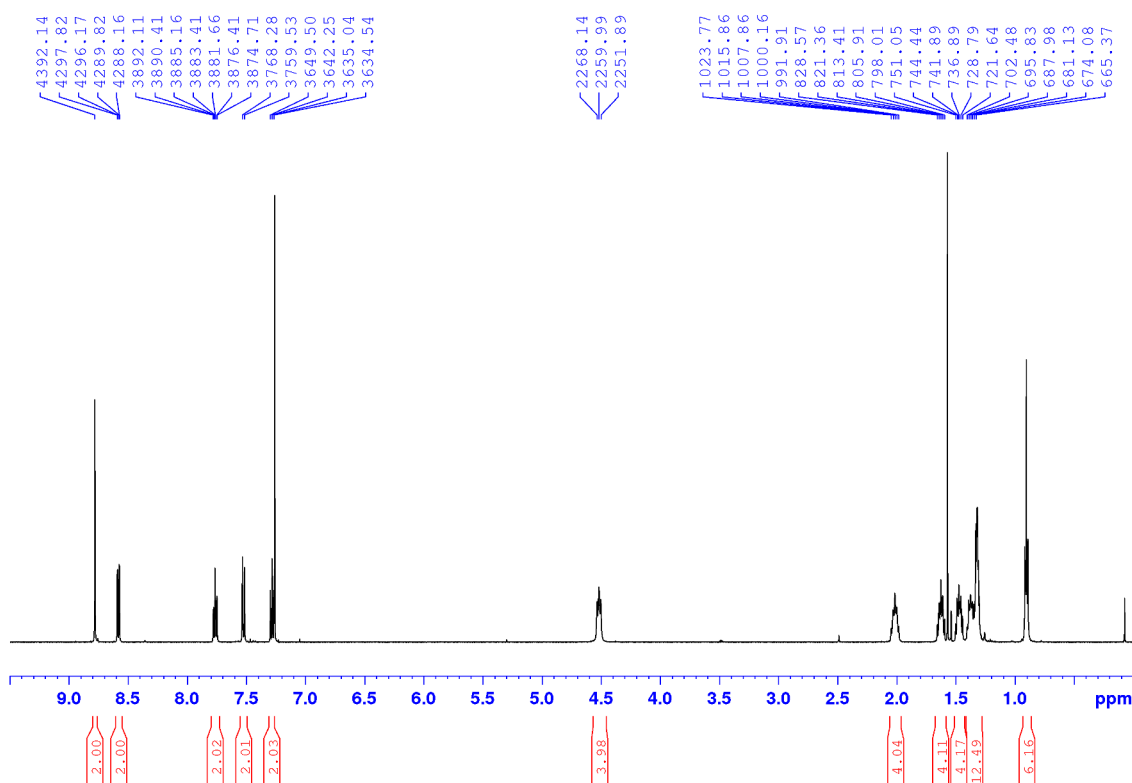
^{13}C NMR (CDCl$_3$, 100.6 MHz*): δ 178.20, 142.37, 135.85, 134.71, 128.18, 126.41, 121.19, 120.92, 114.62, 113.58, 46.46, 31.80, 29.43, 29.32, 27.18, 27.06, 22.66, 14.11.
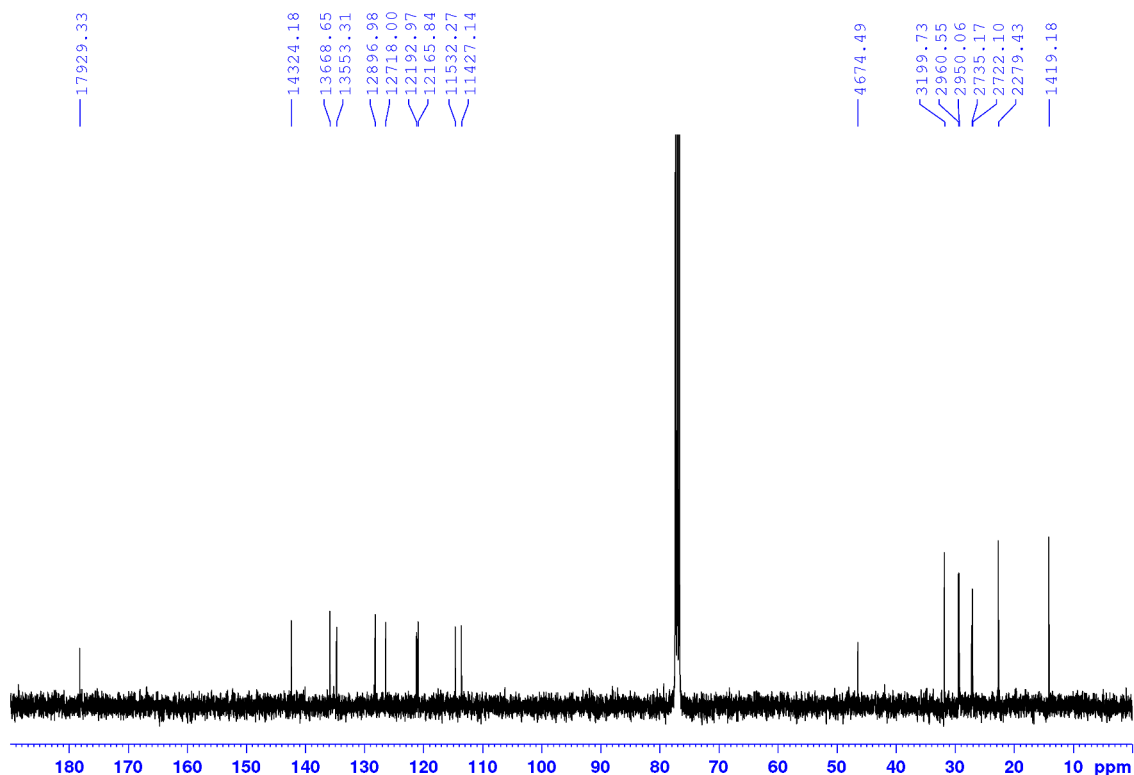
Conditions for polymerization of micellar dispersions

Derivative	MW (g·mol^{-1})	amount (mg)	vol (mL)	n (µmol)
T80	1310	87,0	-	66,4
AP-E4	346,42	33,0	-	95,3
4EDMA (if present)	330,38	1,60	-	4,84
distilled water	-	-	40	-
THF	-	-	1,5	-
radical initiator	-	-	-	3,70

AP-E4 and T80 are dissolved in 1 mL of THF, and the solution is injected in water. 4EDMA is added only in case of crosslinking. The dispersion is stirred overnight before addition of the radical initiator. The initiator is introduced as THF solution (0,5 mL, 7,4 mM), swiftly injected in the stirring dispersion of AP-E4/T80. The final dispersion is allowed to equilibrate for 30 minutes before polymerization.

The chosen concentration of initiator is ∼4 mol% with respect to the co-surfactant AP-E4. This concentration would be extremely high for a classic radical polymerization, nonetheless we decided to use it with the idea of introducing at least three molecules of initiator per micelle (the amount is calculated on the basis of data in table 4.1), in order to allow the polymerization starting in most of the micelles.

Additional information about specific polymerizations are detailed below.

---

*This spectrum only was acquired with a Bruker NMR Avance 400 NEO.

Photopolymerization

The mercury lamp (low pressure, 125 W) and its power supply were purchased from Helios Italquartz Srl. Polymerization is performed in a quartz reactor (20 cm high, 1,5 cm diameter).

The UV curing oven (shown in figure 4.17) was purchased from Proxima Direct® (model number J0202), and it is equipped with four 9 W lamps UV-9W. Polymerization is performed in a quartz reactor (20 cm high, 1,5 cm diameter).

Thermal polymerization

The micellar dispersion is prepared in a 100 mL roundbottom flask and heated in a silicon bath using a heating plate equipped with a temperature controller.

Loading of organic species

Derivative	MW (g · mol^{-1})	amount (mg)	vol (mL)	n (µmol)
Pyrene	202,25	8,10	-	40,0
Qn-Ott	536,75	21,5	-	40,0
THF	-	-	4,00	-
p-xylene	106,16	-	0,50	-

The chosen organic species is dissolved in the solution of THF and p-xylene. p-Xylene is used as co-solvent to obtain a clear solution. 1 mL of the prepared solution is injected in the micellar dispersion, and the latter is allowed to equilibrate for at least 2 h before use.

Characterization of micellar dispersions

Morphological characterization

IR spectra were collected with a PerkinElmer FT-ATR spectrophotometer Spectrum 100.

DLS experiments were performed on a 90Plus Particle Size Analyzer (Brookhaven Instruments Corporation) with scattering angles of 15° and 90°, equipped with a 35 mW solid state 632,8 nm laser and a Brookhaven's TuboCorr correlator with 510 channels. Unless otherwise stated, measurements were run at 20 °C. Zetasizer software was always allowed to optimize both measurement position and attenuator, choosing water as dispersant. Three consecutive measurements have been run on each sample, and mediated to obtain the final intensity distribution. Measurements were run on 1 mL of micellar dispersion in a disposable cuvette.

SEM images were collected by Cristina Cazzaniga, to which the author is truly grateful, in De Nora laboratories (Milano). The used instrument was a SEM/FEG Inspect F 50-FEI.

Optical characterization

Absorption spectra were collected with a Jasco V-570 spectrophotometer.

Photoluminescence spectra were collected with a Varian Cary Eclipse spectrofluorometer.

Appendix: interpretation of DLS measurements

When light hits small particles, it is scattered in all directions, and even if the light source is a laser, the scattering intensity fluctuates over time. This fluctuation is due to Brownian motion of the particles: the distance between the scatterers in the solution constantly changes with time, leading to constructive or destructive interference of the scattered light. The dynamic information of the particles is derived from an autocorrelation of the intensity trace $I(t)$ recorded during the experiment, defined as[79]

$$g^2(\tau) = \frac{\langle I(t)I(t+\tau)\rangle}{\langle I(t)\rangle^2}$$

where τ is the delay time. At short delay times, the correlation is high because the particles do not have a chance to move to a great extent from their initial states. The two signals are thus essentially unchanged when compared after a very short time interval. As the delay times become longer, the correlation decays exponentially, meaning that, after a long time period has elapsed, there is no correlation between the scattered intensity of the initial and final states. This exponential decay is related to the motion of the particles, specifically to the diffusion coefficient, and is described by a function[79]

$$G(\tau) = g(\tau) - 1 = \beta e^{-2Dq^2\tau}$$

β being an instrumental parameter, D being the diffusion coefficient of the particles and q the scattering wavevector. Size of the particles is contained in the diffusion coefficient, and can be calculated using Stokes-Einstein equation.[80]

This mathematical introduction is needed to make aware that, during a DLS measurement, the intensity fluctuation of the scattered light is the only measured quantity, all other information being obtained from calculations performed by the software. This means that, unless the used solution does not scatter light at all, the instrument can always calculate a size distribution, but this does not mean the measurement is reliable.

The right output to look at is therefore not the size distribution, but the correlogram obtained as $g(\tau)^{-1}$, which contains only the scattering intensity. For a reliable measurement, this is a sigmoidal function, whose value is close to 1 for short delay times, and goes to zero for long delay times. If the correlogram does not approach zero, or the shape anyway is not that of a sigmoidal function, the measurement cannot be considered reliable.

It is also important to consider that the size distribution, again, is obtained through a calculation, fitting the correlation function. As the instrument is able to fit it using multiple decay functions (in order to be able to distinguish different families of particles, if necessary), it might be that the software obtains the best fitting using two functions instead of one, therefore reporting more than one family of particles even when only one is present. When two family of particles are reported by the instrument, the size distribution can be considered reliable only when the peaks are completely resolved one from the other, and sizes differ for at least one order of magnitude. In all other cases, if more than one family of particles is present, this technique gives ambiguous results.[75]

Bibliography

[1] Kresheck, G. C., Hamori, E., Davenport, G., and Scheraga, H. A. *J. Am. Chem. Soc.* **1966**, *88*, 246–253. doi: 10.1021/ja00954a013.

[2] Folger, R., Hoffmann, H., and Ulbricht, W. *Ber. Bunsenges. Phys. Chem* **1974**, *78*, 986–997. doi: 10.1002/bbpc.19740781006.

[3] Aniansson, E. A. G. and Wall, S. N. *J. Phys. Chem.* **1974**, *78*, 1024–1030. doi: 10.1021/j100603a016.

[4] Aniansson, E. A. G. and Wall, S. N. *J. Phys. Chem.* **1975**, *79*, 857–858. doi: 10.1021/j100575a019.

[5] Aniansson, E. A. G., Wall, S. N., Almgren, M., Hoffmann, H., Kielmann, I., Ulbricht, W., Zana, R., Lang, J., and Tondre, C. *J. Phys. Chem.* **1976**, *80*, 905–922. doi: 10.1021/j100550a001.

[6] Lessner, E., Teubner, M., and Kahlweit, M. *J. Phys. Chem.* **1981**, *85*, 1529–1536. doi: 10.1021/j150611a014.

[7] Hall, G. D. *J. Chem. Soc. Faraday Trans. 2* **1981**, *77*, 1973–2006. doi: 10.1039/F29817701973.

[8] Ulbricht, W. and Zana, R. *Colloids Surf. A* **2001**, *185*, 487–494. doi: 10.1016/S0927-7757(01)00560-X.

[9] Lund, R., Willner, L., and Richter, D. *Kinetics of block copolymer micelles studied by small-angle scattering methods.*, chap. 2, in *Controlled Polymerization and Polymeric Structures*, vol. 259 of *Advances in Polymer Science*. Springer, Cham, **2013**, pp. 51–158. ISBN 978-3-319-02919-1.

[10] Zana, R. (Editor). *Dynamics of Surfactant Self-Assemblies*. CRC Press, Boca Ranton, **2005**. ISBN 978-0-8247-5822-6.

[11] Patist, A., Kanicky, J. R., Shukla, P. K., and Shah, D. O. *J. Colloid Interface Sci.* **2002**, *245*, 1–15. doi: 10.1006/jcis.2001.7955.

[12] Patist, A., Jha, B. K., Oh, S.-G., and Shah, D. O. *J. Surfactants Deterg.* **1999**, *2*, 317–324. doi: 10.1007/s11743-999-0083-6.

[13] Aniansson, G. E. A. *The mean lifetime of a micelle*, in *Surfactants, Adsorption, Surface Spectroscopy and Disperse Systems*, vol. 70. Steinkopff-Verlag Heidelberg, **1985**, pp. 2–5. ISBN 978-3-662-16084-8.

[14] Larrabee, C. E. and Sprague, E. D. *J. Polym. Sci. Polym. Lett.* **1979**, *17*, 749–751. doi: 10.1002/pol.1979.130171201.

[15] Boutevin, B., Robin, J.-J., Boyer, B., Lamaty, G., Leydet, A., Roque, J.-P., and Senhaji, O. *New J. Chem.* **1996**, *20*, 137–142.

[16] Stähler, K., Selb, J., Barthelemy, P., Pucci, B., and Candau, F. *Langmuir* **1998**, *14*, 4765–4775. doi: 10.1021/la980245d.

[17] Stähler, K., Selb, J., and Candau, F. *Langmuir* **1999**, *15*, 7565–7576. doi: 10.1021/la990431z.

[18] Guyot, A. and Tauer, K. *Reactive surfactants in emulsion polymerization.* Springer, Berlin, Heidelberg, **1994**, pp. 43–65. ISBN 978-3-540-57198-8.

[19] Gadberry, J. F., Otterson, R., Hill, R. M., Bognolo, G., and Thomas, R. R. *Other Types of Surfactants*, chap. 6, in *Chemistry and Technology of Surfactants*. Blackwell Publishing Ltd, **2007**, pp. 153–235. ISBN 978-1-4051-2696-0.

[20] Morizur, J.-F., Irvine, D. J., Rawlins, J. J., and Mathias, L. J. *Macromolecules* **2007**, *40*, 8938–8946. doi: 10.1021/ma0717486.

[21] Sponchioni, M., Palmiero, U. C., and Moscatelli, D. *HPMA-PEG Surfmers and Their Use in Stabilizing Fully Biodegradable Polymer Nanoparticles*, **2017**. Ahead of print on *Macromol. Chem. Phys.* doi: 10.1002/macp.201700380.

[22] Tan, Y. Z., Wu, D., Lee, H. T., Wang, H., Honciuc, A., and Chew, J. W. *Colloids Surf. A* **2017**, *533*, 179–186. doi: 10.1016/j.colsurfa.2017.08.036.

[23] Friedrich, T., Tieke, B., Meyer, M., Pyckhout-Hintzen, W., and Pipich, V. *J. Phys. Chem. B* **2010**, *114*, 5666–5677. doi: 10.1021/jp911358z.

[24] Li, W., An, H., Tan, Y., Lu, C., Liu, C., Li, P., Xu, K., and Wang, P. *Soft Matter* **2012**, *8*, 5078–5086. doi: 10.1039/C2SM07200A.

[25] Sauer, R., Turshatov, A., Baluschev, S., and Landfester, K. *Macromolecules* **2012**, *45*, 3787–3796. doi: 10.1021/ma300090a.

[26] Fischer, V., Lieberwirth, I., Jakob, G., Landfester, K., and Muñoz Espí, R. *Adv. Funct. Mater.* **2013**, *23*, 451–466. doi: 10.1002/adfm.201201839.

[27] Summers, M. and Eastoe, J. *Adv. Colloid Interface Sci.* **2003**, *100-102*, 137–152. doi: 10.1016/S0001-8686(02)00058-1.

[28] Kline, S. R. *Langmuir* **1999**, *15*, 2726–2732. doi: 10.1021/la981451o.

[29] FitzGerald, P. A. and Warr, G. G. *Adv. Colloid Interface Sci.* **2012**, *179-182*, 14–21. doi: 10.1016/j.cis.2012.06.003.

[30] Kotzev, A., Laschewsky, A., Adriaensens, P., and Gelan, J. *Macromolecules* **2002**, *35*, 1091–1101. doi: 10.1021/ma011047n.

[31] Laschewsky, A. *Curr. Opin. Colloid Interface Sci.* **2003**, *8*, 274–281. doi: 10.1016/S1359-0294(03)00049-9.

[32] Wang, D., Ji, W.-X., Li, Z.-C., and Chen, L. *J. Am. Chem. Soc.* **2006**, *128*, 6556–6557. doi: 10.1021/ja060907i.

[33] Peng, M., Liao, Z., Zhu, Z., and Guo, H. *Macromolecules* **2010**, *43*, 9635–9644. doi: 10.1021/ma101953h.

[34] Kopeć, M., Niemiec, W., Laschewsky, A., Nowakowska, M., and Zapotoczny, S. *J. Phys. Chem. C* **2014**, *118*, 2215–2221. doi: 10.1021/jp410808z.

[35] Service, R. F. *Science* **2005**, *309*, 95–95. doi: 10.1126/science.309.5731.95.

[36] Jafvert, C. T., Patricia, L. H., and Heath, J. K. *Water Res.* **1994**, *28*, 1009–1017. doi: 10.1016/0043-1354(94)90185-6.

[37] Li, J.-L. and Chen, B.-H. *Chem. Eng. Sci.* **2002**, *57*, 2825 – 2835. doi: 10.1016/S0009-2509(02)00169-0.

[38] Fischer, E., Fieber, W., Navarro, C., Sommer, H., Benczédi, D., Velazco, M. I., and Schönhoff, M. *J. Surfactants Detergents* **2009**, *12*, 73–84. doi: 10.1007/s11743-008-1104-4.

[39] Pandya, K., Lad, K., and Bahadur, P. *J. Macromol. Sci., Part A* **1993**, *30*, 1–18. doi: 10.1080/10601329308009387.

[40] Mukherjee, P., Padhan, S. K., Dash, S., Patel, S., and Mishra, B. K. *Adv. Colloid Interface Sci.* **2011**, *162*, 59–79. doi: 10.1016/j.cis.2010.12.005.

[41] Salager, J.-L. *Emulsion phase inversion phenomena*, in *Emulsions and emulsion stability*. Boca Raton, **2006**, ISBN 978-0-8247-2695-9.

[42] Witthayapanyanon, A., Harwell, J., and Sabatini, D. *J. Colloid Interface Sci.* **2008**, *325*, 259–266. doi: 10.1016/j.jcis.2008.05.061.

[43] Griffin, W. C. *J. Soc. Cosmetic Chem.* **1954**, *5*, 249–256.

[44] Mollet, H. and Grubenmann, A. *Formulation Technology: Emulsions, Suspensions, Solid Forms*. John Wiley & Sons, **2008**. ISBN 3-527-30201-8.

[45] Fateminia, S. M. A., Wang, Z., and Liu, B. *Small Methods* **2017**, *1*, 1600023. doi: 10.1002/smtd.201600023.

[46] Fery-Forgues, S. *Nanoscale* **2013**, *5*, 8428–42. doi: 10.1039/c3nr02657d.

[47] Xing, P. and Zhao, Y. *Adv. Mater.* **2016**, *28*, 7304–7339. doi: 10.1002/adma.201600906.

[48] Nie, K., Dong, B., Shi, H., Liu, Z., and Liang, B. *Anal. Chem.* **2017**, *89*, 2928–2936. doi: 10.1021/acs.analchem.6b04258.

[49] Buurma, N. J. *Annu. Rep. Prog. Chem., Sect. B: Org. Chem.* **2011**, *107*, 328–348. doi: 10.1039/C1OC90014E.

[50] Matsushima, Y., Nishiyabu, R., Takanashi, N., Haruta, M., Kimura, H., and Kubo, Y. *J. Mater. Chem.* **2012**, *22*, 24124–24131. doi: 10.1039/C2JM34797K.

[51] Baba, K., Kasai, H., Shinohara, Y., Okada, S., Oikawa, H., Matsuda, H., and Nakanishi, H. *Jpn. J. Appl. Phys.* **2008**, *47*, 3769. doi: 10.1143/JJAP.47.3769.

[52] Zhang, X., Zhang, X., Tao, L., Chi, Z., Xu, J., and Wei, Y. *J. Mater. Chem. B* **2014**, *2*, 4398–4414. doi: 10.1039/C4TB00291A.

[53] He, G. S., Tan, L.-S., Zheng, Q., and Prasad, P. N. *Chem. Rev.* **2008**, *108*, 1245–1330. doi: 10.1021/cr050054x.

[54] Nakanishi, H. and Oikawa, H. *Reprecipitation Method for Organic Nanocrystals*, in *Single Organic Nanoparticles*. Springer-Verlag Berlin Heidelberg, **2003**, pp. 17–31. ISBN 978-3-642-62429-2.

[55] http://goldbook.iupac.org/html/I/I03117.html. Accessed 26-11-2017.

[56] Carlucci, L., Ciani, G., and Proserpio, D. M. *Coord. Chem. Rev.* **2003**, *246*, 247–289. doi: 10.1016/S0010-8545(03)00126-7.

[57] Sperling, L. H. and Hu, R. *Interpenetrating Polymer Networks*, in *Polymer Blends Handbook*. Springer Netherlands, Dordrecht, **2003**, pp. 417–447. ISBN 978-0-306-48244-1.

[58] Dragan, E. S. *Chem. Eng. J.* **2014**, *243*, 572–590. doi: 10.1016/j.cej.2014.01.065.

[59] http://www.sigmaaldrich.com/catalog/product/sial/p1754?lang=en&region=US. Accessed 26-11-2017.

[60] Zhang, Q., Wang, A., Meng, Y., Ning, T., Yang, H., Ding, L., Xiao, X., and Li, X. *Anal. Chem.* **2015**, *87*, 9810–9816. doi: 10.1021/acs.analchem.5b02096.

[61] McCarroll, M., Toerne, K., and von Wandruszka, R. *Langmuir* **1998**, *14*, 2965–2969. doi: 10.1021/la971284c.

[62] Duus, J. Ø., Gotfredsen, C. H., and Bock, K. *Chem. Rev.* **2000**, *100*, 4589–4614. doi: 10.1021/cr990302n.

[63] http://www.sigmaaldrich.com/content/dam/sigma-aldrich/docs/Aldrich/ General_Information/photoinitiators.pdf. Accessed 26-11-2017.

[64] Chemtob, A., Kunstler, B., Croutxé-Barghorn, C., and Fouchard, S. *Colloid Polym. Sci.* **2010**, *288*, 579–587. doi: 10.1007/s00396-010-2190-1.

[65] http://www.amazon.it/dp/B006RR7FO4/ref=asc_df_B006RR7FO447667026/?tag= googshopit-21&creative=23402&creativeASIN=B006RR7FO4&linkCode=df0& hvdev=c&hvnetw=g&hvqmt=. Accessed 26-11-2017.

[66] Heine, H.-G., Rosenkranz, H.-J., and Rudolph, H. *Angew. Chem., Int. Ed.* **1972**, *11*, 974–978. doi: 10.1002/anie.197209741.

[67] Hutchison, J. and Ledwith, A. *Photoinitiation of vinyl polymerization by aromatic carbonyl compounds*, vol. 14 of *Advances in Polymer Science*. Springer, Berlin, Heidelberg, **1974**, pp. 49–86. ISBN 978-3-540-06649-1. doi: 10.1007/3-540-06649-7_2.

[68] Bibaut-Renauld, C., Burget, D., Fouassier, J. P., Varelas, C. G., Thomatos, J., Tsagaropoulos, G., Ryrfors, L. O., and Karlsson, O. J. *J. Polym. Scie. Part A: Polym. Chem.* **2002**, *40*, 3171–3181. doi: 10.1002/pola.10407.

[69] Encina, M. V., Lissi, E. A., Koch, V., and Elorza, E. *J. Polym. Sci.: Polym. Chem. Ed.* **1982**, *20*, 73–78. doi: 10.1002/pol.1982.170200108.

[70] Strom, E. T., Russell, G. A., and Schoeb, J. H. *J. Am. Chem. Soc.* **1966**, *88*, 2004–2007. doi: 10.1021/ja00961a028.

[71] Pryor, W. A., Cornicelli, J. A., Devall, L. J., Tait, B., Trivedi, B. K., Witiak, D. T., and Wu, M. *J. Org. Chem.* **1993**, *58*, 3521–3532. doi: 10.1021/jo00065a013.

[72] http://www.sigmaaldrich.com/content/dam/sigma-aldrich/docs/Aldrich/General_Information/thermal_initiators.pdf. Accessed 26-11-2017.

[73] http://www.wako-chemicals.de/files/download/pdf/wako_azo_polymerization_initiators_catalog_25.pdf. Accessed 26-11-2017.

[74] Seinfeld, J. H. and Pandis, S. N. *Atmospheric chemistry and physics: from air pollution to climate change.* John Wiley & Sons, Hoboken, New Jersey, **2006**. ISBN 978-0-471-72018-8.

[75] Till, U., Gibot, L., Mingotaud, C., Vicendo, P., Rols, M.-P., Gaucher, M., Violleau, F., and Mingotaud, A.-F. *Nanotechnology* **2016**, *27*, 315102. doi: 10.1088/0957-4484/27/31/315102.

[76] Kalyanasundaram, J. K. and Thomas, K. *J. Am. Chem. Soc.* **1977**, *99*, 2039–2044. doi: 10.1021/ja00449a004.

[77] Eisfeld, A. and Briggs, J. *Chem. Phys,* **2006**, *324*, 376–384. doi: https://doi.org/10.1016/j.chemphys.2005.11.015.

[78] Sakellariou, E. G., Montalban, A. G., Beall, S. L., Henderson, D., Meunier, H. G., Phillips, D., Suhling, K., Barrett, A. G., and Hoffman, B. M. *Tetrahedron* **2003**, *59*, 9083–9090. doi: 10.1016/j.tet.2003.09.060.

[79] Goldburg, W. I. *Am. J. Phys.* **1999**, *67*, 1152–1160. doi: 10.1119/1.19101.

[80] Atkins, P. and de Paula, J. *Atkins' Physical Chemistry.* Oxford University Press, **2014**. ISBN 978-01-996-9740-3.

Chapter 5

Surfactant-driven self-assembly of hybrid perovskite nanoplatelets

Dadurch kann ich mich dir nun vorstellen.
Und damit ist die Vorstellung zu Ende.

Michael Ende
DER SPIEGEL IM SPIEGEL

Within the frame of the work done, the project presented here may appear a bit out of line. Surfactants, in this case, are again used for their inherent ability to define confined systems, but in a totally different way. We are not speaking of micelles and water, the surfactant is not "the box where things happen" anymore. The surfactant becomes active part, building block in a hybrid material. This difference, although remarkable, does not change the point of the whole work: taking advantage of the peculiar properties of a class of molecules, and their interaction with the environment, to create objects with new and different characteristics. What is more, we are again taking advantage of self-assembly and colloidal methods to do it.

From the point of view of the design of the surfactants, we are totally changing perspective. We move from non-ionic to cationic molecules, in particular the polar head needs to be an ammonium ion. The apolar tail, on the other side, allows more freedom of choice, its characteristics tuning the properties of the final material. We started working with classic long chain alkylammonium salts to learn and practice on the job, as these materials and their interactions are well-known, and have a long track in assembly of colloidal nanocrystals. Subsequently we moved to a way more challenging material, the ammonium salt of a polymeric dimethylsiloxane, which is nearly unexplored for the purpose.

5.1 Perovskites: sometimes they come back

Perovskite is the name of a class of minerals whose chemical formula is ABO_3, A representing a cation with a big ionic radius and B representing a cation with a small ionic radius (O is oxygen, of course), the most famous being $CaTiO_3$. Minerals pertaining to this class have the very peculiar crystal lattice shown in figure 5.1, where the small B ions are surrounded by six oxygen atoms in an octahedral geometry, while the big A cations have a 12-fold cuboctahedral coordination.[1, 2] Synthetic materials, with chemical formula ABX_3 (where X may be oxygen or an halogen) and the same crystal structure, are therefore known as perovskites, and they have been extensively studied since their discovery because they may show a wide variety of interesting properties, such as piezoelectricity in $BaTiO_3$ or superconductivity in $YBa_2Cu_3O_7$*. Since the stability of perovskite structure (namely, the lattice distortion) is described by the Goldschmidt tolerance factor[3, 4]
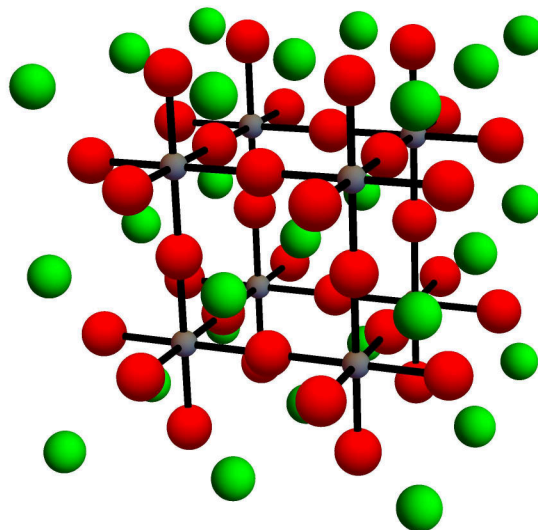
Figure 5.1 Perfect perovskite cubic crystal structure: A, B and O ions are respectively represented in green, gray and red.

$$t = \frac{R_A + R_X}{\sqrt{2}(R_B + R_X)} \in [0.89,\ 1.1]^\dagger$$

(where R_A, R_B and R_X are the ionic radii of A, B and X atoms respectively), the variety of existing perovskite materials - both natural and synthetic - is extremely wide. A very peculiar subclass is represented by the hybrid organic-inorganic perovskites, that have small organic cations in B lattice sites. The interest for these hybrid materials started in the late '70s, when they have been discovered and studied firstly,[5–7] and raised again starting from 2009, with the claim of the first hybrid solar cell.[8] Since then, these materials have met an increasing interest for their optoelectronic properties,[9–17] which last year ended with a perovskite solar cell breaking the record of polycrystalline silicon.[18, 19] $Pb(CH_3NH_3)I_3$ is the main representative of this group, but perovskites with different compositions are also studied, such as having halides different than iodide,[9, 20, 21] formamidinium B cation $CH(NH_2)_2{}^+$ instead of methylammonium $CH_3NH_3{}^+$,[11, 22] or tin instead of lead.[23]

---

*This synthetic mineral has a tripled unit cell, which is oxygen-deficient.

†The lower value is due to geometrical constraints, while the upper one is purely based on empirical observations.

5.2 Ruddlesden-Popper perovskites

The so called Ruddlesden-Popper (R-P) perovskites are a class of perovskite-like minerals with general formula $A_nB_{n-1}X_{3n+1}C_2$, where A, B and C are cations (A and B having the standard perovskite geometry, while C having coordination number of 9), and n represents the number of unit cells in the layer. This means that several layered perovskite structures exist, with layers of different thickness in a double bed of cations.[24] Figure 5.2 represents the crystal lattices for minerals having $n = 1$ and $n = 2$. They clearly owe their name to S. N. Ruddlesden and P. Popper, the discoverers of the crystalline structures.[25, 26]
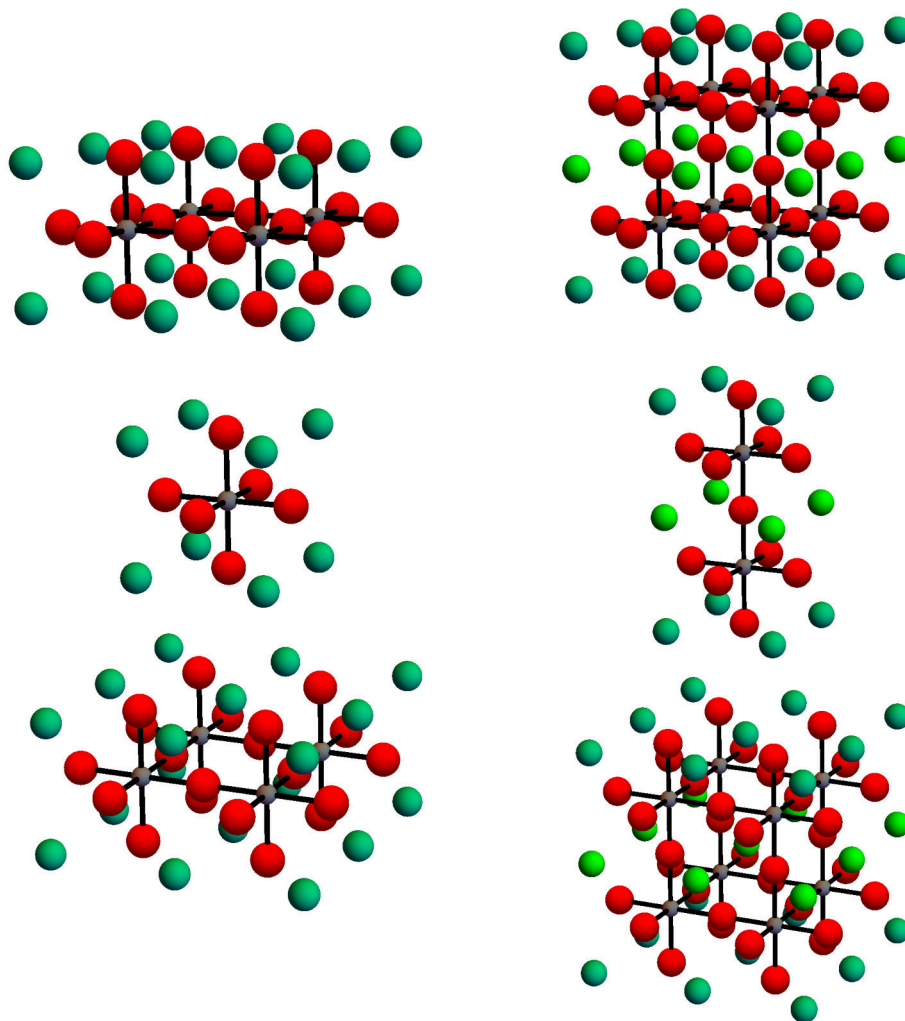
Figure 5.2 Ruddlesden-Popper perovskites $A_{n-1}B_nX_{3n+1}C_2$ lattices with n=1 (top) and n=2 (bottom). A is bright green, B is gray, C is bluish green and X is red.

Hybrid R-P homologous perovskites exist, which have bulky ammonium cations in the C lattice sites, such as alkylammonium cations with chain length of two or more carbon atoms, or arylammonium cations.[27] Lead iodide based materials have been studied in the early 90's,[28] and are now returning to the spotlight for applications in solar cells, transistors, and LEDs.[29–31] However, several synthetic materials with these structures are known, having germanium, tin[32, 33] or a lanthanide[34] as B cation, and different halogens as X anions. The main interest for these synthetic minerals is related to their opto-electronic
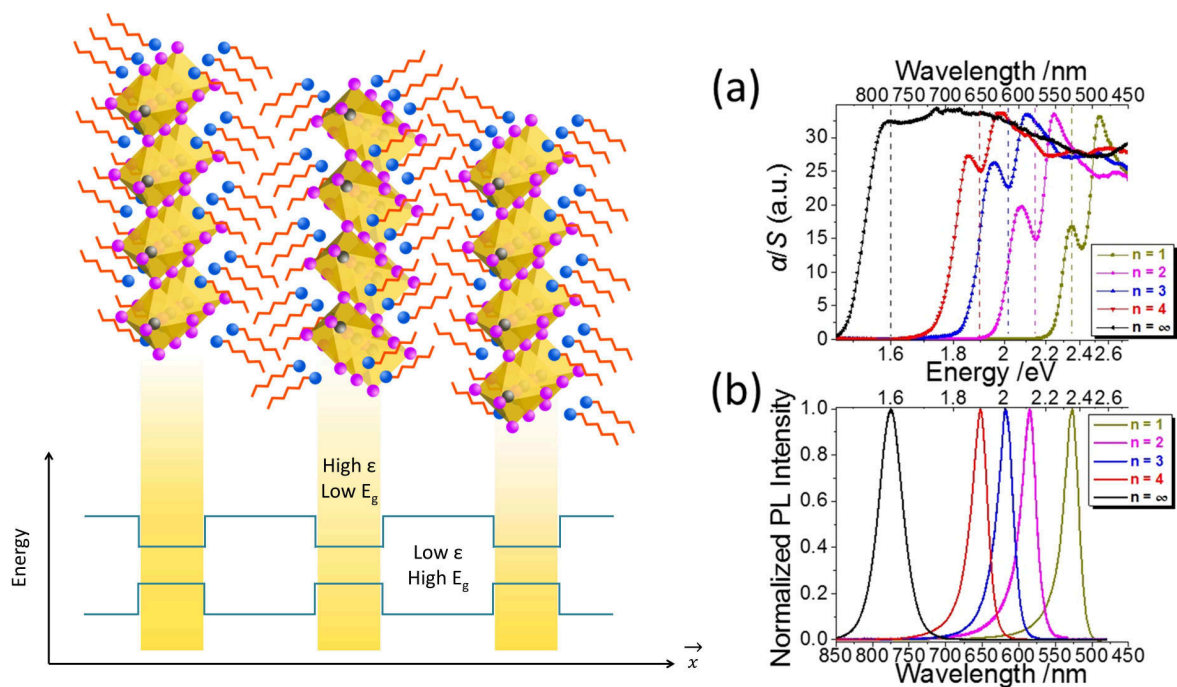
Figure 5.3 On the left: Cartoon of a Ruddlesden-Popper homologous structure for hybrid $PbI_4(R-NH_3)_2$ perovskite (Pb being represented in gray, I in purple, R in orange and NH_3 in blue) and its simplified energy diagram in the real space. On the right: optical absorption (a) and photoluminescence (b) of $Pb_nI_{3n+1}(CH_3-NH_3)_{n-1}(CH_3-CH_2-CH_2-CH_2-NH_3)_2$ perovskites for n = 1, 2, 3, 4, ∞. Reproduced with permission from [37].*

properties, which arise from their peculiar structure. In fact, these materials are composed of alternate layers of inorganic $BX_6{}^{4-}$ octahedra of a material with high dielectric constant and low energy gap, and organic ammonium cations with opposite characteristics. For this reason, the material behave as a natural quantum well, where excitons can form in the inorganic layers, and are stabilized both by a confinement effect and the small Coulombic screening.[35] The energy of the exciton is mainly dependent on the nature of the inorganic semiconductor and the layer thickness. In particular, the valence band maximum is influenced by the p states of the X anion, while the p states of both the X anion and the B cation influence the conduction band minimum. The influence of the ammonium cation is usually considered negligible from the computational point of view. However, bulky organic cations may stack in odd corrugated structures, thus modifying the X$-$B$-$X bond angle. This is known to have an effect on the bandgap, which can vary up to 0,75 eV[36] depending on the angle. The number n of perovskite layers makes the energy gap smaller, so a red shift in the exciton peak is observed for the same material for increasing layer thicknesses. Figure 5.3 shows a cartoon of a $PbI_4(R-NH_3)_2$ material and the variation in the exciton energy for $Pb_nI_{3n+1}(CH_3-NH_3)_{n-1}(CH_3-CH_2-CH_2-CH_2-NH_3)_2$ for n = 1, 2, 3, 4, ∞. This last characteristic is particularly interesting, as it proves how, for a given composition, the exciton energy can be considered a fingerprint of the material, unequivocally identifying its structure.

---

*Direct link to the article: http://pubs.acs.org/doi/abs/10.1021/acs.chemmater.6b00847. Further permissions related to the material excerpted should be directed to the ACS.

5.3   Colloidal 2D perovskite nanoplatelets

The standard growth technique for hybrid layered perovskites is crystallization from an aqueous solution of the precursors, which affords the material as bulky single crystals.[37, 38] However, different synthetic conditions allow to grow the material with different morphologies. For example, growth templated by a substrate - either from vapour phase or solution - ends up promoting in-plane crystallization, the final result being a material with platelet-like morphology.[39, 40]

Recently, precipitation from an antisolvent - a technique borrowed from colloidal chemistry - has been proposed to synthesize perovskites. In this case, growth is under kinetic control: since the crystallization of alkyl chains takes more time than that of the perovskite, nanometer thin platelets are likely to be the synthetic output. Tailoring the synthetic conditions - particularly the nature and the amount of ligand - allows to push the thickness to the limit of single unit cell thick materials.[41, 42] This technique is extremely versatile, as it allows to obtain a huge variety of minerals with different compositions simply modifying the starting amount of precursors. Figure 5.4 shows how the bandgap of $PbX_4(R-NH_3)_2$ - where R is a mixture of butyl and octyl chains, and X may be Cl, Br, or I - may be easily tuned changing the initial ratio of halogens. This strategy is very resourceful. Standard hybrid perovskites with mixed halides composition are studied, as the halides are the species with the highest mobility in the perovskite lattice:[43] understanding how defectivity of the lattice changes as the result of halide motion is fundamental to improve the final performances of the devices.[44–47]

Figure 5.4 Absorption spectra for perovskite nanoplatelets showing continuous tunability as a function of halide composition. Mixtures are made between Cl/Br and Br/I in increments of 10% between the pure compositions. Reproduced with permission from [41].*

Characterization of these materials proves that they are generally less performing, from the optical point of view, with respect to classical 3D perovskites, but they are way more stable to moisture, which is one of the biggest issue for perovskite based devices. This feature, together with the continuous tunability of the bandgap energy, makes these materials particularly attractive for use in optoelectronic devices.
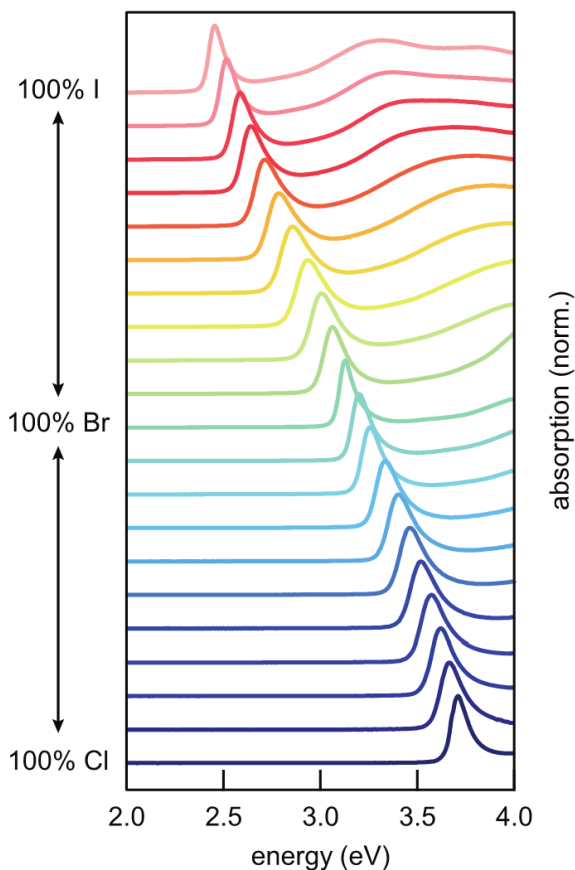
---

*Direct link to the article: http://pubs.acs.org/doi/abs/10.1021/acsnano.6b03496. Further permissions related to the material excerpted should be directed to the ACS.

5.4 Aim of the work

Basing on the literature, a point in particular attracted our attention: despite the reported syntheses, no perovskite materials exist which have an intrinsic two-dimensional nature. The reason is that all the ultra-thin reported perovskites have small molecules in the C lattice sites, which are anyway able to crystallize and form layered structures. The unit-cell thickness feature is only obtained adjusting synthetic conditions properly. Moreover, use of bulky molecules or polymers as ligands, which are less prone to crystallization, may prove challenging, as the increase in the steric hindrance of the ammonium head changes the tolerance factor, and may prevent the formation of the perovskite lattice. Here we report the colloidal synthesis of an intrinsically 2D perovskite through a process of polymer-directed crystallization. The lubricant nature of the polymer used as ligand prevents the formation of a layered perovskite structure, allowing to synthesize a unique material being single unit cell thick.

The synthetic protocol is also suitable to prepare classic R-P homologous perovskites using bulky alkylammonium ligands, which however crystallize as layered structures. We started working with these materials at the beginning, as we needed to become familiar with the colloidal method and the properties of the obtained perovskites. However, we made a nice use of the developed know-how. The possibility of easily synthesize perovskite platelets through a colloidal process, in fact, offers an interesting opportunity around a more fundamental study of the properties of these materials. In particular, taking advantage of both the synthetic method from solution and the responsivness of perovskites to ion-exchange, intercalation and metathesis reactions,[48] one can imagine to vary the morphology -and eventually the properties- of the final material through post-synthetic treatments in dispersion. In particular, we have been able to prove that classic $PbX_4(Alkyl-NH_3)_2$ perovskite nanoplatelets with single halogen composition can be re-configured through a dissolution-recrystallization process to give a material with mixed composition, and whose morphology varies with the applied post-synthetic conditions. In simple terms, one can imagine to reproduce the variety of materials claimed in figure 5.4 just starting from the parent single-halogen platelets.

Again, it is important to stress how the use of surfactants and the colloidal synthetic approach are fundamental to reach these goals. Due to the reduced solubility of the chosen polymeric ammonium salt in polar solvents, the packing of a polymer brush would be impossible through classic spin-coating techniques, which take advantage of a starting solution of the precursors to build the material; on the other side, reconfigurability of synthesized platelets can only take place in dispersion, as ions need a medium to diffuse in and out of the material. As a further benefit, synthesis through colloidal techniques might prove advantageous even from the point of view of the fabrication of a device, as the material can be directly deposited from solution.

5.5 R-P homologous hybrid perovskites with bulky (C8, C12, C16) alkylammonium ligands

R-P lead halide perovskites having long alkylammonium salts as spacers are well known materials. Lead iodide based structures in particular have been studied extensively by K. Pradeesh and G. V. Prakash starting from 2009 as thin film materials. In a series of dedicated papers,[36, 49, 50] they fully characterized their structural, optical and thermal properties. One of their most relevant findings is that the exciton energy is finely tuned by the organic moiety through the bending of the Pb−I−Pb bond. The ligand is also responsible for the thermal properties or the material: different organic species account for different phases, which show different thermal stabilities. A study of the phase transition of these materials has been carried by G. Billing, who collected single crystal XRDs at high and low temperature and gave a full description of the differences between phases.[51] Other studies, more focused on the properties of the ligands, have been carried by S. Vasudevan and N. V. Venkataraman, which took advantage of XRD, DSC, IR and NMR characterization to prove how the alkyl chains assume an all-trans conformation in the crystal, and how the trans-gauche isomerization at high temperature influences the crystal structure.[52, 53] In all the reported studies, however, the material is prepared in the form of single crystal or thin film. In our case instead, the synthesis was performed through crystallization from a non-solvent. This method differs from those mentioned as it affords the perovskite in the form of the kinetic product, and the growth is not templated by a substrate. The first step after synthesis was then a full characterization of the materials through absorbance and PL spectroscopy, DSC and powder XRD.

Figure 5.5 shows the chosen ligands, $Oct-NH_3X$, $Dod-NH_3X$ and $HDec-NH_3X$ (X being Br or I). Usually the synthetic process involves the use of the parent amine and the aqueous solution of the corresponding acid. In our case instead, we synthesized all the ammonium salts, which were subsequently used for the synthesis of perovskites. All iodide based perovskites are well known and characterized, whilst only few articles describe bromide based materials, which report

Figure 5.5 Alkylammonium salts used for the synthesis of colloidal perovskites.

an incomplete characterization.[41, 50] To the best of our knowledge, $PbBr_4(HDec-NH_3)_2$ has never been synthesized before.

5.5.1 Synthesis and characterization of $PbX_4(Alk-NH_3)_2$ perovskite nanoplatelets through colloidal approach

The synthetic process is extremely simple, and it takes advantage of a classical method of colloidal chemistry: precipitation from a nonsolvent (reprecipitation, described in Chapter 4). Details of the procedure are reported in the experimental section. Briefly, the lead halide and the ammonium salt are dissolved in DMF in 1:2 molar ratio, and the solution is injected in vigorously stirring toluene. The reaction can be written as

$$PbX_2 + 2\,Alkyl-NH_3X \xrightarrow{\text{toluene}} PbX_4(Alkyl-NH_3)_2 \downarrow$$
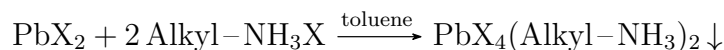
A suspension forms within seconds after the injection, which is brightly fluorescent under UV lamp (λ_{exc}=365 nm). The suspension is allowed to stir for 15 minutes before use. The suspended material is all recovered through centrifugation, after which the supernatant appears transparent and colorless, meaning that nearly all the injected material reacted.
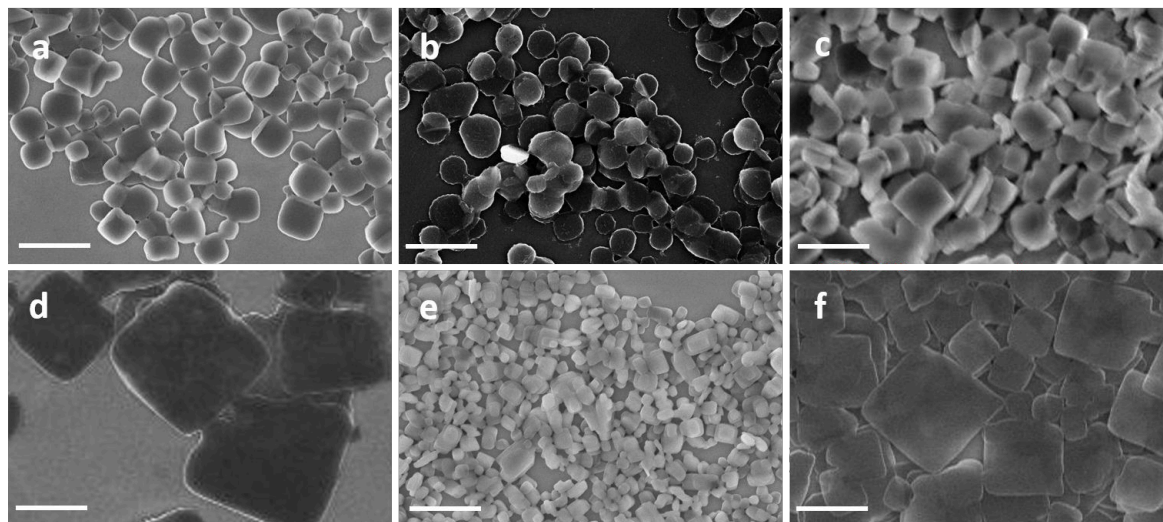
Figure 5.6 SEM images of as synthesized a) $PbBr_4(Oct-NH_3)_2$ b) $PbI_4(Oct-NH_3)_2$ c) $PbBr_4(Dod-NH_3)_2$ d) $PbI_4(Dod-NH_3)_2$ e) $PbBr_4(HDec-NH_3)_2$ and f) $PbI_4(HDec-NH_3)_2$ nanoplatelets. Bar size is 1 µm.

Figure 5.6 shows SEM images of the as synthesized materials after deposition on a silicon substrate. It is possible to see how, in all of the cases, perovskite is obtained in the form of nanoplatelets of different shapes and sizes.

The reason why we obtained the material as relatively large and thin platelets is probably kinetic. Crystallization of the perovskite lattice is favoured respect to Van der Waals interaction between layers, thus growth is likely to happen in the plane instead that out of plane. Even platelets of $PbBr_4(HDec-NH_3)_2$, the smallest of the series, are actually extremely thin: this is proved by STEM. Figure 5.7 in fact shows that the material is mainly formed of very thin platelets which have unaligned edges. These features are invisible in SEM, and suggests that the stacking process happened after the growth, and may be partly due to the precipitation process rather than pairing in solution.

Figure 5.8 shows the optical properties and XRD spectra of as synthesized platelets suspensions. Absorbance and PL spectra show one excitonic peak whose energy is the one expected

Figure 5.7 Dark field STEM picture of $PbBr_4(HDec-NH_3)_2$ platelets. Bar size is 200 nm.

for Ruddlesden-Popper hybrid perovskites with $PbX_4(Alk-NH_3)_2$ structure. XRDs clearly prove the layered morphology of the material, as the peaks can be indexed as $(0,0,l)$. Table 5.1 reports a comparison between literature data known for these materials, and the values we measured of exciton energies and interlayer distances.
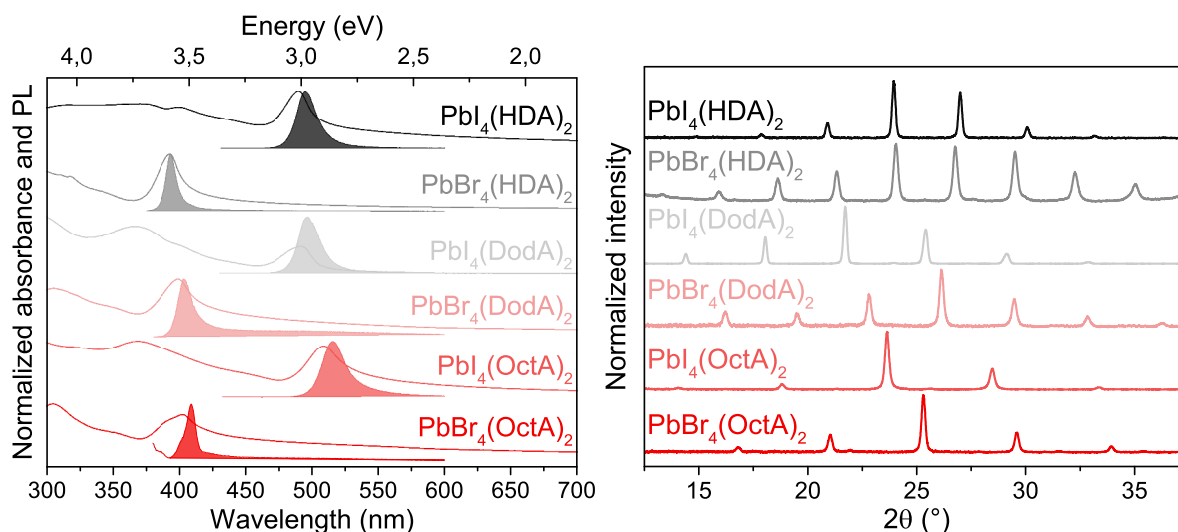
Figure 5.8 Absorption, photoluminescence (left) and XRD spectra (right) measured for as synthesized $PbX_4(Alk-NH_3)_2$ platelets.

Data for all perovskites match well with those reported for all known materials. Therefore we can be quite confident that, even if we synthesized the perovskites through a precipitation technique and the growth is under kinetic control, the characteristics of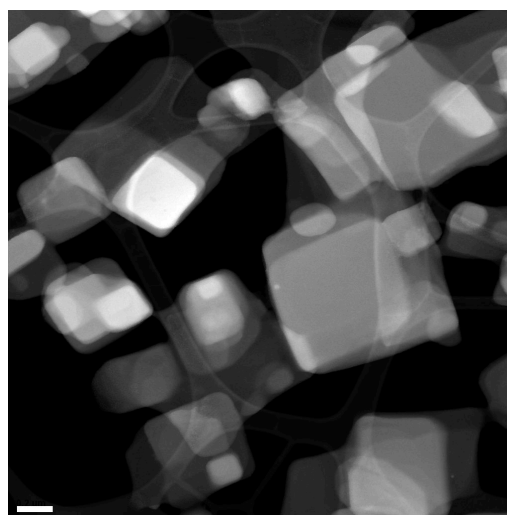 the final material are not really influenced. In particular, our platelets should have the crystal structure known for the same materials grown from solution, for which single crystal XRDs have been collected. This consideration in based not only on the values of interlayer spacing, but also on the exciton energy. As previously stated, in fact, the organic ligand has an influence on the Pb$-$X$-$Pb bond angle, which in turn slightly changes the band structure of the material, and the energy gap as consequence. This means that the exciton energy is diagnostic of the atomic structure of the material. Basing on these reasons, and on DSCs data (v. *infra*), we are confident in assigning the crystal system and the space group to $PbI_4(Oct-NH_3)_2$, $PbI_4(Dod-NH_3)_2$ and $PbI_4(HDec-NH_3)_2$, respectively orthorombic and *Pbca* (61) for all three materials.[51, 54]

Platelets are the kinetic product of the reaction. This clearly does not mean they are also

	Exciton energy (eV)		Interlayer spacing (nm)	
	Measured	Reported	Measured	Reported
$PbBr_4(Oct-NH_3)_2$	3,03	3,08[41]	2,110	2,1[41]
$PbBr_4(Dod-NH_3)_2$	3,07	3,14[50]	2,712	2,7[50]
$PbBr_4(HDec-NH_3)_2$	3,16	-	3,320	-
$PbI_4(Oct-NH_3)_2$	2,40	2,42[41]	1,870	1,874[54]
$PbI_4(Dod-NH_3)_2$	2,49	2,49[36]	2,444	2,451[38, 51]
$PbI_4(HDec-NH_3)_2$	2,50	2,51[36]	2,967	2,965[51]

Table 5.1 Comparison of measured and literature data for $PbX_4(Alk-NH_3)_2$.

the thermodynamic product. Both $PbBr_4(Oct-NH_3)_2$ and $PbI_4(Oct-NH_3)_2$ platelets are not stable in this form, and degrade within few hours from synthesis. Figure 5.9 shows a picture of these two materials one day after the synthesis. $PbBr_4(Oct-NH_3)_2$ platelets degrade and form $PbBr_2$ back, while $PbI_4(Oct-NH_3)_2$ platelets turn into wires.
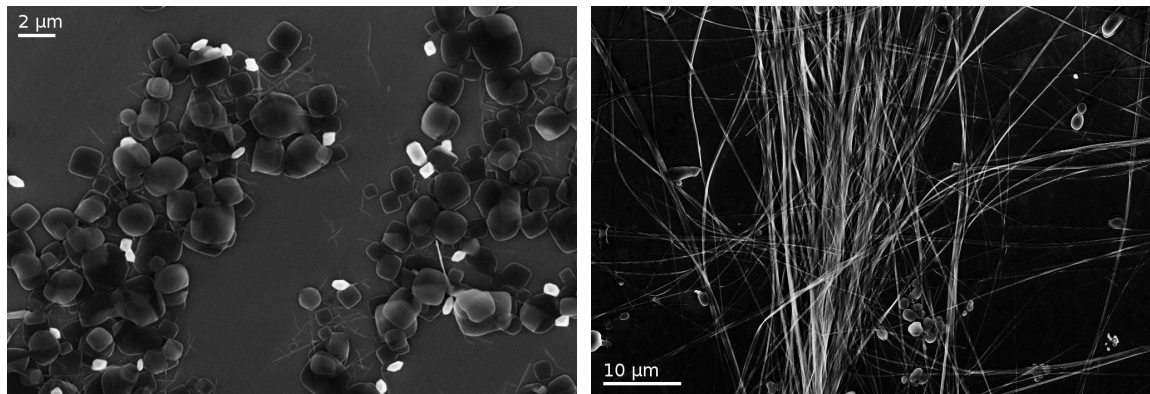
Figure 5.9 SEM picture of $PbBr_4(Oct-NH_3)_2$ (left) and $PbI_4(Oct-NH_3)_2$ (right) one day after the synthesis.

This behaviour may be rationalized in terms of the characteristics of the phase of the perovskite which is stable at room temperature. Figure 5.10 shows DSCs for all the synthesized perovskites - the vertical line being added to help identifying the phase which is stable at room temperature for each material.

All the DSCs show two peaks for both heating and cooling traces. Several studies assigned these transitions to phase transitions of the perovskite. The behaviour was thoroughly studied for $PbI_4(Oct-NH_3)_2$, $PbI_4(Dod-NH_3)_2$ and $PbI_4(HDec-NH_3)_2$.[51, 53, 54] The peak at lower temperature accounts for a phase transition which involves a modification of the ammonium head position and the sliding of the layers, such that octahedra pass from a staggered to an eclipsed configuration (in $PbI_4(Dod-NH_3)_2$ and $PbI_4(HDec-NH_3)_2$) or vice-versa (in $PbI_4(Oct-NH_3)_2$). Moreover, going from low to high temperature, in all three materials the $Pb-I-Pb$

Figure 5.10 DSCs of as synthesized $PbX_4(Alk-NH_3)_2$ platelets. For all measurements, the full line is the cooling trace, and the dashed line is the heating trace.

bridging angle changes from $\sim 150°$ to $\sim 158°$: this explains why the exciton energy in $PbI_4(Oct-NH_3)_2$ is nearly 0,1 eV smaller than that of $PbI_4(Dod-NH_3)_2$ and $PbI_4(HDec-NH_3)_2$. The second DSC peak at higher temperature is related to an "amorphization" of the alkyl chains, which partly undergo to an isomerization from their all-trans configuration with the introduction of gauche defects.

Figure 5.11 Enthalpies of transition determined for $PbX_4(Alk-NH_3)_2$ materials, shown as filled squares, triangles and diamonds, and those reported by Billing,[51, 54] Barman,[53] and Ahmad,[50] shown as open diamonds/squares, crosses and open triangles respectively. Lines are guide to eye. Enthalpy of first phase transition is labeled as ΔH_1, while enthalpy of the order-disorder transition is labeled as ΔH_2.

Figure 5.11 shows a graph with the enthalpies of transition calculated for all materials, and the enthalpies reported by Billing, Barman and Ahmad.[50, 51, 53, 54] In all cases, energy relative to the first transition does not show an obvious dependence from the chain l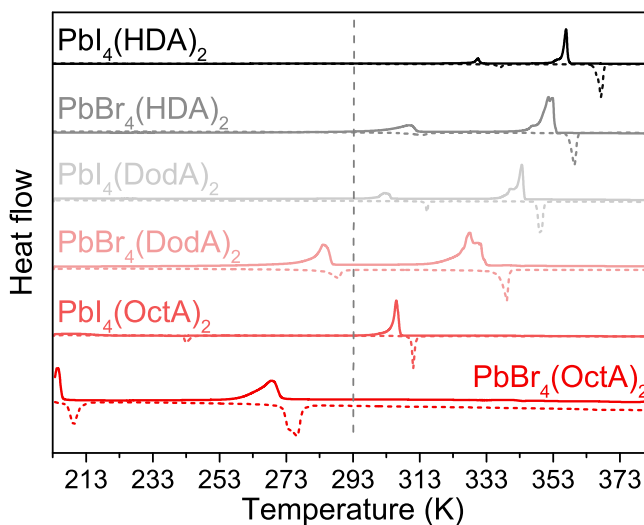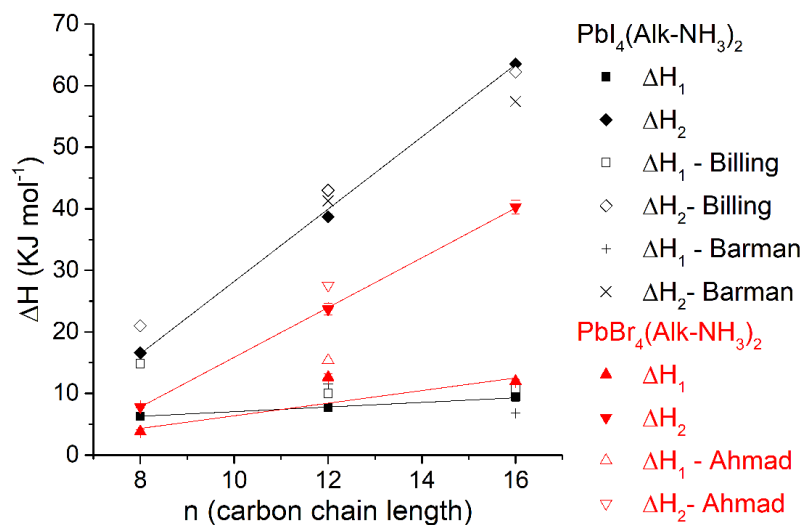ength. This is not strange, as this transition is related to a rearrangement of the layers and chain orientation. Energy relative to the second transition, on the other side, increases with chain length, in agreement with the claim of amorphization of the organic layer. Our data are in fair agreement with the reported values. Moreover, data for bromide materials show the same trends of iodide materials. As the organic chains involved are the same, we expect we are looking at the same phenomena: a phase transition at low temperature, and an order-disorder transition at higher temperature. It is worth noting that bromide based materials show enthalpies of the order-disorder transitions 35-45% lower than the corresponding iodides. This suggests that the packing of the chains is different from the interdigitated one known for iodides. This is also proven by the increase in the interlayer distances for bromide materials.

Coming back to the discussion on the stability of nanoplatelets, DSCs clearly prove that at room temperature $PbI_4(Dod-NH_3)_2$, $PbI_4(HDec-NH_3)_2$ and $PbBr_4(HDec-NH_3)_2$ are in the most stable phase, but this is not true for the other materials. In particular, for $PbI_4(Oct-NH_3)_2$ room temperature is close to the order-disorder transition, and for $PbBr_4(Oct-NH_3)_2$ is well above. This means that, at room temperature, the alkyl chain in these materials have a high kinetic energy. Since the platelets are prepared and stored in solution, this may facilitate the reconfiguration of the material from the kinetic product into a more stable phase. This is particularly true for octylammonium based materials, as the ligand is the most soluble of the series in toluene. Notably, we have not observed this behaviour for $PbBr_4(Dod-NH_3)_2$, which is above the first transition like $PbI_4(Oct-NH_3)_2$. However, in this case room temperature is not close to the temperature of the order-disorder transition, so the material may be stable, or in any case it requires long times before any change in its morphology may be observed.

5.5.2 Reconfigurability of perovskite nanoplatelets: halogen exchange reactions

Since the synthetic method allowed us to prepare a variety of materials with different characteristics, and the dispersion proved a suitable environment to observe the reconfiguration of the platelets from a metastable phase to a more stable one, we decided to test the extension of our control on the reconfiguration process. Since halogens are known for their high mobility in the perovskite lattice,[55, 56] for our testing we tried to build mixed halide perovskites starting from the parental halide nanoplatelets. This process has already been studied for dispersions of perovskite $PbCsX_3$ nanocrystals,[57] and the kinetics are known to be dependent from the presence of any species able to deliver the anions (such as the ammonium salts, or the nanocrystal themselves).

In order to be sure to properly control the process, all the synthesized suspension were purified before use to remove any unreacted species. Details of the purification procedure are reported in the experimental section. In all the cases, equal volumes of parental nanoplatelets suspensions with same concentration were mixed, so the product is expected to exhibit a 1:1 composition of halides.

Mixing parental dispersions: effect of the chain length

Aim of the first experiments was to understand the influence of the ligand in the reconfiguration process. Since the ligand is responsible for the stability of the platelets, the material will be more or less willing to reconfigure depending firstly on its length. A material stable in standard conditions will be poorly reactive or not reactive at all toward halides exchange. On the contrary, a metastable material is a good candidate to obtain the halides mixing. This behaviour is related to the existence of an equilibrium between the crystallized perovskite and the dissolved precursors:

$$\mathrm{m[PbX_4(Alkyl-NH_3)_2]} \rightleftharpoons \mathrm{m[PbX_n{}^{2-n} + (4\text{-}n)X^- + 2\,Alkyl-NH_3{}^+]}$$

The more stable the material is, the less the concentration of solvated precursors, the less efficiently the halide exchange can take place.

As first experiment, we tested all the mixtures for the same ligand: $PbI_4(HDec-NH_3)_2$ with $PbBr_4(HDec-NH_3)_2$; $PbI_4(Dod-NH_3)_2$ with $PbBr_4(Dod-NH_3)_2$; and $PbBr_4(Oct-NH_3)_2$ with $PbI_4(Oct-NH_3)_2$. It is worth highlighting that the mixing process, in all the cases, is performed using the perovskite powder in suspension, because the platelets are too big to remain dispersed in the solvent.

Figure 5.12 shows SEM and EDX analyses of a mixture of $PbI_4(Oct-NH_3)_2$ and $PbBr_4(Oct-NH_3)_2$ after 6 hours mixing. The new obtained platelets show a perfectly mixed composition. Since both the starting materials are "reactive", this result is not surprising. However, it must be underlined that obtaining platelets as product in these conditions is a valuable result itself precisely because we started from two unstable materials. In fact, few examples of these platelets could be imaged, as they tend to degrade back to the perovskite precursors.

Since both the parental suspensions prompt the reconfiguration process, this appear to complete in quite a short time, considering that both the starting suspensions and the final product are made of micrometer-size material.
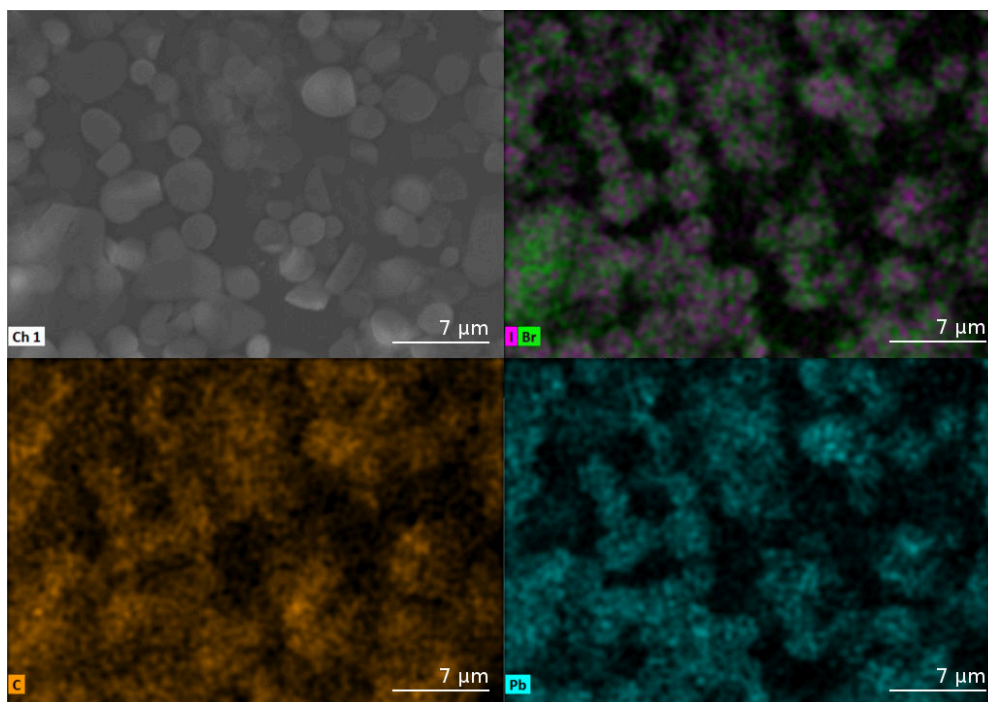
Figure 5.12 SEM image and corresponding EDX analyses of mixed $PbI_4(Oct-NH_3)_2$ and $PbBr_4(Oct-NH_3)_2$ platelets after 6 hours

Figure 5.13 shows SEM and EDX analyses of a mixture of $PbI_4(Dod-NH_3)_2$ and $PbBr_4(Dod-NH_3)_2$ after 6 hours mixing. The synthetic output in this case is more complex, as it looks like two families of platelets are present, one richer in iodine and one richer in bromine. Particles also look like merging into bigger aggregates.
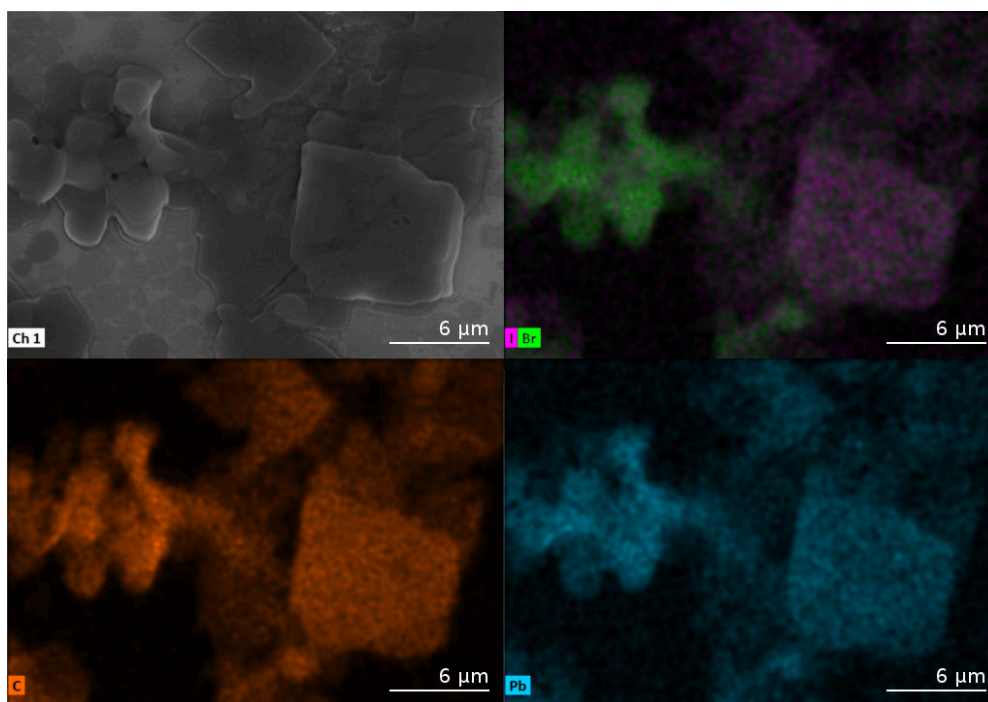
Figure 5.13 SEM image and corresponding EDX analyses of mixed $PbI_4(Oct-NH_3)_2$ and $PbBr_4(Oct-NH_3)_2$ platelets after 6 hours

Basing on the dimension of the platelets, we speculate that the iodide rich platelets are just $PbI_4(Dod-NH_3)_2$ partially substituted with bromine, and the opposite happened to bromine rich platelets. This means that, in the case of dodecyl chain, the halides exchange takes place, but it is extremely inefficient. This is not really surprising, as both the starting materials are supposed to be stable under standard conditions. The merging of the platelets also suggests that solvated precursors may work as mortar for particles.

Figure 5.14 shows SEM and EDX analyses of how a mixture of $PbI_4(HDec-NH_3)_2$ and $PbBr_4(HDec-NH_3)_2$ looks immediately after mixing and after 6 hours.
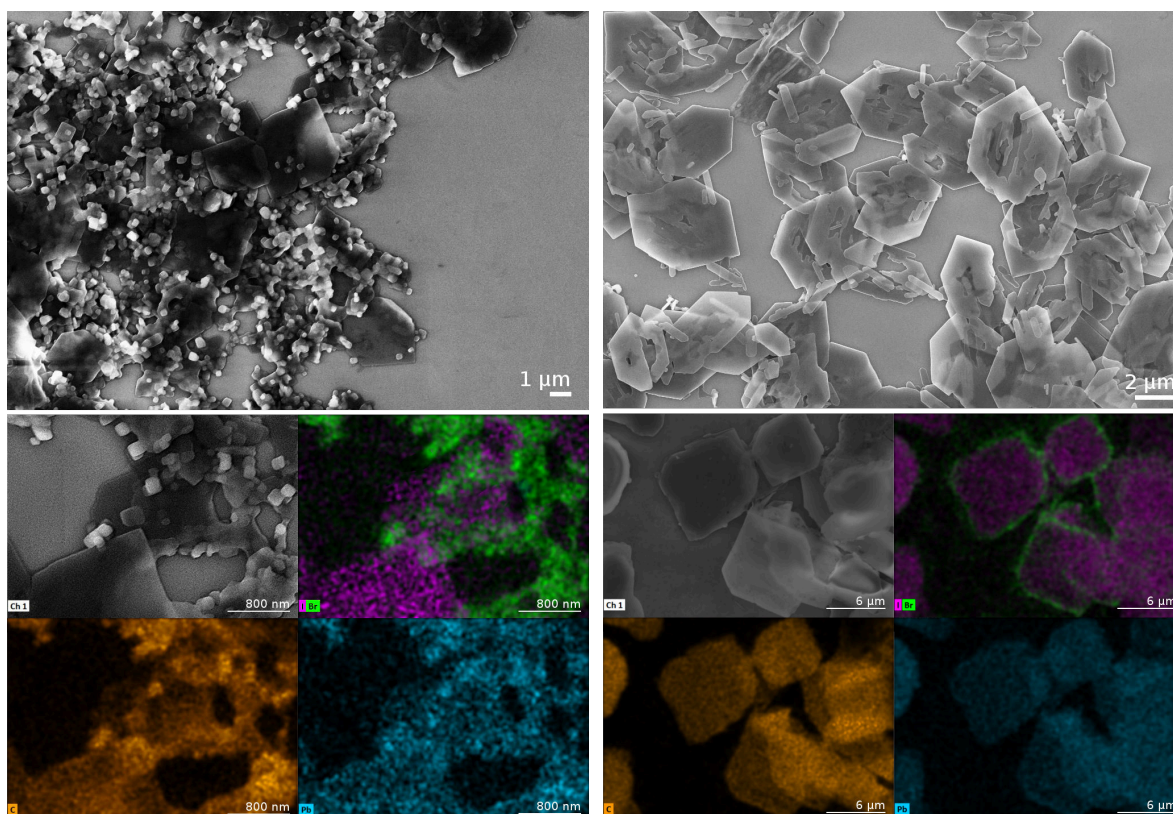
Figure 5.14 SEM images of $PbI_4(HDec-NH_3)_2$ and $PbBr_4(HDec-NH_3)_2$ platelets immediately after mixing (top, left) and after 6 hours (top, right), and corresponding EDX analyses (bottom).

At the beginning of the mixing process, the parental platelets are easily distinguishable, as the $PbBr_4(HDec-NH_3)_2$ platelets are way smaller than the iodide based ones. EDX confirms the initial composition. Anyway, after 6 hours of mixing, $PbBr_4(HDec-NH_3)_2$ platelets are not visible anymore, and only one species of hexagonal platelets is observable. The composition of these platelets is not homogeneous: they are formed by an inner core containing iodine only, while the edges are rich in bromine.

This suggests that $PbI_4(HDec-NH_3)_2$ platelets are stable during mixing, while the bromide based platelets dissolve and recrystallize on the edge of the iodide ones. This behaviour was unforeseen, as we expected to see the same one observed for dodecyl chain materials. This unexpected result is clearly due to a difference in the way $PbBr_4(HDec-NH_3)_2$ platelets behave is dispersion. It is not a matter of stability: PL measurements of $PbBr_4(HDec-NH_3)_2$ parental suspension, visible in figure 5.15, clearly shows that the photoluminescence signal of the material is stable over the same amount of time. Moreover, SEM measurements prove that these platelets are stable in solution for at least one month. Since the material by itself is perfectly stable, a good explanation of the phenomenon comes again from considerations about the equilibrium between solvated precursors an crystallized perovskite. We speculate that $PbBr_4(HDec-NH_3)_2$ platelets can easily dissolve and recrystallize due to their small dimensions and thinness, a feature of this material only. In this scenario, mixing $PbBr_4(HDec-NH_3)_2$ with $PbI_4(HDec-NH_3)_2$ obviously modifies this equilibrium, and prompts the crystallization. Unreacted precursors recrystallize at the edge of iodide based platelets, producing a new material which is less likely to dissolve because of the increased thickness, thus behaving like a well for the reaction outcome.
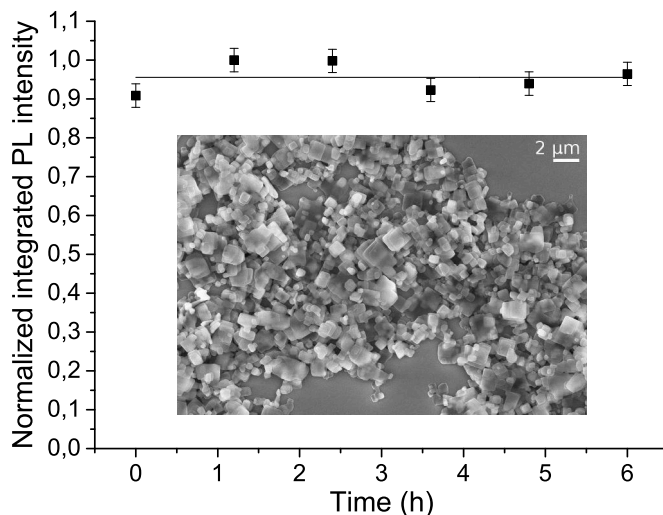
Figure 5.15 Normalized integrated PL intensity of $PbBr_4(HDec-NH_3)_2$ platelets over 6 hours. The black line is a guide to eye. Inset: SEM image of $PbBr_4(HDec-NH_3)_2$ platelets one month after synthesis.

Mixing parental dispersion: effect of promoters

Since the simple mixing of perovskite platelets with stable components produces poorly mixed or heterostructured materials, we attempted to obtain homogeneously mixed material through the use of a "promoter". The promoter should speed up the reaction toward equilibrium composition. The obvious choice was DMF, as this is the solvent used to dissolve all the perovskite precursors for the synthesis. The idea was to push the dissolution-recrystallization process to obtain an homogeneous product. As the mobility of alkyl chains proved to be another key factor for the reconfiguration, we also tried to carry on the process at 60 °C. SEMs and EDX analyses in figure 5.16 show how a 1:1 mixture of $PbI_4(HDec-NH_3)_2$ and $PbBr_4(HDec-NH_3)_2$ platelets looks like after 6 hours with 0,2% vol/vol DMF added, and after 6 hours at 60 °C.

In both cases, the morphology of the material totally changes, as shape of the platelets is not homogeneous anymore, and size is bigger than that of $PbI_4(HDec-NH_3)_2$ platelets. When DMF is present, in particular, platelets are extremely irregular, and they look like Ostwald ripening phenomena took place in suspension. However, in both cases the composition is perfectly homogeneous, thus both DMF and temperature are effective in promoting the dissolution-crystallization process.
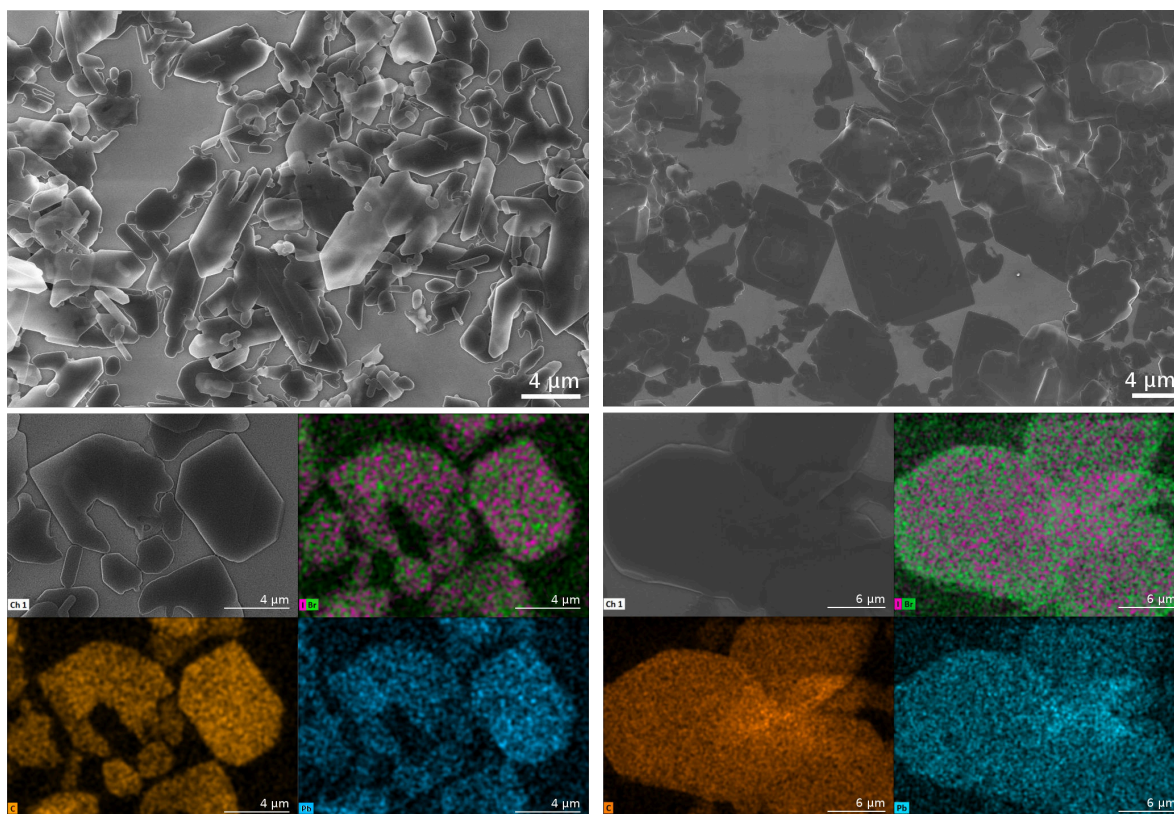
Figure 5.16 SEM of a 1:1 mixture of $PbI_4(HDec-NH_3)_2$, $PbBr_4(HDec-NH_3)_2$ and 0,2% vol/vol of DMF after 6 hours (top, left); SEM of a 1:1 mixture of $PbI_4(HDec-NH_3)_2$, $PbBr_4(HDec-NH_3)_2$ after 6 hours at 60 °C (top, right); and corresponding EDX analyses (bottom).

Finally, figure 5.17 shows SEMs and EDX analyses of a 1:1 mixture of $PbI_4(HDec-NH_3)_2$ and $PbBr_4(HDec-NH_3)_2$ platelets after 6 hours mixing at 60 °C with 0,2% vol/vol DMF added. The result was quite unexpected: we crystallized enormous platelets with a new rose-like morphology. This last result will need a more accurate study, as we actually don't have a theory to explain this weird morphology. DSC and XRD will be collected to understand if we are in front of a new crystalline phase of the material.
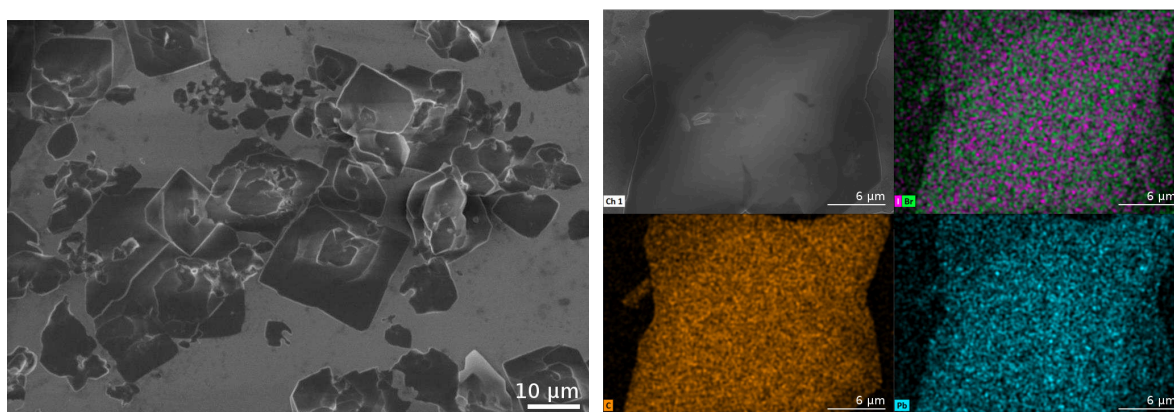
Figure 5.17 SEM of a 1:1 mixture of $PbI_4(HDec-NH_3)_2$, $PbBr_4(HDec-NH_3)_2$ and 0,2% vol/vol of DMF after 6 hours at 60 °C (left), and corresponding EDX analyses (right)

5.5.3 Conclusions

We took advantage of the nonsolvent precipitation method to synthesize nanoplatelets of Ruddlesden-Popper homologous perovskites with long alkyl chains as spacers. The synthetic method is extremely simple, and allows to obtain the final material in high yield in air within seconds. It is worth to underline that the properties of the obtained materials, apart from the morphology, do not differ from those of the same materials grown as single crystal, which are very time-consuming to grow. The perovskites crystallize as square or rounded nanoplatelets several micrometers wide. Because of the high mobility of the alkyl chain, and probably the higher solubility of the ligand in the antisolvent, $PbX_4(Oct-NH_3)_2$ platelets stored in suspension are metastable, and the material degrade back to the precursors in the case of $PbBr_4(Oct-NH_3)_2$, or reconfigure into wires in the case of $PbI_4(Oct-NH_3)_2$.

This synthetic protocol allows to process the final material through post-synthetic treatments and modify its composition and morphology. This is possible thanks to the existence of an equilibrium between the crystallized perovskite and precursors in solution. The concentration of the precursors depends on the ability of the material to dissolve. This characterestic depends in turn from the length of the alkyl chain, and the size and thickness of the synthesized platelets. For this reason, $PbBr_4(Oct-NH_3)_2$, $PbI_4(Oct-NH_3)_2$ and $PbBr_4(HDec-NH_3)_2$ platelets are more reactive in halogen exchange reaction, allowing to reconfigure the parental materials to obtain final particles with fully mixed halides.

In case of parental platelets less prone to dissolution, the reconfiguration process can be facilitated through the use of a promoter, which can be either a solvent for the perovskite, or the temperature. In both cases the reconfiguration into the mixed material can be quickly obtained, to the detriment of homogeneity of size and morphology of the platelets. Use of the solvent, in particular, promotes Ostwald ripening processes. If both the solvent and increased temperature are tested together, the material can be crystallized into an out-of-equilibrium morphology.

5.6 Polymer-directed crystallization of ultra-thin two-dimensional hybrid perovskite nanoplatelets

The idea of synthesizing a perovskite which is two-dimensional by nature is quite challenging, as it naturally implies the use of a capping ligand which is not able to crystallize in a layered structure. Again, this requirement is anything but easy to fulfill. For most organic species, a low tendency to crystallization implies the existence of many degrees of freedom for the molecular backbone, which in turn causes the molecule to have a big Van der Waals volume. This means that molecules suitable in terms of flexibility might be too big to be able to insert in the perovskite lattice. In fact, to fulfill both the lack of crystallinity and tolerance factor requirement, one should use an organic species which is both amorphous and able to pack tightly, two features not easily combined.

A nice way to skip the obstacle is to use a polymer brush. These structures can be obtained through anchorage of long, flexible macromolecules to a non-absorbing substrate. The length of the chains and their grafting density on the substrate are the fundamental parameters which need to be considered to understand the morphology of the coverage: high grafting density and chain length promote the formation of a well-ordered brush, while a small density or short chains promote a mushroom- or a pancake-like coverage of the surface.[58–60]

Among all possible polymers which are suitable to produce a brush-like morphology, we choose poly(dimethylsiloxane) (PDMS). This polymer is well-known to form brush-like structures which show ultralow friction,[61] both suitable characteristics

Cartoon of a unit-cell thick 2D perovskite embedded in a polymer brush made up of flexible polymer chains.

to attempt building up the material. Moreover, the work was performed in Helm's research group, which developed an impressive know-how on the use of PDMS to build hybrid materials.[62–64]

Such a structure would be really unique. Not only it may be a model for the synthesis of materials which are two-dimensional by nature, its properties may prove quite unusual as well. In fact, we are attempting to build a one unit cell thick layer of perovskite embedded in two layers of a polymer which behaves like a liquid. No material more than this can be described as an amorphous- or liquid-like semiconductor. Moreover, both the synthetic method (dispersion in solution, as an ink) and the expected mechanical flexibility make this perovskite an ideal candidate as active material in plastic devices, for example as gate dielectric, as it is formed by an easily polarizable material sandwiched between two insulators. The expected platelet morphology, finally, perfectly fits techniques of

deposition from solution, as there is no need to warry for their orientation with respect to the substrate (a well-known problem for OFETs[65–67]).

5.6.1 Requirements for perovskite formation
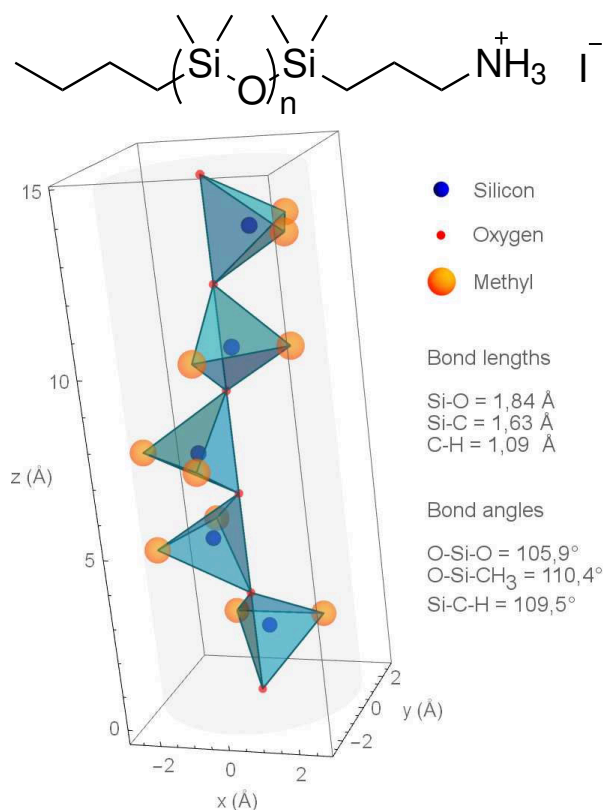
Figure 5.18 Top: chemical structure of PDMS−NH$_3$I used as ligand for the synthesis. Bottom: cartoon of a strand of dimethylsiloxane chain aligned with z axis. Values for bond lengths and angles are taken from [68].

Before attempting to synthesize a perovskite with this ligand, we tried to understand if crystallization was possible for such a bulky polymer on the basis of tolerance factor. Even if this concept applies to three-dimensional perovskites, the same calculation for this material is applicable since it is based on the unit cell of the perovskite, and has a crucial importance. In fact, in the case the polymer is too bulky to allow formation of the perovskite, only a solution of solvated anions and cations is obtained.

Figure 5.18 shows the structure of the ammonium salt of PDMS used for the synthesis of the perovskite. The ionic head can be considered as having the methylammonium ionic radius (1,8 Å[69]), but the polymeric backbone is bulkier. WAXS data for this polymer suggest an inter-chains distance of 7,1 Å.[68] This value corresponds to the thickness of the chain in a "hard cylinders" model, the analogue of a hard sphere model for simple liquids. Tolerance factor calculated from this radius amount to t=1,26*, which is bigger than any known value for a perovskite, meaning that the lattice is not likely to grow. However, this interchain distance is obtained for the polymer in a stochastic configuration. In our case, instead, the chain is pinned to a surface and perpendicularly aligned, as it is supposed to pack into a brush. A rough estimate of the steric hindrance of the polydimethylsiloxane chain in a brush-like conformation can be obtained with a simple model based on bond lengths and angles, shown in figure 5.18. Alignment of the oxygen atoms with z axis accounts for the elongation of the chain, and thus the formation of the brush, while rotation of the silicon-centered tetrahedra around the axis simulates both the chain flexibility and the minimization of interaction between methyl groups. The molecular radius is calculated as the radius of the cylinder described by the rotation of the tetrahedra toward the z axis, represented in gray. On the basis of this model, one can calculate a molecular radius of 2,80 Å, which accounts for a tolerance factor t=1,10. This suggests that, for a brush-packed structure, a PDMS capped perovskite has a chance to grow.

---

*Revised ionic radius is used for lead, as described in [4]

As second requirement, we checked the minimum number of monomeric units needed to build the brush. As PDMS is a polymer with a very flexible backbone, the mushroom-to-brush crossover happens for grafting densities $\sigma > \sigma^*$, where

$$\sigma^* = (l \cdot N^{0,588})^{-2}$$

and l and N are respectively the size and number of monomeric units.[59] The minimum number of monomeric units needed for a fixed grafting density is thus

$$N > (l\sqrt{\sigma})^{1/0,588}$$

We calculated a monomer length $l = 2,93\,\text{Å}$ from bond lengths and angles of PDMS, while as grafting density we considered the number of chains per unit cell surface of the perovskite. Using the unit cell parameters of $PbI_4(HDec-NH_3)_2$,[51] we calculated a grafting density

$$\sigma = \frac{\#\,\text{of chains per unit cell}}{\text{area of unit cell}} = \frac{1}{a \cdot b} = 0,0133\,\text{Å}^{-2}$$

Even if the perovskite has two polymer chains per unit cell, in the calculation of the grafting density we considered one only, as the second chain locates on the opposite side of the platelet, thus on a different surface. Using these values, we calculated $N > 6.3$, which accounts for a relative molar mass higher than 746. For this reason, we used 1K $PDMS-NH_3I$ (calculated $n = 12.7$, $M_r = 1331$), which was synthesized from the corresponding commercial amine (details are given in the experimental section).

5.6.2 Moving first steps

The first attempt we made to synthesize the polymer-capped perovskite immediately proved us how much of a challenging process we were trying to carry out.

Figure 5.19 shows the picture of an as-synthesized $PbI_4(PDMS-NH_3)_2$ perovskite dispersion in toluene, and its absorption and PL spectra. A detailed description of the synthetic procedure is reported in the experimental section. As in the case of alkylammonium based
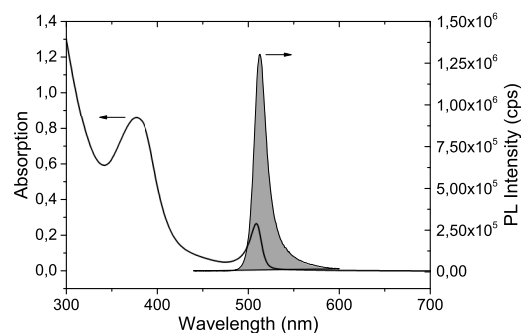
Figure 5.19 Picture of an as-prepared dispersion of $PbI_4(PDMS-NH_3)_2$ nanoplatelets (on the left), and its absorption and PL spectra (on the right)

nanoplatelets, a solution of PbI_2 and $PDMS-NH_3I$ in 1:2 molar ratio is injected in vigorously stirring toluene. The optical characterization proves that the perovskite is present, as there is an absorption peak corresponding to the exciton energy of a lead iodide based perovskite one unit cell thick (see fig. 5.3 and 5.4 as comparison). Figure 5.20 shows two SEM picture of the as synthesized material. None of the pictures is well focused, because

electrons are collected by organic material all around. Even if platelets are visible, they look like embedded in a huge amount of unreacted polymer and lead iodide, which does not allow to see any feature of the material. Controlling the crystallization and cleaning the material, for this very peculiar perovskite, proved to be a very demanding task.
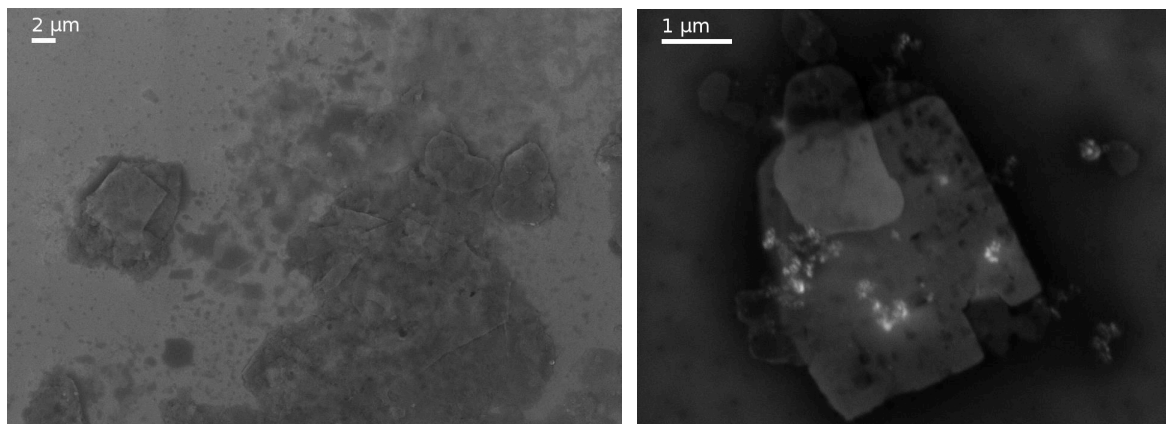
Figure 5.20 SEM pictures of as synthesized $PbI_4(PDMS-NH_3)_2$ nanoplatelets

5.6.3   Polymer directed crystallization as an equilibrium process

The first approach attempted to clean the as-synthesized material was to use the classic techniques for colloidal nanocrystal, likely precipitation and redispersion in clean solvent. We tried several centrifugation rates and times, and even consecutive cleaning runs. No striking improvement was obtained. Different solvents were tested as media for redispersion of cleaned nanoplatelets, with no better results. Size-exclusion chromatography was attempted as well, but apparently the perovskite got stuck on the stationary phase, and no material was recovered.

Figure 5.21 shows an example of a typical outcome of these cleaning procedures. In this particular case, the as-prepared dispersion was centrifuged twice before redispersion. The first low speed centrifugation (2000 rpm for 5 minutes) removes unreacted PbI_2, which crystallizes as dense nanoparticles. The second high speed centrifugation (4400 rpm for 15 minutes) of the supernatant allows to partially precipitate the perovskite. The supernatant is then removed and clean toluene added to redisperse the nanoplatelets. The SEM clearly allows to understand that no significant improvement in the cleanliness of the material is achieved, as again no focused image could be obtained due to the presence of unreacted polymer around the perovskite.
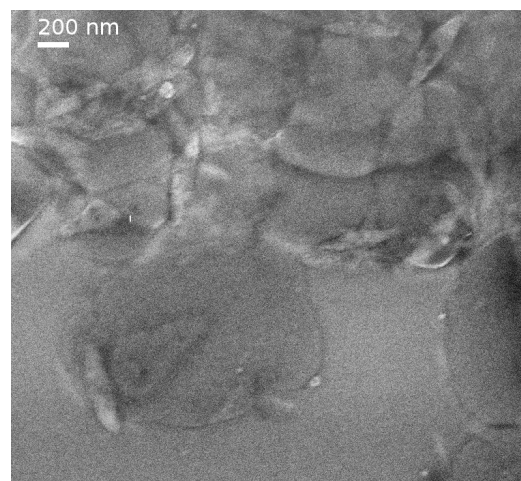
Figure 5.21 SEM picture of $PbI_4(PDMS-NH_3)_2$ nanoplatelets after precipitation and redispersion in toluene

This apparent impossibility to efficiently remove the polymer was quite unexplainable at the beginning, as purifying alkylammonium

based perovskites didn't prove hard. The nature of the ligand, in this case, was completely changing all the synthetic rules: the precipitation process was not controlled by the crystallization of the inorganic layer, as it usually happens for hybrid perovskites. Crystallization was instead under control of the organic ligand. The reason is quite easy to understand: in the chosen conditions, the perovskite can only crystallize as a unit cell thin layer, and uniquely in the eventuality that the polymer packs efficiently into a brush on its surface. This means that, even if the crystallization of the perovskite is kinetically favoured, it cannot simply happen if conditions for the polymer to pack are not optimized. Moreover, as in the case of alkylammonium ligands, we expect the material to exist in equilibrium with the monomers

$$m[PbI_4(PDMS-NH_3)_2] \rightleftharpoons m[PbI_n^{2-n} + (4\text{-}n)I^- + 2\,PDMS-NH_3^+]$$

especially as in this case the ligand is soluble in the antisovent.

In a standard synthesis, after injection of the precursors solution, crystallization of the perovskite immediately starts as it is the kinetically favoured process. However, if condition for assembly of the polymeric brush are not met, crystallization is likely to stop. Some lead iodide crystallizes as nanoparticles, while the remaining material just stays dispersed in toluene, solvated by ammonium cations, in equilibrium with the crystallized phase. Growth of the platelets is then likely to occur slowly over time, through the addition of the dispersed material to the lattice. However, this process is definitely not efficient. It is known, in fact, to slow down over time, as it occurs against entropy and the concentration gradient.[58] Since the final perovskite is a dispersed material and not a precipitate, its crystallization ends up being dictated by thermodynamics instead of kinetics. Moreover, during the precipitation, the platelets probably bring some unreacted polymer entangled in the pinned chains, which comes back to the solution upon redispersion. As the perovskite itself probably partially dissolves with the addition of clean solvent, the impossibility to clean properly the material it is not really surprising.

5.6.4 Tailoring synthetic conditions

5.6.4.1 Variation of the antisolvent

The most important parameter which needs to be taken into account when trying to build a polymer brush is usually the solvent used for the synthesis. In fact, a bad solvent for the polymer is likely to lead a mushroom-like conformation of the chains instead of a brush one, which makes it impossible to growth the perovskite. Our first attempt to improve the synthetic outcome focused on the solvent.

Suitable solvents for perovskite precipitation need to be apolar. Colloidal synthesis of perovskite nanocrystals have been reported in hexanes, toluene, chlorobenzene, chloroform and dichloromethane.[42, 70] Attempting the synthesis in hexanes and dichloromethane was totally unsuccessful: precipitation simply does not occur in hexanes, while in dichloromethane degradation of the perovskite to lead iodide occurs within minutes after the synthesis. Synthesis of the nanoplatelets in chlorobenzene and chloroform instead afforded the desired product. Figure 5.22 shows absorbance spectra of the three dispersions. Using otherwise identical conditions, chloroform appears to lead twice as much product with respect to toluene and chlorobenzene. Unfortunately, sample degradation occurs within few hours after synthesis in this solvent.

The behaviour in hexanes is not unexpected. Synthesis in this solvent is reported for the synthesis of dots, and is based on the formation of an inverse emulsion rather than on nonsolvent precipitation. Perovskite is obtained breaking the emulsion with a polar solvent, such as acetone, followed by immediate crystallization. In our case, after the addition of acetone we observed the breaking of the emulsion (as the mixture turned from opaque to transparent), but no fluorescence. We speculate that the acetone itself is the cause: in fact, addition of small amounts of acetone to a toluene dispersion of platelets immediately causes the disappearance of the fluorescence, as the solvent dissolves the perovskite.
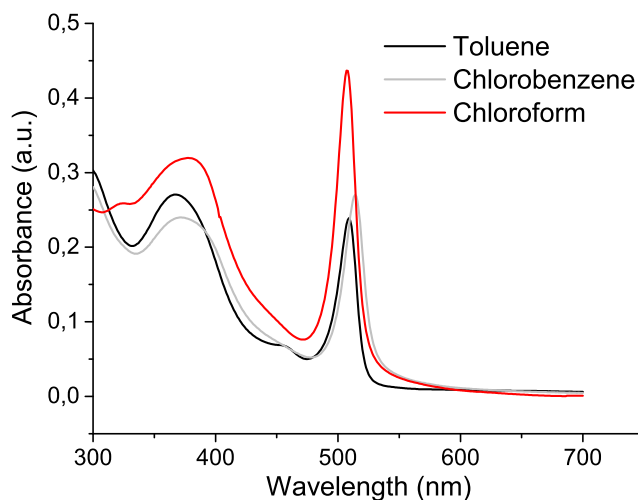

Figure 5.22 Absorption spectra of $PbI_4(PDMS-NH_3)_2$ platelets prepared using different antisolvents.

On the other side, there are two reasons that probably account for the behaviour of chloroform and dichloromethane. The first one is related to the crystallization, thus is a consideration on the kinetic of the process. The use of more polar antisolvents pushes the nucleation rate of the perovskite,[42] so a higher amount of material is obtained at the very beginning, which explain the higher absorbance for chloroform. The second reason is related to the solubility of the ligand in the solvent. Chloroform and dichloromethane are both better solvents than toluene and chlorobenzene for the ligand, as they are more suitable to solvate the ammonium head. This means they push the thermodynamic equilibrium of the system toward the solvated phase instead of the crystallized perovskite. This factor probably leads to the degradation of the perovskite back to the precursors. The expected smaller dimensions of the platelets in the case of dichloromethane, moreover, accelerate the process. Finally, behaviour of chlorobenzene appears slightly better than that of toluene, but no striking improvement was observed in the SEMs of the synthesized platelets.

As all the tested solvents are able to solubilize the PDMS, we realized we were looking at the wrong parameter. All good solvents for PDMS are able to drive its packing into a brush, and the main difference is thus observed in the behaviour of the inorganic material.

5.6.4.2 Variation of the solvent

For this reason, we speculated that the initial solvent should have had a greater influence on the synthetic output. In fact, the choice of the solvent is fundamental for the final morphology of the material, as it influences not only the initial configuration of the polymer, but also the nucleation rate of the perovskite. The ideal solvent should to be able to dissolve all the perovskite precursors, and properly solvate the polymer to avoid the formation of a polymeric random coil.

Looking at the problem from the point of view of the inorganic material, the choice of the solvent mainly influences the grade of solvation of Pb^{2+} cations, the species with lowest solubility. Good solvents for PbI_2, such as DMF, are coordinative for Pb^{2+}, and allow

to obtain highly concentrated solution of the precursors. On the other side, coordinative solvents influence the ability of the ions to correctly pack into the perovskite lattice. The reason is that good solvents for Pb^{2+} are able to interact through the formation of hydrogen bonds, the same kind of bond the ammonium salts form in the perovskite. For this reason non-coordinative solvents, such as acetonitrile, have been demonstrated to grant the growth of crystals with increased stability, as the final material is less defective, and consequently less sensitive to moisture.[71] Since they are not coordinative, however, the only way the material can be solvated is coordination of Pb^{2+} through I^-, and formation of PbI_n^{2-n} species.[72] The final concentration of precursors one can obtain in solution is anyway lower than that obtainable through a coordinative solvent.

Looking at the problem from the point of view of the ligand, different solvents mainly influences the initial conformation of the polymeric chain. A bad solvent for PDMS will not allow solvation of the polymeric chain, and the material will mainly form random coils. This conformation is expected to be detrimental for the growth of the perovskite, as the chains need to unroll before being able to pack in the lattice and form the brush. Unfortunately, we identified only a few good solvents for PDMS, which are hexanes, toluene, chloroform and tetrahydrofuran. Among these, the only solvent suitable to prepare the precursors solution is THF, as the others are antisolvents for the perovskite.

In order to understand the influence of the various factors, we compared results obtained for three different solvents: DMF, acetonitrile and THF. Respective characteristics toward the two identified factors are described in table 5.2 . Unfortunately, no solvent has been identified which is both coordinative for Pb^{2+} and able to solvate PDMS. For this reason, we used a 1:1 mixture of DMF and toluene, which allowed us to obtain a clear solution of the precursors*.

	Coordinative for Pb^{2+}	Solubilize PDMS
1:1 DMF/toluene	Yes	Yes
DMF	Yes	No
THF	No	Yes
Acetonitrile	No	No

Table 5.2 Ability of chosen solvents to coordinate Pb^{2+} and solubilize PDMS.

Figure 5.23 shows a significant SEM picture of the outcome of synthesis for each solvent. Platelets obtained using acetonitrile and DMF as solvents are way smaller than the others, with average dimensions spanning the range 150-300 nm for acetonitrile, and 300 nm-1 μm for DMF. In both the case of DMF/toluene and THF, on the other side, square platelets with dimensions of 2-4 μm can be obtained. This behaviour may be rationalized in terms of conformation of the polymer. Solvents unable to solvate PDMS push it toward a random coil conformation, or formation of aggregates. In both cases, the polymer needs to disgregate and unroll to form a brush on top of the perovskite. Since this process requires time, nucleation of the perovskite may happen before it completes, thus leading to a partially mushroomy packing of the chains. Under such conditions, the perovskite is likely to stop growing earlier simply because there is no room enough for more polymer to add. On the other side, the use of a solvent which solvate the ligand from the beginning facilitate the crystallization and growth of platelets.

Effect of the solvents on the inorganic side of the material is less evident. However, the smaller dimensions of platelets obtained with acetonitrile compared to those observed for

---

*No luminescence was detected from this solution under illumination with UV lamp (λ_{exc}=365 nm)

DMF may probably be accounted to an increased nucleation rate. In fact, Pb_2^+ is only stabilized through formation of complexes with I^-, thus nucleation is more favourable than in DMF. Behaviour in THF is difficult to be properly described, as the PbI_n^{2-n} species are stabilized also by the solvated ligand, so diffusive processes and coalescence are likely to occur besides nucleation and growth.
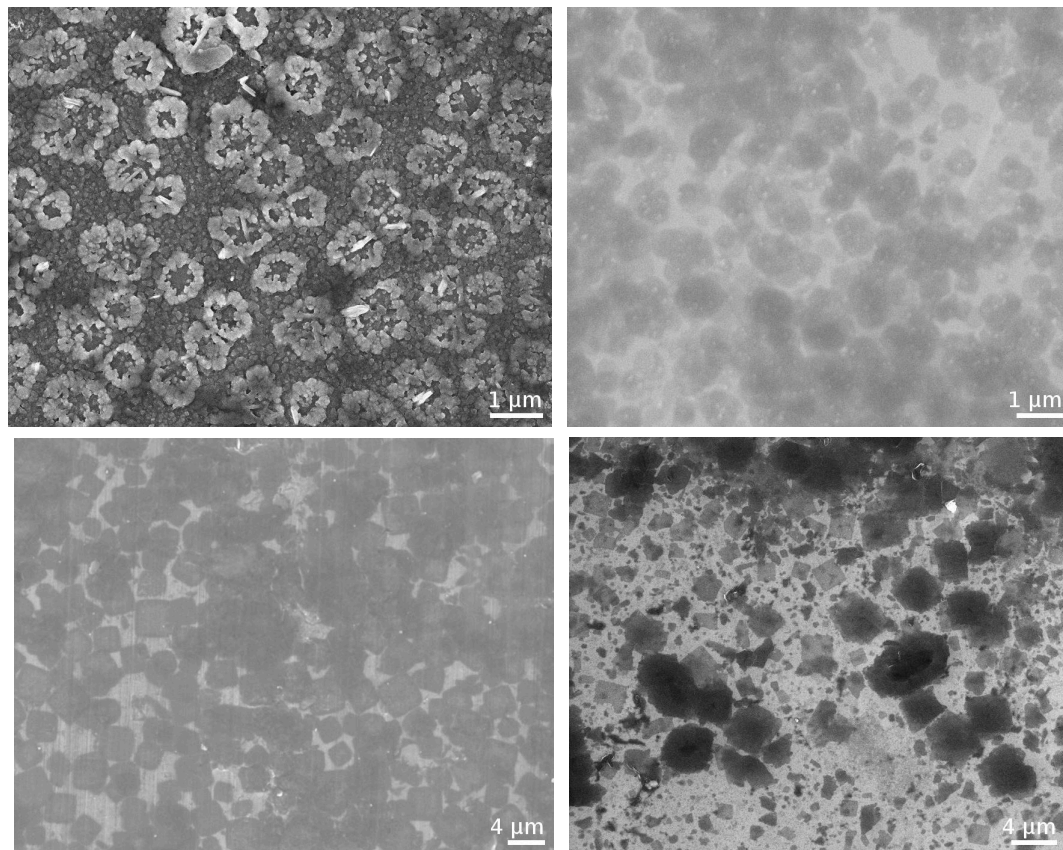
Figure 5.23 SEMs of $PbI_4(PDMS-NH_3)_2$ nanoplatelets synthesized from different starting solvents. Top, left: acetonitrile. Top, right: DMF. Bottom, left: 1:1 DMF/toluene. Bottom, right: THF.

Apparently, use of DMF allowed to synthesize more homogeneous platelets if compared to THF and acetonitrile. For both these solvents, in fact, obtained platelets are way more irregular. Since both THF and acetonitrile are not able to dissolve PbI_2, the starting solution of precursors has been obtained through addition of $HI_{(aq)}$ (details of synthesis are given in the experimental section). The irregularity of shapes may be therefore due to the presence of a high amount of water in the reaction environment, as it is known its presence is detrimental for the growth of hybrid perovskites.

5.6.4.3 Effect of temperature

The effect of solvent proved important in modifying the final morphology of nanoplatelets, but the lacking of a solvent suitable to solubilize both PbI_2 and $PDMS-NH_3I$ pushed us to find another way to improve the synthetic output of the reaction. Since the major problem seemed to be related to the difficulty for the polymer to pack at the lattice surface, we looked for a way to facilitate this process. We speculated the major difficulty to arise from the steric hindrance of the chains: once a molecule takes its place, a second one needs to overcame the energy barrier due to Van der Waals interaction to pack near

it. This means that lowering the energy of interaction of PDMS with itself will facilitate the crystallization of the perovskite. This energy of interaction is the Cohesive Energy Density (CED) of the polymer, which is defined as the energy per unit volume of the liquid required to move a molecule from the liquid state to a vapor state: it is a measure of the interactions between the molecules in the liquid state.[73] For liquids of low molar weight, the cohesive energy is closely related to the molar heat of evaporation ΔH_{vap} (at a given temperature):

$$E_{coh} = \Delta U_{vap} = \Delta H_{vap} - p\Delta V \approx \Delta H_{vap} - RT \tag{5.1}$$

Knowledge of this quantity is fundamental, as it is related to several other variables, such as the Hildebrand solubility parameter, the surface tension and the internal pressure, and makes possible predictions about swelling and interactions with solvents, refraction index and dipole moment[73–76] of the polymer.

Since it is a thermodynamic property of the material, CED depends on temperature, in particular is expected to lower with increasing temperature, as stated by equation 5.1. Figure 5.24 shows the variation of CED with temperature for a variety of polymers. In the case of high molecular weight PDMS, a raise in temperature from 30 °C to 100 °C has the effect of lowering the CED of $\sim 20\%$. We therefore attempt the synthesis at higher temperature. Since the boiling temperature of toluene is 110 °C, we considered to try both an intermediate temperature (60 °C), and one as close as possible to the boiling point (100 °C).

Figure 5.24 Variation of CED with temperature for various polymers. Reproduced with permission from [77]. Copyright © 2017 John Wiley & Sons, Inc

Figure 5.25 shows SEMs for a series of syntheses performed in the standard conditions (DMF as solvent, toluene as antisolvent) with temperature as the only variable. It is immediately clear that temperature raising makes a striking difference on the quality of the final material. At low temperature, platelets are barely distinguishable, even if optical characterization proves their existence. Synthesis at 60 °C allows to obtain cleaner platelets, but apparently a huge amount of material crystallize as PbI_2, visible as white crystals all around. We don't have an explanation for this behaviour yet. Synthesis at 100 °C finally ends up in nice, clean platelets. Temperature has also an influence on the size of the final material, which grows from 2-4 μm at 20 °C to 5-10 μm at 100 °C. This increase in platelets size matches with the proposed model: an increase of temperature lowers the CED, thus it facilitates the packing of the polymer, but has small influence on the nucleation rate, and platelets end up growing wider.
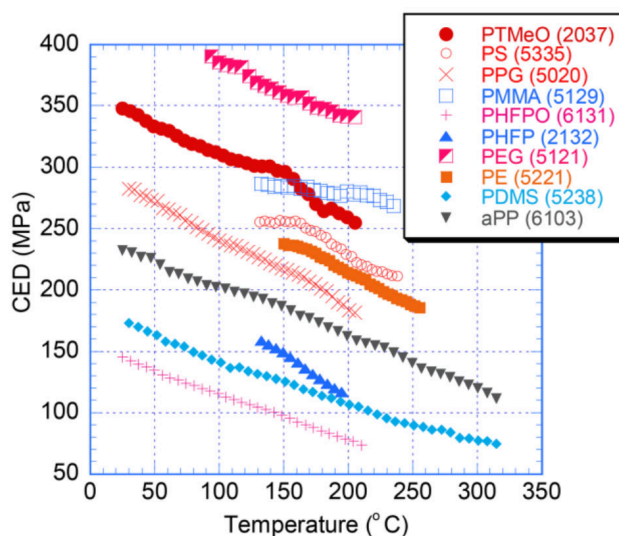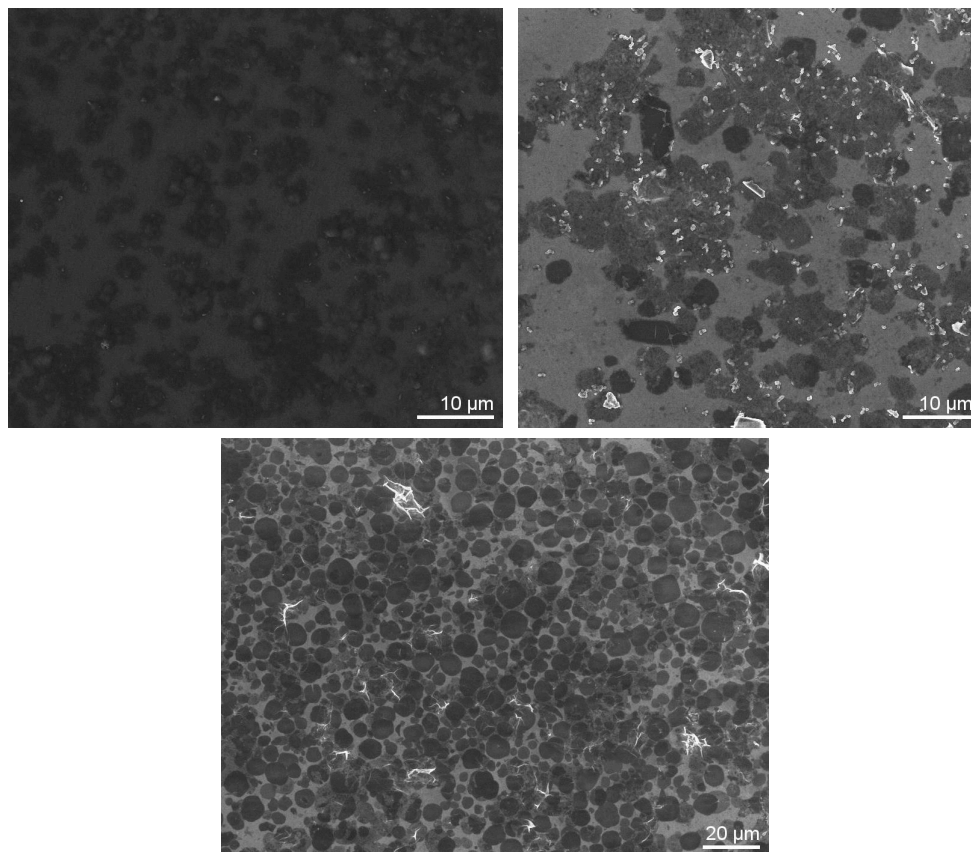
Figure 5.25 SEMs of $PbI_4(PDMS-NH_3)_2$ nanoplatelets synthesized in toluene at 20 ˚C (top, left), 60 ˚C (top, right) and 100 ˚C (bottom).

5.6.4.4   Effect of mixed ligands

As at room temperature the steric hindrance of PDMS inhibits the perovskite crystallization, we attempted with a last, different strategy. The idea was to partially substitute the PDMS with a smaller, less bulky ligand, in order for the PDMS to have more surface available per chain and pack more easily. As co-ligand, we used $HDec-NH_3I$. The reason is that $PbI_4(HDec-NH_3)_2$ platelets have an absorption and emission spectrum blue-shifted with respect to that of $PbI_4(PDMS-NH_3)_2$. We adopted this expedient as the ability of the co-ligand in promoting crystallization of the perovskite is greater than that of PDMS: this means that it's possible to obtain platelets with segregated ligands as synthetic output, which however can be distinguished on the basis of their optical properties. As we also aimed at maintaining the unit cell thickness feature granted by PDMS, we had to balance two opposite needing: on one side, a high amount of co-ligand, to grant more space per chain to the polymer; on the other, a small amount of co-ligand, to avoid the risk to build a layered material. We decided to perform two syntheses, substituting 10% and 25% of the total polymer respectively. Details on the synthesis are given in the experimental section. In the first case, the synthetic output was a dispersion, while in the second case a suspension formed within few minutes after injection.

Figure 5.26 shows SEMs images of the two materials. In the case of a 10% substitution, thin platelets are clearly visible, which look way better than those obtained from $PDMS-NH_3I$ only in the same conditions. They are also quite big, although defective, as holes are visible in nearly all of them. In the case of 25% substitution, on the other

side, the only visible material was made of thick platelets, which look very similar to $PbI_4(HDec-NH_3)_2$. Our hypothesis is that, in the case of 10% substitution, $HDec-NH_3I$ is too diluted to be able to segregate, thus it disperses homogeneously within the polymer, or eventually creates small domains, which however are not big enough to influence the $Pb-I-Pb$ bond angle defined by PDMS. In the case of 25% substitution, instead, we do not substitute the polymer at all, as the amount of $HDec-NH_3I$ is high enough to allow it to crystallize separately. The polymer, anyway, has probably an influence on the crystallization process, as the morphology of the obtained platelets is different from that of $PbI_4(HDec-NH_3)_2$ (visible in figure 5.6).
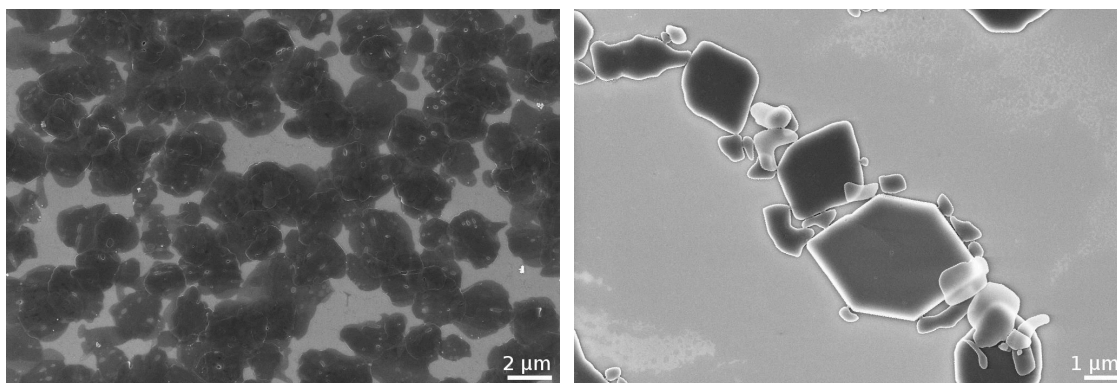
Figure 5.26 SEMs of $PbI_4(PDMS-NH_3)_{2-x}(HDec-NH_3)_x$ for $x = 0.2$ (left) and $x = 0.5$ (right)

Absorption and PL spectra of $PbI_4(PDMS-NH_3)_{2-x}(HDec-NH_3)_x$ for $x = 0$, 0.2, 0.5, 2, shown in figure 5.27, confirm our theory. The 10% substitution of $PDMS-NH_3I$ with $HDec-NH_3I$ does not influence the exciton energy of the material, which is the same of $PbI_4(PDMS-NH_3)_2$, whilst for 25% substitution two peaks are clearly observable, which correspond to the peaks of parent materials.
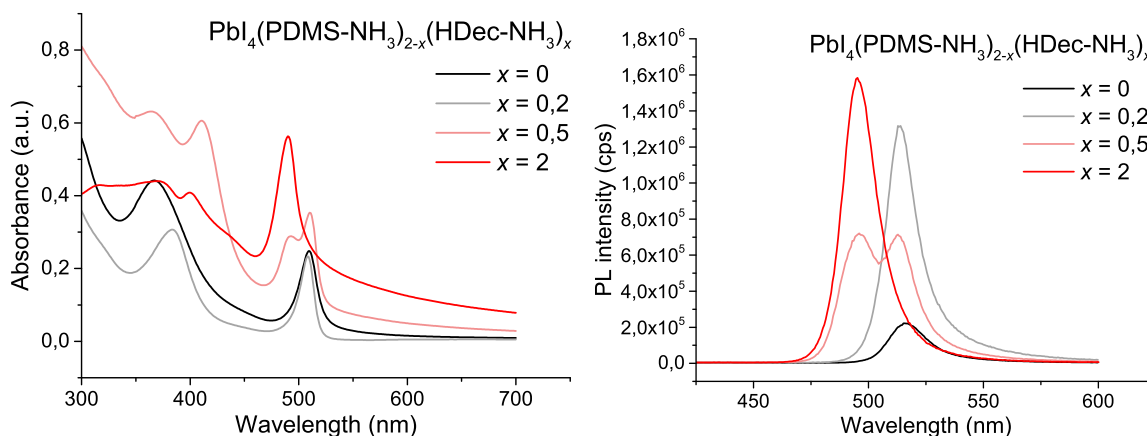
Figure 5.27 Absorption (left) and PL (right) spectra of $PbI_4(PDMS-NH_3)_{2-x}(HDec-NH_3)_x$ for $x = 0, 0.2, 0.5, 2$

PL spectra, on the other side, suggest that the obtained mixed materials do not behave like the parent ones. In fact, $PbI_4(PDMS-NH_3)_{1,8}(HDec-NH_3)_{0,2}$ and $PbI_4(PDMS-NH_3)_2$ have extremely different luminescence intensities, even if their absorbances are similar. There is no obvious explanation for such a behaviour, but it would be interesting to understand if it might be related to a different crystallinity grade of the final material.

5.6.5 Conclusions

We developed the synthesis of a naturally bidimensional hybrid perovskite through a process of polymer-directed crystallization using an ammonium salt of PDMS. To the best of our knowledge, this is the first time such a synthesis is reported. Since the crystallization of the material requires the packing of the PDMS into a polymeric brush on the perovskite surface, the process is mainly under the control of the ligand. For this reason, we rationalized the morphology of the final material in terms of the behaviour of the polymer rather than that of the inorganic perovskite layer.

Use of different starting solvents allows to influence the dimensions of the obtained platelets, as the growth is determined by the initial conformation of the polymeric chain: use of good solvents for PDMS, such a THF or a DMF/toluene mixture, allows to grow bigger platelets, as the polymer is in the best conditions to grow as a brush.

The most important parameter to consider, however, is the cohesive energy density of PDMS. In fact, lowering this energy means favouring the interaction between chains, which can pack more easily. Synthesis of $PbI_4(PDMS-NH_3)_2$ performed at high temperature proves the point, as it allows to grow wider and cleaner platelets.

A lot of work still remains to be done. Since we understood the importance of intrinsic properties of the ligand, a study of the synthesis depending on the chain length, and the nature of the polymer may be performed, to understand if this synthetic method is generalizable or is a unique feature of PDMS. A full study of the characteristics of the obtained material should be attempted through GI-WAXS, DSC, AFM and PL measurements. We never attempted the synthesis of $PbBr_4(PDMS-NH_3)_2$, which has a tolerance factor of 1.14 on the basis of our model, nor perovskites with a cation different than lead. But probably, the most

Figure 5.28 SEM of $PbI_4(PDMS-NH_3)_2$ showing "crumpled" nanoplatelets.

interesting feature of these platelets is their extreme flexibility, which arises from both the extreme aspect ratio (few nanometers thin - several micrometers large material) and the "liquid" nature of the ligand. As visible in figure 5.28, these platelets can fold in crumpled conformations. Macroscopic properties of the material as a bulk are probably close to those of PDMS by means of the so-called "stealth effect",[58] thus it should be something similar to a "liquid semiconductor". A study of the mechanical properties of this weird material may reserve some surprises.
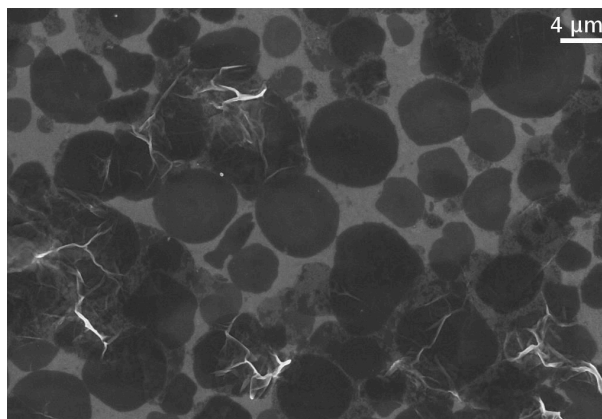
5.7   Experimental

Amine terminated 1K PDMS was purchased from Polymer Source. Lead iodide and bromide were purchased from TCI. All other materials and solvents were purchased from Sigma Aldrich. All reagents were used as received.

Synthesis of ammonium salts

NMR spectra were record on a Bruker Avance II 500 MHz NMR Spectrometer.

Synthesis of octylammonium bromide Oct−NH₃Br
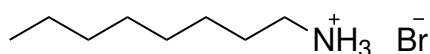
Octylamine (2,00 g, 15,5 mmol) is dissolved in isopropanol (2 mL), then $HBr_{(aq)}$ 48% (2,60 g, 1,75 mL, 15,5 mmol) is added dropwise over 5 minutes. The solution is stirred for 5 minutes more, then solvents are removed at reduced pressure. The product is crystallized from the crude using toluene (3,19 g, yield 97,9%). It appears as a white, cakey solid. The product is stored in the dark to prevent its degradation.

^{1}H NMR (CDCl$_3$, 500 MHz): δ 7.90 (br), 2.96 (t, J=7.7 Hz, 2H), 1.74 (quin, J=7.5 Hz, 2H), 1.34 (quin, J=7.2 Hz, 2H), 1.24-1.19 (m, 8H), 0.81 (t, J=7.0 Hz, 3H)

^{13}C NMR (CDCl$_3$, 125.8 MHz): δ 40.21, 31.71, 29.03, 28.91, 27.51, 26.55, 22.60, 14.08.

Synthesis of dodecylammonium bromide Dod−NH₃Br
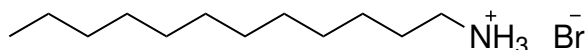
Dodecylamine (2,00 g, 10,8 mmol) is dispersed in isopropanol (2 mL), then $HBr_{(aq)}$ 48% (1,82 g, 1,22 mL, 10,8 mmol) is added dropwise over 5 minutes. The solution is stirred for 5 minutes more, then solvents are removed at reduced pressure. The product is crystallized from the crude using toluene (2,73 g, yield 94,9%). It appears as a white, cakey solid. The product is stored in the dark to prevent its degradation.

^{1}H NMR (CDCl$_3$, 500 MHz): δ 7.96 (br), 2.95 (t, J=7.7 Hz, 2H), 1.73 (quin, J=7.7 Hz, 2H), 1.33 (quin, J=7.2 Hz, 2H), 1.18 (m, 16H), 0.81 (t, J=7.0 Hz, 3H)

^{13}C NMR (CDCl$_3$, 125.8 MHz): δ 40.16, 31.92, 29.63, 29.62, 29.55, 29.38, 29.36, 28.95, 27.55, 26.53, 22.70, 14.13.

## Synthesis of hexadecylammonium bromide HDec−NH₃Br
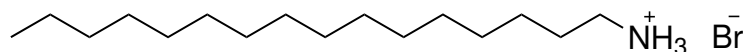
Hexadecylamine (2,00 g, 8,28 mmol) is dispersed in isopropanol (2 mL), then $HBr_{(aq)}$ 48% (1,40 g, 937 μL, 8,28 mmol) is added dropwise over 5 minutes. The solution is stirred for 5 minutes more, then solvents are removed at reduced pressure. The product is crystallized from the crude using toluene (2,62 g, yield 98,2%). It appears as a white, cakey solid. The product is stored in the dark to prevent its degradation.

^{1}H NMR (DMSO−d$_6$, 500 MHz): δ 7.59 (br), 2.77 (t, J=7.6 Hz, 2H), 1.51(quin, J=7.3 Hz, 2H), 1.25 (m, 26H), 0.86 (t, J=7.0 Hz, 3H).

^{13}C NMR (DMSO−d$_6$, 125.8 MHz): δ 31.76, 29.51, 29.47, 29.39, 29.30, 29.17, 29.98, 27.47, 26.23, 22.56, 14.43. One more signal around 40 ppm is expected, but it is covered by solvent peak.

Synthesis of octylammonium iodide Oct−NH₃I
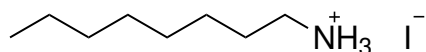
Octylamine (2,00 g, 15,5 mmol) is dissolved in isopropanol (2 mL), then $HI_{(aq)}$ 57% (3,47 g, 2,04 mL, 15,5 mmol) is added dropwise over 5 minutes. The solution is stirred for 5 minutes more, then solvents are removed at reduced pressure. The product is crystallized from the crude using toluene (3,69 g, yield 92,7%). It appears as a white, cakey solid. The product is stored in the dark to prevent its degradation.

^{1}H NMR (CDCl$_3$, 500 MHz): δ 7.58 (br), 3.05 (t, J=7.7 Hz, 2H), 1.78 (quin, J=7.7 Hz, 2H), 1.35 (quin, J=7.2 Hz, 2H), 1.26-1.21 (m, 8H), 0.82 (t, J=7.0 Hz, 3H)

^{13}C NMR (CDCl$_3$, 125.8 MHz): δ 40.52, 31.70, 29.02, 28.90, 27.43, 26.9, 22.61, 14.09.

Synthesis of dodecylammonium iodide Dod−NH₃I
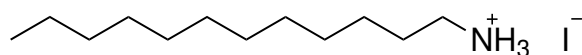
Dodecylamine (2,00 g, 10,8 mmol) is dispersed in isopropanol (2 mL), then $HI_{(aq)}$ 57% (2,42 g, 1,42 mL, 10,8 mmol) is added dropwise over 5 minutes. The solution is stirred for 5 minutes more, then solvents are removed at reduced pressure. The product is crystallized from the crude using toluene (3,10 g, yield 91,6%). It appears as a white, cakey solid. The product is stored in the dark to prevent its degradation.

^{1}H NMR (CDCl$_3$, 500 MHz): δ 7.61 (br), 3.04 (t, J=7.7 Hz, 2H), 1.77 (quin, J=7.7 Hz, 2H), 1.36 (quin, J=7.2 Hz, 2H), 1.19 (m, 16H), 0.81 (t, J=6.9 Hz, 3H)

^{13}C NMR (CDCl$_3$, 125.8 MHz): δ 40.52, 31.92, 29.64, 29.56, 29.40, 29.36, 28.96, 27.47, 26.60, 22.70, 14.13.

Synthesis of hexadecylammonium iodide HDec−NH₃I
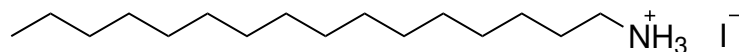
Hexadecylamine (2,00 g, 8,28 mmol) is dispersed in isopropanol (2 mL), then $HI_{(aq)}$ 57% (1,86 g, 1,09 mL, 8,28 mmol) is added dropwise over 5 minutes. The solution is stirred for 5 minutes more, then solvents are removed at reduced pressure. The product is crystallized from the crude using toluene (2,92 g, yield 95,4%). It appears as a white, cakey solid. The product is stored in the dark to prevent its degradation.

^{1}H NMR (DMSO−d₆, 500 MHz): δ 7.58 (br), 2.77 (t, J=7.6 Hz, 2H), 1.51(quin, J=7.2 Hz, 2H), 1.25 (m, 26H), 0.86 (t, J=6.9 Hz, 3H).

^{13}C NMR (DMSO−d₆, 125.8 MHz): δ 31.76, 29.51, 29.47, 29.38, 29.30, 29.17, 29.97, 27.46, 26.22, 22.56, 14.43. One more signal around 40 ppm is expected, but it is covered by solvent peak.

Synthesis of 1K PDMS−NH₃I
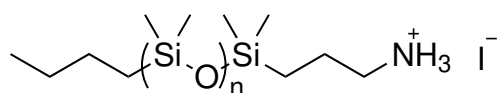
Molecular weight of amine terminated 1K PDMS is determined through ^{1}H NMR simply by integration of the peak of the Si−CH₃ groups with respect to the ending −CH₃ (see NMR below). In this way, we calculated $n = 12, 7$.
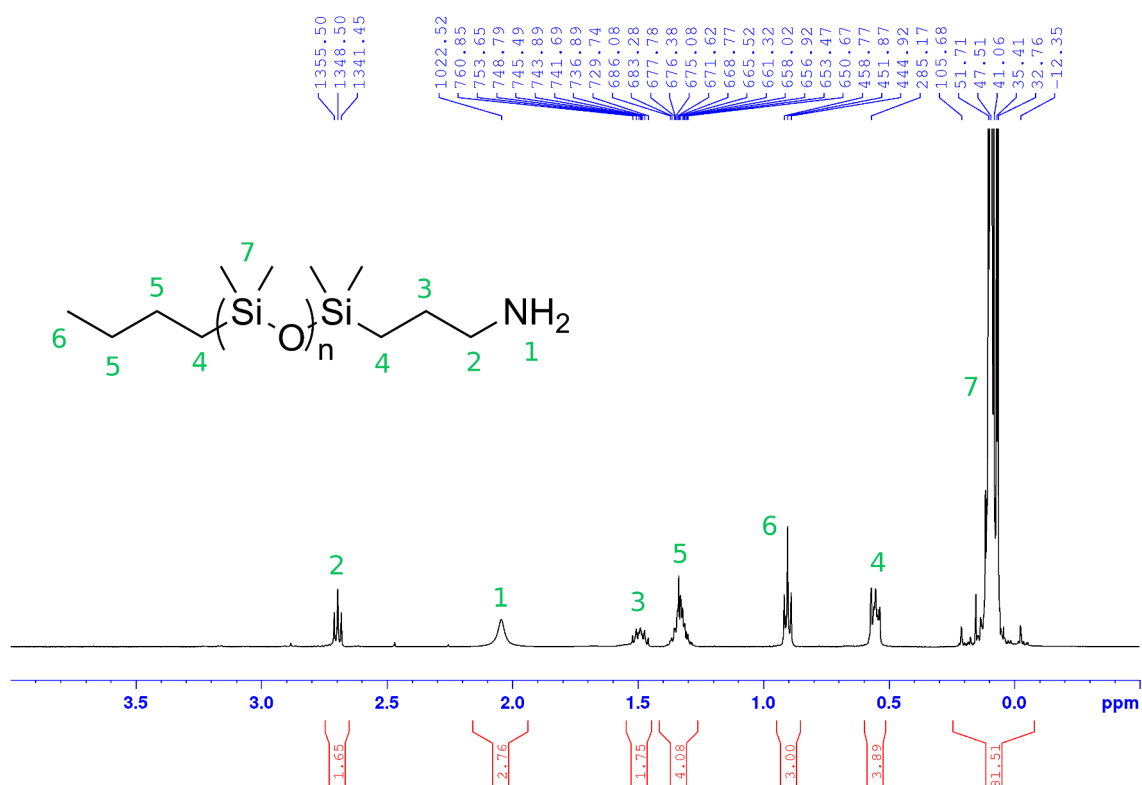
Amine terminated 1K PDMS (MW=1203, 2,00 g, 1,66 mmol) is dissolved in isopropanol (2 mL), then $HI_{(aq)}$ 57% (373 mg, 219,4 μL, 1,66 mmol) is added dropwise over 5 minutes. The solution is stirred for 5 minutes more, then solvents are removed at reduced pressure. The residue is dissolved in CH_2Cl_2, and anhydrous $MgSO_4$ is added to remove any remaining water (water removal is fundamental to prevent product degradation). The white solid is filtered away, and the organic phase is dried at reduced pressure to afford the pure product as a yellowish oil (2,00 g, yield 90,0%). The product is stored at −18 °C in the dark to prevent its degradation.

^{1}H NMR ($CDCl_3$, 500 MHz): δ 5.43 (br), 3.04 (t, J=6.9 Hz, 2H), 1.82 (q, J=7.4 Hz, 2H), 1.33 (m, 4H), 0.90 (t, J=6.9 Hz, 3H), 0.66 (m, 2H), 0.56 (m, 2H), 0.10 (m, 82H). Peaks at 4.06 and 1.24 are due to residual isopropanol, while peak at 5.32 is due to residual CH_2Cl_2.[78]
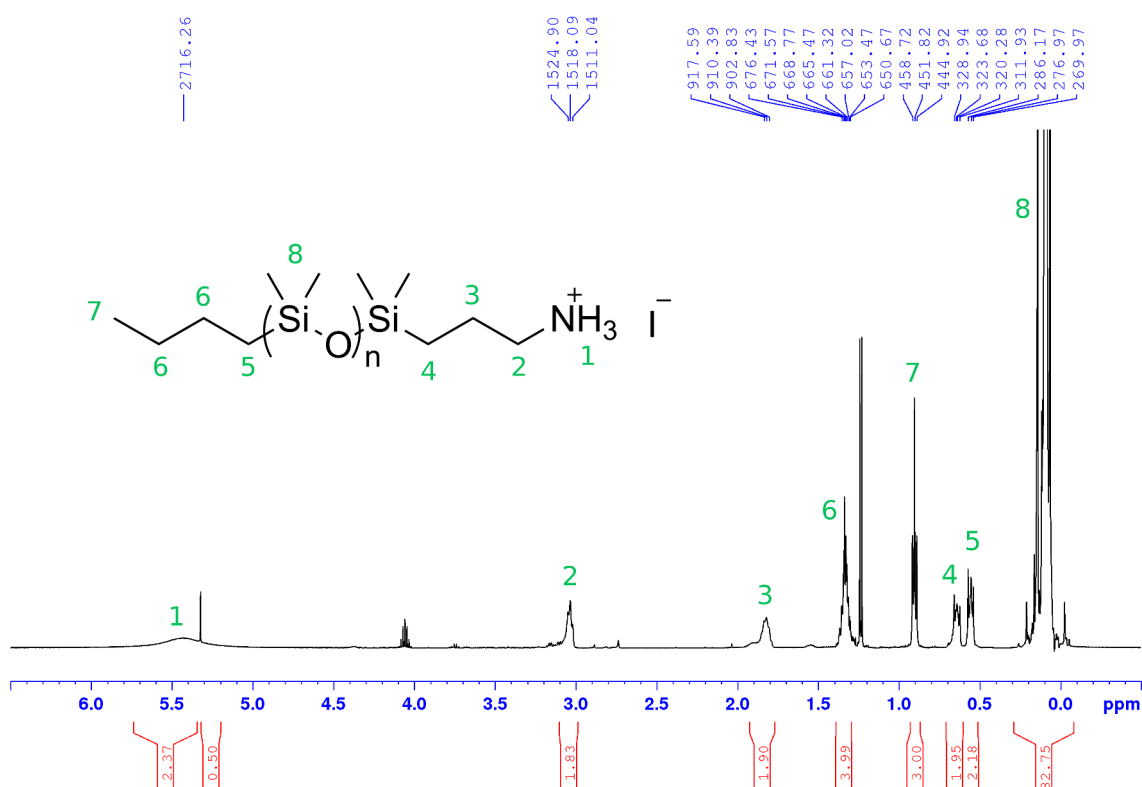
Synthesis of perovskite nanoplatelets

Synthesis of alkylammonium based perovskite nanoplatelets

Synthesis of perovskite material is performed through a nonsolvent precipitation method (reprecipitation).

The chosen lead halide is dissolved in DMF to obtain a solution 0,1 M. In a typical synthesis, 100 μL of this solution are added to 2 eq of ammonium salt, then 100 μL of DMF more are added to facilitate its dissolution. The obtained precursors solution is injected in 100 mL of toluene (the antisolvent) stirring at 1000 rpm to induce the precipitation of the perovskite. The dispersion in stirred for 15 minutes before use.

Synthesis of PDMS based perovskite nanoplatelets

In a typical synthesis, 100 µL of PbI_2 0,1 M solution in DMF are added to 2 eq of $PDMS-NH_3I$, then 100 µL of toluene are added to obtain a clear solution, which is not luminescent under UV lamp (λ_{exc}=365 nm). The obtained precursors solution is injected in 100 mL of toluene (the antisolvent) stirring at 1000 rpm to induce the precipitation of the perovskite. The dispersion in stirred for 15 minutes before use.

For solvents different from 1:1 DMF/toluene, the following procedures were applied.

DMF 100 µL of PbI_2 0,1 M solution in DMF are added to 2 eq of $PDMS-NH_3I$, then 100 µL of DMF more are added. A biphasic mixture is obtained, which was sonicated for 30 minutes before use. The obtained precursors mixture is injected in 100 mL of toluene (the antisolvent) stirring at 1000 rpm to induce the precipitation of the perovskite. The dispersion in stirred for 15 minutes before use.

Acetonitrile 0,050 mmol of PbI_2 (23,0 mg) are dispersed in 1 mL of acetonitrile, then 0,050 mmol of $HI_{(aq)}$ 57 % (11,2 mg, 6,60 µL) are added. Suspension is sonicated until a yellow solution is obtained, then 1 mL of 0,1 M solution of $PDMS-NH_3I$ (0,10 mmol, 132,8 mg) in toluene is added. A biphasic mixture is obtained, which was sonicated for 30 minutes more before use. Finally, 200 µL of the obtained precursors mixture are injected in 100 mL of toluene (the antisolvent) stirring at 1000 rpm to induce the precipitation of the perovskite. The dispersion in stirred for 15 minutes before use.

THF 0,050 mmol of PbI_2 (23,0 mg) are dispersed in 1 mL of THF, then 0,050 mmol of $HI_{(aq)}$ 57 % (11,2 mg, 6,60 µL) are added. Suspension is sonicated until a yellow solution is obtained, then 1 mL of 0,1 M solution of $PDMS-NH_3I$ (0,10 mmol, 132,8 mg) in THF is added. Finally, 200 µL of the obtained precursors solution are injected in 100 mL of toluene (the antisolvent) stirring at 1000 rpm to induce the precipitation of the perovskite. The dispersion in stirred for 15 minutes before use.

Synthesis of $PbI_4(PDMS-NH_3)_{1,8}(HDec-NH_3)_{0,2}$ perovskite nanoplatelets

100 µL of PbI_2 0,1 M solution in DMF are mixed with 20 µL of a 0,1 M solution of $HDec-NH_3I$ in DMF. This solution is then added to 1,8 eq of PDMS, and 100 µL of toluene are added to obtain a clear solution. This final solution is injected in 100 mL of toluene stirring at 1000 rpm to induce the precipitation of the perovskite. The dispersion in stirred for 15 minutes before use.

Synthesis of $PbI_4(PDMS-NH_3)_{1,5}(HDec-NH_3)_{0,5}$ perovskite nanoplatelets

100 µL of PbI_2 0,1 M solution in DMF are mixed with 50 µL of a 0,1 M solution of $HDec-NH_3I$ in DMF. This solution is then added to 1,5 eq of PDMS, and 100 µL of toluene are added to obtain a clear solution. This final solution is injected in 100 mL of toluene stirring at 1000 rpm to induce the precipitation of the perovskite. The dispersion in stirred for 15 minutes before use.

Purification of alkylammonium based perovskite nanoplatelets

10 mL of nanoplatelets suspension are centrifuged for 10 minutes at 4400 rpm. The supernatant is subsequently removed, and 10 mL of clean toluene are added. The flask is then shaken to obtain a new suspension.

Characterization of perovskite nanoplatelets

Morphological characterization

SEM and EDX analyses were performed by Karol Miszta on a Zeiss Gemini Ultra-55 Analytical Field Emission Scanning Electron Microscope. Beam energy used was 5 kV for imaging and 8 kV for elemental analyses. Samples were prepared by drop-casting 40 μL of a purified suspension of nanoplatelets on a clean silicon substrate heated at 40 °C. The substrate is cut from a Czochralski silicon wafer, and cleaned by ultrasonication for 20 minutes in acetone, then isopropanol and finally Milli-Q water.

STEM analysis was performed by Teresa Williams on a JEOL 2100-F 200 kV Field-Emission Analytical Transmission Electron Microscope using a HAADF (high-angle annular dark field) STEM detector. Samples were prepared drop-casting 5 μL of a purified suspension of nanoplatelets diluted 1:20 with clean toluene on a lacey carbon film on 200 mesh copper grid, and subsequently drying the excess solvent with absorbent paper.

XRD analyses were performed by Karol Miszta on a Bruker AXS D8 Discover GADDS X-Ray Diffractometer operated at 35 kV / 40 mA with a Co-Kα wavelength of 1.789 Å. All recorded spectra are converted to be comparable with a Cu-Kα wavelength of 1.541 Å.

Optical characterization

Absorption spectra were recorded on a Cary 5000 UV-Vis-NIR spectrophotometer. 300 μL of nanoplatelets dispersion/suspension in toluene are poured in a 1 mm pathlength quartz cuvette for the measurement.

Photoluminescence spectra were recorded on a NanoLog Spectrofluorometer equipped with a 450 W xenon short-arc as source, and a InGaAs based detector. Excitation wavelength: 365 nm; integration time: 0,01 s. 500 μL of nanoplatelets dispersion/suspension in toluene are poured in a 3 mm pathlength fluorescence quartz cuvette for the measurement.

Thermal characterization

DSC traces were recorded on a TA Instruments DSC Q200 at a constant scanning speed of 5 °C min^{-1}.

Bibliography

[1] Goldschmidt, V. M. *Skr. Nor. Vidensk. Akad. i Oslo* **1927**, *8*, 7–156.

[2] Bhalla, A. S., Guo, R., and Roy, R. *Mat. Res. Innovat.* **2000**, *4*, 3–26. doi: 10.1007/s100190000062.

[3] Kieslich, G., Sun, S., and Cheetham, A. K. *Chem. Sci.* **2015**, *6*, 3430–3433. doi: 10.1039/C5SC00961H.

[4] Travis, W., Glover, E. N. K., Bronstein, H., Scanlon, D. O., and Palgrave, R. G. *Chem. Sci.* **2016**, *7*, 4548–4556. doi: 10.1039/C5SC04845A.

[5] Weber, D. *Z. Naturforsch. B* **1978**, *33*, 1443–1445. doi: 10.1515/znb-1978-1214.

[6] Mischgofsky, F. *J. Cryst. Growth* **1983**, *65*, 500–505. doi: 10.1016/0022-0248(83)90093-3.

[7] Ricard, L., Rey-Lafon, M., and Biran, C. *J. Phys. Chem.* **1984**, *88*, 5614–5620. doi: 10.1021/j150667a031.

[8] Kojima, A., Teshima, K., Shirai, Y., and Miyasaka, T. *J. Am. Chem. Soc.* **2009**, *131*, 6050–6051. doi: 10.1021/ja809598r.

[9] Lee, M. M., Teuscher, J., Miyasaka, T., Murakami, T. N., and Snaith, H. J. *Science* **2012**, *338*, 643–647. doi: 10.1126/science.1228604.

[10] Liu, M., Johnston, M. B., and Snaith, H. J. *Nature* **2013**, *501*, 395–398. doi: 10.1038/nature12509.

[11] Pellet, N., Gao, P., Gregori, G., Yang, T.-Y., Nazeeruddin, M. K., Maier, J., and Grätzel, M. *Angew. Chem., Int. Ed.* **2014**, *53*, 3151–3157. doi: 10.1002/anie.201309361.

[12] Green, M. A., Ho-Baillie, A., and Snaith, H. J. *Nat. Photonics* **2014**, *8*, 506–514. doi: 10.1038/nphoton.2014.134.

[13] Nie, W., Tsai, H., Asadpour, R., Blancon, J.-C., Neukirch, A. J., Gupta, G., Crochet, J. J., Chhowalla, M., Tretiak, S., Alam, M. A., Wang, H.-L., and Mohite, A. D. *Science* **2015**, *347*, 522–525. doi: 10.1126/science.aaa0472.

[14] Sivaram, V., Stranks, S. D., and Snaith, H. J. *Scientific American* **2015**, *313*, 54–59. doi: 10.1038/scientificamerican0715-54.

[15] You, J., Meng, L., Song, T.-B., Guo, T.-F., Yang, Y. M., Chang, W.-H., Hong, Z., Chen, H., Zhou, H., Chen, Q., Liu, Y., De Marco, N., and Yang, Y. *Nat. Nanotechnol.* **2016**, *11*, 75–81. doi: 10.1038/nnano.2015.230.

[16] Lal, N. N., Dkhissi, Y., Li, W., Hou, Q., Cheng, Y.-B., and Bach, U. *Adv. En. Mater.* **2017**, *7*, 1602761. doi: 10.1002/aenm.201602761.

[17] Grancini, G., Roldán-Carmona, C., Zimmermann, I., Mosconi, E., Lee, X., Martineau, D., Narbey, S., Oswald, F., De Angelis, F., Graetzel, M., and Nazeeruddin, M. K. *Nat. Commun.* **2017**, *8*, 15684. doi: 10.1038/ncomms15684.

[18] Yang, W. S., Park, B.-W., Jung, E. H., Jeon, N. J., Kim, Y. C., Lee, D. U., Shin, S. S., Seo, J., Kim, E. K., Noh, J. H., and Seok, S. I. *Science* **2017**, *356*, 1376–1379. doi: 10.1126/science.aan2301.

[19] http://www.nrel.gov/pv/assets/images/efficiency-chart.png. Accessed 26-12-2017.

[20] Edri, E., Kirmayer, S., Cahen, D., and Hodes, G. *J. Phys. Chem. Lett.* **2013**, *4*, 897–902. doi: 10.1021/jz400348q.

[21] Yang, M., Zhang, T., Schulz, P., Li, Z., Li, G., Kim, D. H., Guo, N., Berry, J. J., Zhu, K., and Zhao, Y. *Nat. Commun.* **2016**, *7*, 12305. doi: 10.1038/ncomms12305.

[22] Eperon, G. E., Stranks, S. D., Menelaou, C., Johnston, M. B., Herz, L. M., and Snaith, H. J. *Energy Environ. Sci.* **2014**, *7*, 982–988. doi: 10.1039/C3EE43822H.

[23] Hao, F., Stoumpos, C. C., Cao, D. H., Chang, R. P. H., and Kanatzidis, M. G. *Nat. Photonics* **2014**, *8*, 489–494. doi: 10.1038/nphoton.2014.82.

[24] Beznosikov, B. V. and Aleksandrov, K. S. *Crystallogr. Rep.* **2000**, *45*, 792–798. doi: 10.1134/1.1312923.

[25] Ruddlesden, S. N. and Popper, P. *Acta Cryst.* **1957**, *10*, 538–539. doi: 10.1107/S0365110X57001929.

[26] Ruddlesden, S. N. and Popper, P. *Acta Cryst.* **1958**, *11*, 54–55. doi: 10.1107/S0365110X58000128.

[27] Du, K.-z., Tu, Q., Zhang, X., Han, Q., Liu, J., Zauscher, S., and Mitzi, D. B. *Inorg. Chem.* **2017**, *56*, 9291–9302. doi: 10.1021/acs.inorgchem.7b01094.

[28] Calabrese, J., Jones, N. L., Harlow, R. L., Herron, N., Thorn, D. L., and Wang, Y. *J. Am. Chem. Soc.* **1991**, *113*, 2328–2330. doi: 10.1021/ja00006a076.

[29] Tsai, H., Nie, W., Blancon, J.-C., Stoumpos, C. C., Asadpour, R., Harutyunyan, B., Neukirch, A. J., Verduzco, R., Crochet, J. J., Tretiak, S., Pedesseau, L., Even, J., Alam, M. A., Gupta, G., Lou, J., Ajayan, P. M., Bedzyk, M. J., Kanatzidis, M. G., and Mohite, A. D. *Nature* **2016**, *536*, 312–316. doi: 10.1038/nature18306.

[30] Liu, J., Xue, Y., Wang, Z., Xu, Z. Q., Zheng, C., Weber, B., Song, J., Wang, Y., Lu, Y., Zhang, Y., and Bao, Q. *ACS Nano* **2016**, *10*, 3536–3542. doi: 10.1021/acsnano.5b07791.

[31] Ling, Y., Yuan, Z., Tian, Y., Wang, X., Wang, J. C., Xin, Y., Hanson, K., Ma, B., and Gao, H. *Adv. Mater.* **2016**, *28*, 305–311. doi: 10.1002/adma.201503954.

[32] Mitzi, D. B. *Chem. Mater.* **1996**, *8*, 791–800. doi: 10.1021/cm9505097.

[33] Knutson, J. L., Martin, J. D., and Mitzi, D. B. *Inorg. Chem.* **2005**, *44*, 4699–4705. doi: 10.1021/ic050244q.

[34] Mitzi, D. B. and Liang, K. *Chem. Mater.* **1997**, *9*, 2990–2995. doi: 10.1021/cm970352d.

[35] Ishihara, T. *J. Lumin.* **1994**, *60*, 269–274. doi: 10.1016/0022-2313(94)90145-7.

[36] Pradeesh, K., Rao, K. N., and Prakash, G. V. *J. Appl. Phys.* **2013**, *113*, 083523. doi: 10.1063/1.4792667.

[37] Stoumpos, C. C., Cao, D. H., Clark, D. J., Young, J., Rondinelli, J. M., Jang, J. I., Hupp, J. T., and Kanatzidis, M. G. *Chem. Mater.* **2016**, *28*, 2852–2867. doi: 10.1021/acs.chemmater.6b00847.

[38] Ishihara, T., Takahashi, J., and Goto, T. *Phys. Rev. B* **1990**, *42*, 11099–11107. doi: 10.1103/PhysRevB.42.11099.

[39] Dou, L., Wong, A. B., Yu, Y., Lai, M., Kornienko, N., Eaton, S. W., Fu, A., Bischak, C. G., Ma, J., Ding, T., Ginsberg, N. S., Wang, L.-W., Alivisatos, A. P., and Yang, P. *Science* **2015**, *349*, 1518–1521. doi: 10.1126/science.aac7660.

[40] Zhang, Q., Su, R., Liu, X., Xing, J., Sum, T. C., and Xiong, Q. *Adv. Funct. Mater.* **2016**, *26*, 6238–6245. doi: 10.1002/adfm.201601690.

[41] Weidman, M. C., Seitz, M., Stranks, S. D., and Tisdale, W. A. *ACS Nano* **2016**, *10*, 7830–7839. doi: 10.1021/acsnano.6b03496.

[42] Yang, S., Niu, W., Wang, A.-L., Fan, Z., Chen, B., Tan, C., Lu, Q., and Zhang, H. *Angew. Chem. Int. Ed.* **2017**, *56*, 4252–4255. doi: 10.1002/anie.201701134.

[43] Eames, C., Frost, J. M., Barnes, P. R. F., O'Regan, B. C., Walsh, A., and Islam, M. S. *Nat. Commun.* **2015**, *6*, 7497. doi: 10.1038/ncomms8497.

[44] Stranks, S. D., Eperon, G. E., Grancini, G., Menelaou, C., Alcocer, M. J. P., Leijtens, T., Herz, L. M., Petrozza, A., and Snaith, H. J. *Science* **2013**, *342*, 341–344. doi: 10.1126/science.1243982.

[45] Hoke, E. T., Slotcavage, D. J., Dohner, E. R., Bowring, A. R., Karunadasa, H. I., and McGehee, M. D. *Chem. Sci.* **2015**, *6*, 613–617. doi: 10.1039/C4SC03141E.

[46] DeQuilettes, D. W., Zhang, W., Burlakov, V. M., Graham, D. J., Leijtens, T., Osherov, A., Bulović, V., Snaith, H. J., Ginger, D. S., and Stranks, S. D. *Nat. Commun.* **2016**, *7*, 11683. doi: 10.1038/ncomms11683.

[47] Bischak, C. G., Hetherington, C. L., Wu, H., Aloni, S., Ogletree, D. F., Limmer, D. T., and Ginsberg, N. S. *Nano Lett.* **2017**, *17*, 1028–1033. doi: 10.1021/acs.nanolett.6b04453.

[48] Schaak, R. E. and Mallouk, T. E. *Chem. Mater.* **2002**, *14*, 1455–1471. doi: 10.1021/cm010689m.

[49] Pradeesh, K., Baumberg, J. J., and Vijaya Prakash, G. *J. Appl. Phys.* **2012**, *111*, 013511. doi: 10.1063/1.3674324.

[50] Ahmad, S., Baumberg, J. J., and Vijaya Prakash, G. *J. Appl. Phys.* **2013**, *114*, 233511. doi: 10.1063/1.4851715.

[51] Billing, D. G. and Lemmerer, A. *New J. Chem.* **2008**, *32*, 1736–1746. doi: 10.1039/b805417g.

[52] Venkataraman, N. V., Bhagyalakshmi, S., Vasudevan, S., and Seshadri, R. *Phys. Chem. Chem. Phys.* **2002**, *4*, 4533–4538. doi: 10.1039/B204983J.

[53] Barman, S., Venkataraman, N. V., Vasudevan, S., and Seshadri, R. *J. Phys. Chem. B* **2003**, *107*, 1875–1883. doi: 10.1021/jp026879h.

[54] Lemmerer, A. and Billing, D. G. *Dalton Trans.* **2012**, *41*, 1146–1157. doi: 10.1039/C0DT01805H.

[55] Tress, W., Marinova, N., Moehl, T., Zakeeruddin, S. M., Nazeeruddin, M. K., and Grätzel, M. *Energy Environ. Sci.* **2015**, *8*, 995–1004. doi: 10.1039/C4EE03664F.

[56] Pellet, N., Teuscher, J., Maier, J., and Grätzel, M. *Chem. Mater.* **2015**, *27*, 2181–2188. doi: 10.1021/acs.chemmater.5b00281.

[57] Akkerman, Q. A., D'Innocenzo, V., Accornero, S., Scarpellini, A., Petrozza, A., Prato, M., and Manna, L. *J. Am. Chem. Soc.* **2015**, *137*, 10276–10281. doi: 10.1021/jacs.5b05602.

[58] Rühe, J. *Polymer Brushes: On the Way to Tailor-Made Surfaces*, in *Polymer Brushes*. Wiley-VCH Verlag GmbH & Co. KGaA, **2005**, pp. 1–31. ISBN 978-3-527-60382-4.

[59] Binder, K. and Milchev, A. *J. Polym. Sci. Part B: Polym. Phys.* **2012**, *50*, 1515–1555. doi: 10.1002/polb.23168.

[60] Egorov, S. A., Hsu, H.-P., Milchev, A., and Binder, K. *Soft Matter* **2015**, *11*, 2604–2616. doi: 10.1039/C4SM02862G.

[61] Owen, M. J. *Surface Properties and Applications*, in *Silicon-Containing Polymers*. Springer Netherlands, **2000**, pp. 213–231. ISBN 978-1-4020-0348-6.

[62] Huang, C., Sun, Z., Cui, M., Liu, F., Helms, B. A., and Russell, T. P. *Adv. Mater.* **2016**, *28*, 6612–6618. doi: 10.1002/adma.201600691.

[63] Toor, A., Helms, B. A., and Russell, T. P. *Nano Lett.* **2017**, *17*, 3119–3125. doi: 10.1021/acs.nanolett.7b00556.

[64] Huang, C., Cui, M., Sun, Z., Liu, F., Helms, B. A., and Russell, T. P. *Langmuir* **2017**, *33*, 7994–8001. doi: 10.1021/acs.langmuir.7b01685.

[65] Facchetti, A. *Mater. Today* **2007**, *10*, 28–37. doi: 10.1016/S1369-7021(07)70017-2.

[66] Allard, S., Forster, M., Souharce, B., Thiem, H., and Scherf, U. *Angew. Chem., Int. Ed.* **2008**, *47*, 4070–4098. doi: 10.1002/anie.200701920.

[67] Rivnay, J., Jimison, L. H., Northrup, J. E., Toney, M. F., Noriega, R., Lu, S., Marks, T. J., Facchetti, A., and Salleo, A. *Nat. Mater.* **2009**, *8*, 952. doi: 10.1038/nmat2570.

[68] Sides, S. W., Curro, J., Grest, G. S., Stevens, M. J., Soddemann, T., Habenschuss, A., and Londono, J. D. *Macromolecules* **2002**, *35*, 6455–6465. doi: 10.1021/ma020014k.

[69] Park, N.-G. *Mater. Today* **2015**, *18*, 65–72. doi: 10.1016/j.mattod.2014.07.007.

[70] Huang, H., Zhao, F., Liu, L., Zhang, F., Wu, X.-g., Shi, L., Zou, B., Pei, Q., and Zhong, H. *ACS Appl. Mater. Interfaces* **2015**, *7*, 28128–28133. doi: 10.1021/acsami.5b10373.

[71] Zhang, F., Huang, S., Wang, P., Chen, X., Zhao, S., Dong, Y., and Zhong, H. *Chem. Mater.* **2017**, *29*, 3793–3799. doi: 10.1021/acs.chemmater.7b01100.

[72] Stevenson, J., Sorenson, B., Subramaniam, V. H., Raiford, J., Khlyabich, P. P., Loo, Y. L., and Clancy, P. *Chem. Mater.* **2017**, *29*, 2435–2444. doi: 10.1021/acs.chemmater.6b04327.

[73] Dee, G. T. and Sauer, B. B. *The Cohesive Energy Density of Polymer Liquids*, in *Computational Studies, Nanotechnology, and Solution Thermodynamics of Polymer Systems*. Springer US, Boston, MA, **2002**, pp. 29–36. ISBN 978-0-306-47110-0.

[74] Gee, G. A. G. and Wilson, G. J. *Polymer* **1960**, *1*, 456–466. doi: 10.1016/0032-3861(60)90061-6.

[75] Sauer, B. B. and Dee, G. T. *Macromolecules* **2002**, *35*, 7024–7030. doi: 10.1021/ma0202437.

[76] Krevelen, D. V. and Nijenhuis, K. T. *Cohesive Properties and Solubility*, chap. 7, in *Properties of Polymers*. Elsevier, Amsterdam, fourth edition ed., **2009**, pp. 189–227. ISBN 978-0-08-054819-7.

[77] Dee, G. T. and Sauer, B. B. *J. Appl. Polym. Scie.* **2017**, *134*, 1–14. doi: 10.1002/app.44431.

[78] Gottlieb, H. E., Kotlyar, V., Nudelman, A., G, E., K, V., and Nudelman, A. *J. Org. Chem.* **1997**, *62*, 7512–7515. doi: 10.1021/jo971176v.

List of acronyms

AFM Atomic Force Microscopy

ATR Attenuated Total Reflection

CED Cohesive Energy Density

cmc critical micellar concentration

Cryo-EM Cryo-Electron Microscopy

DLS Dynamic Light Scattering

DSC Differential Scanning Calorimetry

DSSC Dye Sensitized Solar Cell

EDX Energy Dispersive X-Ray Spectroscopy

FDA Food and Drug Administration

FT Fourier-transform

GC-MS Gass Chromatography-Mass Spectroscopy

GIWAXS Grazing-Incidence Grazing-Angle X-Ray Scattering

HLB Hydrophilic-Lipophilic Balance

IPN Interpenetrated Polymer Network

ISC Intersystem Crossing

NIR Near Infrared

NMR Nuclear Magnetic Resonance

OFET Organic Field-Effect Transistor

OLED Organic Light-Emitting Diode

PL photoluminescence

QY quantum yield

ROS reactive oxygen species

SEM Scanning Electron Microscopy

STEM Scanning Transition Electron Microscopy

TADF Thermally Activated Delayed Fluorescence

TTA Triplet-Triplet Annihilation

TTET Triplet-Triplet Energy Transfer

UC Up-Conversion

UCMs up-converting micelles

UV Ultraviolet

XRD X-Ray Diffraction

List of chemicals names

4EDMA tetraethylene glycol dimethacrylate

AAPH 2,2'-azobis(2-amidinopropane) dihydrochloride

AcOEt ethyl acetate

AIBN azobisisobutyronitrile

AP-E4 2-(tetrahydropyranyl)oxy TEG methacrylate

BODIPY boron-dipyrromethene

DABP 4,4'-bis(dimethylamino)benzophenone

DBA 9,10-dibromoanthracene

DCM dichloromethane

DMF N,N-dimethylformamide

DMSO dimethyl sulfoxide

Dod−NH₃X dodecylammonium halide

DPA 9,10-diphenylanthracene

DTE 2-di(3-thienyl)-1,2-ethanedione

HDec−NH₃X hexadecylammonium halide

Ig1 1-hydroxycyclohexyl phenyl ketone

Ig2 2-hydroxy-2-methylpropiophenone

IS 2,3-dioxo-2,3-dihydroindole (isatin)

Kolliphor® EL PEG-35 castor oil. CAS number: 61791-12-6

LPO lauroyl peroxide

N(Et)₃ triethylamine

Oct−NH₃X octylammonium halide

PBS phosphate buffer saline

Pd(dtbpf)Cl$_2$ [1,1'-bis(di-tert-butylphosphino)ferrocene]dichloropalladium(II)

Pd(dppf)Cl$_2$ [1,1'-bis(diphenylphosphino)ferrocene]dichloropalladium(II)

Pd(PPh$_3$)$_2$Cl$_2$ bis(triphenylphosphine)palladium(II) dichloride

Pd(PPh$_3$)$_4$ tetrakis(triphenylphosphine)palladium(0)

PDMS poly(dimethylsiloxane)

Pd(OAc)$_2$ palladium(II) acetate

P-E4 2-[2-[2-[2-[(tetrahydro-2H-pyran-2-yl)oxy]ethoxy]ethoxy]ethoxy]ethanol

PEG polyethylene glycol

PtOEP platinum(II) 2,3,7,8,12,13,17,18-octaethyl-21H,23H-porphyrin

PVA poly(vinyl alcohol)

Qn-Oct 5,12-dioctylquinolino[2,3-b]acridine-7,14(5H,12H)-dione

T80 Tween 80, polyethylene glycol sorbitan monooleate. CAS number: 9005-65-6

TEG tetraethylene glycol

THF tetrahydrofuran

TPGS-750-M DL$-\alpha-$tocopherol methoxy PEG succinate. CAS number: 1309573-60-1

Triton X-100 polyethylene glycol tert-octylphenyl ether. CAS number: 9002-93-1